Earth-Abundant Transition Metal Hydride Complexes for Dehydrocoupling and Hydrosilylation Catalysis

by

Paul Ashley Lummis

A thesis submitted in partial fulfillment of the requirements for the degree of

Doctor of Philosophy

Department of Chemistry
University of Alberta

Abstract

The work described within this thesis details explorations into the realm of transition metal hydride chemistry, in particular for compounds of zirconium and zinc, plus additional ligand design and synthesis.

Chapter 2 features complexes of zirconium bearing sterically hindered bis(amido)silyl ligands, and the functionalisation thereof. In addition, some of the challenges associated with these complexes are described, in particular the installation of these ligands onto Zr, and the functionalisation of the Zr following ligand binding. Additionally, the catalytic activity of these complexes towards dehydrocoupling of amine-boranes is investigated.

Chapter 3 details the synthesis of a new bis(amido)silyl "umbrella" ligand precursor, and the utlisation of 1,1,3,3-tetramethylguanidine towards new bis(imine) ligands tethered by silyl, disilyl and disiloxane linkeages.

Chapter 4 we covers the preparation of neutral and cationic zinc hydride adducts bearing N-hetercyclic carbene ligands, and their use in the catalytic hydrosilylation and hydroboration of ketones. In chapter 5 the ability of these compounds to be utilised as single-source precursors for materials chemistry is described, as well as the design of compounds towards the synthesis of an elusive zinc carbonyl complex.

Dedicated to the memory of Kenneth Finch and Harald Neumann

"Imagination is more important than knowledge. For knowledge is limited to all we now know and understand, while imagination embraces the entire world, and all there ever will be to know and understand." - Albert Einstein

Acknowledgements

First of all, I must thank my advisor Professor Eric Rivard for all of his help and support since he graciously allowed me to join his research group. I benefitted immensely from his guidance, and very much appreciated the fact that he allowed me as much creative freedom as was possible and never once said that I had asked a stupid question, despite proffering many. It was a long and rewarding journey, during which I have grown immensely as a person, a chemist, and perhaps most importantly, as a glove-box/solvent purification system technician. I would also like to thank Prof. Steven Bergens, Prof. Frederick West, Prof. Jon Veinot, Prof. Rylan Lundgren, Prof. Frédéric-Georges Fontaine and Prof. John Davis for serving on my supervisory/examination committee, and for always forcing me to work harder, and to think outside of the box. I would be remiss also to not thank Dr. Terry Kee at the University of Leeds, who advised my earlier studies and began the process of making me a chemist of at least somewhat reasonable ability.

Next, I must thank my amazing wife Erika, without whom this entire process would not have been possible. Simple words cannot express how grateful I am that you have been by my side during these past five years, and I look forward to an exciting future together; I even promise to (try to) get a "real" job soon! In addition to Erika, I am grateful for the support of my family; my brother Ian, Parents Julia and Eric, and grandparents Edith & Kenneth, and Eric Sr. I would also like to thank my mother and father in law, Sigrid and Harry Neumann who welcomed me warmly into their family, and into their home upon my initial move from England to Canada, as well as the

extended Neumann, Knox and Wrona families for the warm welcome to your country and your family.

None of what follows would not have been possible without the amazing staff at the University of Alberta, and to them I offer my sincere thanks, in particular to Dr. Bob McDonald, Dr. Michael Ferguson, Dr. Jason Cooke, Ryan Lewis, Mark Miskolzie, Nupar Dabral, Wayne Moffat, Prof. Alex Brown, the wonderful staff of the machine, electronic and glass shops, and to everybody else that has made my stay so enjoyable.

I must also thank all the previous members of the Rivard lab (in somewhat chronological order); Dr. Ibrahim Al-Rafia, Adam Malcolm, Le Kang, Kelsey Deutsch, Kyle Sabourin, William Ramsay, Marcel Schreier, Christopher Berger, James Goettel, Jason Brandt, Leah Miedema, Sean Liew, Sean MacDonald, Dr. Gang He, Alyona Shynkaruk, William Torres Delgardo, Melanie Lui, Anindya Swarnakar, David Xu, Cieran Tran, Piotr Hubacek, Janelle Smiley-Wiens, Devon Schatz, Laura Lee, Kate Powers, Koichi Nagata, Paul Choi, Fatemeh Shahin, Brandon Furlong, Matthew Roy, Sarah Parke, Dr. Christian Hering-Junghans, Dr. Mike Boone, Derek Zomerman and Nathan Paisley. Thank you to all of the above for your ideas, support, discussion, and most of all for enduring my music.

If I was to list individually every person who has made this journey so enjoyable the result would be a document at least double the size of the one that follows, however I must reserve some special thanks to a few people by name, and offer a sincere apology to anybody that I might miss; I'll buy the beer next time. With that in mind, I'd like to offer my sincere gratitude to the

following for your support and continued friendship: Dr. Matthew Zamora, Dr. Avena Ross, Christopher Sadek, Dr. Lindsay “The Hounje” Hounjet, Dr. Mike Slaney, Dr. Tiffany MacDougall, Dr. Jeremy Gauthier, Kirsten Tomlin, Devin Reaugh, Dr. Mita Dasog, Christina Gonzalez, Sarah Regli, Dr. Melanie Hoffman, Dr. Brenna Brown, Dr. Christian Merten, Lindsay Shearer, Greg Kaufmann, Dr. Brent Rudyk, Dr. Sonja Francis, Dr. Jeremy John, Dr. Teague McGinitie, Dr. Elizabeth McGinitie, Justin Thuss, Colin Diner, and Dr. Katie Nizio. I must also offer my thanks to my friends back in the UK, in particular Rich Jarvis, Scott Greenfield, Steve Haywood, Ross Ballinger, Sean Dunn, Rob Tagg, Danny Middleton, Matt Lane, Steven Collins, Matt Fairbrother, Ian Frost, Chris Kendrick, Liz LeQuelenec, and many, many more. Even though I’ve been gone from the UK for many years now I can still chat with you as though a day has never been lost, and for that I’m forever grateful.

List of Tables

List of Figures

List of Schemes

List of Symbols, Abbreviations and Nomenclature

Symbols	**Meaning**
{X}	Decoupled nucleus X
2D	2-Dimensional
Å	Angström
AIM	Atoms In Molecules
Bp	Boiling point
^{s}Bu	*Sec*-butyl
ca.	circa; approximately
COD	1,5-cyclooctadiene
DMAP	4-Dimethylaminopyridine
DOSY	Diffusion Ordered NMR spectroscopy
equiv.	Equivalent
eV	Electron volt
FT	Fourier transform
g	Gram
HOMO	Highest occupied molecular orbital
Hz	Hertz
IMes	1,3-Bis(2,4,6-trimethylphenyl)imidazole-2-ylidine
$ImMe_2{}^{i}Pr_2$	1,3-Diisopropyl-3,4-dimethylimidazole-2-ylidine
^{i}Pr	Isopropyl
IPr	1,3-Bis(2,6-diisopropylphenyl)imidazole-2-ylidine
IR	Infrared

K	Kelvin
kJ	Kilojoule
kcal	Kilocalorie
LA	Lewis acid
LB	Lewis base
LUMO	Lowest unoccupied molecular orbital
Me	Methyl
Mes	Mesityl
mg	Milligram
MHz	Megahertz
min	Minute
mL	Millilitre
mmol	Millimole
mol	Mole
Mp	Melting point
NBO	Natural bond orbital
NHC	*N*-heterocylic carbene
$^{n}J_{AB}$	n-bond AB coupling constant
NMR	Nuclear Magnetic Resonance
°C	Degrees Celcius/centigrade
ORTEP	Oakridge Thermal Elipsoid Plot
OTf	Trifluoromethansulfonate, triflate
Ph	Phenyl

ppm	Parts per million
PXRD	Powder X-ray diffraction
RDS	Rate determining step
RT	Room temperature
THF	Tetrahydrofuran
TOF	Turnover frequency
TON	Turnover number
vs.	Versus
WBI	Wiberg Bond Index
XPS	X-ray PhotoelectronSpectroscopy
μ	Micro; also mu (to infer a bridging atom)
δ	Partial charge or chemical shift in ppm
η	Eta; the number of atoms through which a ligand coordinates
σ	Sigma

Chapter 1.

Introduction

1.1 Why transition metal chemistry?

Transition metal complexes form a ubiquitous part of modern synthetic chemistry, with applications ranging from mediating catalysis to their use as precursors in the chemical vapour deposition of materials. Early on, metal-containing compounds were used as base colours for paints and pigments, however it was only later in the 1900s that the structure of these coordination complexes were understood, largely due to the pioneering work of Alfred Werner. Naturally, the scope of coordination chemistry has widened over time, moving from simple homoleptic complexes bearing naturally occurring ligands such as CO, halides, NH_3 and H_2O (e.g. $[Co(NH_3)_6]Cl_3$), to include species featuring designer ligands. For example, the development of sterically-encumbered chiral phosphines over the past few decades has led to active metal-containing catalysts for stereoselective transformations of great use in industrial pharmaceutical chemistry.[1]

The field of organometallic chemistry represents an important subdiscipline, and deals with the study of compounds that have at least one carbon atom bound directly to a metal centre. While there were early discoveries such as Zeise's salt $K[Cl_3Pt(\eta^2\text{-}C_2H_4)]$, first reported in 1831,[2] the field of organometallic chemistry came into greater prominence with the discovery of ferrocene $Fe(C_5H_5)_2$ by Pauson and coworkers in 1951.[3] Ferrocene was particularly novel at the time as it displayed a new ligand binding mode, $[\eta^5\text{-}C_5H_5]^-$, and ushered in the ubiquitous use of the

cyclopentadienyl (Cp) ligand to support various related metal complexes, termed metallocenes (see Figure 1.1 for examples). Advantages of the Cp ligand include the potential to substitute at various positions about the five-membered ring to obtain structurally and electronically distinct cyclopentadienyl complexes, and for $[C_5H_5]^-$ (and its analogues) to display various metal coordination modes to allow for other ligands to be accommodated at the metal centre. An example highlighting the potentially fluxional nature of the Cp ligand is zincocene (Cp_2Zn), where the Cp rings are observed to equilibrate between η^1, η^3 and η^5 coordination on the NMR timescale.[4]

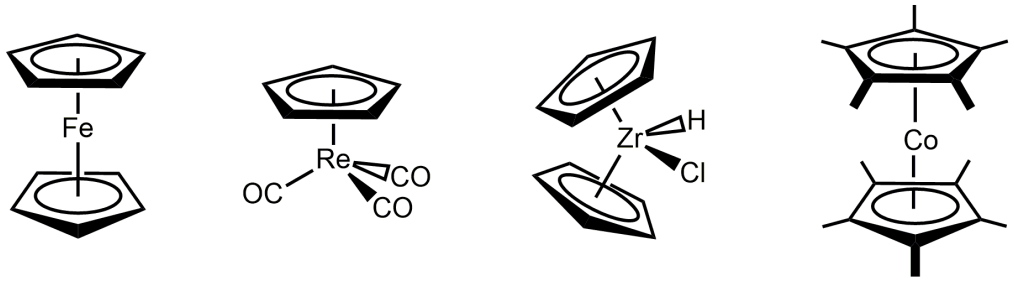

1 **2** **3** **4**

Figure 1.1 Representative examples of compounds bearing cyclopentadienyl (Cp) or pentamethylcyclopentadienyl (Cp*) ligands.

Of the examples listed in Figure 1.1, a notable compound is Schwartz's reagent, $Cp_2Zr(H)Cl$ (**3**), first prepared in the group of Jeffrey Schwartz in 1974.[5] What is particularly interesting about this species is that it contains a hydrogen atom bound directly to a metal centre. Due to the electropositive nature of zirconium relative to hydrogen, the Zr-H bond is polarised such that

the electron density of the bond is closer to the hydrogen atom, and therefore this hydrogen ligand shows *hydridic* character ($H^{\delta-}$). When coupled with the electrophilic nature of the zirconium centre, this compound, and others like it, are excellent candidates for activating organic substrates such as alkynes, alkenes and other unsaturated compounds.[6] As a result, this thesis has a major focus on the preparation of new hydride complexes for catalytic transformations; it was determined that both zirconium and zinc are inexpensive metals whose complexes hold significant promise in this regard. In order to provide background and motivation for the studies in this thesis, the next sections will cover a non-exhaustive overview of the synthesis of metal hydrides, selected advances in metal hydride chemistry, and how these complexes relate to dehydrocoupling and hydrosilylation catalysis.

1.2 Metal hydrides: an overview

1.2.1. Binary metal hydrides

Naturally, the simplest compounds that one can consider when discussing metal hydrides would be homoleptic compounds containing just hydrogen atoms and the metal of choice, otherwise referred to as binary metal hydrides. Many transition metal hydrides exist in the form of MH, with some metals such as Zn, Ca, Mg forming MH_2 species, while other metals such Ti and Zr can form non-stoichiometric hydrides (e.g. $TiH_{1.95}$).[7] Of particular relevance to the work described in this thesis, molecular MH_2, MH_3 and MH_4 species (M = Zr and Hf) have been prepared via laser ablation of the metal in the presence of H_2 at 10 K, however these MH_x species are thermally sensitive

and reductively eliminate H_2 gas when warmed to room temperature.[8] Thermally stable metal hydrides often display poor solubility in most common laboratory solvents due to the formation of extended structures in the solid state, mediated by M-H-M bridges or ionic $M^{(x+)}\cdots H^-$ interactions.[9] An added complication is that the hydridic character of the H atoms makes most metal hydrides reactive towards water (and other protic solvents) to form the corresponding metal hydroxides (and oxides), with the concomitant formation of gaseous H_2. As mentioned, another challenge associated with some binary metal hydrides is their relative thermal instability. Metal-hydrogen covalent bonds are typically weaker (*ca*. 144-235 kJ mol^{-1})[10] than the H-H bond strength observed for the H_2 molecule (*ca*. 432 kJ mol^{-1}), which makes the dissociation of two equivalents of the M-H moiety to form two equivalents of M(0) and one equivalent of H_2 potentially favourable. With a judicious choice of co-ligand however, the thermal stability and solubility of these species can be increased. This is demonstrated in the case of complexes of Lewis base stabilized complexes of AuH, LAu-H, where the choice of ligand L can modulate the Au-H bond strength from 297 kJ mol^{-1} where there is no ligand, to as high as 372 $kJmol^{-1}$ [L = NH_3] and 377 kJ mol^{-1} [L = CO].[9] In addition, the presence of bulky ligands can also suppress bimolecular decomposition pathways, as illustrated by the successful preparation of the Au(I) hydride adduct IPr•AuH (IPr = $[(HCNDipp)_2C:]$; Dipp = 2,6-diisopropylphenyl) .[11]

1.2.2. Ternary metal hydrides

Another class of metal hydride of importance to this thesis is ternary metal hydrides. These compounds are similar to the aforementioned binary metal hydrides in that the metal of choice is only bound to hydrogen atoms, however the number of bound hydrogen atoms is greater than the formal positive charge on the metal centre; the resulting anionic charge of the $[M^{x+}H_n]^{(n-x)-}$ complex is typically balanced by alkali or alkaline earth metal cations. Main group element ternary hydrides such as $Na[BH_4]$ and $Li[AlH_4]$ are well-known reducing agents within organic chemistry,[12] however ternary transition metal hydrides are also known.[13] One interesting feature of many ternary transition metal hydrides is the ability to achieve very high coordination numbers, with $K_2[ReH_9]$[14] being a particularly noteworthy example. In order to better understand the nature of metal hydrides, key synthetic routes and the nature of M-H and M-H_2 bonding will be described below. Of note, additional ligands must be generally tethered to the central metal to generate heteroleptic species with improved solubility and thermal stability.

1.2.3. Synthesis of metal hydride complexes

There are a variety of different pathways by which one can synthesise heteroleptic transition metal hydride complexes, the major routes of which are outlined below:

Oxidative addition of H_2 to a metal centre often can transpire when the metal is electron rich. This occurs via an initial interaction between the metal and H_2, where the metal functions as a Lewis acid, and H_2 donates the σ-bonding electron density to the metal centre (Figure 1.2 **A**; Figure 1.3). At the same time, or in synergy, the metal can donate electron density from an occupied d-orbital to the H-H σ* orbital of dihydrogen, resulting in weakening (**B**) or cleavage (**C**) of the H-H bond; the latter process leads to an increase in the oxidation state of the metal by +2 charge units.

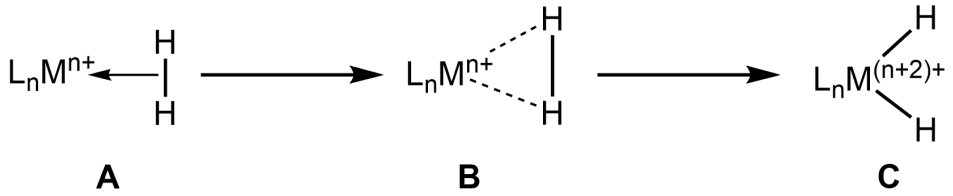

Figure 1.2 (**A**) Initial interaction of H_2 with a metal centre, L_nM; (**B**) partial back-donation to $H_2(\sigma^*)$ with lengthening of H-H bond and decrease in bond order, and (**C**) formal oxidative addition of H_2 to a metal centre with associated increase in oxidation state from n+ to (n+2)+.

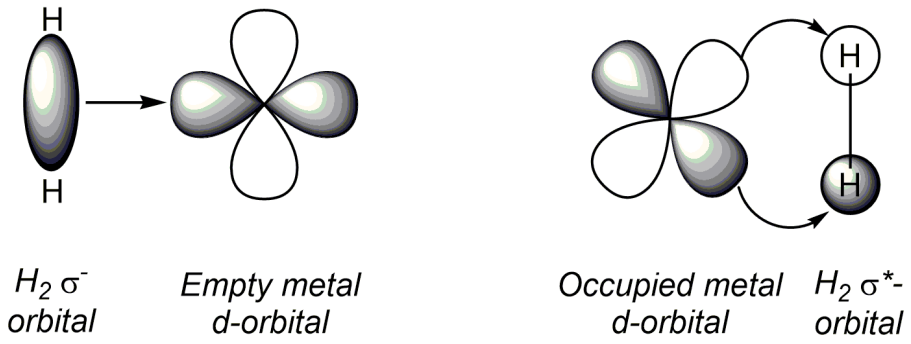

Figure 1.3 (Left) interaction of the occupied σ-bonding orbital in H_2 with an empty d-orbital on a metal centre, and (Right) back donation from an occupied metal d-orbital to the σ* orbital of H_2, which results in H-H bond cleavage and formation of a metal dihydride.

While the oxidative addition of H_2 to metal complexes is one of the more conceptually simple methods of forming metal hydride complexes, there are certain requirements that must be met in order for this reaction to proceed. Firstly, the transition metal complex in question must have an available higher oxidation state; that is to say that the resultant complex and metal oxidation state must be both thermodynamically and kinetically stable. As an example, the oxidative addition of H_2 to a Zr(IV) complex to generate a Zr(VI) dihydride species would not proceed as Zr(IV) represents d^0 configuration, and therefore has neither the available oxidation state, nor the required d-electrons for the effective oxidative addition of H_2. There also exist σ-complexes where H_2 is bound in a side-on, η^2 fashion (**B**, Figure 1.2), with a partial backbonding interaction but with no formal oxidative addition having occurred. This interaction results in the weakening of the H-H bond, however the formal cleavage and oxidation addition to the metal centre does not occur. The first such example was presented by the group of Kubas in 1984 with the crystallographically characterized compounds $[M(PR_3)_2(CO)_3(\eta^2\text{-}H_2)]$ (M = W, Mo; R = ^{i}Pr, cyclohexyl).[15]

Salt metathesis involves the addition of a hydride source, such as $Li[AlH_4]$, to a metal halide substrate. This reaction proceeds via a metathesis pathway, typically with the generation of an alkali or alkaline earth metal halide salt as by-product. In some cases, such as with a simple metal hydride like KH, this is the only by-product, however other commonly employed hydride sources often yield a Lewis acid concurrently. An example of this

reactivity is shown in Equation 1.1, where a metal halide featuring generic ligands, L_n, combines with potassium Selectride $K[HB^sBu_3]$ (Equation 1.1) to give a metal hydride (L_nMH) along with KX and the Lewis acid B^sBu_3 in the process (^{s}Bu = sec-butyl).

$$L_nMX + K[HB^sBu_3] \longrightarrow L_nMH + KX + B^sBu_3 \qquad (1.1)$$

One benefit of using functionalised hydride salts such as $K[HB^sBu_3]$ or $Li[HBEt_3]$ rather than simple ternary hydride salts (e.g. $Na[BH_4]$) is the increased solubility of the organosubstituted species in commonly used organic solvents, which allows for more facile handling and faster reactivity of these hydride sources relative to their less soluble counterparts.

Hydride elimination involves the migration of one hydrogen atom from various positions of an already attached fragment, such as an alkyl group, to a coordination site on the metal centre. In the case illustrated in Figure 1.4, the β-hydrogen atom migrates to the metal, with the generation, and sometimes elimination from the metal coordination sphere of an unsaturated molecular fragment such as an alkene in an overall process termed β-hydride elimination. As hydride elimination initially results in an increase in coordination number at the metal centre, the metal must be coordinatively unsaturated; otherwise this process cannot take place. One way to prevent β–hydride elimination from happening, should it be undesirable, is to choose an alkyl fragment that does not contain any β-hydrogen atoms, such as a neopentyl group ($-CH_2{}^t$Bu). While functional groups such as the aforementioned neopentyl group may

prevent β-hydrogen elimination, there are also α- and γ-hydrogen elimination processes that can occur.

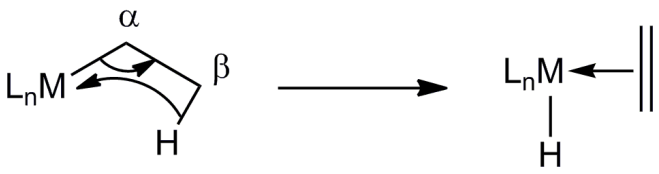

Figure 1.4 Mechanism for β-hydride elimination with generation of a new metal hydride featuring a concurrently generated unsaturated moiety.

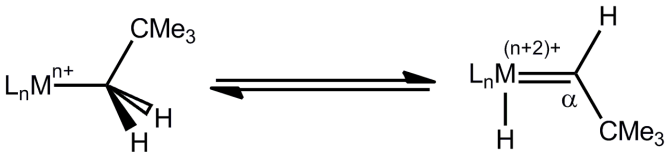

(1.2)

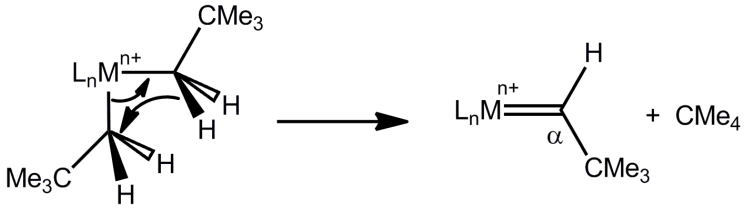

(1.3)

Another process of interest is *α-hydrogen elimination* (Equation 1.2) which occurs with an increase in the formal oxidation state of the metal centre and transfer of hydrogen from the α-position of an organic fragment to a metal centre (the H-acceptor). This is conceptually similar to, but slightly different from *α-hydrogen abstraction* (Equation 1.3) which transpires with no change in formal oxidation state, and where a second organic fragment acts as the hydrogen atom acceptor, thus resulting in deprotonation and loss of this second, now protonated, fragment.

1.3 Introduction to specific catalytic processes of relevance to this thesis

1.3.1 Dehydrocoupling catalysis

Dehydrocoupling, the formation of a new element-element bond with concomitant release of one equivalent of hydrogen gas (Equation. 1.4), is a particularly appealing process for a number of reasons. The ability to form new bonds through an atom-economical route whereby the generation of hydrogen as the sole by-product makes this a desireable method for the formation of a variety of new compounds and materials.[16] In addition to this, many element-hydrogen bonds are relatively weak, thus the dehydrocoupling process is often exergonic. Furthermore, the loss of gaseous hydrogen from the reaction mixture serves to drive the reaction forward, and thus these reactions are typically irreversible. The use of transition metal catalysts in this process allows for reactivity that cannot often be seen in the absence of these species.

(1.4)

These type of dehydrocoupling reactions can be used to couple like elements with each other (e.g. the dehydrocoupling of monomeric silanes to form polysilane polymers and oligomers), or to create new bonds between two different elements (e.g. the dehydrocoupling of amine-borane and phosphine-borane adducts to form new B-N and P-N containing materials). In this thesis,

I will discuss exclusively the dehydrocoupling of amine-borane adducts of the general form $R_2NH•BH_3$; reviews of polysilane ($[R_2Si]_n$)[17] and phosphinoborane ($[RPH-BH_2]_n$)[18] syntheses via dehydrocoupling methodology can be found in the literature.

1.3.2 Catalytic dehydrocoupling of amine-borane adducts

1.3.2.1 The discovery of amine-borane adducts

Amine-boranes are of current interest as precursors to B-N polymers and ceramics, and have been explored within the context of hydrogen storage technologies.[19] These often air-stable adducts have been known for many years, and indeed the first example, $H_3N•BF_3$, was reported by Gay-Lussac in 1809.[20] Despite this early discovery, it was not until over a century later that Schlesinger and coworkers reported the synthesis of an amine-borane adduct of borane, BH_3, when they prepared $Me_3N•BH_3$ via the combination of an excess of trimethylamine with diborane (Equation. 1.5).[21] One drawback to this direct method is the need to handle the extremely pyrophoric gas diborane, B_2H_6 (bp -92.5 °C). In some cases, such as in the formation of $Me_3N•BH_3$, excess amine is used to increase the yield of the amine-borane complex, with any remaining amine collected at the end of the reaction.

$$\underset{\mathbf{5}}{2\,Me_3N} + \underset{\mathbf{6}}{B_2H_6} \xrightarrow{\text{-196 °C} \rightarrow \text{-80 °C}} \underset{\mathbf{7}}{2\,Me_3N•BH_3} \qquad (1.5)$$

With the above in mind, focus turned to the development of new synthetic routes to amine-boranes. One major advance was to utilise Lewis base-stabilised complexes of BH_3, such as $Me_2S{\bullet}BH_3$ and $THF{\bullet}BH_3$, in chemical syntheses. These reagents do however suffer from their own drawbacks which prevent their routine use on large scales, namely the liberation of pungent Me_2S in the former case, and the relatively poor long-term stability of $THF{\bullet}BH_3$ (which tends to afford furan ring-opened products including $B(OBu)_3$ over time). Despite these drawbacks, they have proven to be useful in the relatively small scale preparations of a range of amine-borane adducts, as demonstrated in the preparation of the liquid amine-borane diisopropylamine-borane, $^{i}Pr_2NH{\bullet}BH_3$ (Equation. 1.6),[22] which has shown the ability to effectively remove H_2 from other amine-boranes adducts such as $Me_2NH{\bullet}BH_3$ via transfer dehydrogenation.[23]

$$\underset{\mathbf{8}}{THF{\bullet}BH_3} + \underset{\mathbf{9}}{^{i}Pr_2NH} \xrightarrow[-\ THF]{-78\ ^{\circ}C \rightarrow RT} \underset{\mathbf{10}}{^{i}Pr_2NH{\bullet}BH_3} \qquad (1.6)$$

Another route that may be employed in the synthesis of amine-boranes is the reaction between an ammonium halide and alkali-metal borohydride salts. This will generate the desired amine-borane, accompanied by the release of one equivalent of an alkali metal halide salt, MX (M = Li, Na, K; X = Cl, Br, I) and one equivalent of gaseous H_2. This methodology is particularly useful for two reasons: the first is that the handling of free gaseous amines such as $MeNH_2$ (bp -6 °C) is avoided (Equation 1.7);[24] the second advantage

is when the desired borane is not commercially available, but can be obtained as the corresponding alkali metal borate salt. For example, the lithium borate salt $Li[MeBH_3]$ can be formed from the widely available borate ester $B(O^iPr)_3$, and then combined with the appropriate ammonium halide salt to yield an amine-borane adduct of $MeBH_2$ (Scheme 1.1).[25]

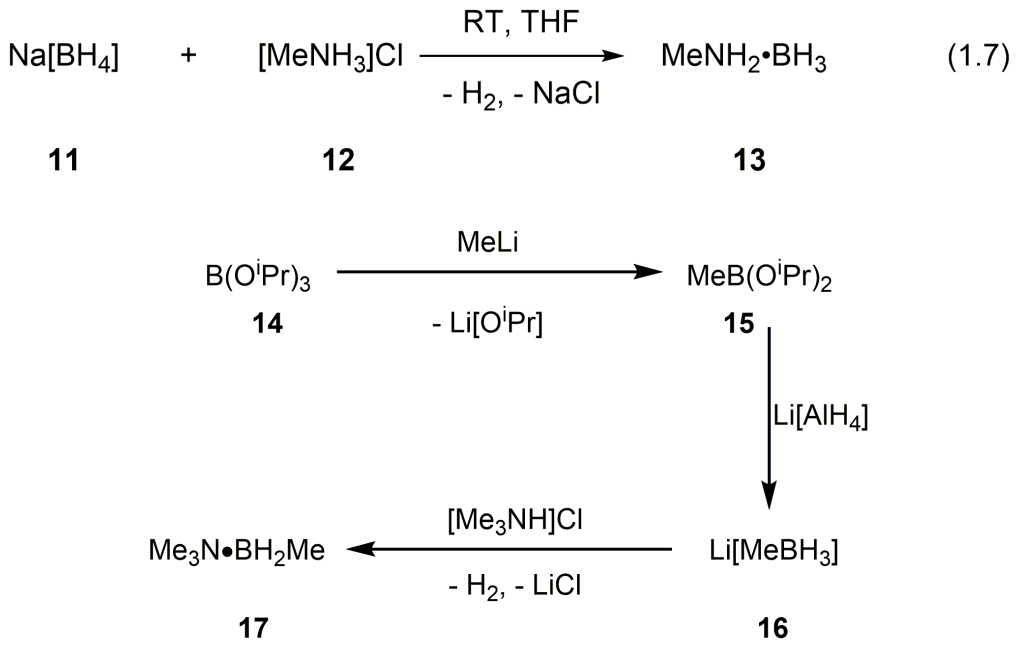

Scheme 1.1 Synthesis of amine-borane adduct $Me_3N•BH_2Me$.

1.3.2.2 Catalytic dehydrocoupling of amine-boranes

Now that the synthesis of amine-boranes has been discussed, the next step is to examine the types of compounds that can mediate the dehydrocoupling of these species. This is of particular interest as the products of dehydrocoupling, both oligomeric and polymeric, hold potential in hydrogen storage technologies and as precursors to ceramics.[17,18] Typically,

efficient dehydrocoupling requires the use of a transition metal complex as a catalyst, however there have been reported examples of non-metal containing species such as *N*-heterocyclic carbenes[26] or even iminoboranes such as $^{i}Pr_2N{=}BH_2$[22] effecting the mild stoichiometric dehydrogenation of amine-borane adducts. For this thesis I will discuss the dehydrocoupling of amine-boranes mediated by group 4 element complexes; a comprehensive discussion as to this chemistry facilitated by other metals has been previously published.[11a]

One of the first examples of group 4 element-catalysed dehydro-coupling of amine-boranes was reported by Manners and coworkers in 2006.[27] In this work, the authors utilised a mixture of Cp_2TiCl_2 with two equivalents of ^{n}BuLi in toluene at 20 °C, and this mixture instigates the complete conversion of $Me_2NH{\bullet}BH_3$ into $[Me_2N\text{-}BH_2]_2$ and $Me_2NH\text{-}BH_2\text{-}NMe_2\text{-}BH_3$ within 4 hours at a 2 mol% Ti catalyst loading. In this work, the authors mentioned that the unknown nature of the titanium products ("Cp_2Ti") generated in this mixture made identification of a reaction mechanism extremely challenging; it should be noted however that the analogous Zr system, termed Negishi's reagent ("Cp_2Zr") has been extensively studied in solution with a wide variety of Zr-containing products and organic by-products conclusively identified by NMR spectroscopy.[28] Later work by the Manners group utilised a different methodology to gain access to a "Cp_2Ti" source, by reducing Cp_2TiCl_2 with Na/Hg amalgam in the presence of PMe_3. The resulting Ti(II) complex $Cp_2Ti(PMe_3)_2$ (**19**) was isolable in pure form

(Equation 1.8),[29] and its ability to act as a dehydrogenation catalyst was investigated. The authors found in this instance that the catalytic dehydrocoupling mediated by this species was essentially the same as when the Cp_2TiCl_2 and ^nBuLi combination was used.

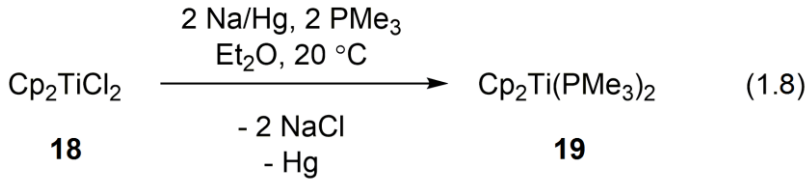

(1.8)

As part of their investigations, the authors also attempted to ascertain whether the active species was homogeneous or heterogeneous in nature, as will be discussed later. From this work, the authors inferred a two-step cycle (Scheme 1.2) that involves the initial generation of the linear dimer, $Me_2NH\text{-}BH_2\text{-}NMe_2\text{-}BH_3$, which is then dehydrogenated in an on-metal process described as follows: phosphine dissociation from $Cp_2Ti(PMe_3)_2$ (**19**) yields transient [Cp_2Ti], and then one equivalent of $Me_2NH{\bullet}BH_3$ oxidatively adds to the Ti centre, to form $Cp_2Ti(H)NMe_2BH(\mu\text{-}H)_2$ (**I**) with two of the hydridic hydrogen substituents on B forming agostic interactions with the Ti centre. This interaction is similar to the one described by Roesler and coworkers who prepared $Cp_2Zr(H)NH_2BH_2(\mu\text{-}H)$, the first crystallographically characterised species that featured a formal agostic interaction between an aminoborane moiety and Zr.[30]

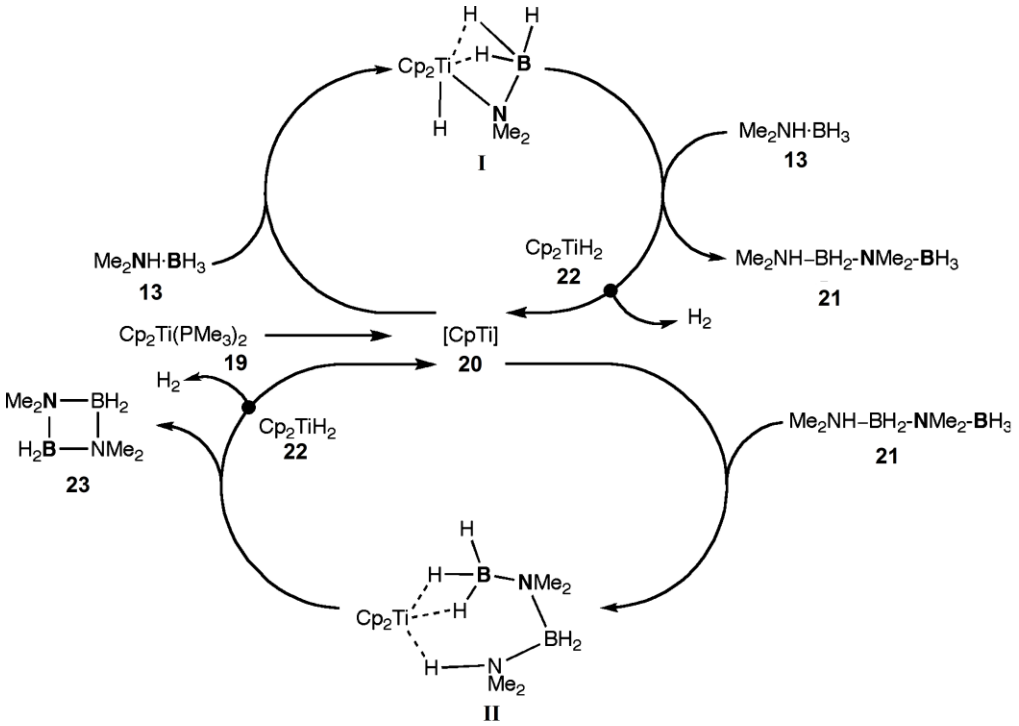

Scheme 1.2 Proposed mechanism for dehydrocoupling of $Me_2NH•BH_3$ by $[Cp_2Ti]$. Adapted with permission from Manners and coworkers, *J. Am. Chem. Soc.*, **2010**, *132*, 3831. Copyright 2010 American Chemical Society.

Following the generation of (**I**), metathesis between this species and one further equivalent of $Me_2NH•BH_3$ yields the linear dimer $Me_2NH\text{-}BH_2\text{-}NMe_2\text{-}BH_3$, in addition to Cp_2TiH_2 (**22**), which the authors then propose reductively eliminates H_2 to regenerate $[Cp_2Ti]$. The authors postulate that the next process involves the interaction of $Me_2NH\text{-}BH_2\text{-}NMe_2\text{-}BH_3$ with $[Cp_2Ti]$, which then removes a proton and a hydride from the terminal nitrogen and boron atom respectively of the B_2N_2 chain to facilitate a ring-closure with formation of a new B-N bond (yielding the cyclic dimer $[Me_2NBH_2]_2$). Once again the Cp_2TiH_2 generated is proposed to reductively eliminate H_2, and reform the active catalyst $[Cp_2Ti]$.

In addition, the Manners group probed whether the active catalyst in Scheme 1.2 was homogeneous or heterogeneous in nature; it is expected that a heterogeneous catalyst formed from a soluble precursor would first undergo an induction period with zero catalytic activity, followed by discernible activity once the heterogeneous catalyst is formed. In the case of a homogeneous catalyst, there would be a minimal induction period, with catalytic activity commencing almost immediately upon the addition of the catalyst to the reaction mixture. Comparison of the consumption of $Me_2NH{\bullet}BH_3$ versus time in the presence of three catalysts "Cp_2Ti" generated *in situ* from a mixture of Cp_2TiCl_2 and $^{n}BuLi$, $Cp_2Ti(PMe_3)_2$, and $[Rh(COD)Cl]_2$ (COD = 1,5-cyclooctadiene) was made (Figure 1.5). Interestingly, both Ti catalysts displayed similar reactivity and instant activity, while an induction period was noted for the Rh catalyst. This suggests that both of the Ti catalysts act in a similar, homogeneous fashion, whereas $[Rh(COD)Cl]_2$ yields colloidal Rh (Figure 1.5). Additional studies by Autrey and coworkers suggest that there may also be present catalytically active, soluble Rh_6 clusters.[31] Furthermore the addition of Hg, which will poison many heterogeneous catalysts, did not decrease the catalytic activity of both of the Ti catalysts, while Hg caused an immediate cease in activity for the Rh-based catalyst system.[28]

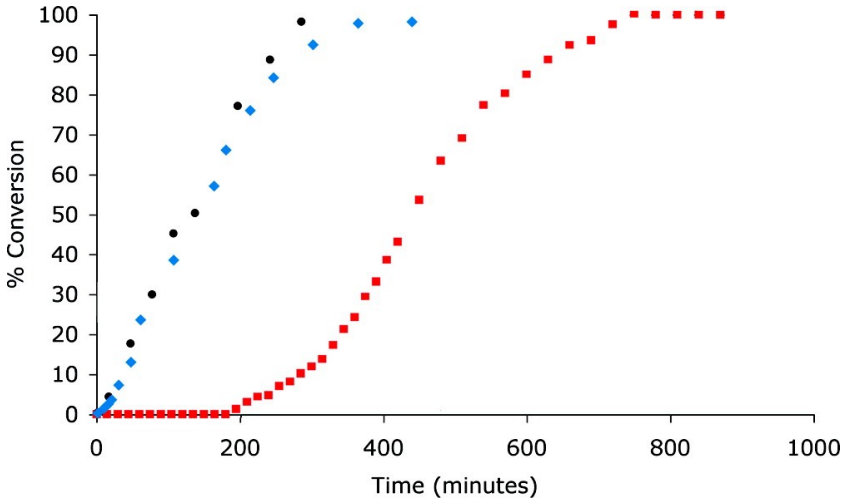

Figure 1.5 Consumption of $Me_2NH{\bullet}BH_3$ versus time in toluene with 2 mol% catalyst loadings for $[Cp_2Ti]$ (circles), $Cp_2Ti(PMe_3)_2$ (diamonds) and $[RhCl(COD)]_2$ (squares). Adapted with permission from Manners and coworkers, *J. Am. Chem. Soc.*, **2010**, *132*, 3831. Copyright 2010 American Chemical Society.

The mechanism of amine-borane dehydrocoupling in the presence of $[Cp_2Ti]$ was investigated computationally by Luo and Ohno,[32] who found two viable routes for this process, with one being intramolecular in nature (Scheme 1.3), and the other being intermolecular. Unlike the pathway proposed by Manners and coworkers which features a formal oxidative addition process at Ti, the intramolecular pathway involves a two-step transfer hydrogenation facilitated by the titanium centre which first deprotonates the nitrogen of $Me_2NH{\bullet}BH_3$, before abstracting a hydride from the adjacent boron centre (Scheme 1.3). This pathway is characterised by a transient interaction between the Ti and N, unlike the formal oxidative addition proposed by Manners, and this generates the aminoborane $Me_2N{=}BH_2$, which can then undergo a spontaneous dimerization to form the cyclic dimer $[Me_2NBH_2]_2$. The authors

report that all attempts to find a concerted rather than a step-wise mechanism for the dehydrogenation of $Me_2NH•BH_3$ were unsuccessful.

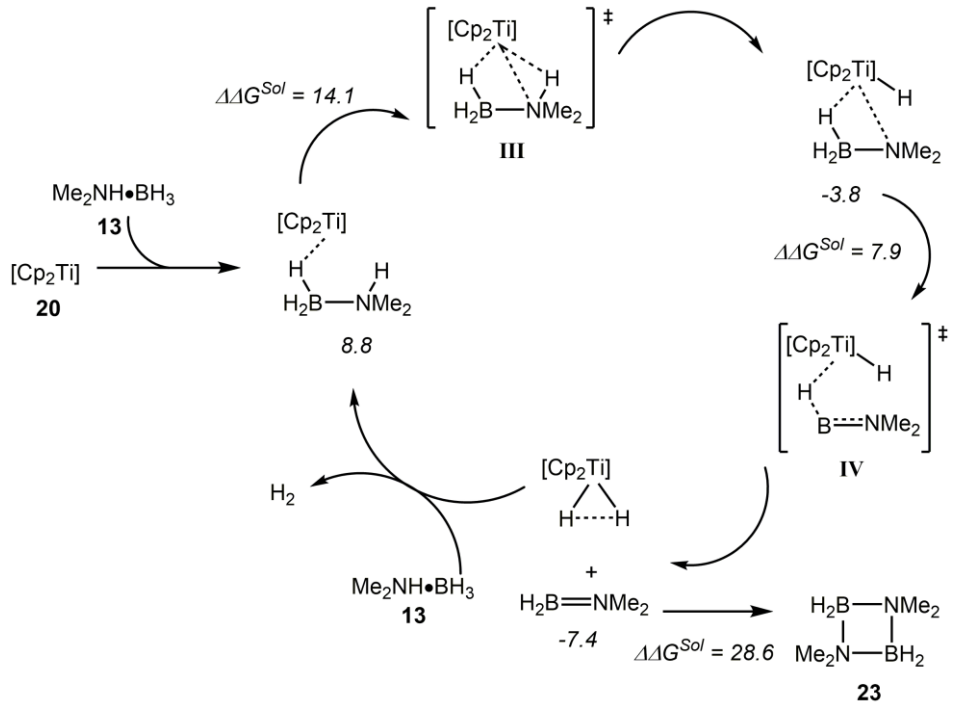

Scheme 1.3 Computed mechanism for the intramolecular dehydrocoupling of $Me_2NH•BH_3$ mediated by $[Cp_2Ti]$. The solvation free energies ($\Delta\Delta G^{sol}$, kcal/mol) are relative to unreacted $Me_2NH•BH_3$ and $[Cp_2Ti]$. Adapted with permission from Ohno and coworkers, *Organometallics*, **2007**, *26*, 3597. Copyright 2007 American Chemical Society.

The authors also investigated a second, intermolecular route, as this type of pathway have been suggested previously for the Rh catalysed dehydrocoupling of $Me_2NH•BH_3$.[14] This intermolecular pathway involves the interaction of two equivalents of $Me_2NH•BH_3$ with the $[Cp_2Ti]$ centre, and stepwise proton and hydride abstraction, with formation of one new B-N bond occurring while both substrates are attached to the metal centre; this is then followed by the elimination of one equivalent of the linear dimer Me_2NH-BH_2-NMe_2-BH_3. However they found that the rate determining step (RDS) for

the intermolecular route was less kinetically favourable (35.8 kcal/mol) in relation to the RDS for the intramolecular route listed in Scheme 1.3 (computed to be 22.9 kcal/mol).

More recently, Manners and coworkers explored the use of Ti(III) and Zr(III) species as pre-catalysts for the dehydrocoupling of amine-boranes.[33] The authors were able to identify one Ti(III) species [Cp_2Ti-$NMe_2BH_2(\mu$-H)] that catalysed the dehydrocoupling of amine-boranes with a reasonable turnover frequency [TOF = 10.6 hr^{-1}, 97 % conversion] in toluene at 20 °C with a 2 mol % catalyst loading; this value is comparable to the performance of "Cp_2Ti" (*cf.* TOF = 11.1 hr^{-1}, 88 % conversion). Furthermore, electron paramagnetic resonance (EPR) spectroscopy revealed identical spectra for a sample of pure [Cp_2Ti-$NMe_2BH_2(\mu$-H)] and that of the reaction mixture using *in situ* generated "Cp_2Ti" as a catalyst, which would infer that the same Ti(III) species is an active catalyst in these dehydrocoupling processes.

In a complementary study by Wass and coworkers, a cationic zirconocene complex [$Cp_2ZrOC_6H_4P^tBu_2$][$B(C_6F_5)_4$] was developed for the catalytic dehydrocoupling of $Me_2NH{\bullet}BH_3$.[34] This zirconium complex featured a cationic zirconocene centre bearing an ortho-phosphinoaryloxide ligand, with the tetrakis(pentafluorophenyl)borate unit as a counteranion. In this case, the hemilabile pendent phosphine was able to stabilise the cationic centre, and also played a role in the dehydrocoupling which was postulated to follow a frustrated Lewis pair (FLP)-type mechanism (as shown in Scheme 1.4). The authors also prepared an analogous species featuring an unsubstituted –OPh

ligand in place of the $-OC_6H_4P(^tBu)_2$ group, and found that there was no observed activity, adding support for the FLP-assisted dehydrogenation of an amine-borane (Scheme 1.4). In addition, the proposed reaction intermediate $[Cp_2Zr(H)OC_6H_4P(H)(^tBu)_2][B(C_6F_5)_4]$ was independently synthesised via the direct reaction of $[Cp_2ZrOC_6H_4P(^tBu)_2][B(C_6F_5)_4]$ with one equivalent of H_2, and this species proved to be equally as efficacious as the initial active catalyst $[Cp_2ZrOC_6H_4P(^tBu)_2][B(C_6F_5)_4]$ towards the dehydrocoupling of $Me_2NH{\bullet}BH_3$. Interestingly, the activity of this catalyst, TOF = 600 hr^{-1}, is far superior to that of any other zirconocene system reported.[12] Despite the high activity of the aforementioned FLP-mediated system, it should be mentioned that zirconium systems that do not employ FLP-assisted dehydrogenation are typically are less active than analogous titanium catalysts. A 2007 study by Chirik and coworkers investigated the ability of a variety of group 4 metallocene complexes to affect the catalytic dehydrocoupling of $Me_2NH{\bullet}BH_3$ (Figure 1.6).[35]

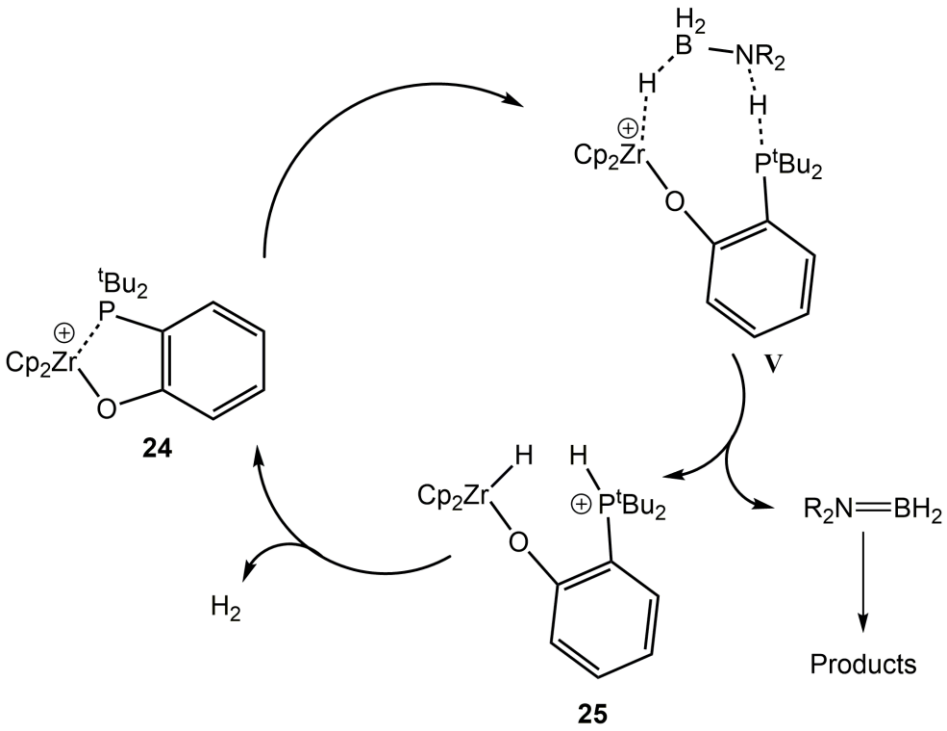

Scheme 1.4 Proposed catalytic cycle for the dehydrocoupling of Me_2NHBH_3 catalysed by $[Cp_2ZrOC_6H_4P(^tBu)_2][B(C_6F_5)_4]$. Adapted with permission from Wass and coworkers, *J. Am. Chem. Soc.*, **2011**, *133*, 8826. Copyright 2011 American Chemical Society.

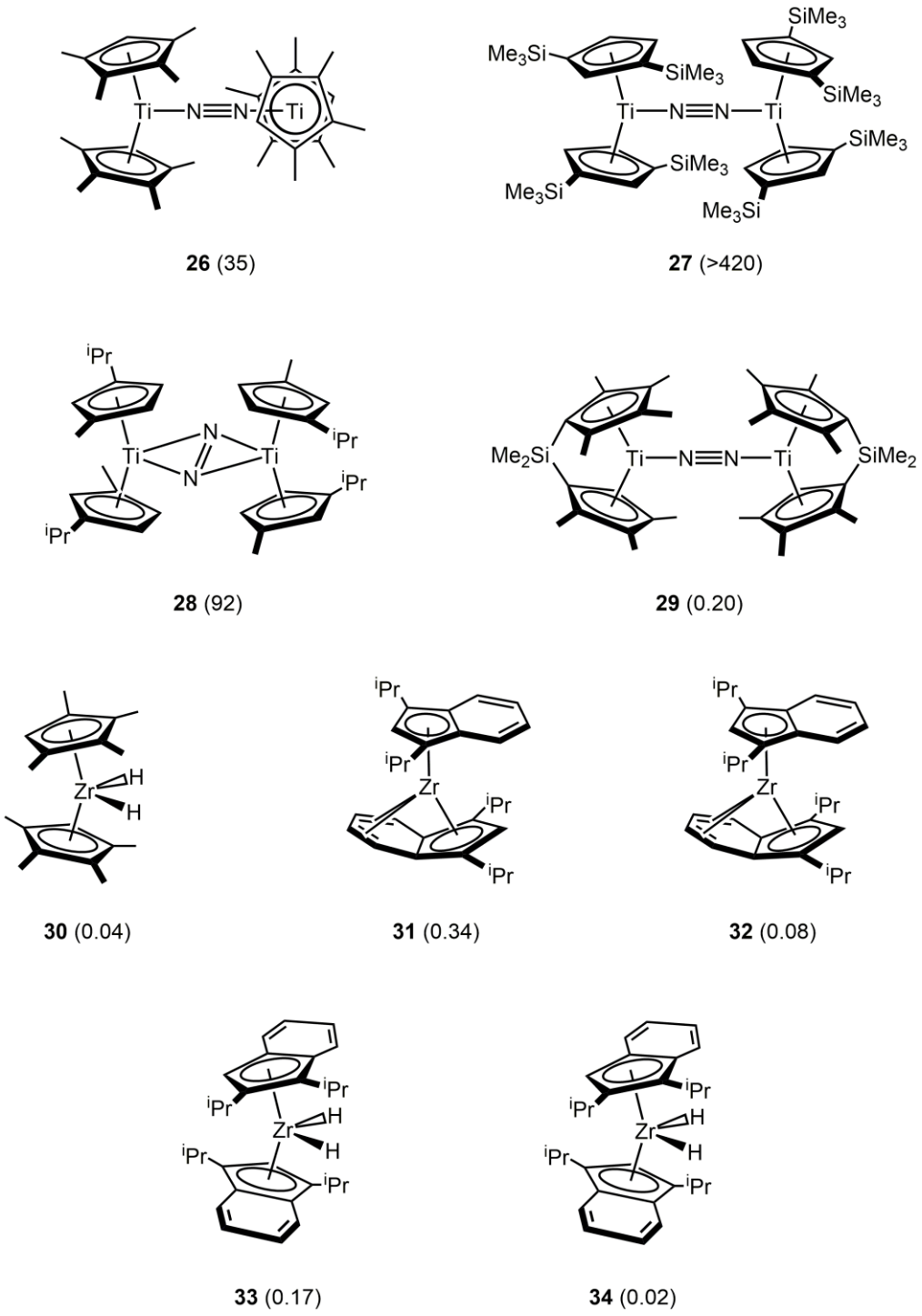

Figure 1.6 Ti and Zr complexes investigated for efficiency towards the catalytic dehydrocoupling of $Me_2NH{\bullet}BH_3$. All reactions were performed at 2 mol% catalyst loading in C_6D_6, with turnover frequencies (TOF, hr^{-1}) given below each compound in parentheses. All reactions containing Ti catalysts were carried out at 23 °C with all Zr reactions carried out at 65 °C. Adapted from: D. Pun, E. Lobkovsky, P. J. Chirik, *Chem. Commun.*, **2007**, 3297. Reproduced by permission from The Royal Society of Chemistry.

In this work, it was found that the titanium complexes performed significantly better than the zirconium complexes, and also functioned at lower temperature than their Zr analogues. Chirik and coworkers also noted that in instances where the cyclopentadienyl ring was substituted with -$SiMe_3$ groups, the activities were increased relative to the analogous complexes featuring the organic groups Me and ^{i}Pr.[34]

From the aforementioned work, I decided to investigate the synthesis and dehydrocoupling chemistry of zirconium complexes bearing bis(amido)silyl ligands such as $[(DippN)_2Si^{i}Pr_2]^{2-}$ ($[NSiN^{Dipp}]$). These dianionic ligands benefit from facile synthesis, with the potential for modification to allow for a similar steric environment at the metal centre as in Cp_2MX_2 systems. Furthermore, these ligands would be formally $4e^-$ donors, versus the $12e^-$ donation of two Cp ligands, resulting in more electropositive and potentially more Lewis-acidic metal centres. The original hypothesis was that the generation of such systems would allow for significantly higher turnover frequencies relative to the relatively modest TOF observed for the previously known neutral, non-FLP assisted metallocene complexes. As the rate determining step for amine-borane dehydrogenation by $[Cp_2Ti]$ was shown to be the addition of the substrate to the metal centre, we suggest that a more electrophilic metal centre would facilitate this initial interaction, thereby increasing the relative rate of catalysis.

1.4 Recent developments in zinc coordination chemistry and applications

1.4.1 Introduction to zinc chemistry

The chemistry of zinc, a first-row transition element located in group 12, is diverse. Zinc is an important element in biochemistry and has been identified as an essential micronutrient for both humans and plants.[36] Zinc is also the central metal ion in many metalloenzymes such as alcohol dehydrogenase.[37] In addition, many zinc compounds are found in commercial products, such as zinc(II) chloride in deodorants and zinc(II) sulfide in paints and dyes. Zinc has three available oxidation states: Zn(0) for the metallic element, Zn(II) as the most commonly encountered oxidation state within coordination complexes, and a few recently prepared compounds contain stable Zn(I) states accompanied by Zn-Zn bonds. Furthermore, many zinc species have been shown to be of great use for a variety of stoichiometric and catalytic transformations, as will be discussed in Sections 1.4.2 and 1.4.3.

1.4.2 The chemistry of Zn(I) complexes

For many years, the chemistry of zinc was focused mainly on Zn(II) species or zinc metal itself. This changed in 2004 when Carmona and coworkers reported the synthesis of decamethyldizincocene Cp*Zn-ZnCp* (**37**), the first example of a stable compound with formal Zn(I) centres.[38] Cp*Zn-ZnCp* (**37**) was prepared from the reaction between diethylzinc and bis(pentamethylcyclopentadienyl)zinc (Cp^*_2Zn) (**36**) wherein the elimination of butane and the insertion of the remaining Zn atom into a Zn-Cp* bond

(Equation 1.9) transpires to yield a Zn(I) dimer, caused by the overlap of the singly-filled 4s orbital on each Zn centre to yield the central Zn-Zn bond.[37] This reaction may be facilitated by the somewhat unusual solid-state structure of Cp^*_2Zn (**36**), which is shown to have one η^5-bound Cp* moiety, while the other Cp* unit is ligated via a single carbon atom in an η^1-fashion; it should be noted however that in solution only one peak is observed by ^1H NMR spectroscopy, and only two peaks by $^{13}C\{^1H\}$ NMR spectroscopy, suggesting that the ring slippage is occurring faster than the NMR timescale.[39]

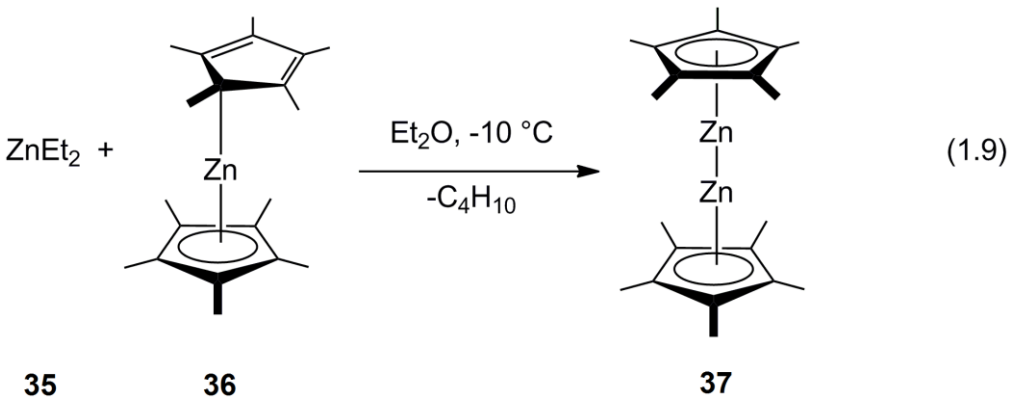

35 **36** **37** (1.9)

Since this initial discovery, there have been additional reports of Zn(I) complexes featuring a variety of sterically encumbered ligands. Shortly after the report by Carmona, Robinson and coworkers reported the synthesis and computational analysis of a Zn(I) dimer bearing a Nacnac ligands (Nacnac)Zn-Zn(Nacnac) (**39**) (Nacnac = $[HC(CMeNDipp)_2]$; Dipp = 2,6-$^iPr_2C_6H_3$).[40] This species was prepared in a two-step procedure where the ligand was first installed at zinc by comibining *in situ* generated Li[Nacnac] with ZnI_2; the resultant species $[(Nacnac)Zn(\mu\text{-}I)_2Li(OEt_2)_2]$ was then stirred with finely cut

potassium in toluene for two days to yield the desired Zn(I) species (**39**) (Equation 1.10). The X-ray crystallographic structure of **39** revealed that the two Nacnac ligands were nearly orthogonal with respect to each other, with a N-Zn-Zn-N torsion angle of 86.6°. Computational analysis at the BY3LP/DZP^{++} and BZ86/DZP^{++} levels revealed that this D_{2d} conformation was slightly favoured [by 0.26 kcal/mol (B3LYP) and 0.37 kcal/mol (BZ86)] relative to the D_{2h} conformation where the ligands would lie in the same plane.

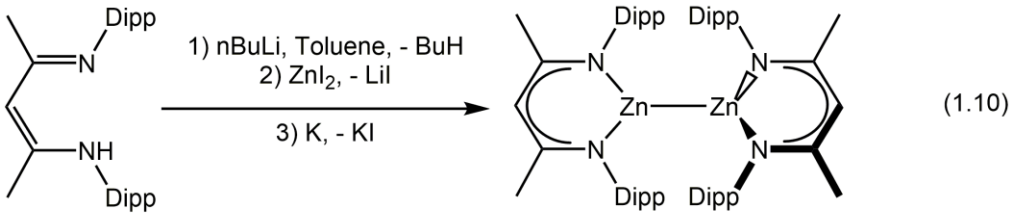

(1.10)

38 **39**

Soon after, the group of Philip Power reported a terphenyl-substituted Zn(I) species, again featuring a central Zn-Zn bond, Ar′Zn-ZnAr′ (**41)** (Ar′ = 2,6-(C_6H_3-2,6-$^{i}Pr_2$)$_2C_6H_3$).[41a] This compound was accessible by reduction of the dimeric Zn(II) iodide [Ar′Zn(μ-I)]$_2$ (**40**) with sodium metal (Scheme 1.5). In order to rule out the formation of a Zn(II) hydride, the corresponding species [Ar′Zn(μ-H)]$_2$ (**42**) was independently prepared by reacting **40** with two equivalents of NaH. This was done as a similar Zn···Zn distance was predicted and later observed in **42** [2.4084(3) Å] as for the direct Zn-Zn bond in **41** [2.3591(9) Å]. It was also shown that the product Ar′Zn-ZnAr′ (**41**) had different physical and spectroscopic characteristics from those of [Ar′Zn(μ-H)]$_2$ (**42**). Curiously, the addition of one further equivalent of NaH to [Ar′Zn(μ-H)]$_2$ (**42**) results in the formal reduction of the Zn(II) centre, and

generation of a new species (**43**; Scheme 1.5) featuring a Zn-Zn interation, and an anionic hydride ligand bridging symmetrically between the two Zn(I) centres to create a planar, $4e^-$ anti-aromatic ring.[40b] In addition to this bridging hydride (which was identified in the ^1H NMR spectrum in C_6D_6 as a broad peak at +2.04 ppm), there is also a sodium atom that forms not only a weak interaction with the two Zn(I) centres, but is further coordinated by flanking η^6-interactions with two adjacent substituted phenyl rings.

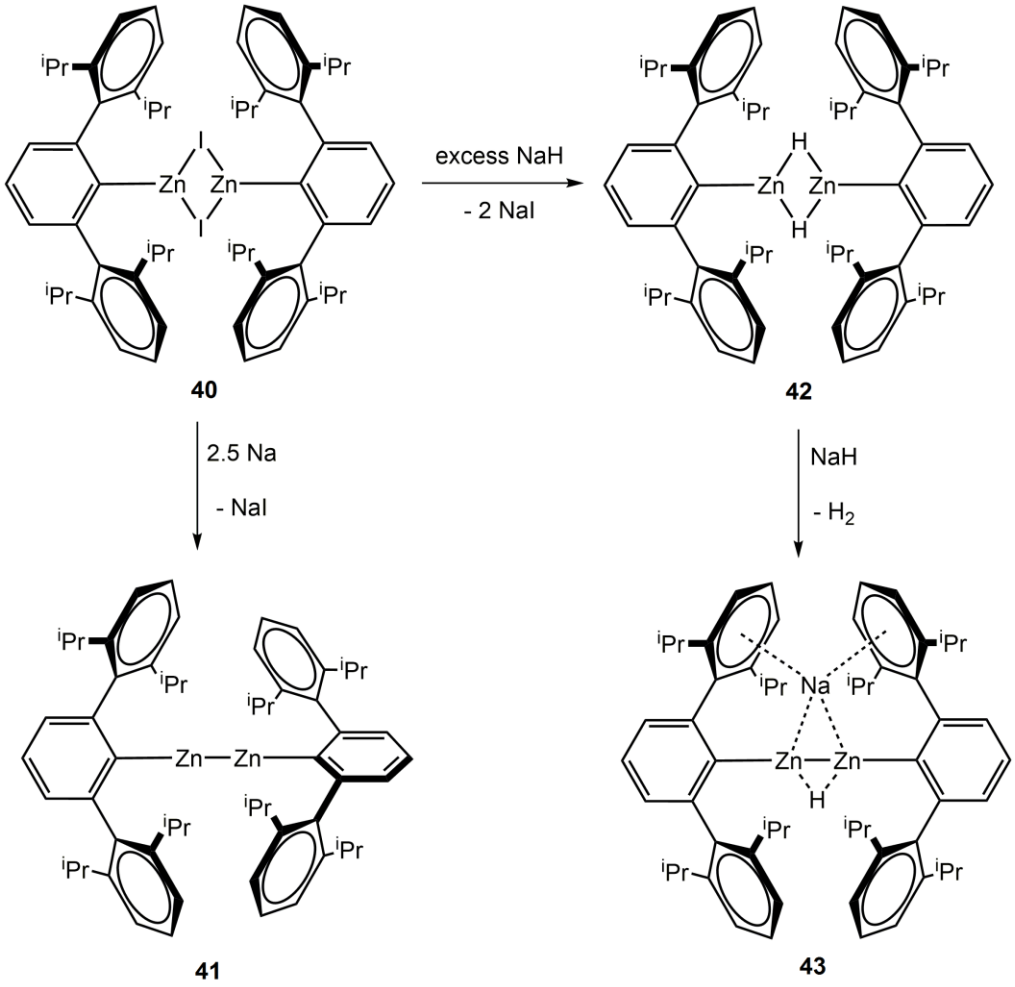

Scheme 1.5 Synthesis of the zinc(I) dimer Ar′Zn-ZnAr′ (**41**), the related zinc(II) hydride $[Ar'Zn(\mu\text{-}H)]_2$ (**42**), and zinc(I) complex Ar′Zn(μ-H)(μ-Na)ZnAr′ (**43**).

In 2012 Andreas Stasch reported an analogous Zn(I) species featuring a Zn-Zn bond stabilised by sterically demanding bis(imino)phosphinate $[(DippN)_2PPh_2]^-$ ligands (Equation 1.11);[42] attempts to form a related Zn(I) dimer bearing the bidentate guanidinate ligand $[(DippN)_2CNCy_2]^-$ was unsuccessful.[43]

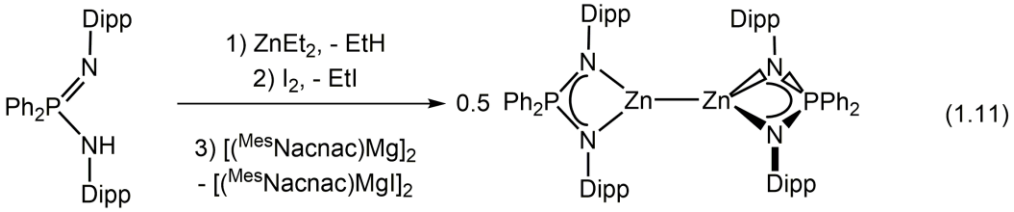

44 **45** (1.11)

Very recently, Fischer and coworkers described the synthesis of a solvated dizinc congener of the calomel dication, $[Hg_2]^{2+}$ (Equation 1.12).[44]

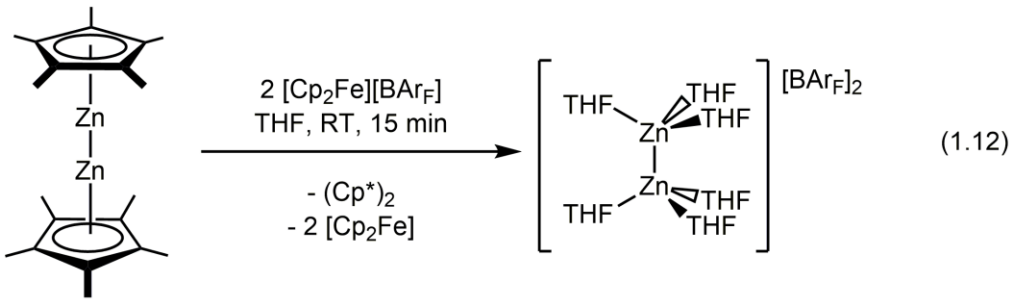

$[BAr_F] = [B\{C_6H_3\text{-}3,5\text{-}(CF_3)_2\}_4]^{\ominus}$

37 **46** (1.12)

This particular species, $[Zn_2(THF)_6][BAr_F]_2$ (**46**), was shown to be a versatile reagent for the synthesis of new Zn(I) and Zn(II) species. For example, the addition of two equivalents of the potassium salts KCp^* or K[Nacnac] led to the formation of the previously described $[Cp^*Zn]_2$ (**37**) and $[(Nacnac)Zn]_2$ (**39**) dimers, respectively. Furthermore, the addition of 6 equivalents of phenylisonitrile, PhNC, afforded the structurally related salt

$[Zn_2(CNPh)_6][BAr_F]_2$ (**47**) (Scheme 1.6). The use of the strong σ-donor PMe_3 however led to the cleavage of the Zn-Zn bond, and the isolation of the Zn(II) species $[Zn(PMe_3)_4][BAr_F]_2$ (**48**) and Zn metal via a disproportionation reaction (Scheme 1.6). The authors also reported that the solvated dication $[Zn_2(THF)_6][BAr_F]_2$ (**46**) does not react with CO, even when a solution of this species is sparged with CO for over 90 minutes. Nevertheless, this report introduces a useful potential synthon in the realm of Zn(I) chemistry. It should be noted that the isolation of a neutral Zn(I) hydride moiety is conspicuously absent from the literature, as is the utilization of many of these aforementioned Zn(I) compounds in catalysis, an area which is well established for Zn(II) complexes.

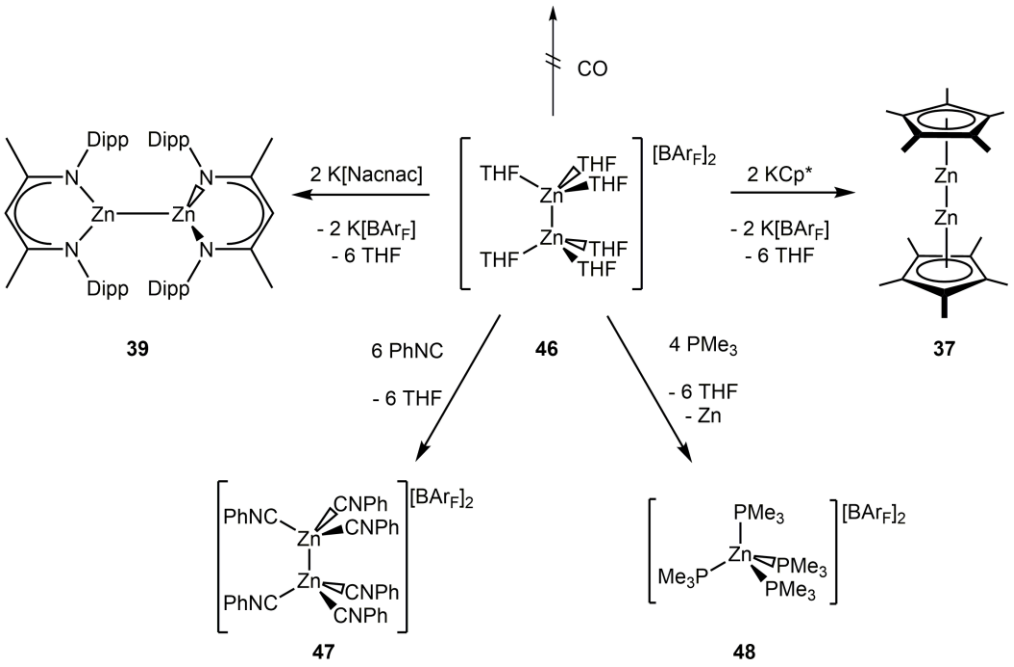

Scheme 1.6 Reactivity of $[(THF)_6Zn_2][B(Ar_F)_4]_2$ (**46**). Adapted from: H. Banh, C. Gemel, R. W. Seidel, R. A. Fischer, *Chem. Commun.*, **2015**, *51*, 2170. Reproduced by permission from The Royal Society of Chemistry.

1.4.3 The chemistry of Zn(II) complexes

The +2 oxidation state is very much dominant within the realm of zinc chemistry. There are a variety of known compounds between Zn and the p-block elements such as the zinc pnictides (Zn_3N_2, Zn_3P_2 and Zn_3As_2), zinc chalcogenides (ZnO, ZnS, ZnSe and ZnTe), and zinc halides (ZnF_2, $ZnCl_2$, $ZnBr_2$ and ZnI_2). ZnO is particularly interesting due to its amphoteric nature, and is being explored for optoelectronic applications as an n-type semiconductor, with a band-gap (3.3 eV) that is comparable to that of TiO_2 (*cf.* band-gap of TiO_2 = 3.2-3.35 eV). In addition, ZnS is of interest as a wide band-gap semiconductor [cf. band-gap 3.54 eV (cubic) and 3.91 eV (hexagonal)]; in addition, ZnS is utilised commercially in many "glow-in-the-dark" products. Beyond the realm of binary zinc compounds lies a rich chemistry of coordination compounds bound by a myriad of main group element containing ligands.[45] As many such compounds have been discussed previously,[44] I will not provide a detailed overview in this thesis, but rather focus on hydrosilylation catalysis mediated by Zn(II) complexes, in addition to the chemical reactivity of Zn(II) hydride complexes.

1.4.3.1 Zn(II) complexes for hydrosilylation

Hydrosilylation, the addition of a Si-H bond across an unsaturated substrate, provides us with the ability to functionalise organic species such as ketones, esters, amides and alkenes. In the case of compounds containing carbonyl group, this results in production of a new Si-O siloxy linkage with concomitant C-H bond formation. In the case of alkenes and alkynes the

hydrosilylation can proceed with either *Markovnikov* or *anti-Markovnikov* selectivity as shown in Scheme 1.7.

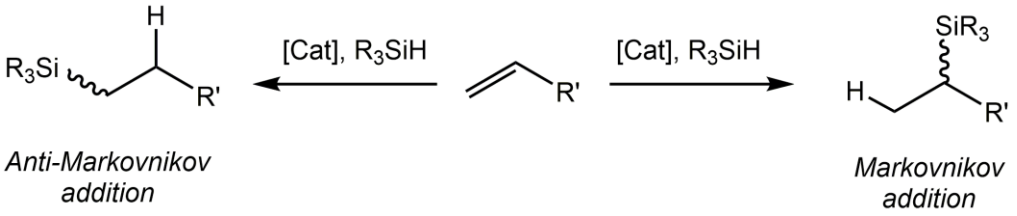

Scheme 1.7 Selectivity dictated by Markovnikov or anti-Markovnikov addition of silane, R_3SiH to terminal alkene (R, R′ = alkyl, aryl, heteroalkyl, heteroaryl group; [Cat] = catalyst).

In hydrosilylation (and hydroboration), the polarity of the E-H bond (E = Si or B) lies towards the hydrogen atom, and therefore the hydride will typically add to the more substituted carbon atom, thus making anti-Markovnikov addition more favourable.

Industrially, hydrosilylation is used to produce a variety of consumer products which can be used as surfactants, or as additives to cosmetic products.[46] Typically, these products are synthesised using platinum catalysts such as Karstedt's or Speier's catalysts ($Pt_2\{[H_2C{=}CHSiMe_2]_2O\}_3$ and $K_2PtCl_6{\bullet}6H_2O$, respectively); these processes have been previously reviewed and will not be further discussed in this thesis.[47] It should however be pointed out that due to the large amount of platinum used industrially for hydrosilylation catalysis [*ca.* 5.6 metric tonnes in 2007],[45] that there has been significant interest in the utilisation of more earth-abundant, low cost metal options as catalysts.

In 2012, Beller and coworkers reported the reduction of tertiary amides catalysed by $Zn(OAc)_2$ in the presence of a small excess (3 equivalents) of $(EtO)_3SiH$.[48] An initial test run was performed on N,N-dimethylbenzamide $PhC(O)NMe_2$ at a 10 mol% Zn loading, and resulted in a 97 % conversion of the substrate to the corresponding amine $PhCH_2NMe_2$ at 20 °C (Scheme 1.8).

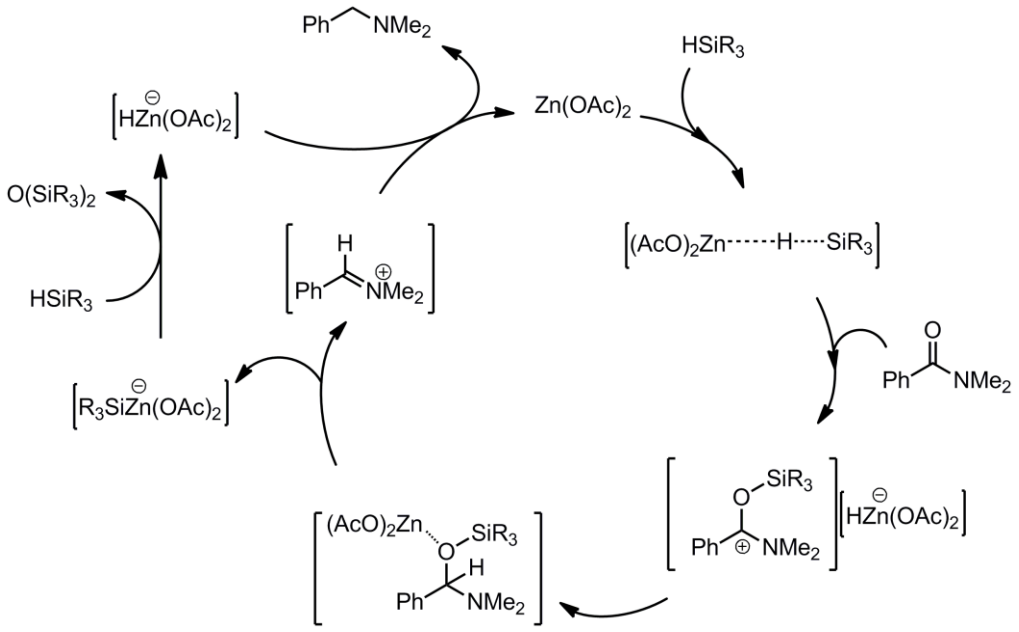

Scheme 1.8 Proposed catalytic cycle for the hydrosilation of amides catalyzed by $Zn(OAc)_2$. Adapted with permission from Beller and coworkers, *J. Am. Chem. Soc.*, **2012**, *132*, 1770. Copyright 2012 American Chemical Society.

To rule out the likelihood of other contaminants playing a role in the catalysis, $Zn(OAc)_2$ was sourced from multiple vendors, and in each case comparable results were obtained. Also of note is that the other ZnX_2 salts (X = F, Cl, Br, OTf) leads to negligible conversions at best, while Cu and Fe-based acetate salts were completely inactive at promoting hydrosilylation; the reasons for the specificity of Zn and –OAc were not discussed however. The authors also reported that while using other silanes such as $PhSiH_3$, Ph_2SiH_2, and

$(EtO)_2MeSiH$ do not result in significant activity at room temperature, raising the temperature to 65 °C led to >90 % conversion to the corresponding amine, with over 20 examples of different amide substrates explored. The mechanism proposed by the authors implies that the $Zn(OAc)_2$ first abstracts H^- from the silane to generate a transient cationic silylium species, $[SiR_3]^+$. This in turn adds to the carbonyl moiety, with concerted addition of the hydride to the carbon adjacent to the newly generated siloxy group. The regenerated $Zn(OAc)_2$ can then activate the siloxy group, leading to C-O bond cleavage and generation of anionic zinc silanoate $[R_3SiOZn(OAc)_2]^-$ along with an iminium cation; this is similar to that observed by the group of Piers in their investigations into FLP-mediated hydrosilation.[49] The anionic zinc silanoate then undergoes metathesis to form an anionic zinc hydride $[HZn(OAc)_2]^-$ which can then add the hydride to the iminium salt with generation of the desired amine, and reformation of the $Zn(OAc)_2$ (Scheme 1.8).

In 2010 the groups of Enthaler and Driess reported a highly active catalyst for the achiral hydrosilylation of ketones, with complete conversion of the ketones explored to their corresponding alcohols following acidic work up (Equation 1.13).[50] The Zn-based catalyst (**49**) contained a dianionic O-S-O pincer ligand and gave TOF values of up to 970 hr^{-1} for simple substrates such as acetone. In this particular system there was no observed enantioselectivity when a variety of asymmetrically substituted aromatic and aliphatic ketones were tested as substrates. The authors propose that the silane $(EtO)_3SiH$ is first activated by coordination of silicon to a Zn-bound oxygen atom and is held in

such a position so that when the incoming ketone binds to Zn, displacement of one arm of the TMEDA ligand transpires (Scheme 1.9). The silicon-bound hydride can then add to the electrophilic carbon of the carbonyl, leading to alkoxide, $[R^1R^2C(H)O]^-$ formation. This is subsequently followed by loss of $R^1R^2C(H)OSi(OEt)_3$ via a metathesis pathway to regenerate the catalyst (Scheme 1.9).

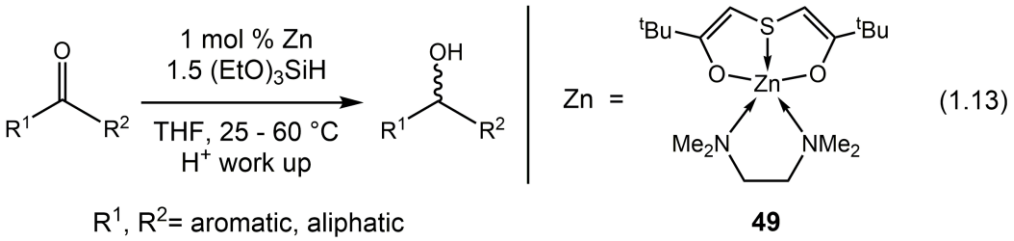

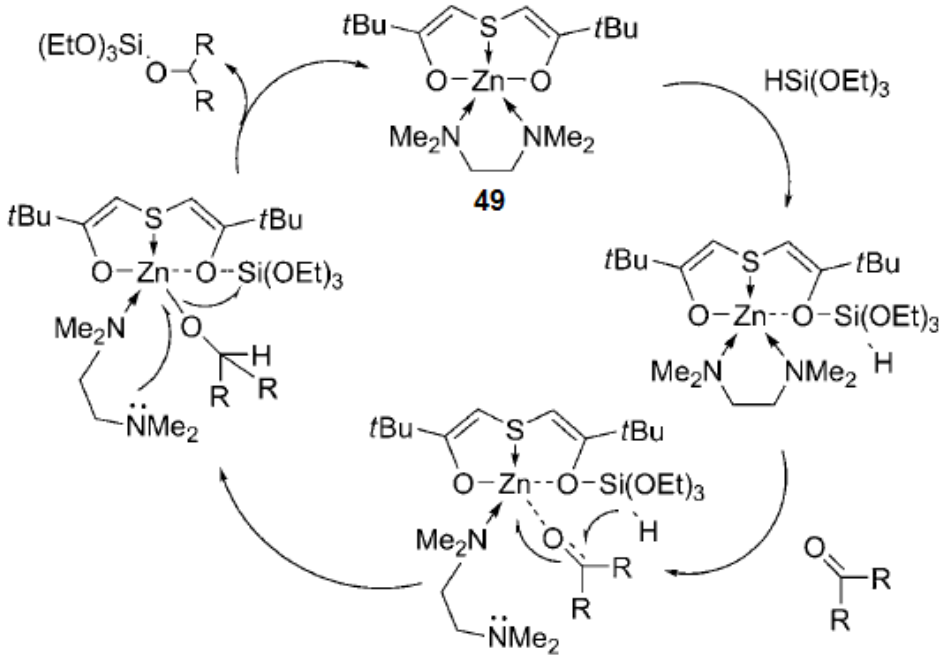

Scheme 1.9 Proposed catalytic cycle for hydrosilation of ketones mediated by compound **49**. Reprinted with permission from Enthaler and coworkers, *ChemCatChem*, **2010**, *2*, 846. Copyright 2010 WileyVCH.

Another example of a zinc-based catalyst for the hydrosilylation and methanolysis of silanes was presented by Parkin and coworkers in 2012.[51] The precatalyst (**50**) featured a tripodal tris(2-pyridylthio)methyl [Tptm] ligand, which when bound to Zn could either be in a κ^3 or κ^4 binding mode, depending on how electron withdrawing the other substituent on Zn was (Equation 1.14). For example, the hydride complex [κ^3-Tptm]ZnH could be converted to [κ^4-Tptm]ZnOSiMe$_3$ following addition of Me_3SiOH. Both of the species described in Equation 1.14 (Compounds **50** and **51**)were shown to be excellent catalysts for the hydrosilylation of acetone, acetaldehyde and CO_2 at low catalyst loadings of 0.1 mol % with good turnover numbers (>10^3) and respectable turnover frequency (up to 4.2 hr^{-1}).

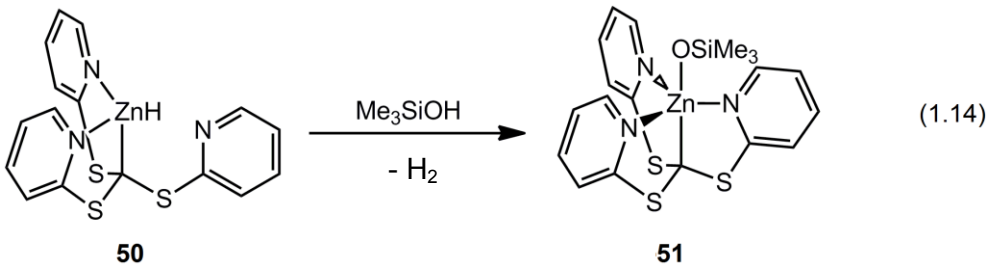

50 **51** (1.14)

A common theme in many of the listed catalytic processes is the presence of either well-defined Zn-H species or the possible formation of zinc hydrides as intermediates. As a result, it was decided that zinc hydride complexes, particularly Lewis base adducts of neutral ZnH_2 would be explored as potential pre-catalysts for the hydrosilation of ketones, aldehydes and alkenes in this thesis.

1.4.3.2 Introduction to zinc hydride chemistry

The simplest zinc hydride species, ZnH_2, was initially prepared by Schlesinger and coworkers in 1947, and was obtained from the reaction between dimethylzinc and lithium borohydride (Equation 1.15).[52] Zinc dihydride is a thermally sensitive solid that will decompose into zinc metal and hydrogen over the course of a few hours when stored at room temperature. In addition, ZnH_2 is essentially insoluble in almost all solvents, and will react vigorously with water (as is the case with many metal hydrides).

$$Li[AlH_4] + ZnMe_2 \xrightarrow{Et_2O} ZnH_2 + Li[Me_2AlH_2] \qquad (1.15)$$

Undaunted by the challenges associated with handling ZnH_2, researchers have been able to isolate various zinc hydride complexes by replacing one H^- group with anionic co-ligands (Figure 1.7).

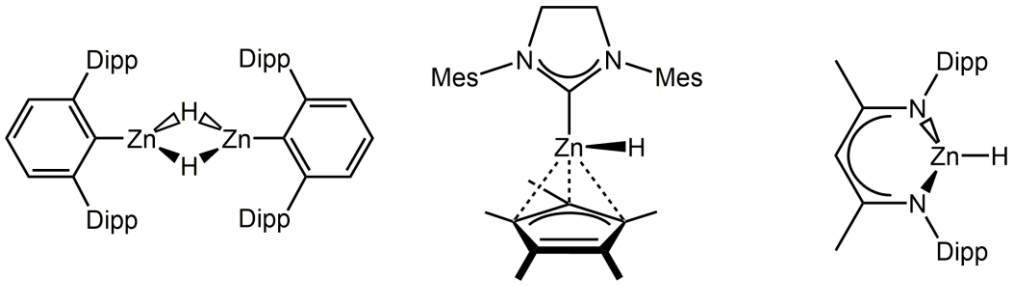

42 **52** **53**

Figure 1.7 A selection of zinc hydride complexes previously reported in the literature; Mes = 2,4,6-$Me_3C_6H_2$.

One previously mentioned example of a stable and soluble zinc(II) hydride, $[Ar'Zn(\mu\text{-}H)]_2$ (**42**), features sterically demanding terphenyl ligands.[32a] More

recently, Stephan and Jochmann formed the *N*-heterocyclic carbene bound zinc hydride SIMes•ZnH(η^3-Cp*), (**52**), [SIMes = $(H_2CNMes)_2C$:; Mes = 2,4,6-$Me_3C_6H_2$] from the reaction between $ZnCp^*_2$ and SIMes in the presence of hydrogen gas.[53] Furthermore, the authors describe the use of this species as an effective catalyst for the hydrogenation of a wide variety of aromatic and aliphatic imines.

A final example of an RZnH complex (to be mentioned here) was prepared by the group of Harder, and contains a three coordinate zinc centre with a terminally positioned hydride (**53**, Figure 1.7) that is kinetically stabilised from dimerization due to the presence of large flanking diisopropylphenyl (Dipp) groups on the attached Nacnac ligand.[54] This species, [(Nacnac)ZnH] (**53**), could be prepared from the chloro congener [(Nacnac)ZnCl] (**54**) via either treatment with one half equivalent of CaH_2 (Equation 1.16), or by treatment with $K[^iPr_2N•BH_3]$, which would yield the desired hydrido species along with elimination of KCl and $^iPr_2N{=}BH_2$. Work from the same group using the less sterically demanding $Nacnac^{Mes}$ ligand ($Nacnac^{Mes}$ = $[(2,4,6\text{-}Me_3C_6H_2)NC(Me)]_2CH$) results in the formation of a centrosymmetric dimer $[(Nacnac^{Mes})Zn(\mu\text{-}H)]_2$ with a Zn_2H_2 core.[55]

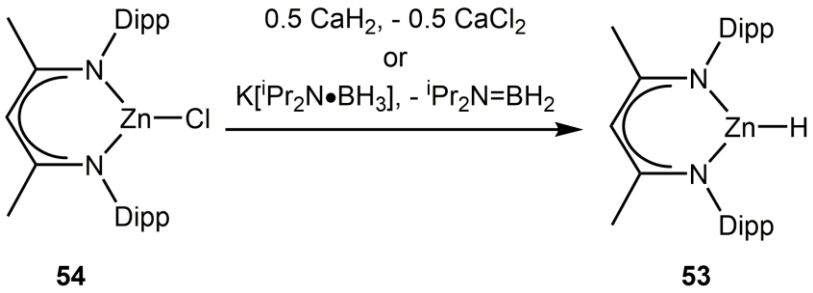

54 **53** (1.16)

A main target of interest upon the commencement of this thesis was to prepare a soluble adduct of ZnH_2. Unfortunately, this achievement was reported in 2013 by Okuda and coworkers in the form of the dimeric species (**55a** and **55b**) stabilised by the known *N*-heterocyclic carbene ligands IMes and IPr [IMes = $(HCNMes)_2C$:, IPr = $(HCNDipp)_2C$:].[56] In this work, two pathways were presented for the synthesis of these NHC adducts of ZnH_2 (Scheme 1.10): the first pathway involved mixing the carbene donor with ZnH_2 in THF, followed by stirring overnight. The second synthetic pathway involved the methanolysis of an NHC•$ZnEt_2$ adduct, followed by the silane-induced hydride transfer to Zn with loss of R_3SiOMe.

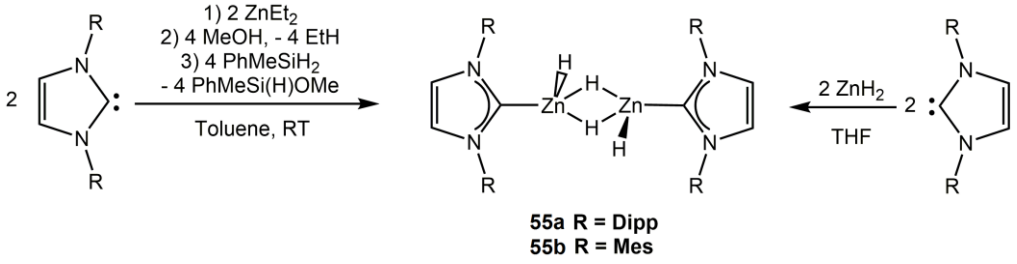

Scheme 1.10 Synthesis of [NHC•Zn(H)(μ-H)]$_2$ complexes **55a** and **55b**; R = Mes, Dipp.

These two routes represent useful methodologies with which one can access a variety of metal hydride species. The resultant species are highly soluble in aromatic solvents such as toluene and benzene, and were also demonstrated to be efficient catalysts for the methanolysis of silanes. However these species still suffer from the thermal decomposition into zinc metal, hydrogen gas and the free NHC over time at room temperature. As a result, our group sought to improve the stability of these species to make them more viable candidates as catalysts for hydrosilylation and hydroboration processes.

1.5 Acknowledgement of collaborators

Portions of the work discussed in this thesis were completed in collaboration with other researchers within the Rivard group in the Department of Chemistry at the University of Alberta.

All X-ray crystallographic studies described in this thesis were performed by Dr. R. McDonald and Dr. M. J. Ferguson, including the mounting of crystals, set-up and operation of the diffractometer, refinement of the structures and preparation of all crystallographic data tables.

In chapter 2, the preparation of the bis(amido)silyl ligands and catalytic trials were performed with the assistance of L. J. Miedema and P. Hubacek.

In chapter 3, the preparation of bis(amido)silyl umbrella ligand was performed with the assistance of L. J. Miedema. The preparation of the bis(guanidine) ligands and study of their reactivity was performed in collaboration with D. Golec.

In chapter 4, the catalytic trials were performed in collaboration with M. W. Lui. All computational analysis was performed by M. R. Momeni, under the supervision of Prof. A. Brown. Variable temperature NMR spectroscopy and DOSY NMR spectroscopy was performed with the assistance of Ms. N. Dabral and Mr. M. Miskolzie.

In chapter 5, all computational analysis was performed by E. Antoniuk, under the supervision of Prof. A. Brown. Carbon monoxide reactions were performed with the assistance of Prof. J. Takats.

According to the policy within our research group, each chapter of this thesis is essentially self-contained, and prepared in the form of a paper that is intended for publication in peer-reviewed journals.

A portion of this thesis has been published previously elsewhere, and these publications are listed below:

Chapter 2

(1) S. M. I. Al-Rafia, P. A. Lummis, M. J. Ferguson, R. McDonald, E. Rivard, *Inorg. Chem.*, **2010**, *49*, 5471.

(2) P. A. Lummis, R. McDonald, M. J. Ferguson, E. Rivard, *Dalton Trans.*, **2015**, *44*, 7009.

Chapter 4

(1) S. M. I. Al-Rafia, P. A. Lummis, A. K. Swarnakar, K. C. Deutsch, M. J. Ferguson, R. McDonald, E. Rivard, *Aus. J. Chem.*, **2013**, *66*, 1235.

(2) P. A. Lummis, M. R. Momeni, M. W. Lui, R. McDonald, M. J. Ferguson, M. Miskolzie, A. Brown, E. Rivard, *Angew. Chem. Int. Ed.*, **2014**, *53*, 9347.

1.6 References

1 A. Marinetti, A. Voituriez, *Synlett*, **2010**, *2*, 174.

2 W. C. Zeise, *Ann. der Phys. Chem.*, **1831**, 97, 497.

3 (*a*) T. J. Kealy, P. L. Pauson, *Nature*, **1951**, *168*, 1039; (*b*) G. Wilkinson, *J. Organomet. Chem.*, **1975**, *100*, 273.

4 A. Haaland, S. Samdal, N. V. Tverdova, G. V. Girichev, N. I. Giricheva, S. A. Schlykov, A. G. Garkusha, B. V. Lokshin, *J. Organomet. Chem.*, **2003**, *684*, 351.

5 D. W. Hart, J. Schwartz, *J. Am. Chem. Soc.*, **1974**, *96*, 8115.

6 (*a*) T. Takahashi, M. Hasegawa, N. Suzuki, M. Saburi, C. J. Rousset, P. E. Fanwick, E. Negishi, *J. Am. Chem. Soc.,* **1991**, *113*, 8564; (*b*) L. Jia, J. Zhao, E. Ding, W. W. Brennessel, *J. Chem. Soc., Dalton Trans.,* **2002**, 2608; (*c*) S. Anga, K. Naktode, H. Adimulam, T. K. Panda, *Dalton Trans.,* **2014**, *43*, 14876

7 N. N. Greenwood, A. Earnshaw, *Chemistry of the Elements, 2nd Ed.,* Butterworth-Heinemann, **1997**, ISBN: 0080379419.

8 G. V. Chertihin, L. Andrews, *J. Phys. Chem.*, **1995**, *99*, 15004.

9 G. He, O. Shynkaruk, M. Lui, E. Rivard, *Chem. Rev.* **2014**, *114*, 7815.

10 Values given for neutral, first row metal hydride species. J. Uddin, C. M. Morales, J. H. Maynard, C. R. Landis, *Organometallics*, **2006**, *25*, 5566.

11 E. Y. Tsui, P. Müller, J. P. Sadighi, *Angew. Chem. Int. Ed.*, **2008**, *47*, 8937.

12 J. Clayden, N. Greaves, S. Warren, *Organic Chemistry, 2nd Ed.*, Oxford University Press, **2012**, ISBN: 0199270295.

13 R. B. King, *Coord. Chem. Rev.*, **2000**, *200*, 813.

14 J. G. Floss, A. V. Grosse, *J. Inorg. Nucl. Chem.*, **1960**, *16*, 36.

15 G. J. Kubas, R. R. Ryan, B. I. Swanson, P. J. Vergamini, H. J. Wasserman, *J. Am. Chem. Soc.*, *106*, 451.

16 R. Waterman, *Chem. Soc. Rev.*, **2013**, *42*, 5629.

17 J. F. Harrod, *ACS Symp. Ser.*, **1988**, *360*, 89.

18 For a review covering phosphine-boranes in addition to amine-boranes, see: A. Staubitz, A. P. M. Robertson, M. E. Sloan, I. Manners, *Chem. Rev.*, **2010**, *110*, 4023.

19 A. Staubitz, A. P. M. Robertson, I. Manners, *Chem. Rev.*, **2010**, *110*, 4079.

20 J. L. Gay-Lussac, *Mem. Phys. Chim. Soc. D'Accueil*, **1809**, *2*, 211.

21 A. B. Burg, H. I. Schlesinger, *J. Am. Chem. Soc.* **1937**, *59*, 780.

22 C. A. Jaska, K. Temple, A. J. Lough, I. Manners, *J. Am. Chem. Soc.*, **2003**, *125*, 9424.

23 A. P. M. Robertson, E. M. Leitao, I. Manners, *J. Am. Chem. Soc.*, **2011**, *133*, 19322.

24 M. E. Bowdon, I. W. M. Brown, G. J. Gainsford, H. Wong, *Inorg. Chim. Acta*, **2008**, *361*, 2147.

25 B. Singaram, T. E. Cole, H. C. Brown, *Organometallics*, **1984**, *3*, 774.

26 K. J. Sabourin, A. C. Malcolm, R. McDonald, M. J. Ferguson, E. Rivard, *Dalton Trans.*, **2013**, *42*, 4625.

27 T. J. Clark, C. A. Russell, I. Manners, *J. Am. Chem. Soc.*, **2006**, *128*, 9582.

28 V. K. Dioumaev, J. F. Harrod, *Organometallics*, **1997**, *16*, 1452.

29 C. Jegat, M. Fouassier, M. Tranquille, J. Mascetti, *Inorg. Chem.*, **1991**, *30*, 1529.

30 T. D. Forster, H. M. Tuononen, M. Parvez, R. Roesler, *J. Am. Chem. Soc.*, **2009**, *131*, 6689.

31 Y. Chen, J. L. Fulton, J. C. Linehan, T. Autrey, *J. Am. Chem. Soc.*, **2005**, *127*, 3254.

32 Y. Luo, K. Ohno, *Organometallics*, **2007**, *26*, 3597.

33 H. Helten, B. Dutta, J. R. Vance, M. E. Sloan, M. F. Haddow, S. Sproules, D. Collison, G. R. Whittell, G. C. Lloyd-Jones, I. Manners, *Angew. Chem. Int. Ed.*, **2013**, *52*, 437.

34 A. M. Chapman, M. F. Haddow, D. F. Wass, *J. Am. Chem. Soc.*, **2011**, *133*, 8826.

35 D. Pun, E. Lobkovsky, P. J. Chirik, *Chem. Commun.*, **2007**, 3297.

36 K. M. Hambidge, N. F. Krebs, *J. Nutr.*, **2007**, *137*, 1101.

37 E. G. Brandt, M. Hellgren, T. Brinck, T. Bergman, O. Edholm, *Phys. Chem. Chem. Phys.*, **2009**, *11*, 975.

38 I. Resa, E. Carmona, E. Gutierrez-Puebla, A. Monge, *Science*, **2004**, *305*, 1136.

39 G. van Koten, B. Fisher, P. Wijkens, P. H. M. Budzelaar, J. Boersma, *J. Organomet. Chem.*, **1989**, *376*, 223.

40 Y. Wang, B. Quillian, P. Wei, H. Wang, X.-J. Yang, Y. Xie, R. B. King, P. v. R. Schleyer, H. F. Schaefer, III, G. H. Robinson, *J. Am. Chem. Soc.*, **2005**, *127*, 11944.

41 (*a*) Z. Zhu, R. J. Wright, M. M. Olmstead, E. Rivard, M. Brynda, P. P. Power, *Angew. Chem. Int. Ed.*, **2006**, *45*, 5807; (*b*) Z. Zhu, M. Brynda, R. J. Wright, R. C. Fischer, W. A. Merrill, E. Rivard, R. Wolf, J. C. Fettinger, M. M. Olmstead, P. P. Power, *J. Am. Chem. Soc.*, **2007**, *129*, 10847.

42 A. Stasch, *Chem. Eur. J.*, **2012**, *18*, 15105.

43 (*a*) S. Schmidt, S. Schulz, D. Bläser, R. Boese, M. Bolte, *Organometallics*, **2010**, *29*, 6097; (*b*) C. Jones, L. Furness, S. Nembenna, R. P. Rose, S. Aldridge, A. Stasch, *Dalton Trans.*, **2010**, *39*, 8788.

44 H. Banh, C. Gemel, R. W. Seidel, R. A. Fischer, *Chem. Commun.*, **2015**, *51*, 2170.

45 For a comprehensive review on the chemistry of organozinc and zinc coordination complexes, see: S. J. Archibald*, Comprehensive Coordination Chemistry II*, *Vol. 6* (Ed.: D. E. Fenton*),* Elsevier*,* London*,* **2004***,* 1147.

46 A. M. Tondreau, C. C. H. Atienza, K. J. Weller, S. A. Nye, K. M. Lewis, J. G. P. Delis, P. J. Chirik, *Science*, **2012**, *335*, 567.

47 D. Troegel, J. Stohrer, *Coord. Chem. Rev.*, **2011**, *225*, 1440.

48 S. Das, D. Addis, S. Zhou, K. Junge, M. Beller, *J. Am. Chem. Soc.*, **2012**, *132*, 1770.

49 A. Y. Houghton, J. Hurmalainen, A. Mansikkamäki, W. E. Piers, H. M. Tuononen, *Nature Chem.*, **2014**, *6*, 983.

50 N. A. Marinos, S. Enthaler, M. Driess, *ChemCatChem*, **2010**, *2*, 846.

51 W. Sattler, G. Parkin, *J. Am. Chem. Soc.*, **2012**, *134*, 17642.

52 A. E. Finholt, A. C. Bond, Jr., H. I. Schlesinger, *J. Am. Chem. Soc.*, **1947**, *69*, 1199.

53 P. Jochmann, D. W. Stephan, *Angew. Chem., Int. Ed.* **2013**, *52*, 9831.

54 J. Spielmann, D. Piesik, B. Wittkamp, G. Jansen, S. Harder, *Chem. Commun.* **2009**, 3455.

55 S. Schulz, T. Eisenmann, D. Schuchmann, M. Bolte, M. Kirchner, R. Boese, J. Spielmann, S. Harder, *Z. Naturforsch.*, **2009**, *64b*, 1397.

56 A. Rit, T. P. Spaniol, L. Maron, J. Okuda, *Angew. Chem. Int. Ed.* **2013**, *52*, 4664.

Chapter 2: Synthesis, characterisation and reactivity of complexes of zirconium bearing hindered bis(amido)silyl ligands

2.1 Abstract

Herein the synthesis and characterisation of a series of zirconium compounds featuring the bis(amido)silyl ligand $[^{i}Pr_2Si(NDipp)_2]^{2-}$ (Dipp = 2,6-diisopropylphenyl) is described. The functionalisation of bis(amido)silyl zirconium halide complexes with a variety of nucleophiles such as $LiNMe_2$, $LiBH_4$ and MeLi, was explored and the resulting products showed a propensity to form anionic zirconate salts when the syntheses were carried out in THF. One of the zirconate products, $[^{i}Pr_2Si(NDipp)_2]Zr(NMe_2)_2{\bullet}ClLi(THF)_3$, has the ability to catalyse the dehydrocoupling of primary and secondary amine-boranes at room temperature in aromatic solvents.

2.2 Introduction

Zirconium has long attracted interest as a metal of choice for catalysis since it is relatively inexpensive and abundant in comparison to many other transition metals. Moreover, its electropositive nature leads to polar Zr-E bonds (E = C, N, O, P etc.), thus making Zr complexes amenable to catalytic sigma-bond metathesis pathways.[1] Indeed, many zirconium complexes are active olefin polymerisation catalysts,[2] can promote the dehydrocoupling of amine-boranes[3] and silanes,[4] as well as the hydroamination of unsaturated substrates such as ketones[5] and alkenes.[6] Furthermore, key examples involving the activation of small molecules such as N_2[7] and CO[8] by zirconium centres have been reported.

Of the many catalytically active Zr complexes known, metallocene complexes remain prevalent within the literature (Figure 2.1, **I-IV**), due to their exceptional thermal stability and ease of synthesis associated with the use of cyclopentadienyl units as ligands. It should be noted that in addition to traditional zirconocene compounds, there also exist various *ansa*-metallocenes, e.g. (**IV**), wherein two cyclopentadienyl moieties are linked by spacer units such as Me_2C or Me_2Si. This structural feature leads to a contraction of the $Cp_{(centroid)}$-M-$Cp_{(centroid)}$ angle thereby changing the steric environment around the metal, conferring structural rigidity and in some instances stereospecific reactivity in relation to their non-tethered analogues.[9] Conceptually, tethered *ansa*-metallocene ligands are similar to the sterically

modifiable $[^{i}Pr_2Si(NR)_2]^{2-}$ ligand scaffolds previously explored within our laboratory (R = Dipp, $SiPh_3$ or $Si(4\text{-}^{i}Pr\text{-}C_6H_4)_3$).[10] The ability to readily modify the steric and electronic nature of these $[R'_2Si(NR)_2]^{2-}$ ligands via altering the R and R′ substituents has been used to advance low oxidation state main group element chemistry.[11] Moreover, these bis(amido)silyl ligands are expected to be less electron donating than their tethered bis(cyclopentadienyl) counterparts, thus it was hypothesised that bis(amido)silyl chelates would lead to more electron deficient and sterically accessible metal centres within the context of advancing metal-mediated catalysis.

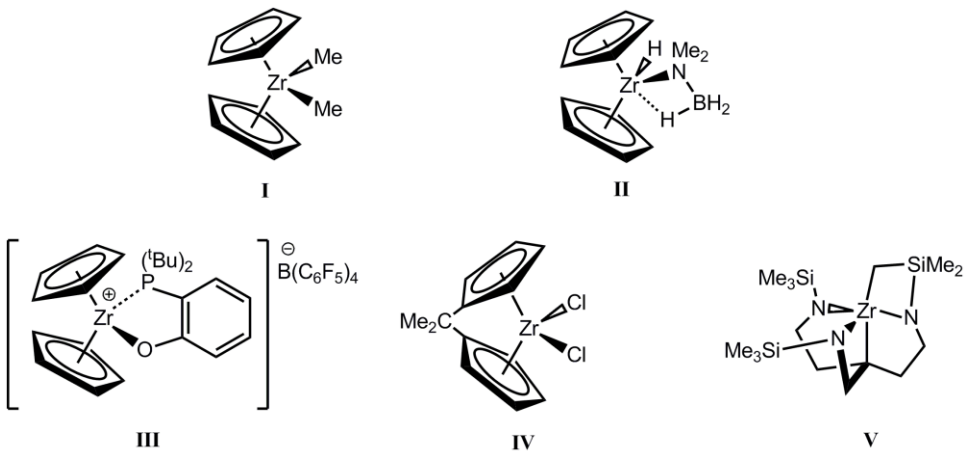

Figure 2.1. Examples of metallocene (**I-IV**) and non-metallocene (**V**) complexes as pre-catalysts for the dehydrocoupling of amine-boranes and/or silanes.

There has been a resurgence in the chemistry of amine-boranes as a result of their potential use as hydrogen storage materials.[12] It was recently demonstrated that while neutral zirconocene complexes such as **II** are able to induce the catalytic dehydrocoupling of amine-boranes with modest turnover

frequencies of *ca.* 0.6 hr^{-1},[13] the generation of a formally cationic zirconium centre in **III** led to a marked increase in activity (up to 1000 fold) towards the same substrates.[14] This corresponds well with our postulate that a more Lewis acidic metal centre will facilitate the binding of target substrates. With the aforementioned chemistry in mind, we explored the synthesis of new low coordinate zirconium complexes supported by [NSiN] chelates as pre-catalysts for dehydrocoupling methodologies was explored.

2.3 Results and discussion

2.3.1 Synthesis of bis(amido)silyl zirconium complexes

The requisite ligand precursor for these studies $H_2[NSiN]^{Dipp}$ (**1**), ($[NSiN]^{Dipp}$ = $[DippNSi(^iPr)_2NDipp]^{2-}$) was readily synthesised as a crystalline white solid in high yield (*ca.* 80 %) starting from the commercially available amine, $DippNH_2$ (Dipp = 2,6-diisopropylphenyl) (Scheme 2.1).[10a,15] Conversion of $H_2[NSiN]^{Dipp}$ into the dilithiobis(amido) salt, $Li_2[NSiN]^{Dipp}$ is possible by treating the bis(amine) (**1**) with 2 equivalents of ^nBuLi in Et_2O; this dilithio reagent can be used *in situ*, or isolated as a white air-sensitive solid that is highly soluble in aromatic and aliphatic solvents. If the synthesis is conducted in THF, then $Li(THF)_4\{[NSiN]^{Dipp}Li(THF)_2\}$ (**2a**) can be crystallised upon layering the THF solution with hexanes at -35 °C. Removal of all volatiles *in vacuo* afforded the neutral species, $Li_2[NSiN]^{Dipp}$•3THF, as confirmed by NMR spectroscopy and elemental analysis.

Compound **2a** shows two distinct fragments, each containing a central lithium atom. The cationic $Li(THF)_4$ fragment features a slightly distorted tetrahedral Li centre, with all of the Li-O bond lengths [1.912(5) Å avg.] the same within three standard deviations of experimental error. The anionic fragment has the $[NSiN]^{Dipp}$ ligand bound to a distorted tetrahedral Li centre, with a N(1)-Li(1)-N(1′) angle of 81.41(17)° and a N(1)-Li(1)-O(1) angle of 137.65(7)°.

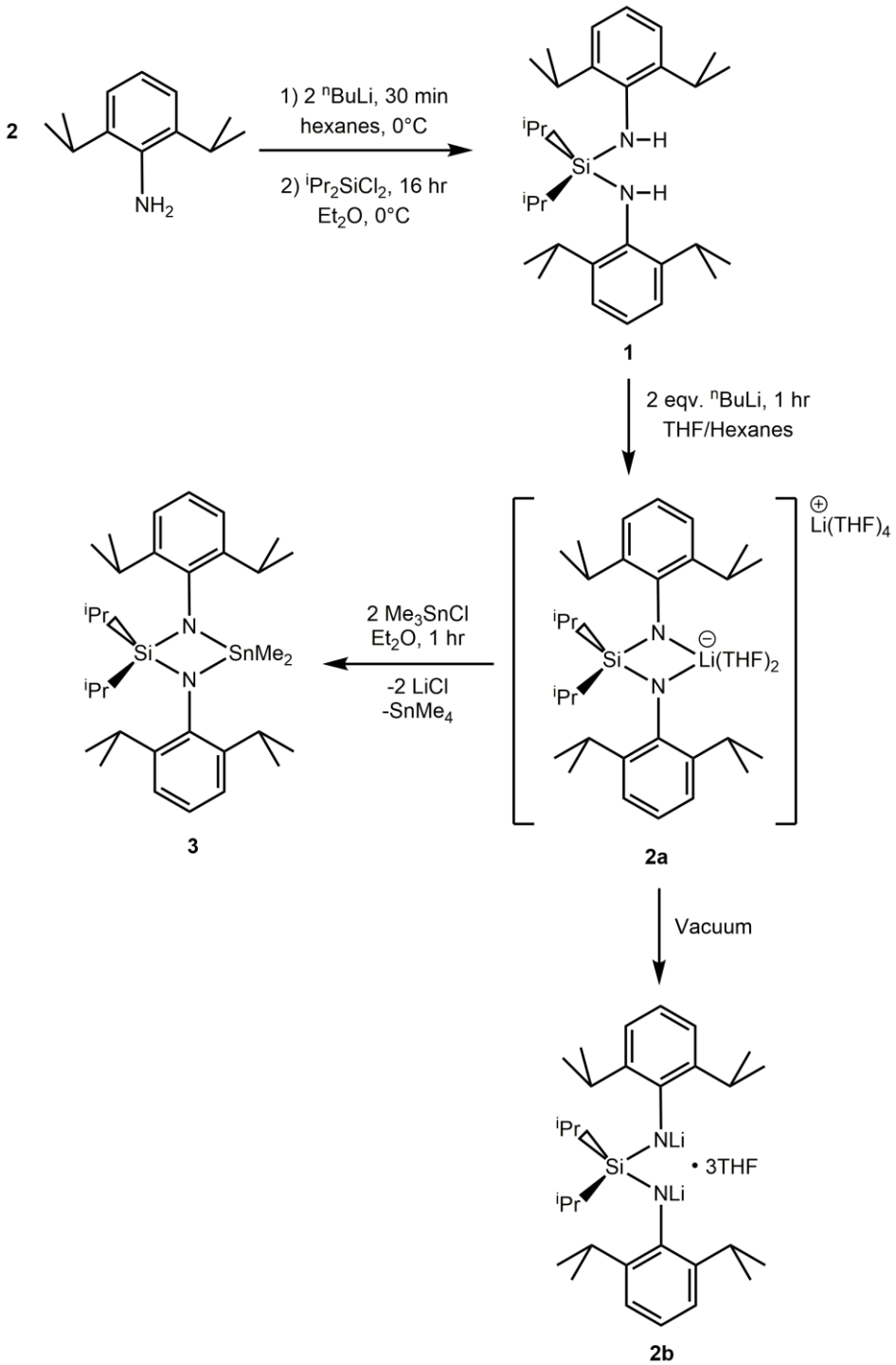

Scheme 2.1. Synthesis of neutral ligand $H_2[NSiN]^{Dipp}$ (**1**), dilithio congeners $Li_2[NSiN]^{Dipp}$•XTHF (X = 6, **2a**; X = 3, **2b**) and dimethylstannyl congener $Me_2Sn[NSiN]^{Dipp}$ (**3**).

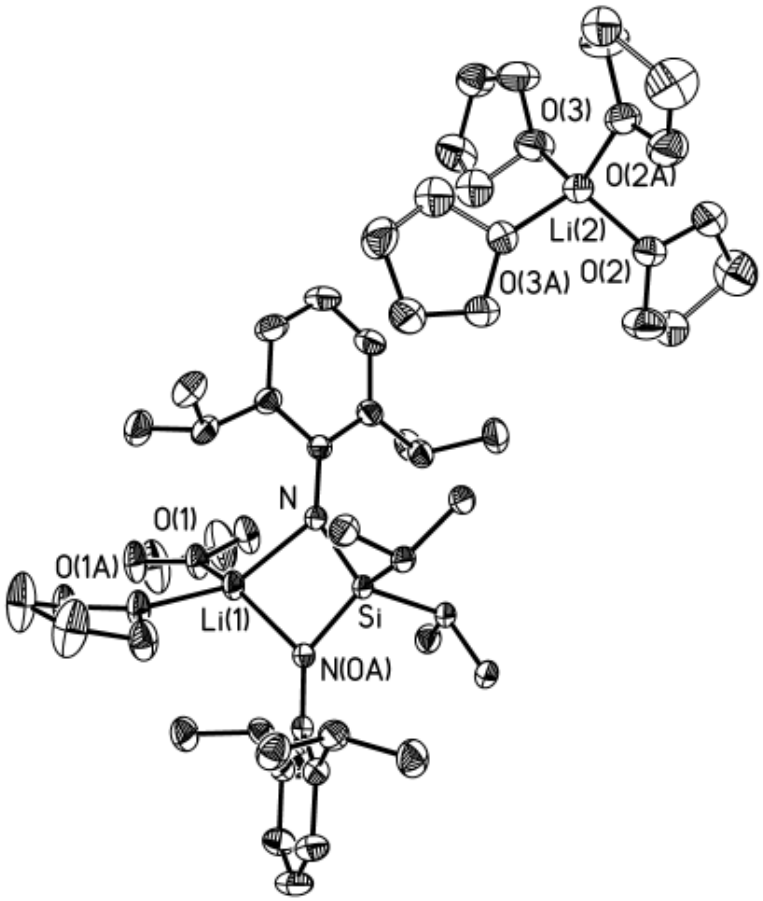

Figure 2.2. Molecular structure of $Li(THF)_4\{[NSiN]^{Dipp}Li(THF)_2\}$ (**2a**) with thermal elipsoids at the 30 % probability level. All hydrogen atoms have been omitted for clarity. Selected bond lengths (Å): Si(1)-N(1) 1.6971(15), Si(1)-C(1) 1.92257(19), N(1)-Li(1) 2.038(3), Li(1)-O(1) 2.038(3), Li(2)-O(2) 1.924(4), Li(2)-O(3) 1.901(4).

In addition to the dilithio salts described, the preparation of a softer transmetallating agent was achieved by treating a solution of either **2a** or **2b** with 2 equivalents of Me_3SnCl in diethyl ether. Somewhat to our surprise, rather than forming the anticipated bisstannylated ligand precursor $(Me_3Sn)_2[NSiN]^{Dipp}$ as originally intended, the elimination of one equivalent

of Me_4Sn in addition to the expected loss of two equivalents of LiCl occurred. Independent synthesis of **3** via treatment of a diethyl ether solution of **2a** with one equivalent of Me_2SnCl_2 was also achieved. It was found that **3** was able to perform a transmetallation to install the $[NSiN]^{Dipp}$ chelate onto Ge, however no new product formation was noted when combined with $Cl_4Zr(THF)_2$, $Cl_4Ti(THF)_2$ or $CoCl_2$.

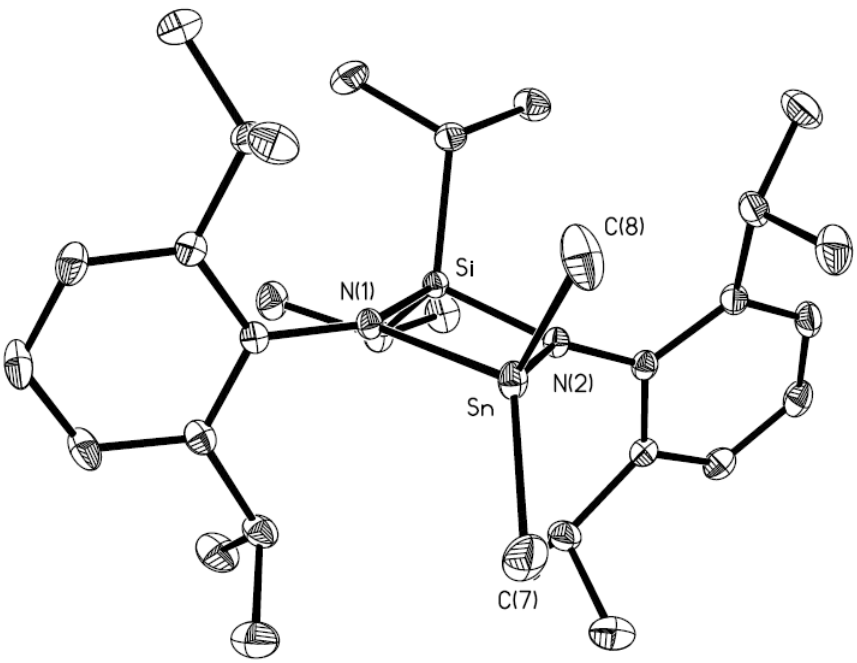

Figure 2.3 Molecular structure of $[NSiN]^{Dipp}SnCl_2$ (**3**) with thermal ellipsoids presented at the 30 % probability level. All hydrogen atoms have been omitted for clarity. Selected bond lengths (Å) and angles (°): Sn-N(1) 2.0557(16), Sn-N(2) 2.0647(16), Sn-C(7) 2.124(3), Sn-C(8) 2.132(3), Si-N(1) 1.7432(17), Si-N(2) 1.7491(16); N(1)-Sn-N(2) 75.72(6), N(1)-Si-N(2) 92.78(8), Si-N(1)-Sn 95.39(7), Si-N(2)-Sn 94.89(7).

Addition of *in situ* generated $Li_2[NSiN]^{Dipp}$ to a suspension of $ZrCl_4$•2THF in Et_2O afforded the zirconate complex $[NSiN]^{Dipp}ZrCl(\mu$-

$Cl)_2Li(THF)_2$ (**4**) (Scheme 2.2) as a colourless, moisture-sensitive solid in 69 % yield. As is seen by X-ray crystallography, compound **4** contains one equivalent of lithium chloride within the coordination sphere of zirconium (Figure 2.4). A similar bonding motif was noted by Sun and coworkers in their synthesis of $[Me_2NSi(Me)_2NDipp]ZrCl_2(\mu\text{-}Cl)_2Li(THF)_2$; the same group also reported the formation of the LiCl-free compound $[Me_2NSi(Me)_2NDipp]_2ZrCl_2$.[15c] By contrast, a series of Zr[NSiN] heterocycles supported by the $[DippNSi(Me)_2NDipp]^{2-}$ ligand retains two equivalents of THF at zirconium with no evidence of LiCl encapsulation.[15a] The observed inclusion of LiCl in **4** is caused by the bulky ligand causing the dissociation of THF from the Zr centre, which in turn renders the Zr more electron deficient. This increased Lewis acidity then allows for the binding of one equivalent of LiCl to satisfy the coordinative unsaturation of the Zr centre. The C_{ipso}-N-Zr angles involving the Dipp groups in $[DippNSiMe_2NDipp]ZrCl_2(THF)_2$,[15a] [136.72(19)° and 139.9(2)°] are wider than the corresponding values found in $[NSiN]^{Dipp}ZrCl(\mu\text{-}Cl)_2Li(THF)_2$ (**4**) [131.91(13)° and 132.87(13)°], a reflection of the different coordination numbers at Zr observed in these two compounds. As noted in previous work with the $[NSiN]^{Dipp}$ ligand, there is restricted rotation about the N-C_{ipso} bond involving the Dipp groups in **4**, leading to two spectroscopically distinct methyl environments within the isopropyl groups (in C_6D_6).[10]

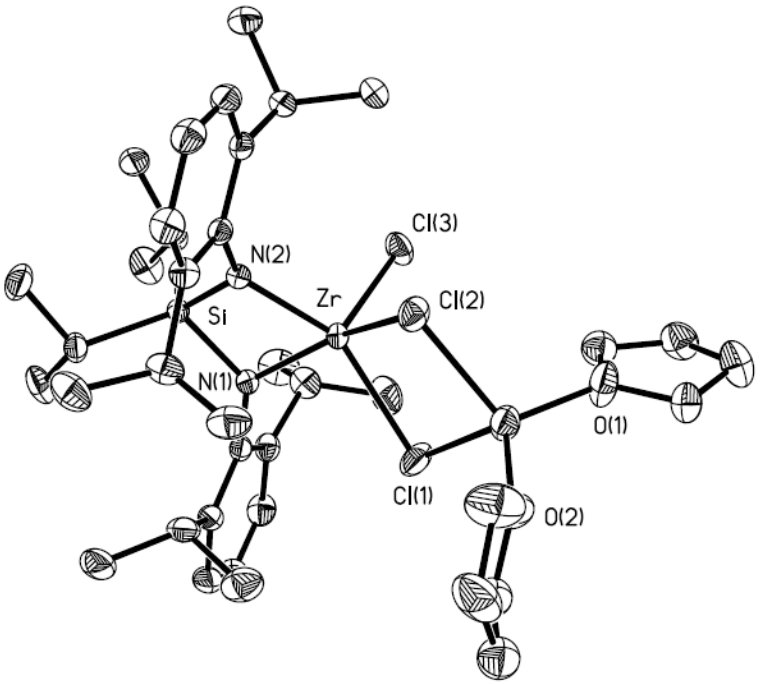

Figure 2.4. Molecular structure of $[NSiN]^{Dipp}ZrCl(\mu\text{-}Cl)_2Li(THF)_2$ (**4**) with thermal ellipsoids presented at the 30 % probability level. All hydrogen atoms have been omitted for clarity. Selected bond lengths (Å) and angles (°): Zr–N(1) 2.0521(16), Zr–N(2) 2.0495(16), Zr–Cl(1) 2.4966(6), Zr–Cl(2) 2.5199(6), Zr–Cl(3) 2.3910(6), Cl(1)–Li 2.399 (5), Cl(2)–Li 2.372(5); N(1)–Zr–N(2) 75.69(6), N(1)–Zr–Cl(1) 92.70(5), N(1)–Zr–Cl(2) 150.17(5), N(1)–Zr–Cl(3) 106.41(5), N(2)–Zr–Cl(1) 149.13(5), N(2)–Zr–Cl(2) 91.08(5), N(2)–Zr–Cl(3) 105.70(5), Cl(1)–Zr–Cl(2) 85.15(2), Cl(1)–Zr–Cl(3) 105.01(3), Cl(2)–Zr–Cl(3) 102.86(2), Cl(1)–Li–Cl(2) 90.70(15).

Somewhat to our surprise, the attempted formation of $[NSiN]^{Dipp}Zr(NMe_2)_2$ via a protonolysis reaction between $H_2[NSiN]^{Dipp}$ and $Zr(NMe_2)_4$ resulted in no reaction, despite heating the mixture in toluene to reflux for 72 hours. Possible explanations for this lack of reactivity include the increased steric bulk of **1** relative to $DippNH_2$ (which reacts readily with $Zr(NMe_2)_4$) and the hyperconjugative interaction between the nitrogen lone

pairs within $H_2[NSiN]^{Dipp}$ (**1**) and the adjacent Si-C σ* orbitals which reduce the nucleophilicity of the amine sites.

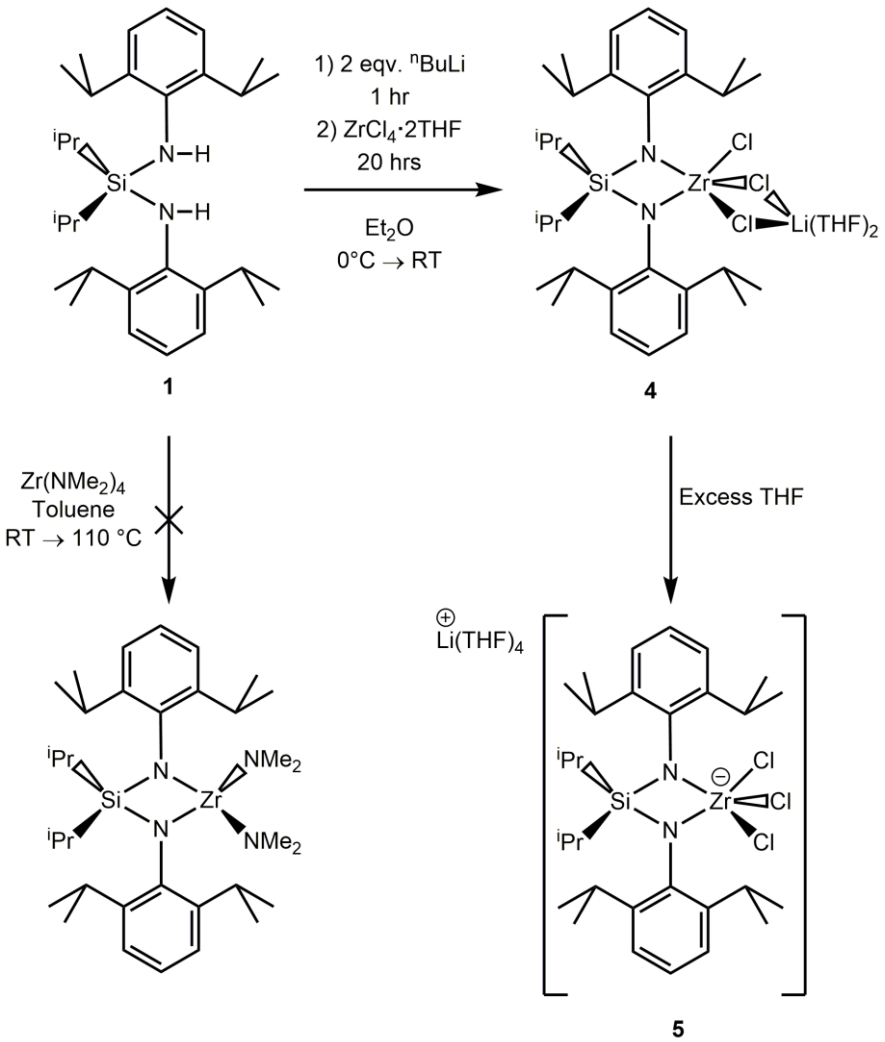

Scheme 2.2. Synthesis of the halogenato zirconium complexes $[NSiN]^{Dipp}ZrCl(\mu\text{-}Cl)_2Li(THF)_2$ (**4**) and $Li(THF)_4\{[NSiN]^{Dipp}ZrCl_3\}$ (**5**).

It was also observed that dissolution of **4** in THF led to the irreversible formation of the zirconate salt $Li(THF)_4\{[NSiN]^{Dipp}ZrCl_3\}$ (**5**). While high

quality crystals of **5** of suitable quality for single-crystal X-ray analysis were not obtained, ^{1}H NMR spectroscopy showed the incorporation of four equivalents of THF, corresponding to the formation of the $[Li(THF)_4]^+$ cation. To our surprise, attempts to remove a chloride from the zirconate **5** via reaction with TlOTf and AgOTf in Et_2O resulted in the observation of **1** as the major soluble product by ^{1}H NMR spectroscopy. Further explorations indicate that the formally anionic nature of the zirconate centre in $Li(THF)_4\{[NSiN]^{Dipp}ZrCl_3\}$ (**5**) made nucleophilic substitution of the Zr-bound halides more challenging in relation to **4**. For example, attempts to install Me_2N- groups at Zr to form $[NSiN]^{Dipp}Zr(NMe_2)_2$ only resulted in the exclusive generation of the mono-dimethylamido zirconate salt, $Li(THF)_4\{[NSiN]^{Dipp}ZrCl_2(NMe_2)\}$ (**6**), even when four equivalents of $LiNMe_2$ were added to **5** (or compound **4** in the presence of THF; Scheme 2.3). This may be due to the presence of a formally anionic pentacoordinate Zr centre, which would in turn be less reactive towards nucleophiles such as $[NMe_2]^-$ and $[BH_4]^-$; this trend is seen throughout this work. The X-ray structure of **6** reveals a distorted square pyramidal geometry at Zr, with the central zirconium atom raised slightly out of the plane of the square base of ligating atoms. While the $[NSiN]^{Dipp}$ chelate affords a narrow N(1)-Zr-N(2) angle [71.9(1)°], all remaining bond angles involving adjacent ligating atoms in the base of the pyramid fall in the range of 90.93(8) to 90.07(4)° with the –NMe_2 group occupying the axial position (Figure 2.5).

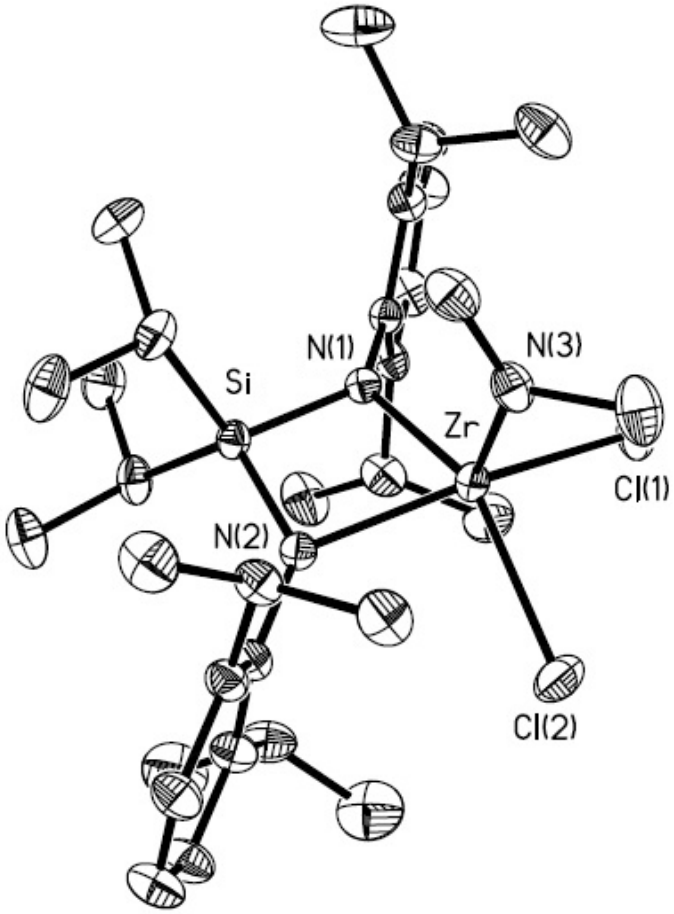

Figure 2.5. Molecular structure of $Li(THF)_4\{[NSiN]^{Dipp}ZrCl_2(NMe_2)\}$ (**6**) with thermal ellipsoids presented at the 30 % probability level. All carbon-bound hydrogen atoms and the cationic $Li(THF)_4$ units have been omitted for clarity. Selected bond lengths (Å) and angles (°): Zr–N(1) 2.139(3), Zr–N(2) 2.114(3), Zr–N(3) 2.032(3), Zr–Cl(1) 2.4487(1), Zr–Cl(2) 2.468(1); N(1)–Zr–N(2) 71.9(1), N(1)–Zr–N(3) 109.7(1), N(1)–Zr–Cl(1) 90.83(8), N(1)–Zr–Cl(2) 145.74(8), N(2)–Zr–N(3) 108.2(1), N(2)–Zr–Cl(1) 149.68(7), N(2)–Zr–Cl(2) 90.93(8), N(3)–Zr–Cl(1) 100.98(9), N(3)–Zr–Cl(2) 103.72(9), Cl(1)–Zr–Cl(2) 90.07(4)

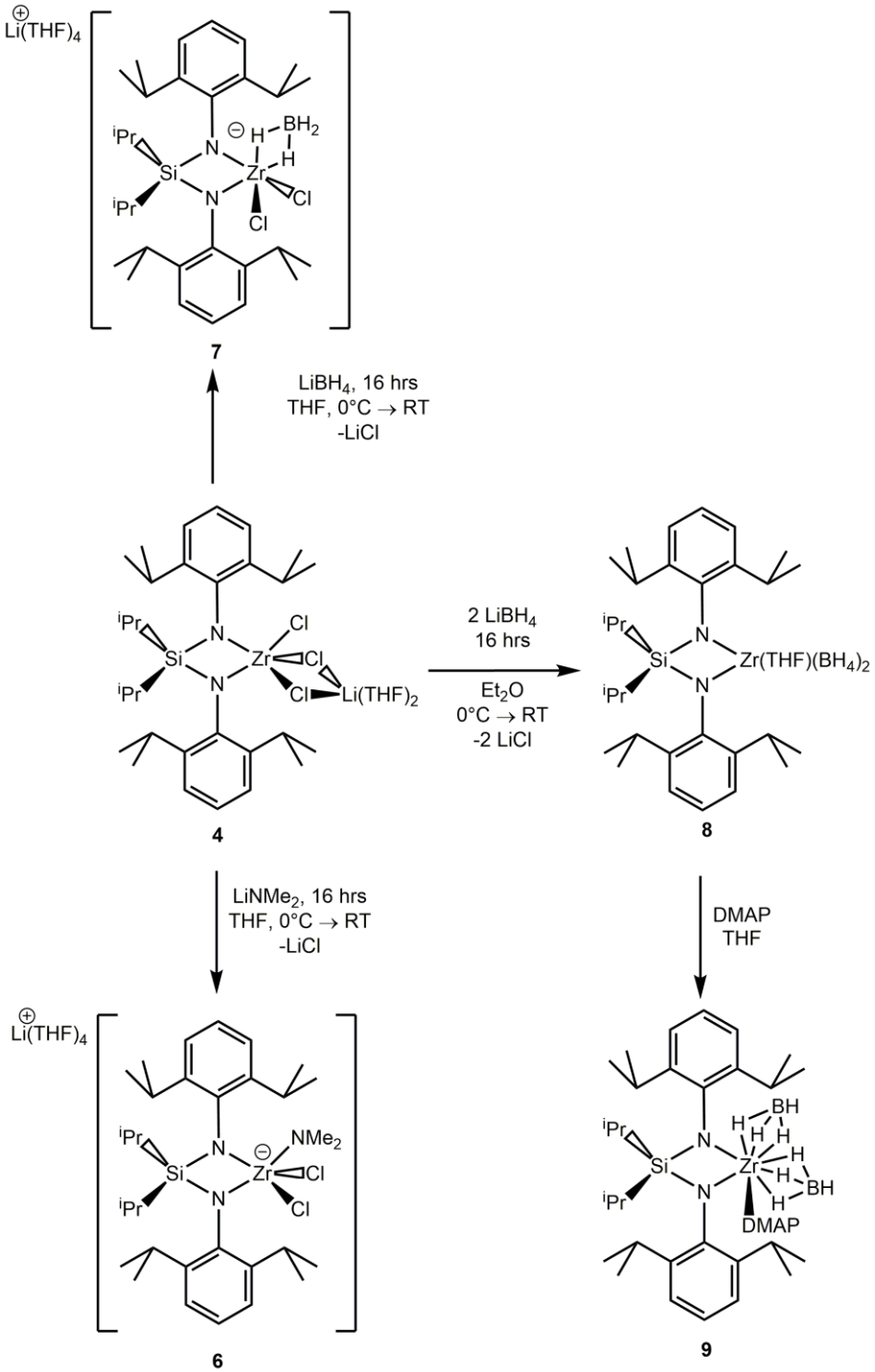

Scheme 2.3. Synthesis of $Li(THF)_4\{[NSiN]^{Dipp}ZrCl_2(NMe_2)\}$ (**6**), $Li(THF)_4\{[NSiN]^{Dipp}Zr(BH_4)Cl_2\}$ (**7**), $[NSiN]^{Dipp}Zr(BH_4)_2$•THF (**8**) and $[NSiN]^{Dipp}Zr(BH_4)_2$•DMAP (**9**).

In a similar fashion, the mono-substituted product $Li(THF)_4\{[NSiN]^{Dipp}ZrCl_2(BH_4)\}$ (**7**) is exclusively formed when $[NSiN]^{Dipp}ZrCl(\mu\text{-}Cl)_2Li(THF)_2$ (**4**) is treated with an excess of $Li[BH_4]$ in THF; as mentioned above, this process likely involves the initial formation of the zirconate salt **5** when **4** is combined with THF. The borohydride complex **7** (Figure 2.6) bears structural similarity to the amido complex $Li(THF)_4\{[NSiN]^{Dipp}ZrCl_2(NMe_2)\}$ (**6**) as both complexes contain five-coordinate Zr centres, with distorted square pyramidal geometries.

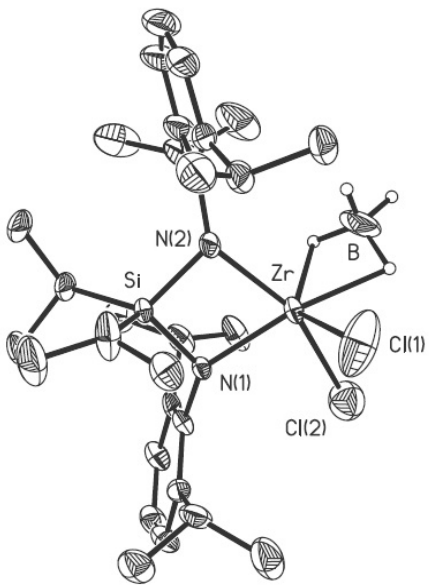

Figure 2.6. Molecular structure of $Li(THF)_4\{[NSiN]^{Dipp}ZrCl_2(BH_4)\}$ (**7**) with thermal ellipsoids presented at the 30 % probability level. All carbon-bound hydrogen atoms and the cationic $Li(THF)_4$ unit have been omitted for clarity. Selected bond lengths (Å) and angles (°): Zr–N(1) 2.094(4), Zr–N(2) 2.102(5), Zr–Cl(1) 2.465(4), Zr–Cl(2) 2.4973(3), Zr---B 2.370(13); N(1)–Zr–N(2) 73.4(2), N(1)–Zr–Cl(1) 110.3(2), N(1)–Zr–Cl(2) 85.0(1), N(2)–Zr–Cl(1) 102.6(2), N(2)–Zr–Cl(2) 155.1(1), Cl(1)–Zr–Cl(2) 96.1(1).

Despite the use of THF as a solvent medium, neither complex **6** or **7** have THF bound to Zr in the solid state, in contrast to the previously discussed bis(amido)silyl complex [DippNSiMe$_2$NDipp]ZrCl$_2$(THF)$_2$.[15a] By changing the THF solvent in the reaction between [NSiN]^{Dipp}ZrCl(μ-Cl)$_2$Li(THF)$_2$ **4** and two equivalents of Li[BH$_4$] with the less coordinating Et$_2$O, the bis(borohydride)zirconium species [NSiN]^{Dipp}Zr(BH$_4$)$_2$•THF (**8**) was obtained in moderate yield (69 %) as a colourless, moisture-senstive solid. While crystals of **8** suitable for X-ray diffraction studies were not able to be grown, the structure of **8** was inferred by NMR spectroscopy and elemental analysis. Specifically, the ^{11}B NMR spectrum of **8** yielded a well-defined pentet, suggesting that the coordination of the [BH$_4$]$^-$ anions to Zr is fluxional in solution, and that this process occurs quickly relative to the NMR timescale. In an attempt to remove BH$_3$ from the [BH$_4$]$^-$ anion and form reactive Zr-H units, two equivalents of the Lewis base 4-dimethylaminopyridine (DMAP) were added to a solution of **8** in Et$_2$O. In place of BH$_3$ removal from the borohydride ions however, direct THF/DMAP exchange with one equivalent of 4-dimethylaminopyridine (DMAP) displacing the previously bound THF molecule transpired, thus yielding [NSiN]^{Dipp}Zr(BH$_4$)$_2$•DMAP (**9**) after purification. Indeed the same product can be obtained cleanly upon addition of just one equivalent of DMAP to **8**.

Crystals of [NSiN]^{Dipp}Zr(BH$_4$)$_2$•DMAP (**9**) were obtained from a 1:1 mixture of toluene and hexanes (Figure 2.7), and the refined structure has two

η^3-coordinated BH_4^- groups linked to zirconium via inner-sphere Zr-H-B interactions in the solid state. These interactions bear remarkable similarity to those observed within the previously reported complex $Zr(BH_4)_4$, with similar Zr---B distances in **7** [2.372(3) and 2.378(3) Å] as the average Zr---B separations in $Zr(BH_4)_4$ [2.342(5) Å].[16] Haaland and coworkers reported the IR spectrum for $Zr(BH_4)_4$,[17] which showed a $\nu(B\text{-}H_{terminal})$ stretching band at 2560-2600 cm^{-1}, in addition to two $\nu(B\text{-}H_{bridging})$ vibrations in the 2090-2185 cm^{-1} range. The IR spectrum of compound **7** exhibits similar features with a sharp $\nu(B\text{-}H_{terminal})$ resonance at 2509 cm^{-1} along with two peaks at 2091 and 2189 cm^{-1} corresponding to $\nu(B\text{-}H_{bridging})$ stretching modes. As previously observed with compound **8**, the appearance of a pentet resonance for the $[BH_4]^-$ units in the ^{11}B NMR spectrum of **9** suggests that BH_4^- coordination is not static, and that each hydride can move between bridging (Zr-H-B) and terminal binding modes on the NMR timescale in solution.

With the above in mind efforts were made to convert $[NSiN]^{Dipp}ZrCl(\mu\text{-}Cl)_2Li(THF)_2$ **4** into the corresponding dihydride congener. The early attempts to generate a zirconium hydride complex were by the direct addition of soluble hydride sources to **4**. The addition of two equivalents of either $Li[HBEt_3]$ and $K[HB^sBu_3]$ to **4** yielded the protio ligand $H_2[NSiN]^{Dipp}$ (**1**) and the concomitant formation of the free boranes (BEt_3 or B^sBu_3) as the only detectable products by ^1H and ^{11}B NMR spectroscopy; the fate of the Zr is unknown in this instance.

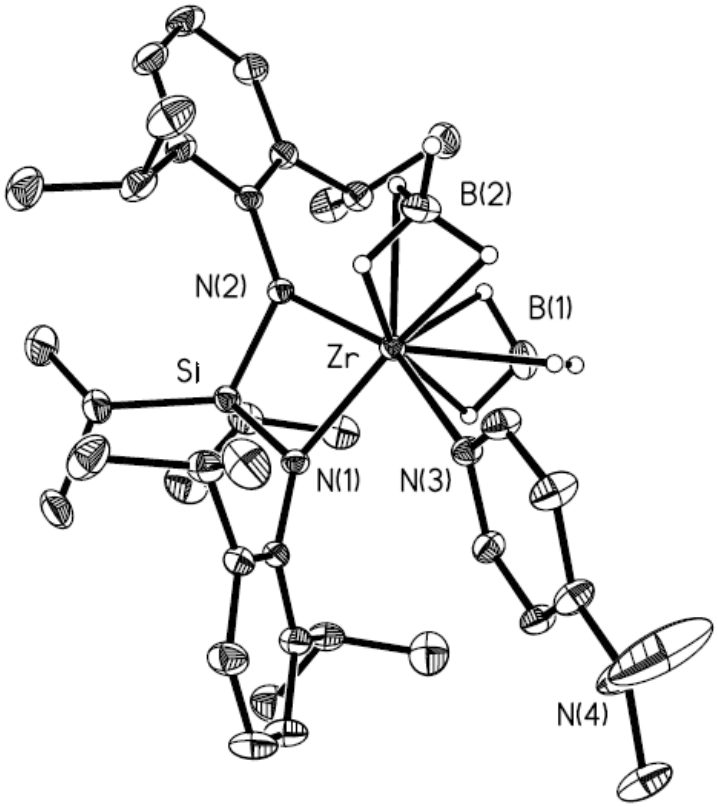

Figure 2.7. Molecular structure of $[NSiN]^{Dipp}Zr(BH_4)_2$•DMAP (**9**) with thermal ellipsoids presented at the 30 % probability level. All carbon-bound hydrogen atoms have been omitted for clarity. Selected bond lengths (Å) and angles (°): Zr–N(1) 2.0988(16), Zr–N(2) 2.0758(16), Zr–N(3) 2.3907(17), Zr---B(1) 2.372(3), Zr---B(2) 2.378(3); N(1)–Zr–N(2) 74.03(6), N(1)–Zr–N(3) 86.31(6), N(1)–Zr–B(1) 111.59(9), N(1)–Zr–B(2) 140.08(9), N(2)–Zr–N(3) 154.38(6), N(2)–Zr–B(1) 108.12(8), N(2)–Zr–B(2) 98.12(8), N(3)–Zr–B(1) 94.19(8), N(3)–Zr–B(2) 86.36(8), B(1)–Zr–B(2) 108.06(10).

In addition to the aforementioned work, we also attempted other routes to directly synthesize the Zr(IV)dihydride complex $[NSiN]^{Dipp}ZrH_2$. This was motivated by the recent work of Roesler and coworkers, who prepared the zirconocene complex, $[Cp_2Zr(H)NH_2BH_2(\mu\text{-}H)]$.[18] Later Manners and

coworkers showed that the structurally related Zr(III) complex [($Cp_2ZrPPh_2BH_2(\mu$-H)] bearing a similar Zr-H-B bridge can catalyse the dehydrocoupling of select amine-borane adducts.[13] Moreover the role of terminal zirconium hydride groups within the catalytic cycle of group(IV) metallocene mediated dehydrocoupling of amine-boranes was examined.[19]

Despite the predilection of this chemistry towards yielding mono-substituted species when THF is used as a solvent, the use of the MeLi as a source of the strongly nucleophilic methyl anion allows for the generation of both the neutral di-substituted $[NSiN]^{Dipp}ZrMe_2$•THF (**10**) and the tri-substituted zirconate $Li(THF)_4\{[NSiN]^{Dipp}ZrMe_3\}$ (**11**) complexes as colourless crystalline solids (Scheme 2.4). Crystals of **10** suitable for X-ray crystallography were grown from a solvent combination of toluene/hexanes at -35 °C (Figure 2.8).

This study identified the presence of a slightly distorted trigonal bipyramidal structure, with the NSiN chelate in **10** occupying one axial and one apical position [N(1)-Zr-N(2) angle = 75.69(4)°]. The adjacent N(1)-Zr-O angle of 162.24(4)° is significantly more narrow than the 180° angle that would be expected from an ideal trigonal bipyramid. Even with this structural distortion, the remaining equatorially arranged atoms are largely unperturbed with a sum of the equatorial bond angles at Zr of 358.66(6)°.

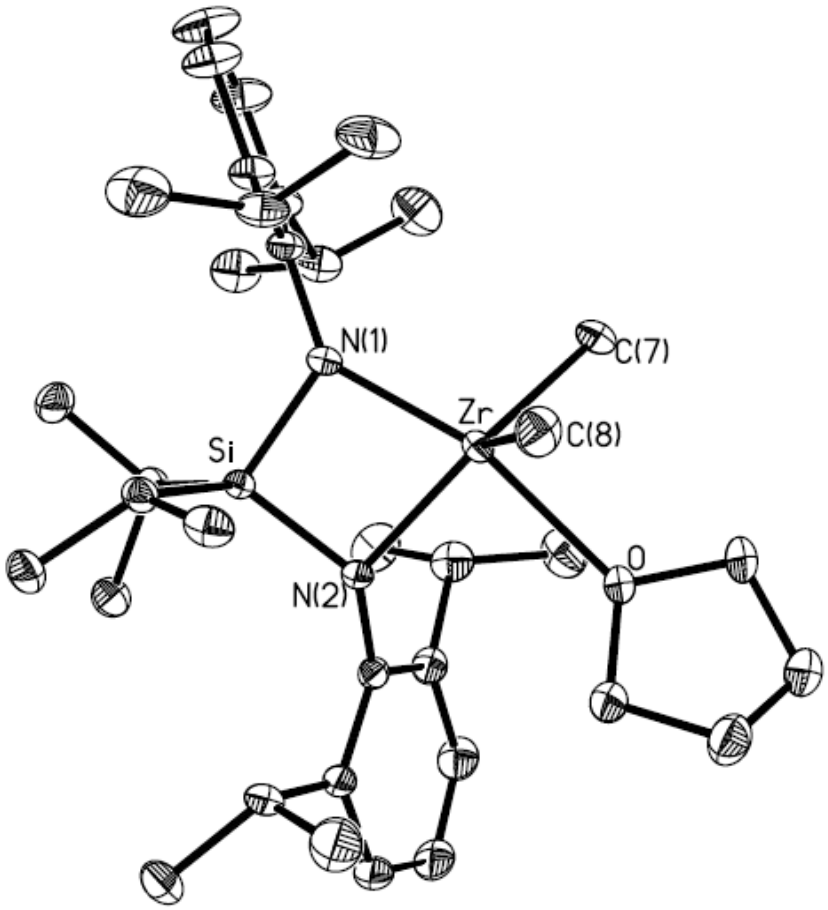

Figure 2.8. Molecular structure of $[NSiN]^{Dipp}ZrMe_2$•THF (**10**) with thermal ellipsoids presented at the 30 % probability level. All hydrogen atoms have been omitted for clarity. Selected bond lengths (Å) and angles (°): Zr–N(1) 2.0620(12), Zr–N(2) 2.1176(11), Zr–C(7) 2.2780(16), Zr–C(8) 2.2562(17), Zr–O 2.3215(11); N(1)–Zr–N(2) 75.69(4), N(1)–Zr–C(7) 102.17(6), N(1)–Zr–C(8) 107.44(6), N(1)–Zr–O 162.24(4), N(2)–Zr–C(7) 136.69(6), N(2)–Zr–C(8) 115.60(6), N(2)–Zr–O 87.65(4), C(7)–Zr–C(8) 106.37(7), C(7)–Zr–O 85.62(5), C(8)–Zr–O 85.14(6).

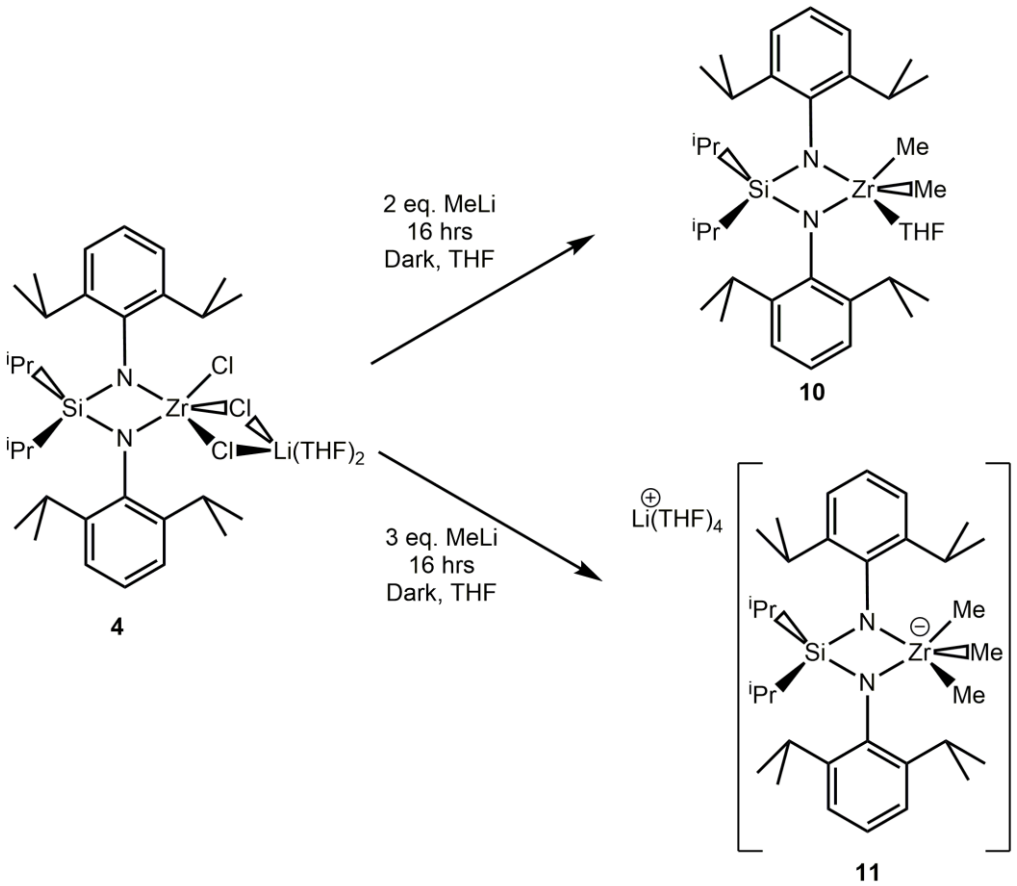

Scheme 2.4. Synthesis of dimethyl and trimethyl zirconium bis(amido)silyl complexes $[NSiN]^{Dipp}ZrMe_2$•THF (**10**) and $Li(THF)_4\{[NSiN]^{Dipp}ZrMe_3\}$ (**11**).

While evidence in the literature of alkyl zirconium complexes which facilitate the dehydrocoupling of amine-boranes could not be found, it was hypothesised that protonolysis of the methyl groups at Zr by an acidic N-H residue within the HNR_2•BH_3 adducts (with concomitant loss of CH_4) would provide clean access to catalytically active species of related stucture to **II** (Figure 2.1). One complication that was discovered was that compounds **10** and **11** proved to be sensitive to light, and allowing solutions of the complexes in Et_2O, THF or toluene to stir overnight while exposed to light resulted in the

formation of metallic precipitates and the recovery of only the protio ligand $H_2[NSiN]^{Dipp}$ (**1**) from the soluble fractions. As such, the preparations of **10** and **11** were performed in either scintillation vials or Schlenk flasks that had been completely wrapped in aluminum foil to exclude ambient light. Any attempts to handle solutions of pure **10** and **11** in the presence of ambient light, resulted in the rapid (< 30 min) decomposition of the starting compounds to $H_2[NSiN]^{Dipp}$ and presumably Zr metal. Allowing a C_6D_6 solution of **10** within a J-Young tube to be exposed to light for 48 hours revealed that in addition to free $H_2[NSiN]^{Dipp}$, both C_2H_6 and CH_4 were present, which suggests that this decomposition proceeds via reductive elimination, and possibly α-elimination pathways.[20] In addition, **10** and **11** proved to be thermally sensitive, which necessitated their storage in the dark at -35 °C. When compounds **10** and **11** were stored in the solid state at room temperature, the quantitative decomposition of these methylated complexes occurred over the course of a few days to yield the free protio ligand, $H_2[NSiN]^{Dipp}$ as the only soluble product identifiable by NMR spectroscopy; the mechanism for this thermolysis however remains as of yet unconfirmed. Attempts to generate $[NSiN]^{Dipp}ZrH_2$ via the hydrogenolysis of the methyl groups from both **10** and **11** using 1 atmosphere of H_2 at room temperature in an aluminium-foil covered Schlenk flask led once again to the formation of **1** as the only product as determined by ^{1}H NMR spectroscopy.

One alternate route to accessing a bis(dimethylamido)-substituted zirconium $[NSiN]^{Dipp}$ complex would be to pre-install the -NMe_2 groups at Zr

before ligation with $[DippNSi(^{i}Pr)_2NDipp]^{2-}$. Fortuitously, Kempe and coworkers described the conproportionation of $ZrCl_4$ and $Zr(NMe_2)_4$ in a diethyl ether/THF solvent mixture to afford the requisite precursor $Cl_2Zr(NMe_2)_2$•2THF.[21] In a subsequent step, this zirconium amide was combined with *in situ* generated $Li_2[NSiN]^{Dipp}$ to yield the bis(dimethylamido) analogue $[NSiN]^{Dipp}Zr(NMe_2)_2(\mu\text{-}Cl)Li(THF)_3$ (**12**) which again contained one equivalent of lithium chloride within the coordination sphere of zirconium (Equation 2.1, Figure 2.9).

As with many of the other compounds bearing the $[NSiN]^{Dipp}$ ligand, compound **12** adopts a pseudo trigonal bipyramidal geometry at zirconium with $Zr\text{-}N_{(NSiN\ ligand)}$ bond lengths of 2.143(2) and 2.152(2) Å, and a narrow N(1)-Zr-N(2) intraring angle of 73.30(8)° that is of similar value as observed within the abovementioned $[NSiN]^{Dipp}Zr$ chelates. It should be pointed out that the $Zr\text{-}N_{(NMe2)}$ bond lengths [2.068(3) Å avg.] are shorter than those observed for the $Zr\text{-}N_{(NSiN\ ligand)}$ linkages, which suggests that there are some additional Zr-N π-interactions present involving the $–NMe_2$ substituents. This is further supported by the sp^2 geometry around these nitrogen atoms [N(3) and N(4)], where the sum of all bond angles around N(3) and N(4) are 360.0(4)° and 359.7(4)°, respectively.

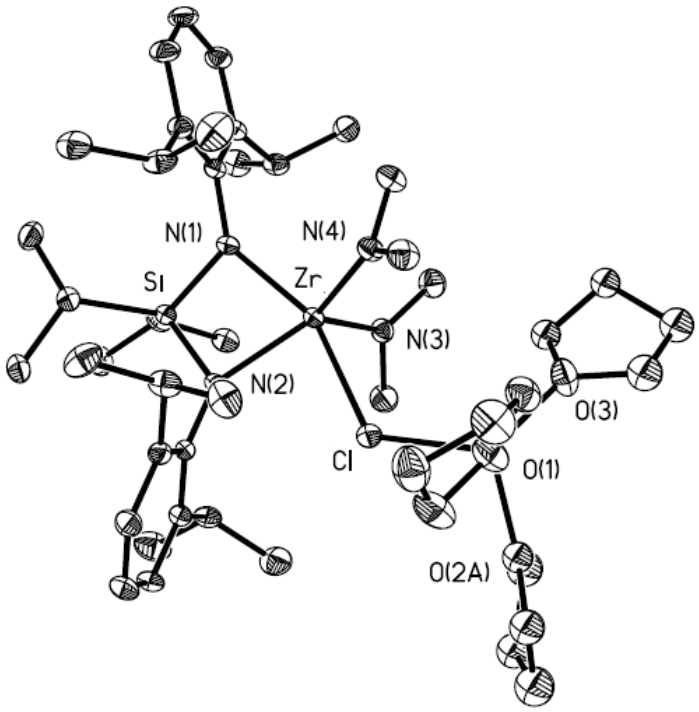

Figure 2.9. Molecular structure of $[NSiN]^{Dipp}Zr(NMe_2)_2(\mu\text{-}Cl)Li(THF)_3$ (**12**) with thermal ellipsoids presented at the 30 % probability level. All hydrogen atoms have been omitted for clarity. Selected bond lengths (Å) and angles (°): Zr–N(1) 2.143(2), Zr–N(2) 2.152(2), Zr–N(3) 2.067(2), Zr–N(4) 2.069(3), Zr–Cl 2.5999(8), Cl–Li 2.368(5); N(1)–Zr–N(2) 73.30(8), N(1)–Zr–N(3) 107.61(9), N(1)–Zr–N(4) 100.45(9), N(1)–Zr–Cl 154.29(6), N(2)–Zr–N(3) 113.08(9), N(2)–Zr–N(4) 139.80(9), N(2)–Zr–Cl 84.53(6), N(3)–Zr–N(4) 106.7(1), N(3)–Zr–Cl 92.80(7), N(4)–Zr–Cl 88.01(7).

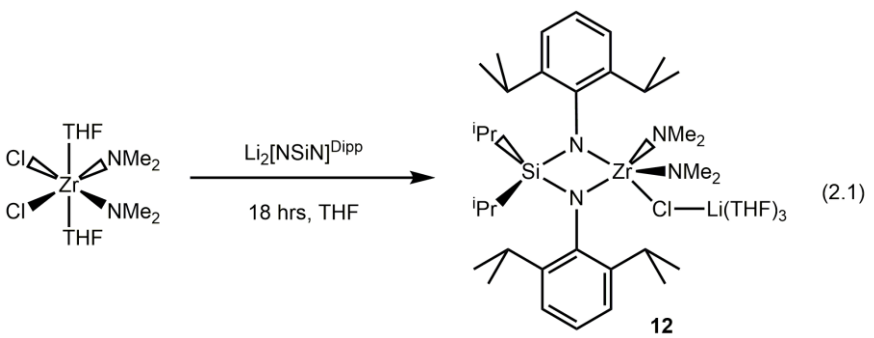

(2.1)

2.3.2 Dehydrocoupling chemistry mediated by bis(amido)silyl zirconium complexes

As has been previously mentioned, zirconium complexes show excellent promise as catalysts for promoting dehydrocoupling.[13,14] Many of these complexes exhibit polar covalent bonds with their ligands, which makes them prime candidates for the σ–bond metathesis steps likely involved during many dehydrogenative coupling processes. To begin, the ability of the dimethylated Zr complex $[NSiN]^{Dipp}ZrMe_2$·THF (**10**) to act as a dehydrogenation catalyst for amine-boranes was tested. As anticipated, this species was able to instigate the dehydrocoupling of Me_2NH•BH_3 in C_6D_6 at a 1 mol % catalyst loading; however the sensitivity of this species led to poor overall performance due to decomposition of the catalyst during the reaction. Specifically only *ca.* 20 % of the starting amine-borane was dehydrogenated before catalyst deactivation occurred. To further explore the ability of the reported Zr complexes to act as pre-catalysts for dehydrocoupling, compounds **1**, **4**, **10** and **11** were combined with Me_2NH•BH_3 in C_6D_6, however no catalysis was observed up to catalyst loadings of 5 mol%.

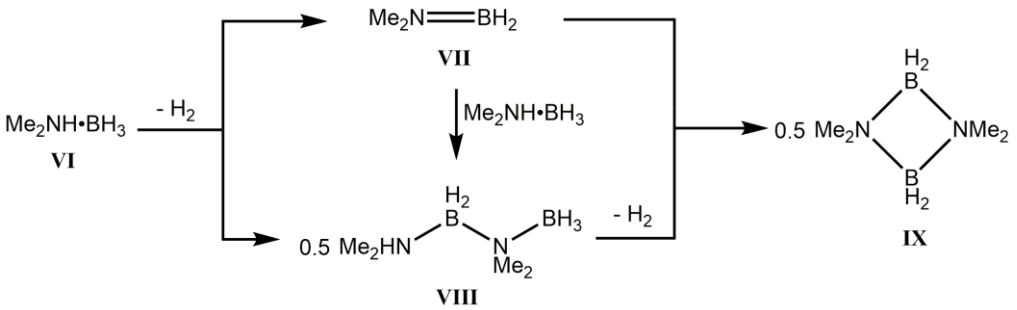

Scheme 2.5. Formation of observed products from the dehydrocoupling of dimethylamine-borane

In contrast to the poor catalytic activity of the methylated complex $[NSiN]^{Dipp}ZrMe_2$•THF (**10**), the dimethylamino-appended zirconacycle $[NSiN]^{Dipp}Zr(NMe_2)_2(\mu\text{-}Cl)Li(THF)_3$ (**12**) proved to be efficacious as a catalyst for the dehydrocoupling of Me_2NH•BH_3. Compound **12** was able to dehydrocouple Me_2NH•BH_3 (**VI**) into the known products $[Me_2N\text{-}BH_2]_2$ (**IX**) and $Me_2NH\text{-}BH_2\text{-}NMe_2\text{-}BH_3$ (**VIII**) (Schemes 2.5 and 2.6) with a turnover frequency of 420 hr^{-1} at a very low catalyst loading of 0.1 mol % in C_6D_6. Interestingly, using a 0.1 mol % vs. a 1 mol % catalyst loading led to a higher observed proportion of the linear product $Me_2NH\text{-}BH_2\text{-}NMe_2\text{-}BH_3$ being formed over the cyclic dimer $[Me_2N\text{-}BH_2]_2$. For example, when 1 mol % of catalyst was used, *ca*. 85 % of the product observed by ^{11}B NMR spectroscopy was that of the cyclic dimer $[Me_2N\text{-}BH_2]_2$ (**IX**), whereas with a 0.1 mol % catalyst loading, the linear dimer $Me_2NH\text{-}BH_2\text{-}NMe_2\text{-}BH_3$ (**VIII**) accounted for 90% of the product observed by ^{11}B NMR spectroscopy. The formation of the linear dimer has been attributed to on-metal bond-forming processes, and

suggests the possible formation of $[NSiN]^{Dipp}Zr(H)NMe_2BH_2(\mu\text{-}H)$ as an intermediate; a similar complex has been reported by Roesler and coworkers $Cp_2Zr(H)NMe_2BH_2(\mu\text{-}H)$.[18] The *in situ* generated $[NSiN]^{Dipp}Zr(H)NMe_2BH_2(\mu\text{-}H)$ might react with free $Me_2NH{\bullet}BH_3$ to generate the linear dimer, $Me_2NH\text{-}BH_2\text{-}NMe_2\text{-}BH_3$ and $[NSiN]ZrH_2$.

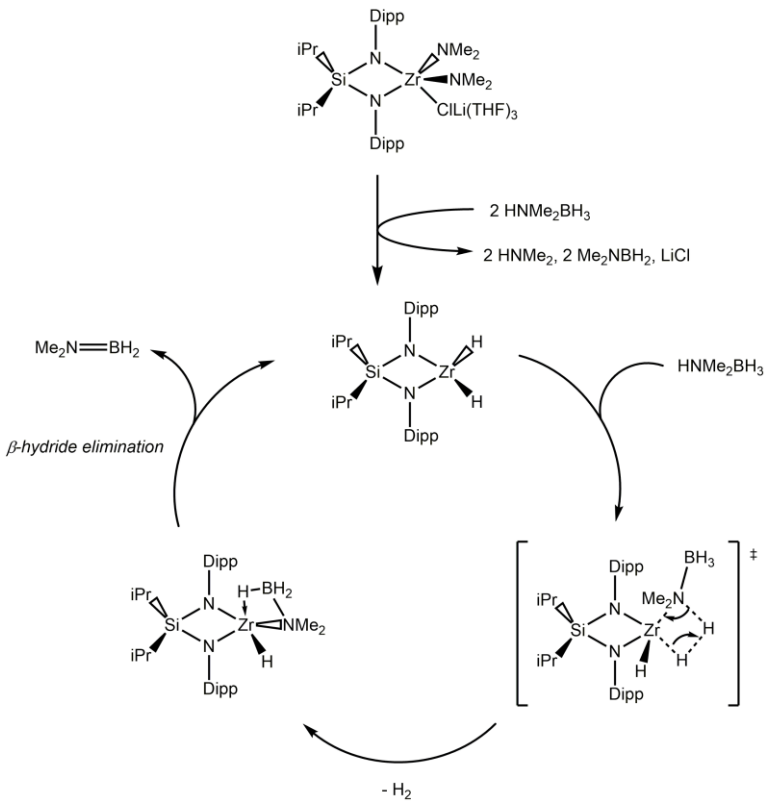

Scheme 2.6. Proposed catalytic cycle for the dehydrocoupling of $Me_2NH{\bullet}BH_3$ by **12**.

In addition, there may also be an off-metal process occurring whereby the aminoborane $Me_2N{=}BH_2$ (**VII**) reacts directly with another equivalent of $Me_2NH{\bullet}BH_3$, thus generating $Me_2NH\text{-}BH_2\text{-}NMe_2\text{-}BH_3$ (**VIII**) without the

need for a metal centre.[22] When the dehydrocoupling was performed in cyclohexene (a known substrate for transfer hydrogenation), the only observed product was the dimeric species $[Me_2NBH_2]_2$ (**IX**), with no trace of linear dimer Me_2NH-BH_2-NMe_2-BH_3 (**VIII**). Manners and coworkers[23] also noted that when the dehydrocoupling of $Me_2NH{\bullet}BH_3$ was performed in the presence of cyclohexene (one equivalent), $[Me_2NBH_2]_2$ (**IX**), was the only observed product by ^{11}B NMR spectroscopy. These results contrast what has been noted with $MeNH_2BH_3$, wherein the aminoborane generated via dehydrogenation, $MeNH{=}BH_2$, reacts with excess cyclohexene to yield $MeNH{=}BCy_2$.[24]

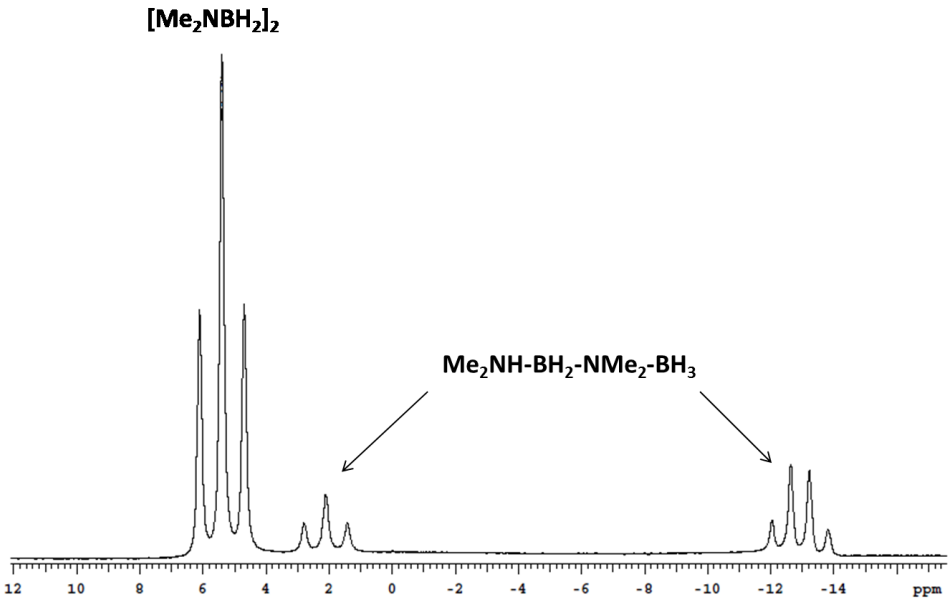

Figure 2.10. ^{11}B NMR spectrum (in C_6D_6) of the product mixture resulting from the dehydrocoupling of $Me_2NH{\bullet}BH_3$ (**VII**) after 1 hour at a 1 mol % catalyst loading of **12**.

A significant solvent dependance on the dehydrocoupling ability of compound **12** was also observed. For instance, the catalytic reactivity of **12** towards $Me_2NH•BH_3$ was quenched in THF, which is possibly due to the formation of $Li(THF)_4\{[NSiN]^{Dipp}Zr(NMe_2)_2(Cl)\}$ in solution, similar to what was observed for related $[NSiN]^{Dipp}Zr$ chelates. The generation of a formally anionic zirconium centre via strong ligation by Cl^- could inhibit the binding of incoming substrates, preventing catalysis from proceeding. This solvent dependence unfortunately decreases the available substrate scope, due to the low solubility of amine-boranes such as $H_3N•BH_3$ and $MeNH_2•BH_3$ in many aliphatic and aromatic solvents, as well as in less coordinating ethereal solvents such as diethyl ether; these solvents would be required to prevent the aforementioned zirconate salts from forming. Compound **12** was also found to be effective as a catalyst at between 0.1 and 1 mol % catalyst loadings for the dehydrocoupling of $^{i}Pr_2NH•BH_3$ in C_6D_6, leading to the quantitive generation of the known aminoborane $^{i}Pr_2N=BH_2$[13] as an isolable monomeric species with a distinct ^{11}B NMR triplet resonance at 35.0 ppm. The catalytic dehydrocoupling of $^{i}Pr_2NH•BH_3$ with **12** as a catalyst proceeded with a slightly lower average TOF [220 hr^{-1}] in relation to $Me_2NH•BH_3$ [420 hr^{-1}] as determined over three catalytic trials, likely due to the more hindered nature of the ^{i}Pr-substituted amine-borane. In addition, the dehydrocoupling of the primary amine borane complexes methylamine-borane and ^{n}butylamine-borane was also explored. In the case of $MeNH_2•BH_3$, no catalysis transpired due to the inherent insolubility of this adduct in benzene.

In the case of the hydrocarbon soluble amine-borane $^{n}BuNH_2 \bullet BH_3$, dehydrocoupling was observed at a moderate rate [TOF = ca. 58 hr^{-1}] with a 0.5 mol % catalyst loading of **12**, and proceeded to 87 % completion. ^{11}B NMR spectroscopy revealed the formation of multiple products: the main components of which were identified as $[^{n}BuNBH]_3$ (16 %), $[^{n}BuNH\text{-}BH_2]_3$ (60 %) and unreacted $^{n}BuNH_2 \bullet BH_3$ (13 %);[25] the remaining products were made up by unidentified broad singlets at +22.1 ppm (2 %) and +18.3 ppm (5 %), in addition to a quartet resonance at -13.6 ppm (2 %). The dehydrocoupling of $^{n}BuNH_2 \bullet BH_3$ was also performed without any additional solvent, and similar results to those observed in concentrated C_6D_6 solution were noted.

In an attempt to further address the role of solvent in our catalysis, the dehydrocoupling of $^{i}Pr_2NH \bullet BH_3$ was also attempted in CD_2Cl_2, however only a small number of turnovers (< 50) were achieved before catalyst deactivation occurred, thus halting the conversion of the amine-borane into the corresponding aminoborane. Despite this deactivation, compound **12** is stable for long periods of time in CH_2Cl_2; a sample of **12** stirred at room temperature for 72 hours displayed no sign of degradation by ^{1}H NMR spectroscopy. This would suggest that the catalytically active species, presumably a zirconium hydride, is reactive towards chlorinated solvents, as has been reported in the past.[26]

2.3.3 Formation and reactivity of a zirconium complex featuring a bis(amido)silyl "umbrella" ligand

Another goal of this work was the synthesis of a zirconium compound featuring one of the larger "umbrella" ligands, and as such we began by utilising the previously described $[(Ph_3SiN)_2Si^iPr_2]^{2-}$ ligand (referred to herein as $[NSiN]^{SiPh3}$).[10a] By employing methodology similar to that described previously for the related $[NSiN]^{Dipp}$ ligand (**1**), we were able to install the desired ligand onto zirconium in reasonable yield.

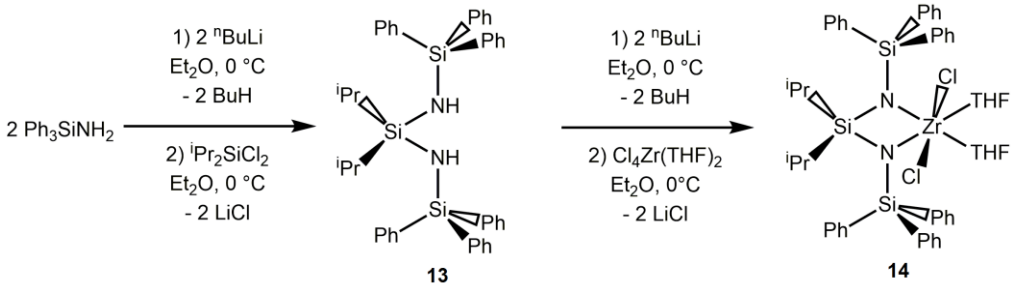

Scheme 2.7 Synthesis of protio ligand $H_2[NSiN]^{SiPh3}$ (**13**) and the zirconium complex $[NSiN]^{SiPh3}ZrCl_2(THF)_2$ (**14**).

X-ray crystallographic analysis of **14** revealed (Figure 2.11), somewhat to our surprise, an octahedral complex of zirconium, featuring two equivalents of THF within the coordination sphere of zirconium; this bears a discernible similarity to $[(DippN)_2SiMe_2]ZrCl_2(THF)_2$ reported by Hill and coworkers.[15a] This is quite different to what was observed when utilising the $[NSiN]^{Dipp}$ ligand, which showed the coordination of one molecular equivalent of LiCl within the coordination sphere of Zr. This suggests that while the $-SiPh_3$ unit

is more sterically demanding than the –Dipp group, the directionality of this bulk is different, with the $SiPh_3$ projecting in a cone-shape away from the metal, and the ortho-isopropyl groups of the Dipp moiety projecting into the metal, thus creating localised crowding of the metal centre.

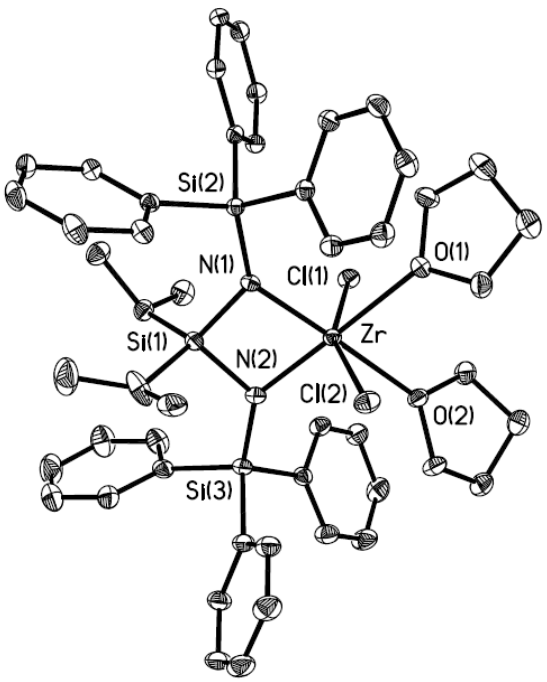

Figure 2.11 Molecular structure of $[NSiN]^{SiPh3}ZrCl_2(THF)_2$, (**14**) with thermal ellipsoids presented at the 30% probability level. All hydrogen atoms have been omitted for clarity. Selected bond lengths (Å) and angles (°): Zr–N(1) 2.078(2), Zr–N(2) 2.055(2), Zr–Cl(1) 2.4657(7), Zr–Cl(2) 2.4588(7), Zr–O(1) 2.3425(18), Zr–O(2) 2.3328(17); N(1)–Zr–N(2) 78.70(8), N(1)–Zr–Cl(1) 98.06(6), N(1)–Zr–Cl(2) 101.55(6), N(1)–Zr–O(1) 100.15(7), N(1)–Zr–O(2) 177.18(7), N(2)–Zr–Cl(1) 99.05(6), N(2)–Zr–Cl(2) 98.24(6), N(2)–Zr–O(1) 178.79(7), N(2)–Zr–O(2) 98.93(5),

We found that while the addition of the desired ligand to zirconium proceeded smoothly, attempts to further substitute the chloride with other groups via reaction with $LiBH_4$, $LiNMe_2$ and MeLi did not as yet yield any

clean products, whether the reaction was run in Et_2O, THF or toluene. In addition to this, the reaction of in situ generated $Li_2[NSiN]^{SiPh3}$ with $Cl_2Zr(NMe_2)_2(THF)_2$ also yielded multiple products. Further work in this area will focus on modifying the reaction conditions to yield clean mono- and di-substituted Zr complexes bearing the $[NSiN]^{SiPh3}$ chelate.

2.4 Conclusions

In conclusion, a variety of zirconium complexes featuring the sterically encumbered dianionic bis(amido)silyl ligand $[DippNSi(^iPr)_2NDipp]^{2-}$ were synthesised. This ligand is sufficiently bulky to suppress the formation of dimeric zirconium complexes (via Zr-E-Zr bridges; E = N or Cl). One drawback of these systems is their proclivity to bind halide ions from the LiCl by-product to yield five-coordinate zirconate complexes which, when allowed to form the corresponding zirconate salts in THF, are generally unreactive towards dehydrocoupling due to coordinative saturation. Effective dehydrocoupling catalysis mediated by one $[NSiN]^{Dipp}$ supported complex $[NSiN]^{Dipp}Zr(NMe_2)_2(\mu\text{-}Cl)Li(THF)_3$ (**12**) was noted with catalytic activity superior to that of analogous zirconocene complexes. Encouraged by these results, we are continuing to investigate the reactivity of tethered bis(amido)zirconium complexes with respect to catalysis.

2.5 Experimental procedures

2.5.1. General.

All reactions were performed using standard Schlenk techniques under an atmosphere of nitrogen or in a nitrogen-filled glovebox (Innovative Technology, Inc.). Solvents were dried using a Grubbs-type solvent purification system manufactured by Innovative Technology, Inc., degassed, and stored under an atmosphere of nitrogen prior to use.[27] Zirconium tetrachloride, tetrakis(dimethylamido)zirconium, *n*-butyl lithium (2.5 M solution in hexanes), methyl lithium (1.6 M solution in diethyl ether), borane-tetrahydrofuran (1.0 M solution in tetrahydrofuran), lithium borohydride, 4-dimethylamidopyridine (DMAP), chlorotrimethyltin, dichlorodimethyltin, lithium dimethylamide, and borane-dimethylamine ($Me_2NH{\bullet}BH_3$), $Li[HBEt_3]$ (1.0 M solution in THF) and $K[H^sBBu_3]$ (1.0 M solution in THF) were purchased from Aldrich and used as received. ^{n}Butylamine was purchased from Aldrich, dried over molecular sieves and distilled prior to use. 2,6-Diisopropylaniline was purchased from VWR and used as received. Dichlorodiisopropylsilane was obtained from Gelest, degassed (freeze-pump-thaw), and stored over molecular sieves under an N_2 atmosphere prior to use. $MeNH_2{\bullet}BH_3$,[28] $^iPr_2NH{\bullet}BH_3$,[29] $^nBuNH_2{\bullet}BH_3$,[23] $Cl_2Zr(NMe_2)_2(THF)_2$,[21] and $Cl_4Zr{\bullet}2THF$[30] were prepared according to literature procedures. ^1H, $^{13}C\{^1H\}$, $^{11}B\{^1H\}$, ^{11}B NMR and $^{119}Sn\{^1H\}$ spectra were recorded on a Varian Inova-

400 or Varian Inova-500 spectrometer and referenced externally to $SiMe_4$ (^1H, $^{13}C\{^1H\}$), $F_3B{\bullet}OEt_2$ and $SnMe_4$ respectively. Elemental analyses were performed by the Analytical and Instrumentation Laboratory at the University of Alberta. Infrared spectra were recorded using Nic-Plan FTIR microscope. Melting points were obtained in sealed glass capillaries under nitrogen using a MelTemp melting point apparatus and are uncorrected.

2.5.2 X-ray Crystallography

Crystals of appropriate quality for X-ray diffraction studies were removed either from a Schlenk tube under a stream of nitrogen or a vial (glovebox) and immediately covered with a thin layer of hydrocarbon oil (Paratone-N). A suitable crystal was then selected, attached to a glass fibre, and quickly placed in a low-temperature stream of nitrogen.[31] All data were collected using a Bruker APEX II CCD detector/D8 diffractometer using Mo Kα or Cu Kα radiation, with the crystal cooled to −100 °C. Refinements were completed using the program SHELXL-97.[32] Hydrogen atoms were assigned positions based on the sp^2 or sp^3 hybridisation geometries of their attached carbon or nitrogen atoms and were given thermal parameters 20 % greater than those of their parent atoms. See Tables 2.1 to 2.4 for a listing of relevant crystallographic data. For compound **2a**, The O2–C55, O2–C58A and O2–C58B distances were restrained to be the same using the SHELXL SADI instruction. Likewise, the C56–C57A and C56–C57B distances were restrained to be the same. For **4**, restraints were applied to distances within the

disordered tetrahydrofuran ligands of the $[Li(OC_4H_8)_4]^+$ ion: d(O3–C71A) = d(O3–C74A) = d(O3–C71B) = d(O3–C74B) = d(O4–C84A) = d(O4–C84B) = 1.46(1) Å; d(C71A–C72A) = d(C72A–C73A) = d(C73A–C74A) = d(C71B–C72B) = d(C72B–C73B) = d(C73B–C74B) = d(C81–C82A) = d(C82A–C83A) = d(C83A–C84A) = d(C81–C82B) = d(C82B–C83B) = d(C83B–C84B) = 1.52(1) Å; d(O3···C72B) = d(O3···C73B) = 2.34(1) Å; d(C71B···C74B) = 2.38(1) Å; d(C71A···C73A) = d(C71B···C73B) = 2.46(1) Å. For **5**, the B–H and H···H distances within the tetrahydroborate ligand were restrained during refinement: d(B–H1BA) = d(B–H1BB) = d(B–H1BC) = d(B–H1BD) = 1.10(1) Å; d(H1BA···H1BB) = d(H1BA···H1BC) = d(H1BA···H1BD) = d(H1BB···H1BC) = d(H1BB···H1BD) = d(H1BC···H1BD) = 1.79(1) Å. For **7**, the coordinated BH_4 groups were restrained to have approximately equal B–H distances and approximately tetrahedral H–B–H angles. For **10**, restraints were applied to distances within the inversion-disordered solvent tetrahydrofuran molecule during refinement: d(O1S–C1S) = d(O1S–C4S) = 1.46(1) Å; d(C1S–C2S) = d(C2S–C3S) = d(C3S–C4S) = 1.52(1) Å.

2.5.3 Synthetic procedures

2.5.3.1 Synthesis of $Li_2[NSiN]^{Dipp}$•3THF (2b)

Compound **1** (0.163 g, 0.35 mmol) was dissolved in 5 mL of hexanes, and this solution was cooled to -35 °C. To this solution was added ^{n}BuLi (2.5

M solution in hexanes, 280 μL, 0.70 mmol), and stirring of the mixture for 30 min resulted in the formation of a white slurry. THF (1 mL) was then added, followed by stirring for 30 min to yield a pale yellow solution. The volume of the solution was then concentrated to ca. 2 mL *in vacuo*, and subsequent cooling to – 35 °C resulted in the formation of colourless crystals of suitable quality for X-ray analysis. This analysis revealed the presence of the mixed dilithio adduct, $Li(THF)_4\{[NSiN]^{Dipp}Li(THF)_2\}$. These crystals rapidly released THF upon exposure to vacuum to yield a pure material containing three equivalents of THF per $[NSiN]^{Dipp}$ ligand. Yield of $\{Li_2[NSiN]^{Dipp}\bullet 3THF$ = 0.238 g (0.34 mol, 98 %). ^{1}H NMR (C_6D_6, 300 MHz): δ 1.18 (m, 12H, THF), 1.35 (d, 24H, ArCH(CH_3)$_2$, $^3J_{HH}$ = 6.9 Hz), 1.36 (d, 12H, SiCH(CH_3)$_2$, $^3J_{HH}$ = 7.2 Hz), 1.56 (septet, 2H, SiCH(CH$_3$)$_2$, $^3J_{HH}$ = 7.2 Hz), 3.24 (m, 12H, THF), 4.04 (septet, 4H, ArCH(CH_3)$_2$, $^3J_{HH}$ = 6.9 Hz), 6.90 (t, 2H, p-ArH, $^3J_{HH}$ = 6.9 Hz), 7.24 (d, 4H, CH(CH_3)$_2$, $^3J_{HH}$ = 6.9 Hz); ^{13}C{^{1}H} NMR (C_6D_6, 126 MHz): δ 20.9 (SiCH(*C*H$_3$)$_2$), 21.9 (Si*C*H(CH$_3$)$_2$), 25.1 (Ar*C*H(CH$_3$)$_2$), 25.5 (THF), 27.4 (ArCH(*C*H$_3$)$_2$), 68.1 (THF), 115.1 (Ar*C*), 123.3 (Ar*C*), 141.7 (Ar*C*), 151.7 (Ar*C*). Mp (°C): 132-134. Anal. Calcd. for $C_{42}H_{72}O_3N_2Li_2Si$: C, 72.58; H, 10.44; N, 4.03. Found: C, 72.54; H, 10.41; N, 4.03.

2.5.3.2 Synthesis of $[NSiN]^{Dipp}SnMe_2$ (3)

To a pale yellow solution of Li_2[NSiN]Dipp·3THF (0.176 g, 0.253 mmol) in 5 mL of Et_2O at -35°C was added a colourless solution of Me_3SnCl (0.101 g, 0.507 mmol) in 3 mL of Et_2O, drop-wise over one minute.

Immediately upon addition of Me_3SnCl, the solution turned bright lemon yellow, with the colour disappearing to give a colourless solution along with white precipitate within one minute of final addition. The mixture was stirred overnight, and then filtered through Celite to remove the insoluble solid. Finally, the resulting filtrate was concentrated *in vacuo* until the appearance of crystals (*ca*. 3 mL solvent removed), and then cooled to -35 °C overnight to yield colourless X-ray quality crystals (0.102 g, 65 %). ^{1}H NMR (C_6D_6, 500 MHz): δ 0.51 (s with satellites, 6H, Sn(CH_3)$_2$), 1.10 (d, 12H, SiCH(CH_3)$_2$, $^3J_{HH}$ = 7.5 Hz), 1.31 (d, 24H, ArCH(CH_3)$_2$, $^3J_{HH}$ = 6.9 Hz), 1.56 (sept, 2H, SiC*H*Me$_2$, $^3J_{HH}$ = 7.5 Hz), 4.22 (sept, 4H, ArC*H*Me$_2$, $^3J_{HH}$ = 6.9 Hz), 7.08-7.19 (m, 6H, Ar*H*). ^{13}C{^{1}H} NMR (C_6D_6, 126 MHz): δ 3.0 (Sn(*C*H$_3$)$_2$), 19.2 (ArCH(*C*H$_3$)$_2$), 19.8 (SiCH(*C*H$_3$)$_2$), 23.3 (Si*C*H(Me$_2$), 27.6 (Ar*C*H(Me$_2$), 123.1 (Ar*C*), 123.4 (Ar*C*), 143.6 (Ar*C*), 146.4 (Ar*C*). ^{119}Sn{^{1}H} NMR (C_6D_6, 186 MHz): δ 90.7 ([NSiN]^{Dipp}*Sn*Me$_2$). Mp (°C): 213-218. Anal. Calcd. for $C_{32}H_{54}N_2SiSn$: C, 62.64; H, 8.87; N, 4.57. Found: C, 62.83; H, 9.01; N, 4.61.

2.5.3.3 Synthesis of [NSiN]^{Dipp}Ge;[10a] metallocycle transfer reaction between [NSiN]^{Dipp}SnMe$_2$ and GeCl$_2$•dioxane (confirmed by ^{1}H NMR)

To a solution of [NSiN]^{Dipp}SnMe$_2$ (0.094 g, 0.15 mmol) in 3 mL of Et_2O was added a solution of Cl_2Ge•dioxane (0.035 g, 0.15 mmol) in 4 mL of Et_2O. The resulting mixture was allowed to stir for 16 hours, and then the volatiles were removed *in vacuo* to yield [NSiN]^{Dipp}Ge as a white solid (0.053 g, 65 %), with ^{1}H NMR spectrum being consistent with the literature.[10a]

2.5.3.4 Synthesis of $[NSiN]^{Dipp}ZrCl(\mu\text{-}Cl)_2Li(THF)_2$ (4)

To a white suspension of $H_2[NSiN]^{Dipp}$ (0.998 g, 2.14 mmol) in 15 mL of Et_2O at -35 °C was added *n*-butyl lithium (2.5 M solution in hexanes, 1.71 mL, 4.28 mmol) and the resultant pale yellow solution was allowed to stir for 1 hour. This solution was then added to a suspension of $ZrCl_4$•2THF (0.806 g, 2.14 mmol) in 25 mL of Et_2O to yield an orange solution along with a white precipitate. The mixture was stirred for 20 hours, and then filtered. The volatiles were removed from the filtrate, and the resulting crude solid was then extracted into a minimum volume of Et_2O (3 mL) and cooled to -35 °C overnight to give colourless X-ray quality crystals of **4** (1.20 g, 69 %). ^{1}H NMR (C_6D_6, 500 MHz): δ 1.10 (d, 12H, SiCH(CH_3)$_2$, $^3J_{HH}$ = 7.6 Hz), 1.15 (m, 8H, THF *β*–CH_2), 1.37 (d, 12H, ArCH(CH_3)$_2$, $^3J_{HH}$ = 7.6 Hz), 1.45 (d, 12H, ArCH(CH_3)$_2$, $^3J_{HH}$ = 7.6 Hz), 1.56 (sept, 2H, SiC*H*(CH$_3$)$_2$, $^3J_{HH}$ = 7.6 Hz), 3.48 (m, 8H, THF *α*–CH_2), 3.79 (sept, 4H, ArC*H*(CH$_3$)$_2$, $^3J_{HH}$ = 6.8 Hz), 7.00-7.13 (m, 6H, Ar*H*). ^{13}C{^{1}H} NMR (C_6D_6, 126 MHz): δ 17.0 (Si*C*H(CH$_3$)$_2$), 19.1 (SiCH(*C*H$_3$)$_2$), 24.5 (ArCH(*C*H$_3$)$_2$), 25.0 (ArCH(*C*H$_3$)$_2$), 27.1 (*βC*-THF), 29.3 (Ar*C*H(CH$_3$)$_2$), 65.9 (*αC*-THF), 124.2 (p-Ar-*C*), 124.3 (m-Ar-*C*), 142.1 (o-Ar-*C*), 146.7 (ipso-Ar-*C*). Mp (°C): 131-134 (dec). Anal. Calcd. for $C_{38}H_{64}Cl_3LiN_2O_2SiZr$: C, 56.10; H, 7.93; N, 3.44. Found: C, 56.51; H, 7.99; N, 3.27.

2.5.3.5 Synthesis of $Li(THF)_4\{[NSiN]^{Dipp}ZrCl_3\}$ (5)

To a pale yellow solution of $[NSiN]^{Dipp}ZrCl(\mu\text{-}Cl)_2Li(THF)_2$ (0.102 g, 0.125 mmol) in 5 mL of Et_2O was added THF (4.45 g, 61.6 mmol) and the resultant pale yellow solution was allowed to stir for 1 hour. The volatiles were removed from the filtrate, and the resulting white solid was then washed with 2 × 2 mL of hexanes to yield **5** as an off-white powder (0.115 g, 96 %). ^{1}H NMR (C_6D_6, 500 MHz): δ 1.12 (d, 12H, SiCH(C*H*$_3$)$_2$, $^3J_{HH}$ = 8.0 Hz), 1.30 (broad s, 16H, THF *β*–C*H*$_2$), 1.39 (d, 12H, ArCH(C*H*$_3$)$_2$, $^3J_{HH}$ = 6.5 Hz), 1.47 (d, 12H, ArCH(C*H*$_3$)$_2$, $^3J_{HH}$ = 6.5 Hz), 1.58 (sept, 2H, SiC*H*(CH$_3$)$_2$, $^3J_{HH}$ = 7.0 Hz), 3.56 (broad s, 16H, THF *α*–C*H*$_2$), 3.83 (sept, 4H, ArC*H*(CH$_3$)$_2$, $^3J_{HH}$ = 6.8 Hz), 7.03 (t, 2H, Ar*H*, $^3J_{HH}$ = 8.0 Hz), 7.13 (d, 4H, Ar*H*, $^3J_{HH}$ = 8.0 Hz). ^{13}C{^{1}H} NMR (C_6D_6, 126 MHz): δ 17.3 (Si*C*H(CH$_3$)$_2$), 19.8 (SiCH(*C*H$_3$)$_2$), 25.0 (ArCH(*C*H$_3$)$_2$), 25.6 (ArCH(*C*H$_3$)$_2$), 28.2 (*β*C-THF), 30.1 (Ar*C*H(CH$_3$)$_2$), 68.9 (*α*C-THF), 124.0 (p-Ar-*C*), 124.4 (m-Ar-*C*), 141.8 (o-Ar-*C*), 148.7 (ipso-Ar-*C*). Mp (°C): 201-204. Anal. Calcd. for $C_{46}H_{80}Cl_3LiN_2O_4SiZr$: C, 57.69; H, 8.42; N, 2.92. Found: C, 56.28; H, 8.03; N, 3.11.

2.5.3.6 Synthesis of $Li(THF)_4\{[NSiN]^{Dipp}ZrCl_2(NMe_2)\}$ (6)

To a suspension of $LiNMe_2$ (0.027 g, 0.52 mmol) in 3 mL of Et_2O at -35 °C was added a solution of $[NSiN]^{Dipp}ZrCl(\mu\text{-}Cl)_2Li(THF)_2$ (0.2090 g, 0.257 mmol) in 3 mL of Et_2O. The resultant mixture was stirred for 18 hours, and then filtered. Removal of the solvent from the filtrate *in vacuo* gave **4** as

an off-white powder. This product was then dissolved in 2 mL of toluene, and the solution stored at -35 °C for three days to yield X-ray quality crystals of **6** (0.076 g, 31 %). ^{1}H NMR (C_6D_6, 400 MHz): δ 1.16 (d, 12H, SiCH(CH_3)$_2$, $^{3}J_{HH}$ = 7.6 Hz), 1.36 (broad d, 24H, ArCH(CH_3)$_2$, $^{3}J_{HH}$ = 6.0 Hz), 1.64 (sept, 2H, SiCH(CH$_3$)$_2$, $^{3}J_{HH}$ = 7.6 Hz), 2.71 (s, 6H, ZrN(CH_3)$_2$), 3.15 (m, 16H, THF β–CH_2), 3.97 (sept, 4H, ArCH(CH$_3$)$_2$, $^{3}J_{HH}$ = 6.8 Hz), 7.04 (t, 2H, p-ArH, $^{3}J_{HH}$ = 7.6 Hz), 7.18 (d, 4H, m-ArH, $^{3}J_{HH}$ = 7.6 Hz). ^{13}C{^{1}H} NMR (C_6D_6, 126 MHz): δ 19.9 (SiCH(CH$_3$)$_2$), 20.3 (SiCH(CH$_3$)$_2$), 24.2 (ArCH(CH$_3$)$_2$), 26.2 (ArCH(CH$_3$)$_2$), 28.1 (O-CH$_2$-CH$_2$), 44.0 (ZrN(CH$_3$)$_2$), 69.1 (O-CH$_2$-), 122.1 (p-Ar-C), 123.9 (m-Ar-C), 142.6 (o-Ar-C), 150.4 (ipso-Ar-C). Mp (°C): 126-128. Anal. Calcd. for $C_{48}H_{86}Cl_2LiN_3O_4SiZr$: C, 59.66; H, 8.97; N, 4.35. Found: C, 58.81; H, 8.41; N, 4.19.

2.5.3.7 Synthesis of Li(THF)$_4${[NSiN]^{Dipp}ZrCl$_2$(BH$_4$)} (7)

To a suspension of Li[BH$_4$] (5.8 mg, 0.27 mmol) in 4 mL of Et$_2$O at -35 °C was added a solution of [NSiN]^{Dipp}ZrCl(μ-Cl)$_2$Li(THF)$_2$ (0.1080 g, 0.133 mmol) in 3 mL of Et$_2$O. The resultant pale yellow suspension was stirred for 18 hours, and then filtered through Celite, and the volatiles removed from the filtrate *in vacuo* to yield a white solid. This solid was recrystallised from hexanes at -35 °C to give **7** (0.0898 g, 72 %) as colourless X-ray quality crystals. ^{1}H NMR (C_6D_6, 500 MHz): δ 1.11 (d, 12H, SiCH(CH_3)$_2$, $^{3}J_{HH}$ = 7.6 Hz), 1.29 (m, 16H, THF α–CH_2), 1.39 (broad d, 24H, ArCH(CH_3)$_2$, $^{3}J_{HH}$ = 6.0 Hz), 1.54 (sept, 2H, SiCH(CH$_3$)$_2$, $^{3}J_{HH}$ = 7.6 Hz), 3.47 (m, 16H, THF β–CH_2),

3.95 (sept, 4H, ArC*H*$(CH_3)_2$, $^3J_{HH}$ = 6.8 Hz), 7.02 (t, 2H, p-Ar*H*, $^3J_{HH}$ = 6.8 Hz), 7.11 (d, 4H, m-Ar*H,* $^3J_{HH}$ = 6.8 Hz). $^{13}C\{^1H\}$ NMR (C_6D_6, 126 MHz): δ 16.9 (Si*C*H$(CH_3)_2$), 19.4 (Si*C*H$(CH_3)_2$), 25.2 (ArCH(*C*$H_3)_2$), 25.8 (*βC*-THF), 28.4 (ArCH(*C*$H_3)_2$), 70.7 (*αC*-THF), 123.9 (p-Ar*C*), 124.4 (m-Ar*C*), 141.6 (o-Ar*C*), 148.9 (ipso-Ar*C*). ^{11}B NMR (C_6D_6, 160 MHz): δ -16.5 (pentet, $^1J_{BH}$ = 80 Hz). Mp (°C): 158-163. Despite multiple attempts, satisfactory analyses were not obtained; see Figures 2.12-2.14 for NMR the corresponding spectra.

2.5.3.8 Synthesis of $[NSiN]^{Dipp}Zr(BH_4)_2(THF)$ (8)

Compound **4** (0.403 g, 0.495 mmol) was dissolved in 4 mL of Et_2O to form a colourless solution. This solution was added to a suspension of lithium borohydride (15.0 mg, 0.68 mmol) in 6 mL of Et_2O. The resultant mixture was stirred for 20 hours, and then filtered through Celite. The volatiles were removed from the filtrate *in vacuo* to yield **8** as a white solid (0.223 g, 69 %). $^1H\{^{11}B\}$ NMR (C_6D_6, 500 MHz): δ 0.99 (m, 4H, THF α–C*H*$_2$), 1.09 (d, 12H, SiCH(C*H*$_3)_2$, $^3J_{HH}$ = 7.5 Hz), 1.37 (d, 24H, ArCH(C*H*$_3)_2$, $^3J_{HH}$ = 6.5 Hz), 1.55 (sept, 2H, SiC*H*$(CH_3)_2$, $^3J_{HH}$ = 7.5 Hz), 3.37 (m, 4H, THF *β*–C*H*$_2$), 3.92 (sept, 4H, ArC*H*$(CH_3)_2$, $^3J_{HH}$ = 6.5 Hz), 7.02 (t, 2H, p-Ar*H*, $^3J_{HH}$ = 7.5 Hz), 7.10 (d, 4H, m-Ar*H*, $^3J_{HH}$ = 7.5 Hz). $^{13}C\{^1H\}$ NMR (C_6D_6, 126 MHz): δ 17.0 (SiCH(*C*$H_3)_2$), 19.3 (ArCH(*C*$H_3)_2$), 24.7 (*βC*-THF), 25.8 (ArCH(*C*$H_3)_2$), 28.3 (Ar*C*H$(CH_3)_2$), 73.2 (*αC*-THF), 124.0 (p-Ar*C*), 124.3 (m-Ar*C*), 141.9 (o-Ar-*C*), 149.0 (ipso-Ar*C*). ^{11}B NMR (C_6D_6, 160 MHz): δ –16.0 (pentet, $^1J_{HB}$ = 79 Hz). IR (Nujol/cm^{-1}): 2078 ν(B-$H_{bridging}$), 2190 ν(B-$H_{bridging}$), 2514 ν(B-

$H_{terminal}$). Mp (°C): 128-131. Anal. Calcd. for $C_{34}H_{64}B_2N_2OSiZr$: C, 62.08; H 9.81; N, 4.26. Found: C, 61.04; H, 9.97; N, 4.03.

2.5.3.9 Synthesis of $[NSiN]^{Dipp}Zr(BH_4)_2(DMAP)$ (9)

Compound **8** (0.197 g, 0.300 mmol) was dissolved in 3 mL of toluene and this solution was added dropwise to a solution of DMAP (30.5 mg, 0.250 mmol) in 2 mL of toluene, and the resultant white suspension was stirred for 18 hours. The solution was then filtered and the volatiles were removed from the filtrate *in vacuo* to yield a faint orange solid. This product was recrystallised by dissolution in 1 mL of toluene, followed by layering with 2 mL of hexanes. This mixture was then cooled to -35 °C for 48 hours to yield colourless X-ray quality crystals of **9** (0.132 g, 62 %). ^{1}H NMR (C_6D_6, 500 MHz): δ 1.20 (d, 12H, SiCH(CH_3)$_2$, $^3J_{HH}$ = 7.2 Hz), 1.42 (d, 12H, ArCH(CH_3)$_2$, $^3J_{HH}$ = 6.8 Hz), 1.45 (d, 12H, ArCH(CH_3)$_2$, $^3J_{HH}$ = 6.8 Hz), 1.67 (sept, 2H, SiCH(CH$_3$)$_2$, $^3J_{HH}$ = 7.2 Hz), 1.76 (s, 6H, DMAP-N(CH_3)$_2$), 4.13 (sept, 4H, ArCH(CH$_3$)$_2$, $^3J_{HH}$ = 6.8 Hz), 5.43 (d, 2H, DMAP-Ar*H,* $^3J_{HH}$ = 7.2 Hz), 7.02 (t, 2H, p-Ar*H*, $^3J_{HH}$ = 7.2 Hz), 7.13 (d, 4H, m-Ar*H*, $^3J_{HH}$ = 7.5 Hz), 8.05 (d, 2H, DMAP-Ar*H,* $^3J_{HH}$ = 7.2 Hz). ^{13}C{^{1}H} NMR (C_6D_6, 126 MHz): δ 19.1 (SiCH(*C*H$_3$)$_2$), 25.0 (ArCH(*C*H$_3$)$_2$), 26.1 (ArCH(*C*H$_3$)$_2$), 27.8 (Ar*C*H(CH$_3$)$_2$), 37.3 (DMAP-N(*C*H$_3$)$_2$), 104.8 (DMAP-*C*), 123.0 (p-Ar-*C*), 123.8 (m-Ar-*C*), 141.7 (o-Ar-*C*), 150.9 (DMAP-*C*), 153.7 (ipso-Ar-*C*). ^{11}B NMR (C_6D_6): δ -16.8 (pentet, $^1J_{BH}$ = 78 Hz). IR (Nujol/cm^{-1}): 2091 ν(B-$H_{bridging}$), 2189 ν(B-$H_{bridging}$), 2509 ν(B-$H_{terminal}$). Mp (°C): 146-148. Anal.

Calcd. for $C_{37}H_{66}B_2N_4SiZr$: C, 62.78; H, 9.40; N, 7.91. Found: C, 64.15; H, 8.98; N, 8.02.

2.5.3.10 Synthesis of $[NSiN]^{Dipp}ZrMe_2$·THF (10)

To a pale yellow solution of $[NSiN]^{Dipp}ZrCl(\mu\text{-}Cl)_2Li(THF)_2$ (0.235 g, 0.289 mmol) in 4 mL of THF at -35 °C in an aluminium foil wrapped scintillation vial was added MeLi (1.6 M solution in hexanes, 361 μL, 0.578 mmol). The resultant deep yellow solution was allowed to warm to room temperature, and the mixture was stirred for 16 hours. The solvent was removed from the filtrate *in vacuo* and the crude residue extracted with 3 mL of toluene and then filtered through Celite. The filtrate was then layered with 2 mL of hexanes and cooled to -35 °C to yield colourless crystals of $[NSiN]^{Dipp}ZrMe_2$•THF (0.120 g, 63 %). ^{1}H NMR (C_6D_6, 500 MHz): δ 0.48 (s, 6H, Zr-CH_3), 1.10 (d, 12H, SiCH(CH_3)$_2$, $^3J_{HH}$ = 7.6 Hz), 1.24 (m, 4H, THF *α*–CH_2), 1.33 (d, 12H, ArCH(CH_3)$_2$, $^3J_{HH}$ = 7.6 Hz), 1.38 (d, 12H, ArCH(CH_3)$_2$, $^3J_{HH}$ = 7.6 Hz), 1.48 (sept, 2H, SiCH(CH$_3$)$_2$, $^3J_{HH}$ = 7.6 Hz), 3.40 (m, 4H, THF *β*–CH_2), 7.02 (t, 2H, p-ArH, $^3J_{HH}$ = 7.6 Hz), 7.13 (d, 4H, m-ArH, $^3J_{HH}$ = 7.6 Hz). ^{13}C{^{1}H} NMR (C_6D_6, 126 MHz): δ 16.9 (SiCH(CH$_3$)$_2$), 19.2 (SiCH(CH$_3$)$_2$), 24.8 (ArCH(*C*H$_3$)$_2$), 27.0 (*β*C-THF), 28.7 (ArCH(*C*H$_3$)$_2$), 28.1 (ArCH(CH$_3$)$_2$), 41.0 (Zr-*C*H$_3$), 71.5 (*α*C-THF), 122.6 (p-ArC), 124.0 (m-ArC), 142.2 (o-ArC), 148.4 (ipso-ArC). Mp (°C): 80-83 (decomp.). Anal. Calcd. for $C_{36}H_{62}N_2OSiZr$: C, 65.69; H, 9.49; N, 4.26. Found: C, 64.88; H, 9.21; N, 4.08.

2.5.3.11 Synthesis of $Li(THF)_4\{[NSiN]^{Dipp}ZrMe_3\}$ (11)

Compound **4** (0.468 g, 0.576 mmol) was dissolved in 10 mL of THF in an aluminum foil wrapped scintillation vial to form a colourless solution. This solution was cooled to -35 °C, and then MeLi (1.6 M solution in Et_2O, 1.08 mL, 1.73 mmol) was added slowly and the bright yellow mixture was warmed to room temperature and stirred for 4 hours before the volatiles were removed from the solution *in vacuo*. The resulting solid was dissolved in 3 mL of Et_2O and the mixture was filtered. The solvent was removed *in vacuo* to yield **11** as an off-white solid (0.347 g, 68 %). ^{1}H NMR (C_6D_6, 500 MHz): δ 0.19 (s, 9H, Zr-CH_3), 1.28 (m, 16 H, *βH*-THF), 1.31 (d, 12H, SiCH(CH_3)$_2$, $^3J_{HH}$ = 6.9 Hz), 1.52 (d, 12H, ArCH(CH_3)$_2$, $^3J_{HH}$ = 7.5 Hz), 1.59 (d, 12H, ArCH(CH_3)$_2$, $^3J_{HH}$ = 7.5 Hz), 1.77 (sept, 2H, SiC*H*(CH$_3$)$_2$, $^3J_{HH}$ = 7.5 Hz), 3.21 (m, 16 H, α*H*-THF), 4.47 (sept, 4H, ArC*H*(CH$_3$)$_2$, $^3J_{HH}$ = 6.9 Hz), 7.01 (t, 2H, p-Ar*H*, $^3J_{HH}$ = 7.5 Hz), 7.25 (d, 4H, m-Ar*H*, $^3J_{HH}$ = 7.5 Hz). ^{13}C{^{1}H} NMR (C_6D_6, 126 MHz): δ 20.0 (SiCH(*C*H$_3$)$_2$), 24.8 (ArCH(*C*H$_3$)$_2$), 25.4 (*βC*-THF), 27.3 (ArCH(*C*H$_3$)$_2$), 28.1 (Ar*C*H(CH$_3$)$_2$), 34.0 (Zr-*C*H$_3$), 68.2 (α*C*-THF), 120.5 (p-Ar*C*), 123.3 (m-Ar*C*), 142.7 (o-Ar*C*), 152.3, (ipso-Ar*C*). Mp (°C): 138-142. Despite multiple attempts, satisfactory analyses were not obtained; see the Figures 2.15 and 2.16 for the corresponding NMR spectra.

2.5.3.12 Synthesis of $[NSiN]^{Dipp}Zr(NMe_2)_2(\mu\text{-}Cl)Li(THF)_3$ (12)

$H_2[NSiN]^{Dipp}$ (0.429 g, 0.919 mmol) was dissolved in 5 mL of Et_2O to form a pale yellow solution, and ^{n}BuLi (2.5 M solution in hexanes, 735 μL,

1.84 mmol) was added dropwise. This solution was allowed to stir for one hour, and then the solution of $Li_2[NSiN]^{Dipp}$ added dropwise to a yellow suspension of $Cl_2Zr(NMe_2)_2(THF)_2$ (0.360 g, 0.917 mmol) in 5 mL of Et_2O. The resultant mixture was stirred for 18 hours and then filtered through Celite. The volatiles were then removed from the filtrate *in vacuo* to yield **12** as an off-white solid (0.379 g, 46 %). Crystals suitable for X-ray diffraction were grown by dissolving **12** in 3 mL of toluene followed by layering of this solution with 3 mL of hexanes and cooling to -35 °C for one week. ^{1}H NMR (C_6D_6, 500 MHz): δ 1.18 (d, 12H, SiCH(C*H*$_3$)$_2$, $^3J_{HH}$ = 7.6 Hz), 1.31 (m, 12H, *β*-THF-C*H*$_2$, $^3J_{HH}$ = 7.2 Hz), 1.38 (br m, 24H, ArCH(C*H*$_3$)$_2$, $^3J_{HH}$ = 7.2 Hz), 1.65 (sept, 2H, SiC*H*(CH$_3$)$_2$, $^3J_{HH}$ = 7.6 Hz), 2.72 (s, 6H, ZrN(C*H*$_3$)$_2$), 3.43 (m, 8H, *α*–THF–C*H*$_2$), 4.00 (sept, 4H, ArC*H*(CH$_3$)$_2$, $^3J_{HH}$ = 6.8 Hz), 7.05 (t, 2H, p-Ar*H*, $^3J_{HH}$ = 7.6 Hz), 7.20 (d, 4H, m-Ar*H*, $^3J_{HH}$ = 7.6 Hz). ^{13}C{^{1}H} NMR (C_6D_6, 126 MHz): δ 19.8 (Si*C*H(CH$_3$)$_2$), 20.6 (SiCH(*C*H$_3$)$_2$), 23.9 (ArCH(*C*H$_3$)$_2$), 25.7 (Ar*C*H(CH$_3$)$_2$), 28.1 (O-CH$_2$-*C*H$_2$), 42.8 (ZrN(*C*H$_3$)$_2$), 68.9 (O-*C*H$_2$-), 122.0 (p-Ar-*C*), 123.8 (m-Ar-*C*), 143.1 (o-Ar-*C*), 149.5 (ipso-Ar-*C*). Mp (°C): 97-100. Anal. Calcd. for $C_{46}H_{84}ClLiN_4O_3SiZr$: C, 61.19; H, 9.38; N, 6.21. Found: C, 61.14; H, 9.10; N, 6.28.

2.5.3.13 Representative dehydrocoupling of $Me_2NH•BH_3$ catalysed by 12

A scintillation vial was charged with 4 mg of **12** (5 μmol) and 0.5 mL of C_6D_6 was added to yield a colourless solution. To this mixture was added a solution of $Me_2NH•BH_3$ (0.312 g, 5.29 mmol) in 1 mL of C_6D_6, and the

resultant solution allowed to stir for 1 hour. At this time, a small aliquot (ca. 0.2 mL) was removed and diluted to 0.7 mL with C_6D_6 for ^{11}B NMR analysis. Upon being stirred for 2 further hours, similar ^{11}B NMR analysis revealed the absence of $Me_2NH•BH_3$. All dehydrocoupling reactions for $Me_2NH•BH_3$ were performed in this manner.

2.5.3.14 Representative dehydrocoupling of $^{i}Pr_2NH•BH_3$ catalysed by 12

A scintillation vial was charged with 6 mg of **12** (7 μmol) and 0.5 mL of C_6D_6 was added to yield a colourless solution. To this mixture was added a solution of $^{i}Pr_2NH•BH_3$ (0.162 g, 1.41 mmol) in 1 mL of C_6D_6, and the resultant solution allowed to stir for 1 hour. At this time, a small aliquot (ca. 0.2 mL) was removed and diluted to 0.7 mL with C_6D_6 for ^{11}B NMR analysis. Upon being stirred for 4 further hours, similar ^{11}B NMR analysis revealed the absence of $^{i}Pr_2NH•BH_3$. All dehydrocoupling reactions for $^{i}Pr_2NH•BH_3$ were performed in this manner.

2.5.3.15 Representative dehydrocoupling of $^{n}BuNH_2•BH_3$ catalysed by 12

A scintillation vial was charged with 6 mg of **12** (7 μmol) and 0.5 mL of C_6D_6 was added to yield a colourless solution. To this solution was added to a solution of $^{n}BuNH_2•BH_3$ (0.312 g, 5.29 mmol) in 1 mL of C_6D_6, and the resultant mixture allowed to stir for 1 hour. At this time, a small aliquot (ca. 0.2 mL) was removed and diluted to 0.7 mL with C_6D_6 for ^{11}B NMR analysis. Upon being stirred for 12 further hours, similar ^{11}B NMR analysis showed

further consumption of $^{n}BuNH_2 \bullet BH_3$, however analysis after a further 12 hours show no additional reactivity. All dehydrocoupling reactions for $^{n}BuNH_2 \bullet BH_3$ were performed in this manner.

2.5.3.16 Synthesis of $[NSiN]^{SiPh3}ZrCl_2(THF)_2$ (14)

To a solution of $H_2[NSiN]^{SiPh3}$ (0.130 g, 0.196 mmol) in 8 mL of Et_2O was added $^{n}BuLi$ (2.5 M solution in hexanes, 156.8 μL, 0.192 mmol), and the resultant solution allowed to stir for 3 hours. This was then added to a slurry of $Cl_4Zr(THF)_2$ (74 mg, 0.20 mmol) in 5 mL of Et_2O, and the resultant mixture was stirred for 20 hours, upon which time the mixture was filtered. Removal of the volatiles from the filtrate *in vacuo* yielded the crude product as an off-white solid (0.112 g, 60 %). Crystals of **14** were obtained by redissolving the product in 4 mL of Et_2O, and storing at -35 °C for 3 days. ^{1}H NMR (500 MHz, C_6D_6): δ 0.96 (d, 12H, $SiCH(CH_3)_2$, $^{3}J_{HH}$ = 7.5 Hz), 1.12 (broad s, 8H, THF), 1.27 (broad s, 2H, $SiCH(CH_3)_2$), 3.26 (broad s, 8H, THF), 7.27 (mult, 12H, Ar*H*), 7.80 (m, 6H, Ar*H*), 7.97 (m, 12H, Ar*H*). $^{13}C\{^{1}H\}$ NMR (126 MHz, C_6D_6): δ 18.5 (THF), 18.9 ($SiCH(CH_3)_2$), 25.0 ($SiCH(CH_3)_2$), 67.9 (THF), 129.7 (Ar*C*), 136.1 (Ar*C*), 136.2 (Ar*C*), 144.2 (Ar*C*). Mp (°C): 187-190. Anal. Calcd. for $C_{50}H_{60}Cl_2N_2O_2Si_3Zr$: C, 62.08; H, 6.25; N, 2.90. Found: C, 61.80; H, 6.33; N, 3.12.

2.3.4. NMR Spectra for compounds 7 and 11

Figure 2.12: ^{1}H NMR spectrum (C_6D_6) of $Li(THF)_4\{[NSiN]^{Dipp}ZrCl_2(BH_4)\}$ (**7**) [(*) denotes residual solvent]

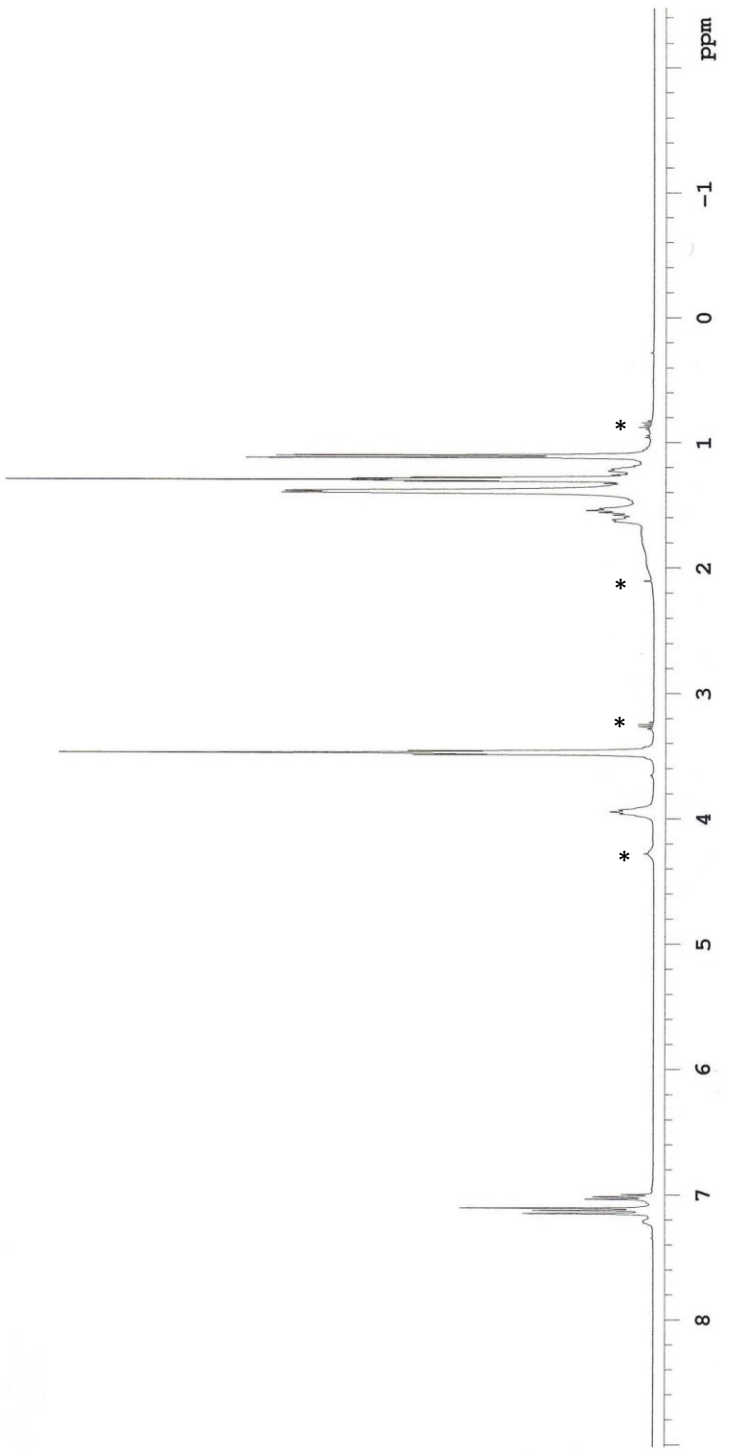

Figure 2.13: ^{11}B NMR spectrum (C_6D_6) of $Li(THF)_4\{[NSiN]^{Dipp}ZrCl_2(BH_4)\}$ (**7**)**.**

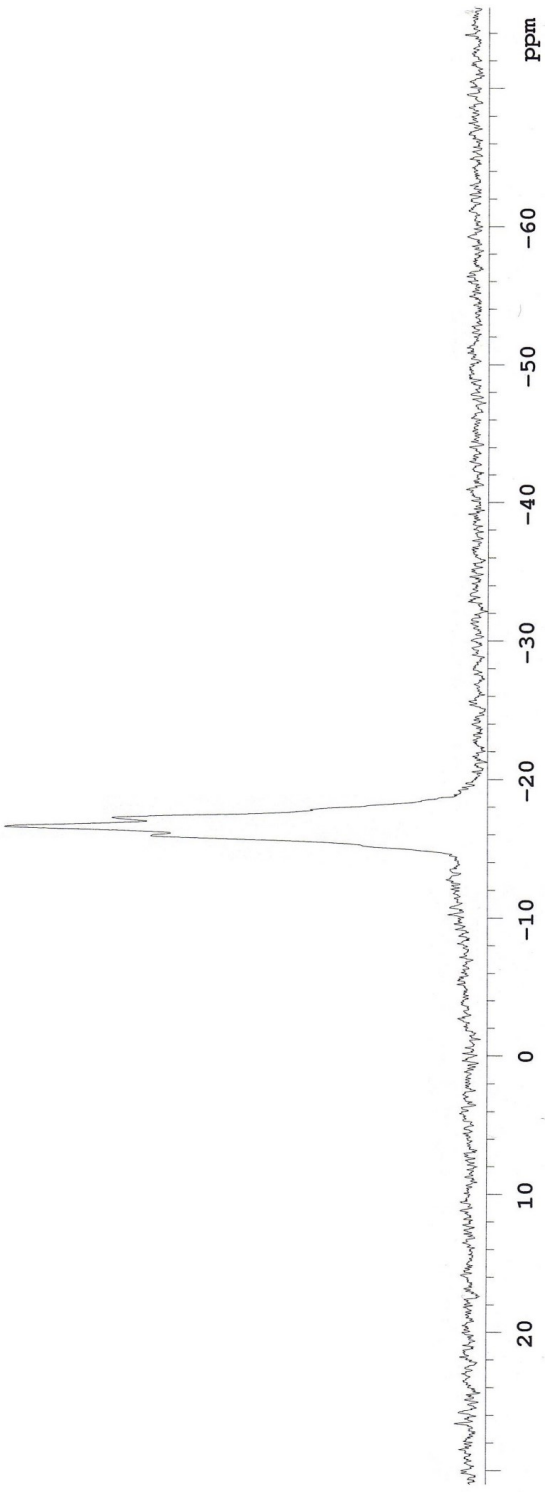

Figure 2.14: $^{13}C\{^{1}H\}$ NMR spectrum (C_6D_6) of $Li(THF)_4\{[NSiN]^{Dipp}ZrCl_2(BH_4)\}$ (**7**) [(*) denotes residual solvent]

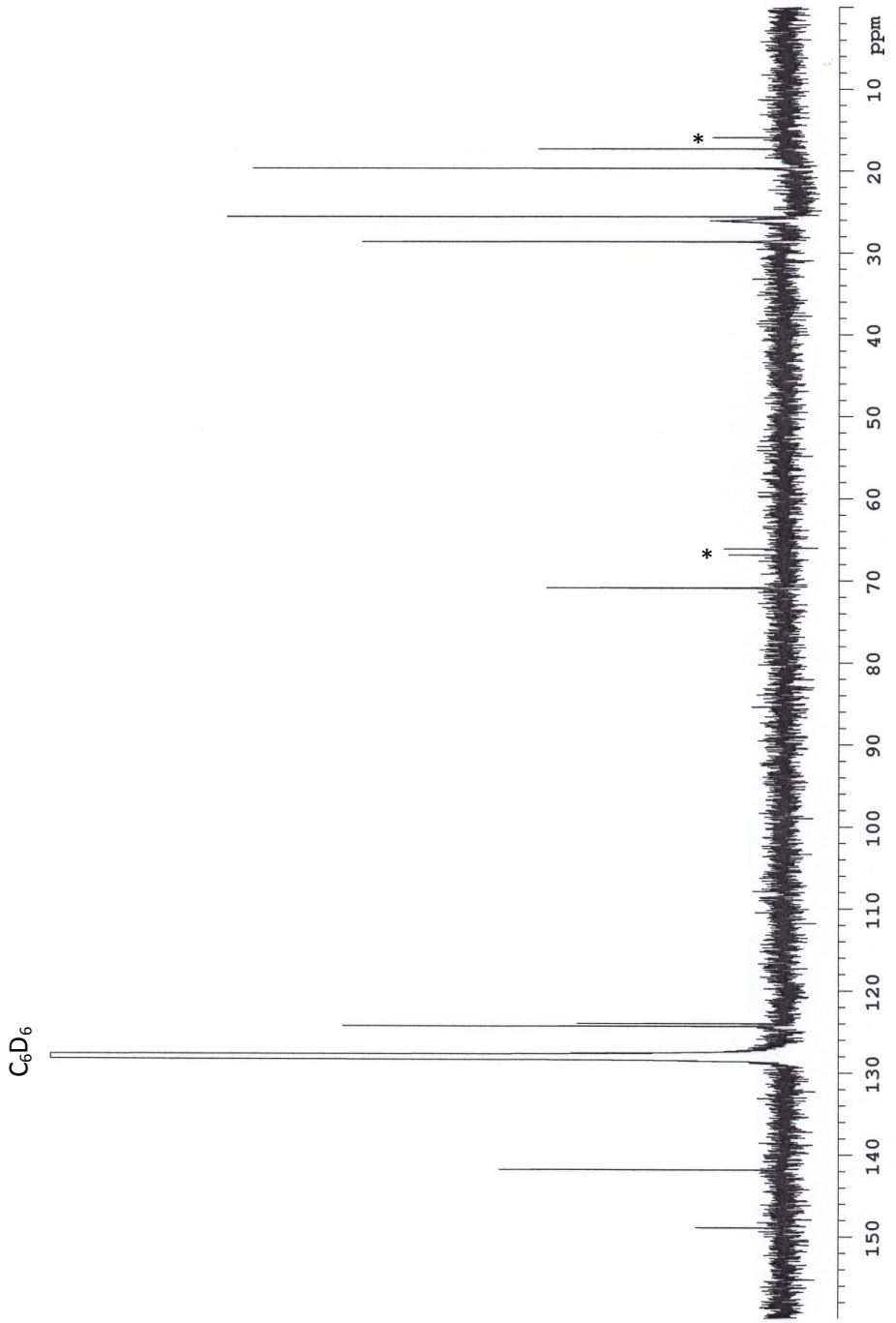

Figure 2.15: ^{1}H NMR spectrum (C_6D_6) of $Li(THF)_4\{[NSiN]^{Dipp}ZrMe_3\}$ (**11**) [(*) denotes residual solvent]

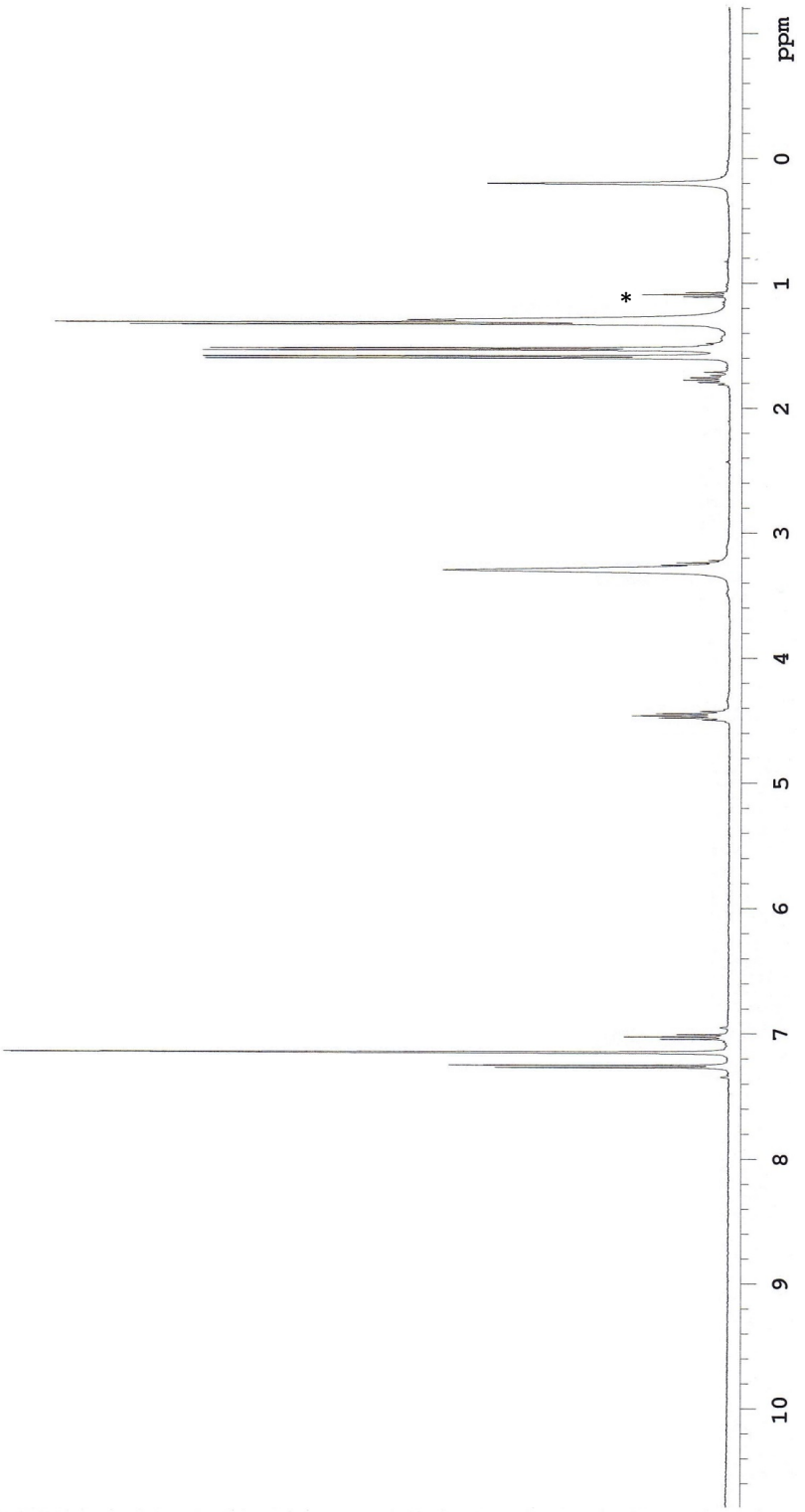

Figure 2.16: $^{13}C\{^{1}H\}$ NMR spectrum (C_6D_6) of $Li(THF)_4\{[NSiN]^{Dipp}ZrMe_3\}$, (**11**) [(*) denotes residual solvent]

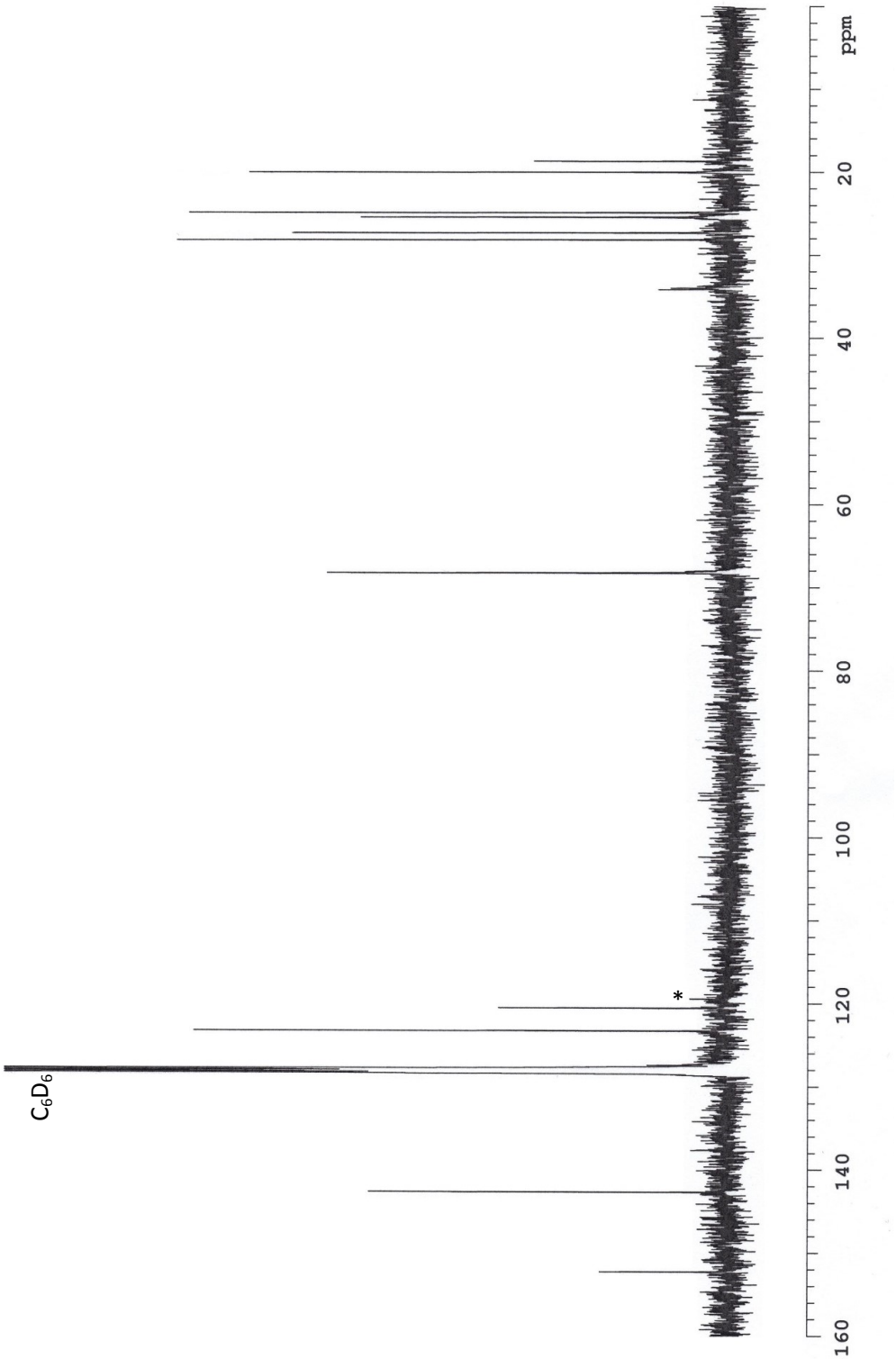

Table 2.1 Crystallographic Data for Compounds **2a** and **3**

	2a	**3**
empirical formula	$C_{54}H_{96}Li_2N_2O_6Si$	$C_{32}H_{54}N_2SiSn$
fw	911.30	613.55
cryst dimens (mm^3)	0.31 × 0.31 × 0.27	0.58 × 0.12 × 0.09
cryst syst	orthorhombic	orthorhombic
space group	$P2_12_12_1$	*Pbca*
unit cell dimensions		
a (Å)	14.7015 (5)	10.4637 (4)
b (Å)	18.1668 (6)	17.5352 (7)
c (Å)	10.5297 (3)	35.7151 (14)
α (deg)		
β (deg)		
γ (deg)		
V ($Å^3$)	2812.26 (16)	6553.1 (4)
Z	2	8
ρ (g cm^{-3})	1.076	1.244
abs coeff (mm^{-1})	0.087	0.838
T (K)	173 (1)	173 (1)
$2\theta_{max}$ (deg)	55.16	53.54
total data	25138	52524
unique data (R_{int})	6490 (0.0247)	6983 (0.0280)
obs data [$I > 2\sigma(I)$]	5559	6071
Params	303	327
R_1 [$I > 2\sigma(I)$][a]	0.0491	0.0259
wR_2 [all data][a]	0.1470	0.714
Max/Min $\Delta\rho$ (e^- $Å^{-3}$)	0.333/-0.167	0.843/-0.780

[a] $R_1 = \Sigma \left| \left| F_o \right| - \left| F_c \right| \right| / \Sigma \left| F_o \right|$; $wR_2 = [\Sigma\, w(F_o^2 - F_c^2)^2 / \Sigma\, w(F_o^4)]^{1/2}$.

Table 2.2 Crystallographic Data for Compounds **4** and **5**

	4	**5**
empirical formula	$C_{38}H_{64}Cl_3LiN_2O_2SiZr$	$C_{48}H_{86}Cl_2LiN_3O_4SiZr$
fw	813.51	966.34
cryst dimens (mm^3)	0.38 × 0.34 × 0.30	0.24 × 0.23 × 0.20
cryst syst	monoclinic	orthorhombic
space group	$P2_1/n$	$P2_12_12_1$
unit cell dimensions		
a (Å)	10.2481 (4)	15.266 (2)
b (Å)	27.2915 (11)	18.419 (3)
c (Å)	15.7628 (6)	19.316 (3)
α (deg)		
β (deg)	101.8171(4)	
γ (deg)		
V ($Å^3$)	4315.2 (3)	5431.5 (14)
Z	4	4
ρ (g cm^{-3})	1.252	1.182
abs coeff (mm^{-1})	1.102	0.363
T (K)	173 (1)	173 (1)
$2\theta_{max}$ (deg)	55.16	53.34
total data	38542	43340
unique data (R_{int})	9969 (0.0157)	11293 (0.0788)
obs data [$I > 2\sigma(I)$]	9002	9794
Params	442	536
R_1 [$I > 2\sigma(I)$][a]	0.0379	0.0485
wR_2 [all data][a]	0.0989	0.1135
Max/Min $\Delta\rho$ (e$^-$ $Å^{-3}$)	0.644/-0.580	0.664/-0.570

[a] $R_1 = \Sigma \| \|F_o\| - \|F_c\| \| / \Sigma |F_o|$; $wR_2 = [\Sigma\, w(F_o^2 - F_c^2)^2 / \Sigma\, w(F_o^4)]^{1/2}$.

Table 2.3 Crystallographic Data for Compounds **7** and **9**

	7	**9**•0.5THF
empirical formula	$C_{46}H_{84}BCl_3LiN_2O_4SiZr$	$C_{39}H_{70}B_2N_4O_{0.5}SiZr$
fw	937.11	743.92
cryst dimens (mm^3)	0.52 × 0.39 × 0.27	0.47 × 0.18 × 0.06
cryst syst	orthorhombic	Monoclinic
space group	$P2_12_12_1$	$P2_1/c$
unit cell dimensions		
a (Å)	15.4463 (17)	10.8302 (4)
b (Å)	18.451 (2)	16.9778 (7)
c (Å)	18.574 (2)	23.5656 (9)
α (deg)		
β (deg)		91.9980 (10)
γ (deg)		
V ($Å^3$)	5293.6 (10)	4330.4 (10)
Z	4	4
ρ (g cm^{-3})	1.176	1.141
abs coeff (mm^{-1})	0.0370	0.312
T (K)	173 (1)	173 (1)
$2\theta_{max}$ (deg)	53.05	52.92
total data	38542	34513
unique data (R_{int})	10870 (0.0534)	8913 (0.0498)
obs data [$I > 2\sigma(I)$]	10278	7012
Params	537	441
R_1 [$I > 2\sigma(I)$][a]	0.0795	0.0357
wR_2 [all data][a]	0.02096	0.0967
Max/Min $\Delta\rho$ (e$^-$ $Å^{-3}$)	0.760/-1.221	0.387/-0.358

[a] $R_1 = \Sigma \| \|F_o\| - \|F_c\| \| / \Sigma |F_o|$; $wR_2 = [\Sigma\, w(F_o^2 - F_c^2)^2 / \Sigma\, w(F_o^4)]^{1/2}$.

.

Table 2.4 Crystallographic Data for Compounds **10** and **12**

	10	**12**•0.5THF
empirical formula	$C_{36}H_{62}N_2OSiZr$	$C_{48}H_{88}ClLiN_4O_{3.5}SiZr$
fw	658.19	938.92
cryst dimens (mm^3)	0.34 × 0.34 × 0.28	0.36 × 0.31 × 0.17
cryst syst	Monoclinic	Monoclinic
space group	$P2_1/c$	$C2/c$
unit cell dimensions		
a (Å)	11.3162 (4)	15.266 (2)
b (Å)	13.2629 (5)	18.419 (3)
c (Å)	24.9183 (9)	19.316 (3
α (deg)		
β (deg)	94.8730 (4)	90.0434 (6)
γ (deg)		
V ($Å^3$)	3726.4 (2)	10392.1 (8)
Z	4	8
ρ (g cm^{-3})	1.173	1.200
abs coeff (mm^{-1})	0.355	0.328
T (K)	173 (1)	173 (1)
$2\theta_{max}$ (deg)	55.10	52.92
total data	32860	41191
unique data (R_{int})	8605 (0.0196)	10729 (0.0619)
obs data [$I > 2\sigma(I)$]	7457	7893
Params	376	525
R_1 [$I > 2\sigma(I)$][a]	0.0272	0.0461
wR_2 [all data][a]	0.0767	0.1288
Max/Min $\Delta\rho$ (e$^-$ $Å^{-3}$)	0.441/-0.290	0.773/-0.629

[a] $R_1 = \Sigma \| \|F_o\| - \|F_c\| \| / \Sigma |F_o|$; $wR_2 = [\Sigma\, w(F_o^2 - F_c^2)^2 / \Sigma\, w(F_o^4)]^{1/2}$.

2.4.1. References

1 For papers detailing mechanisms involving sigma-bond metathesis, see: (*a*) R. Waterman, *Organometallics*, **2013**, *32*, 7249; (*b*) H. G. Woo, J. F. Walzer, T. D. Tilley, *J. Am. Chem. Soc.,* **1992**, *114*, 7047; (*c*) T. D. Tilley, *Acc. Chem. Res.,* **1993**, *26*, 22; (*d*) J. F. Harrod, *ACS Symp. Ser.,* **1988**, *360*, 89.

2 For a review of select zirconium-based complexes as polymerization catalysts, see: (*a*) P. Sobota, *Coord. Chem. Rev.*, **2004**, *248*, 1047; (*b*) J. J. Eisch, *Organometallics*, **2012**, *31*, 4917.

3 A. Staubitz, A. P. M. Robertson, M. E. Sloan, I. Manners, *Chem. Rev.*, **2010**, *110*, 4023.

4 A. J. Roering, S. N. MacMillan, J. M. Tanski, R. Waterman, *Inorg. Chem.*, **2007**, *46*, 6855.

5 W. Zhou, S. L. Marquard, M. W. Bezpalko, B. M. Foxman, C. M. Thomas, *Organometallics*, **2013**, *32*, 1766.

6 (*a*) T. Takahashi, M. Hasegawa, N. Suzuki, M. Saburi, C. J. Rousset, P. E. Fanwick, E. Negishi, *J. Am. Chem. Soc.,* **1991**, *113*, 8564; (*b*) L. Jia, J. Zhao, E. Ding, W. W. Brennessel, *J. Chem. Soc., Dalton Trans.,* **2002**, 2608; (*c*) S. Anga, K. Naktode, H. Adimulam, T. K. Panda, *Dalton Trans.,* **2014**, *43*, 14876; (*d*) N. Yonson, J. C.-H. Yim, L. L. Schafer, *Inorg. Chim. Acta,* **2014**, *422*, 14.

7 (*a*) J. M. Manriquez, D. R. McAlister, E. Rosenberg, A. M. Shiller, K. L. Williamson, S. I. Chan, J. E. Bercaw, *J. Am. Chem. Soc.*, **1978**, *100*, 3078; (*b*) M. D. Fryzuk, T. S. Haddad, S. J. Rettig, *J. Am. Chem. Soc.*, **1990**, *112*, 8185; (*c*) M. D. Fryzuk, J. B. Love, S. J. Rettig, V. G. Young, *Science*, **1997**, *275,* 1445; (*d*) J. A. Pool, E. Lobkovsky, P. J. Chirik, *Nature*, **2004**, *427*, 527; (*e*) D. Pun, C. A. Bradley, E. Lobkovsky, I. Keresztes, P. J. Chirik, *J. Am. Chem. Soc.,* **2008**, *130*, 14046; (*f*) D. Pun, D. J. Knobloch, E. Lobkovsky, P. J. Chirik, *Dalton Trans.,* **2011**, *40*, 7737; (*g*) G. W. Margulieux, S. P. Semproni, P. J. Chirik, *Angew. Chem., Int. Ed.,* **2014**, *53*, 9189.

8 (*a*) T. D. Tilley, *J. Am. Chem. Soc.*, **1985**, *107*, 4084; (*b*) L. Chen, W. – L. Nie, J. Paradies, G. Kehr, R. Fröhlich, K. Wedeking, G. Erker, *Organometallics*, **2006**, *25,* 5333; (*c*) D. J. Knobloch, E. Lobkovsky, P. J. Chirik, *J. Am. Chem. Soc*., **2010**, *132*, 10553.

9 (*a*) G. Erker, G. Kehr, R. Fröhlich, *J. Organomet. Chem*., **2004**, *689*, 1402; (*b*) Y. Nakayama, T. Shiono, *Molecules*, **2005**, *10*, 620.

10 (a) S. M. I. Al-Rafia, P. A. Lummis, M. J. Ferguson, R. McDonald, E. Rivard, *Inorg. Chem*., **2010**, *49*, 9709; (*b*) S. K. Liew, S. M. I. Al-Rafia, J. T. Goettel, P. A. Lummis, S. M. McDonald, L. J. Miedema, M. J. Ferguson, R. McDonald, E. Rivard, *Inorg. Chem*., **2012**, *51*, 5471.

11 (*a*) M. Veith, *Chem. Rev*., **1990**, *90*, 3; (*b*) G. He, O. Shynkaruk, M. W. Lui, E. Rivard, *Chem. Rev*., **2014**, *114*, 7815.

12 (*a*) A. Staubitz, A. P. M. Robertson, I. Manners, *Chem. Rev*., **2010**, *110*, 4079; (*b*) F. H. Stephens, V. Pons, R. T. Baker, *Dalton Trans.*, **2007**, *36*, 2613.

13 H. Helton, B. Dutta, J. R. Vance, M. E. Sloan, M. F. Haddow, S. Sproules, D. Collison, G. Whittell, G. C. Lloyd-Jones, I. Manners, *Angew. Chem., Int. Ed.*, **2013**, *52*, 437.

14 A. M. Chapman, M. F. Haddow, D. F. Wass, *J. Am Chem. Soc*., **2011**, *133*, 8826.

15 For related syntheses, see: (*a*) M. S. Hill, P. B. Hitchcock, *Organometallics*, **2002**, ***21***, 3258; (*b*) S. M. Mansell, C. A. Russell, D. F. Wass, *Inorg. Chem.*, **2008**, *47,* 11367; (*c*) S. Yuan, X. Wei, H. Tong, L. Zhang, D. Liu, W. –H. Sun, *Organometallics*, **2010**, *29*, 2085; (*d*) D. Yang, J. Guo, H. Wu, Y. Ding, W. Zheng, *Dalton Trans.*, **2012**, *41*, 2187.

16 P. H. Bird, M. R. Churchill, *J. Chem. Soc., Chem. Commun.*, **1967**, 403.

17 A. Haaland, D. J. Shorokhov, A. V. Tutukin, H. V. Volden, O. Swang, G. S. McGrady, N. Kaltsoyannis, A. J. Downs, C. Y. Tang, J. F. C. Turner, *Inorg. Chem.*, **2002**, *41*, 6646.

18 T. D. Forster, H. M. Tuononen, M. Parvez, R. Roesler. *J. Am. Chem. Soc.*, **2009**, *131*, 6689.

19 M. E. Sloan, A. Staubitz, T. J. Clark, C. A. Russell, G. C. Lloyd-Jones, I. Manners, *J. Am. Chem. Soc.*, **2010**, *132*, 3831.

20 For examples of decomposition of bis(amido) Zr-Me complexes via reductive elimination and C-H bond activation pathways, see: (*a*) Y. Schrodi, R. R. Schrock, P. J. Bonitatebus, Jr., *Organometallics*, **2001**, *20*, 3560; (*b*) P. Mehrkhodavandi, R. R. Schrock, P. J. Bonitatebus, Jr., *Organometallics*, **2002**, *21*, 5785.

21 S. Brenner, R. Kempe, P. Arndt, *Z. Anorg. Allg. Chem.*, **1995**, *621*, 2021.

22 L. J. Sewell, G.C. Lloyd-Jones, A. S. Weller, *J. Am. Chem. Soc.*, **2012**, *134*, 3598.

23 T. J. Clark, C. A. Russell, I. Manners, *J. Am. Chem. Soc.,* **2006**, *128*, 9582.

24 (*a*) A. P. M. Robertson, E. M. Leitao, I. Manners, *J. Am. Chem. Soc.,* 2011, **133**, 19322; (*b*) A. P. M. Robertson, E. M. Leitao, T. Jurca, M. F. Haddow, H. Helten, G. C. Lloyd-Jones, I. Manners, *J. Am. Chem. Soc.*, **2013**, *135*, 12670.

25 E. Framery, M. Vaultier, *Heteroatom Chem.*, **2000**, *11*, 218.

26 P. C. Wailes, H. Weigold, *J. Organomet. Chem.*, **1970**, *24*, 405.

27 A. B. Pangborn, M. A. Giardello, R. H. Grubbs, R. K. Rosen, F. J. Timmers, *Organometallics*, **1996**, *15*, 1518.

28 M. E. Bowden, I. W. M. Brown, G. J. Gainsford, H. Wong, *Inorg. Chim. Acta*, **2008**, *361*, 2147.

29 C. A. Jaska, K. Temple, A. J. Lough, I. Manners, *J. Am. Chem. Soc.*, **2003**, *125*, 9424.

30 L. E. Manzer, J. Deaton, P. Sharp, R. R. Schrock *Inorg. Synth.,* **1982**, *21*, 135.

31 H. Hope, *Prog. Inorg. Chem.*, **1993**, *41*, 1.

32 G. M. Sheldrick, *Acta. Cryst.,* **2008**, *A64*, 112.

Chapter 3

The design and synthesis of new bis(amido)silyl and bis(guanidine) ligands for use in main group and transition metal coordination chemistry

3.1 Abstract

The design of a series of new bis(amine) NSiN chelates containing two nitrogen donor atoms linked by $Si^{i}Pr_2$ units was explored. In the first case, in order to increase the steric bulk about the ligating nitrogen centres, ligands containing hindered triarylsilyl groups, such as $–Si(C_6H_3\text{-}3,5\text{-}Me_2)$ were prepared. In the second part of this chapter, I discuss the use of tetramethylguanidine $[(Me_2N)_2C=N]^-$ units as ligand components. The resulting neutral bis(imine) donors containing two $[(Me_2N)_2C=N]^-$ units joined by silane, disilane, and disiloxane spacers were evaluated for their abilities to stabilise low valent main group element centres.

3.2 Introduction

The design of new ligands is of utmost importance in furthering the study of coordination chemistry amongst the transition metal and main group elements. The rational design of ligands to satisfy the desired electronic and physical properties of the target compound can open new pathways of reactivity leading to advances in catalysis. Through the judicious choice of both the element to which the ligand is bound, and the functional groups found within the ligand, one can tailor physical characteristics such as the thermal stability, electrophilicity and the solubility of the resulting complexes.[1] In some cases, one can obtain multiple desirable properties at once; for instance, the incorporation of substituted phenyl rings within a ligand (e.g. 2,6-diisopropylphenyl or "Dipp" groups) can not only improve the solubility and steric bulk of the final ligand, but also facilitate straightforward spectroscopic analysis of compounds containing these groups due to the distinct coupling pattern observed by ^{1}H NMR spectroscopy.

Due to their ease of synthesis and high degree of structural tunability, nitrogen-based ligands are widely explored.[2] These investigations have led to the discovery of many new transition metal-mediated transformations, both stoichiometric and catalytic in nature.[3] Some highlights of this field include the catalytic reduction of N_2 to NH_3 at a Mo centre facilitated by the tris(amido)amine complex $[(HIPT)NCH_2CH_2)_3N]Mo$ (HIPT = hexaisopropylterphenyl = 3,5-$(C_6H_2$-2,4,6-$^{i}Pr_3)_2C_6H_3)$,[4] as well as the highly selective, high turnover hydrosilylation of alkenes achieved by an iron catalyst bearing a bis(imido)pyridine ligand.[5] In addition, amido ligands (R_2N^-) feature

prominently in the chemistry of the main group elements, and have facilitated the isolation of species with novel bonding and reactivity.[6] Recently, Jones and coworkers reported the high turnover hydroboration of aldehydes and ketones catalyzed by *in situ* generated [Ar*(Si^{i}Pr$_3$)N]EH (E = Ge, Sn; Ar* = C_6H_2-4-^{i}Pr-2,6-$(CHPh_2)_2$); this work is particularly novel as it demonstrates a rare example of main group element-mediated catalysis.[7] It should be noted that part of the reason for the success of nitrogen-containing ligands is that in addition to having σ-donation from each the nitrogen centre, there are also π-electrons available to donate to the metal (2 π-electrons in the case of $[R_2N]^-$ fragments and up to 4 π-electrons in the case of $[R{=}N]^-$ and $[R{-}N]^{2-}$ units), which in turn increases the strength of the N-M interactions. Moreover, the ability to easily tune the substituents via modular synthetic routes allows for a high level of control over the steric and electronic properties of the ligated element.[2-4]

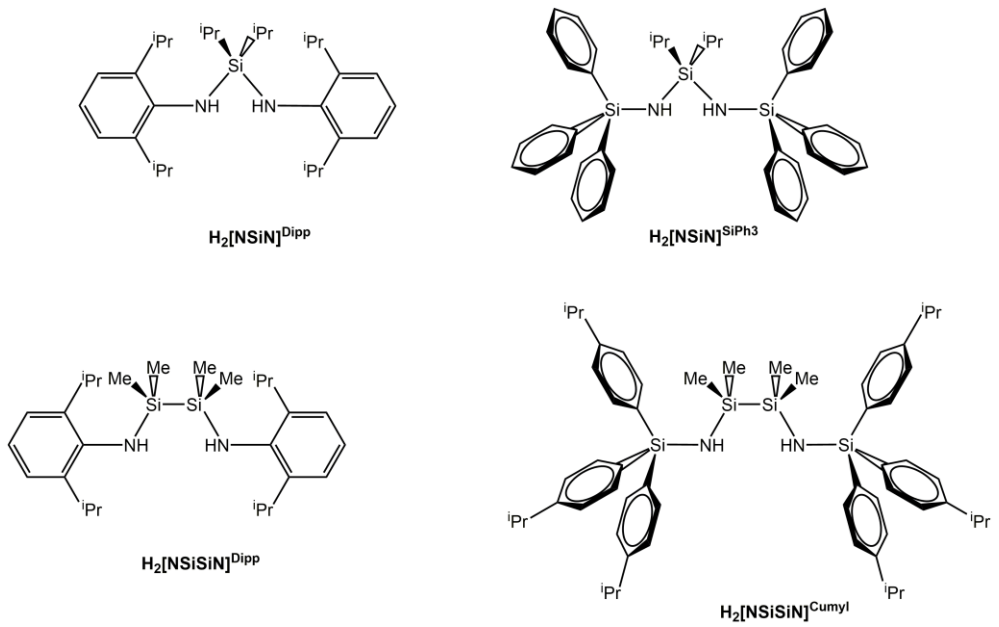

Figure 3.1 Examples of previously synthesised bis(amido)silyl and bis(amido)disilyl ligand precursors.

The synthesis of a variety of bis(amido)silyl ligands, [(2,6-$^{i}Pr_2C_6H_3N)_2Si^{i}Pr_2]^{2-}$ and $[(Ar_3SiN)_2Si^{i}Pr_2]^{2-}$ (where Ar = Ph, 4-$^{i}PrC_6H_4$) was reported by our research group (Figure 3.1),[8] and it was found that these ligands benefit from relatively facile syntheses, as well as conferring excellent steric protection about the target element upon ligation to form the low-coordinate germylenes and stannylenes [(2,6-$^{i}Pr_2C_6H_3N)_2Si^{i}Pr_2$]E: and $[(Ar_3SiN)_2Si^{i}Pr_2]$E: (E = Ge and Sn).[8] As such, I set out to both expand the library of known bis(amido)silyl ligands, and to use them within the realm of transition metal coordination chemistry for catalytic applications (see chapter 2).

3.3 Results and discussion

3.3.1 Synthesis of new "umbrella" ligands featuring tris(3,5-dialkylphenyl)silyl amine groups

In addition to the aforementioned $[NSiN]^{Dipp}$ and $[NSiN]^{SiPh3}$ ligands that were previously synthesised by our group, the synthesis of new NSiN chelates with functionalised aryl groups within the nitrogen-appended $SiAr_3$ "umbrella"-shaped substituents was sought. To begin, the synthesis of the meta-Dipp analogue, $H_2[NSiN]^{SiDipp3}$ was explored, however the planned route first necessitated the preparation of 5-bromo-1,3-diisopropylbenzene (**1a**) which can be synthesised from the commercially available 2,6-diisopropylaniline according to the procedure listed in Scheme 3.1.[9]

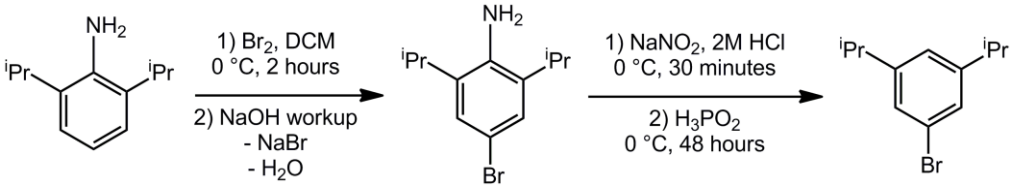

Scheme 3.1 Preparation of 5-bromo-1,3-diisopropylbenzene (**1a**).

It was found that the coupling of **1a** to silicon to yield the triarylsilane $(Dipp)_3SiH$ (**2a**) proceeded smoothly (Scheme 3.2); however attempts to convert this compound cleanly into the corresponding bromotriarylsilane $(Dipp)_3SiBr$ using a known bromination procedure in CCl_4[10] yielded multiple products, as determined by ^1H NMR spectroscopic analysis. Nevertheless, the protocol outlined in Scheme 3.2 was later used to obtain the xylated ligand $H_2[NSiN]^{SiXyl3}$ (**5**).

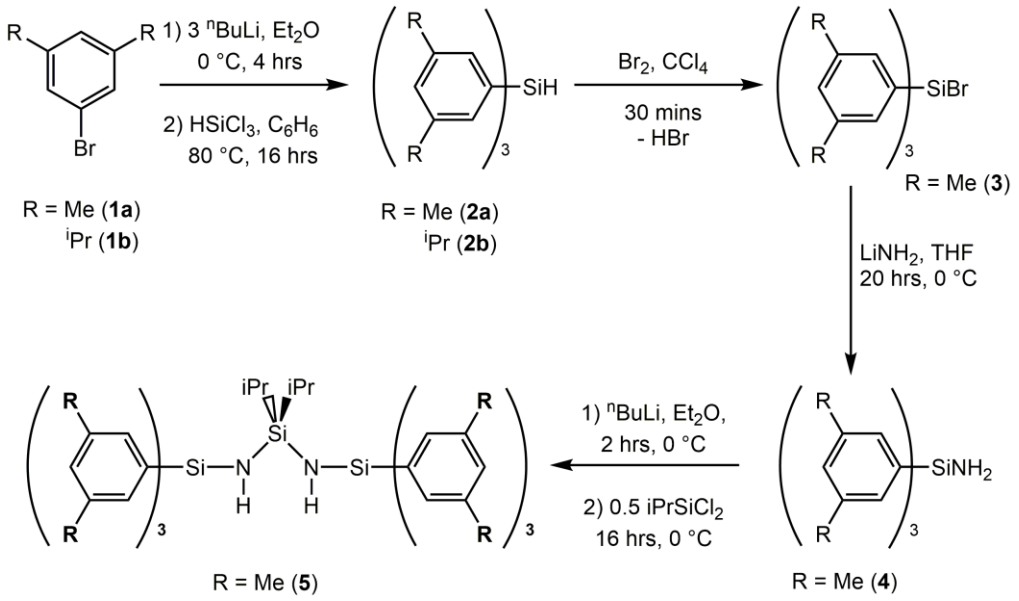

Scheme 3.2 Synthesis of triarylsilanes Xyl_3SiH, **2a**, and $(3,5\text{-}^{i}Pr_2\text{-}C_6H_3)_3SiH$ **2b**, with conversion to Xyl_3SiBr (**3**), Xyl_3SiNH_2 (**4**) and the ligand precursor $H_2[NSiN]^{SiXyl3}$ (**5**).

The conversion of 5-bromo-m-xylene to bromotris(m-xylyl)silane (Xyl_3SiH, Xyl = 3,5-$Me_2C_6H_3$, **3**) has been previously described,[10] and from this reagent the corresponding silylamine Xyl_3SiNH_2 (**4**) was synthesised in nearly quantitative yield by combining **3** with lithium amide in THF. The same methodology as was previously described in chapter 2 was then applied to convert this amine (**4**) into the desired bis(amido)silyl ligand precursor $H_2[NSiN]^{SiXyl3}$ (**5**). Specifically, a solution of **4** was combined with one equivalent of $^{n}BuLi$, stirred for 4 hours, before $^{i}Pr_2SiCl_2$ was added to the *in situ* generated lithium amide $LiN(H)SiXyl_3$. Removal of the solvent *in vacuo* and extraction of the remaining solid into Et_2O gave a pale yellow solution from which $H_2[NSiN]^{SiXyl3}$ (**5**) could be isolated in a 74 % yield. Crystals of sufficient quality for single crystal X-ray crystallographic analysis could not be obtained, however compound **5** afforded satisfactory elemental analyses.

With the goal of installing the $[NSiN]^{SiXyl3}$ ligand onto both germanium[5] and zirconium, compound **5** was combined with 2 equivalents of ^{n}BuLi to generate the bis(amide) salt $Li_2[NSiN]^{SiXyl3}$, followed by addition of this species to either Cl_2Ge•dioxane or $Cl_4Zr(THF)_2$. In each instance a reaction transpired however pure $[NSiN]^{SiXyl3}Ge$ or $[NSiN]^{SiXyl3}ZrCl_2$ were not obtained. This may be due, perhaps, to the increased steric hindrance of the trixylylsilyl group relative to the triphenyl- or tricumyl- derivatives,[5] and accordingly future endeavours will concentrate on first isolating spectroscopically pure bis(amide) $Li_2[NSiN]^{SiXyl3}$ prior to its reaction with Cl_2Ge•dioxane or $Cl_4Zr(THF)_2$.

3.3.2 Synthesis and reactivity of bis(guanidine)ligands with silyl and disilyl spacers

As part of our further investigations into the reactivity of hindered bidentate nitrogen-based ligands, the design of new neutral ligands featuring guanidine moieties was explored. While there are some reports of *N*-heterocyclic guanidine ligands being used in the literature,[11] a 1,1,3,3,-tetramethylguanidine (TMG) array was chosen as a key structural component, as these units would in theory be stronger donors than typical imine ligands due to donation of electron density from the adjacent $–NMe_2$ groups to the binding nitrogen atom (Figure 3.2). It should also be mentioned that there have been examples within the literature of complexes featuring bidentate guanidinate ligands which form a four-membered chelate with the element centre of choice.[12]

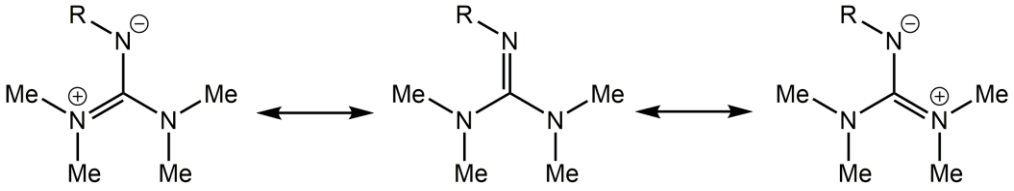

Figure 3.2 Resonance structures showing the stabilisation of negative charge on the imino-nitrogen of 1,1,3,3-tetramethylguanidine (TMG) fragments.

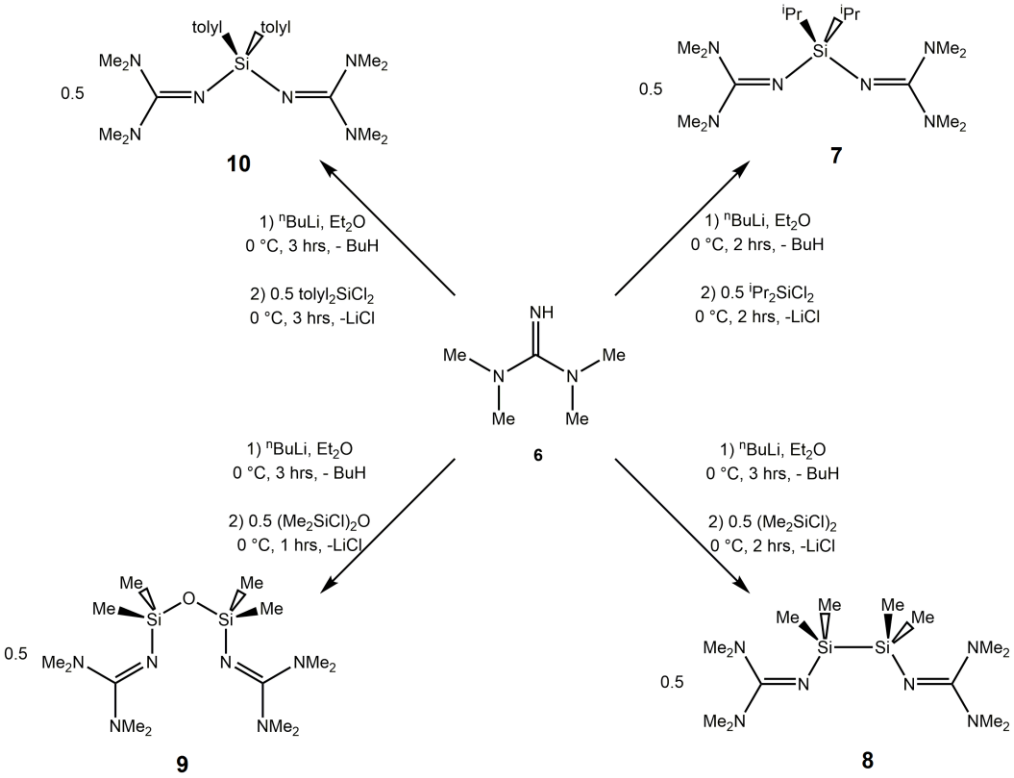

Scheme 3.3 Synthesis of bis(guanidine) ligands $[(Me_2N)_2C{=}N]_2Si^iPr_2$ (**7**), $[\{(Me_2N)_2C{=}N\}_2SiMe_2]_2$ (**8**), $[\{(Me_2N)_2C{=}N\}_2SiMe_2]_2O$ (**9**), and $[(Me_2N)_2C{=}N]_2Si(tolyl)_2$ (**10**).

Scheme 3.3 shows the bis(guanidine) ligands (**7**-**10**) prepared in this study. Fortunately, these ligands can be readily synthesised in moderate to good yields via relatively facile salt metathesis chemistry. While the corresponding lithium salt $Li[N{=}C(NMe_2)_2]$ can be prepared and isolated from the imine $HN{=}C(NMe_2)_2$ (**6**), this was deemed unnecessary, as *in situ*

deprotonation of **6** by one equivalent of ^{n}BuLi, followed by the addition of a dihalogenateddiorgano silane was able to furnish the target ligands in high yield. Compounds **7-9** were obtained as colourless, air sensitive liquids that are thermally stable when handled under nitrogen. $[(Me_2N)_2C{=}N]_2Si(tolyl)_2$ (**10**) is initially obtained as a colourless oil, however trituration with small portions of hexanes, or recrystallisation of this oil from a minimum volume of hexanes at -35 °C gives the product as a low-melting (35-38 °C) colourless solid.

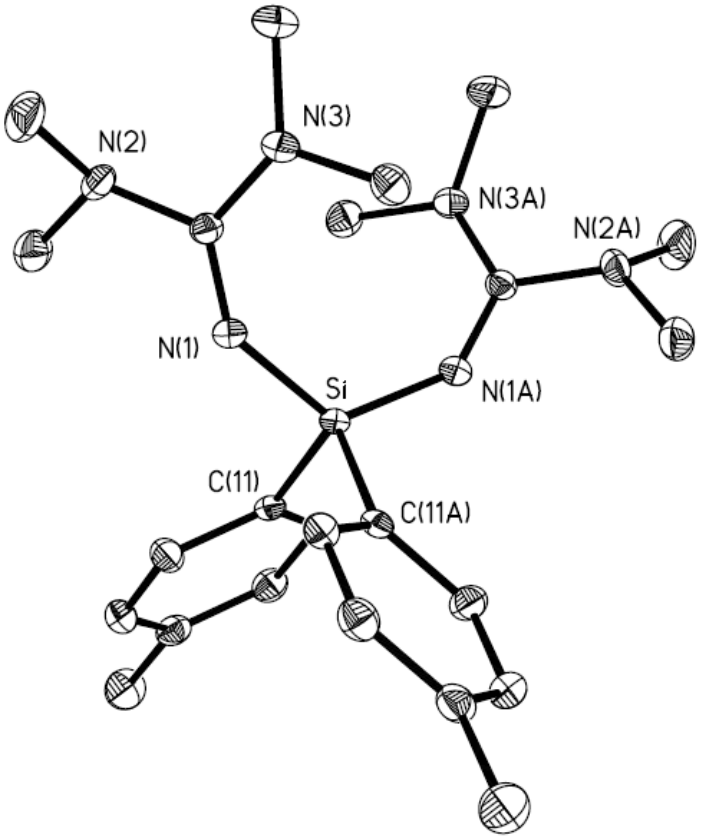

Figure 3.3 Molecular structure of $[(Me_2N)_2C{=}N]_2Si(tolyl)_2$, (**10**) with thermal ellipsoids presented at the 30% probability level. All hydrogen atoms have been omitted for clarity. Selected bond lengths (Å) and angles (°): Si-N(1) 1.6881(10), Si-C(11) 1.8840(12), N(1)-C(1) 1.2704(16), N(2)-C(1) 1.3988(15), N(1)-C(1) 1.3740(16); N(1)-Si-N(1A) 121.69(7), N(1)-Si-C(11) 105.90(5), N(1)-Si-C(11A) 108.02(5), C(11)-Si-C(11A) 106.44(7).

As illustrated in Figure 3.3, compound **10** adopts a distorted tetrahedral arrangement about the bridging silicon centre with a widened N(1)-Si-N(1A) angle of 121.69(7)°; the imine [N(1)-C(1)] bond length is 1.2704(16), and is comparable with other C=N bonds observed in related imines. In addition, the C-N bond lengths within the dimethylamino groups [1.3988(15) and 1.3740(16) Å], while different within standard error, are both shorter than typical C-N single bonds, thus implying the partial presence of double bond character as described in Figure 3.2.

Despite the facile nature of the syntheses outlined in Scheme 3.3 however, a problem was encountered when it came to utilising compounds **7-10** as ligands. Initial mixing **7-10** with $Cl_4Zr(THF)_2$ in Et_2O revealed that no reaction had occurred. Similarly, when compounds **7** or **10** were combined with Cl_2Ge•dioxane in toluene, ^1H NMR spectroscopic analysis revealed that no reaction had occurred. This may be due to the lone pair on each potentially ligating nitrogen atom interacting preferentially with the low-lying neighbouring Si-C σ* orbitals, which reduces the nucleophilicity of the ligands. This would result in a lengthening of the Si-C bond, and the observed distance of 1.8840(12) Å is slightly outside of the typical range for $Si\text{-}C_{Ar}$ bonds [1.857-1.878 Å],[13] suggesting that this interaction may be contributing to the observed bond elongation.

A different result was seen when $[\{(Me_2N)_2C{=}N\}_2SiMe_2]_2$ (**8**) was combined with Cl_2Ge•dioxane. Upon mixing these two reagents in toluene, a white precipitate appeared after ten hours. The resulting insoluble solid product was separated from the soluble fraction, washed with hexanes, and

dried *in vacuo* to yield a fine white powder that was insoluble in all readily available aromatic and aliphatic solvents. Addition of $CDCl_3$ to this powder resulted in a solubilisation followed by a rapid and exothermic reaction with the solvent leading to the formation of a dark brown mother liquor along with an insoluble solid. However, when this product was dissolved in CD_2Cl_2 no such reaction was observed, and the resulting ^1H NMR spectrum contained a single peak at 3.04 ppm, in line with with the presence of equivalent -NMe_2 environments. The $^{13}C\{^1H\}$ NMR spectrum contained a resonance at 40.6 ppm and a second signal at 164.8 ppm, congruent with the presence of [$N=C(NMe_2)_2$] fragments. Fortunately crystals of this product of suitable quality for X-ray crystallography were obtained from a CH_2Cl_2/hexanes mixture. As shown in Figure 3.4 and Equation 3.1, the product obtained was the Ge(II) imine dimer $[(Me_2N)_2C=NGeCl]_2$ (**11**).

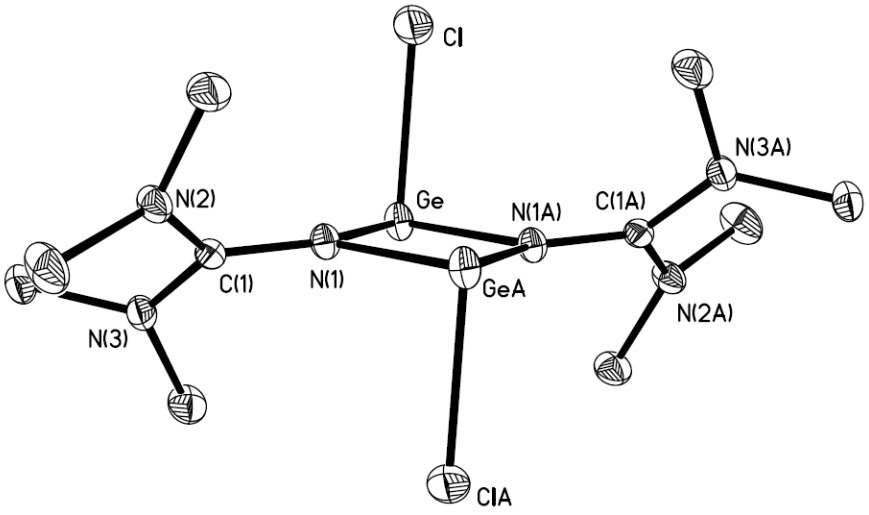

Figure 3.4 Molecular structure of $[(Me_2N)_2C=NGeCl]_2$ (**11**) with thermal ellipsoids presented at the 30% probability level. All hydrogen atoms have been omitted for clarity. Selected bond lengths (Å) and angles (°): Ge(1)-Cl(1) 2.3750(5), Ge(1)-N(1) 1.9429(11), Ge(1)-N(1A) 1.9551(12), N(1)-C(1) 1.3183(17), N(2)-C(1) 1.3567(18); N(1)-Ge(1)-Cl(1) 94.20(4), N(1)-Ge(1)-N(1A) 78.04(5), Ge(1)-N(1)-C(1) 130.05(10).

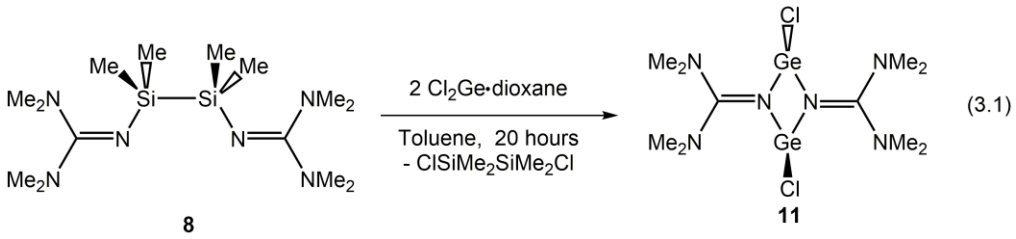

8 **11** (3.1)

Compound **11** adopts a dimeric structure in the solid state with two GeCl units bridged by two guanidinato units. Particularly noteable are the shorter N(2)-C(1) distances [1.3567(18) Å (**11**) vs. 1.3864(16) Å avg. (**8**)] and elongated imine N=C distances [1.3183(17) Å (**11**) vs. 1.2704(16) Å (**8**)] when $[(Me_2N)_2C{=}NGeCl]_2$ (**11**) is compared with $[(Me_2N)_2C{=}N]_2Si(tolyl)_2$ (**8**), the only bis(guanidine)silyl ligand which has been crystallographically characterised in this study. Compound **11** also adopts a planar Ge_2N_2 core with the Cl substituents perpendicular to the central Ge_2N_2 ring due to the presence of a lone pair at each Ge centre as shown by the sum of bond angles around Ge totalling 264.08(5)°. This Ge_2N_2 core arrangement is similar to that observed in the structurally related compound $[Ge(\mu\text{-}NAr)]_2$ (Ar = C_6H_3-2,6-(C_6H_2-2,4,6-Me_3)$_2$), which shows slightly shorter average Ge-N bond lengths of 1.8858(15) Å.[14] Also related to compound **11** is the Ge(II) amido dimer $[Ar^{\#}Ge(\mu\text{-}NH_2)]_2$ ($Ar^{\#}$ = C_6H_3-2,6-C_6H_3-2,6-$^{i}Pr_2$)$_2$), which once again has a dimeric structure with a planar Ge_2N_2 ring, with the germanium-bound $Ar^{\#}$ substituents perpendicular to the core due to the pyramidal geometry at Ge.[15] The average Ge-N bond length in $[Ar^{\#}Ge(\mu\text{-}NH_2)]_2$ of 2.007(3) Å is somewhat longer than observed in compound **11**. Due to the presence of substitutionally labile Cl atoms at Ge, compound **11** could potentially be functionalised with a variety of other groups such as H, alkyl and amido substituents via salt

metathesis pathways. Of note, low-valent group 14 compounds have recently been shown to be active as hydroboration catalysts, and thus structural variants of **11** could be explored for main group element-based catalysts, which would represent a new avenue of research in our research group.[7]

3.4 Conclusions

In this chapter the synthesis of a new NSiN chelate, $H_2[NSiN]^{SiXyl3}$ (**5**) was described, which expands upon our previous work involving the use of bis(amido)silyl ligands to stabilise reactive bonding environments within the main group. Furthermore, the synthesis and characterization of a new class of bis(imino)silyl species featuring tetramethylguanidine arrays bridged by a series of silane (**7**, **10**), disilane (**8**) and disiloxane (**9**) units was reported; while compounds **7**, **9** and **10** did not show any proclivity towards binding germanium(II) chloride following mixing with Cl_2Ge•dioxane, $[\{(Me_2N)_2C=N\}_2SiMe_2]_2$ (**8**) underwent Si-N bond cleavage to yield $[(Me_2N)_2C=NGeCl]_2$ (**11**), which may be a useful synthon towards a class of catalytically active, main group element containing species.

3.5 Experimental procedures

3.5.1. General

All reactions were performed using standard Schlenk techniques under an atmosphere of nitrogen or in a nitrogen-filled glovebox (Innovative Technology, Inc.). Solvents were dried using a Grubbs-type solvent purification system[16] manufactured by Innovative Technology, Inc., degassed, and stored under an atmosphere of nitrogen prior to use. Zirconium tetrachloride, tetramethylguanidine, germanium dichloride-dioxane, dichlorotetramethylsilane, dichlorotetramethyldisiloxane, and *n*-butyl lithium (2.5 M solution in hexanes) were purchased from Aldrich and used as received. 2,6-Diisopropylaniline and 5-bromo-meta-xylene were purchased from VWR and used as received. Dichlorodiisopropylsilane was obtained from Gelest, degassed (freeze-pump-thaw), and stored over molecular sieves under an N_2 atmosphere prior to use. Dichlorodi-p-tolylsilane was obtained from Oakwood Chemicals, degassed (freeze-pump-thaw), and stored over molecular sieves under an N_2 atmosphere prior to use. 3,5-$^{i}Pr_2C_6H_3Br$[7] and $Cl_4Zr(THF)_2$[17] were prepared according to literature procedures. ^{1}H and $^{13}C\{^{1}H\}$ and $^{29}Si\{^{1}H\}$ NMR spectra were recorded either on a Varian Inova-400 or Varian Inova-500 spectrometer and referenced externally to $SiMe_4$. Elemental analyses were performed by the Analytical and Instrumentation Laboratory, and all mass spectra were recorded by the Mass Spectrometry lab at the University of Alberta. Infrared spectra were recorded using Nic-Plan FTIR microscope. Melting points were obtained in sealed glass capillaries under nitrogen using a MelTemp melting point apparatus and are uncorrected.

3.5.2. X-ray Crystallography

Crystals of appropriate quality for X-ray diffraction studies were removed either from a Schlenk tube under a stream of nitrogen or a vial (glovebox) and immediately covered with a thin layer of hydrocarbon oil (Paratone-N). A suitable crystal was then selected, attached to a glass fibre, and quickly placed in a low-temperature stream of nitrogen.[18] All data were collected using a Bruker APEX II CCD detector/D8 diffractometer using Mo Kα or Cu Kα radiation, with the crystal cooled to −100 °C. Refinements were completed using the program SHELXL-97.[19] Hydrogen atoms were assigned positions based on the sp^2 or sp^3 hybridisation geometries of their attached carbon or nitrogen atoms and were given thermal parameters 30 % greater than those of their parent atoms.

3.5.3.1 Synthesis of Xyl_3SiH (2b)

To a solution of 5-bromo-m-xylene (5.42 g, 29.4 mmol) in 150 mL of Et_2O at 0 °C, ^nBuLi (1.6 M solution in hexanes, 27.5 mL, 44 mmol) was added dropwise. The solution turned from colourless to pale yellow, and was stirred overnight during which time a white precipitate of $XylLi{\cdot}(OEt_2)_x$ had formed. The mother liquor was decanted via a cannula, and 150 mL of C_6H_6 was added. To the resulting clear, colourless solution was added $HSiCl_3$ (1.32 g, 0.97 mL, 9.8 mmol) leading to the immediate formation of a white precipitate. The mixture was heated to reflux overnight, and then the mother liquor was decanted through a filter cannula to yield a pale yellow filtrate. The volatiles were removed from the filtrate, and the remaining material was triturated with 3 × 5 mL portions of hexanes to yield Xyl_3SiH as a white

crystalline solid (1.99 g, 59 %). A second batch of the product was obtained following extraction of the original solid with 100 mL of C_6H_6, followed by removal of C_6H_6, and the residue was triturated with 3 × 5 mL portions of hexanes. The resultant solid was dried *in vacuo* yielded a further 1.02 g of product (combined yield 89 %). ^{1}H NMR (400 MHz, C_6D_6): δ 2.08 (s, 18H, ArC*H*$_3$), 5.87 (s with satellites, 1H, Ar$_3$Si*H*, $^1J_{SiH}$ = 195 Hz), 6.87 (s, 3H, p-Ar*H*), 7.50 (s, 6H, o-Ar*H*). ^{13}C{^{1}H} NMR (126 MHz, C_6D_6): δ 21.3 (Ar*C*H$_3$), 132.0 (Ar*C*), 134.1 (Ar*C*), 134.3 (Ar*C*), 137.7 (Ar*C*). Mp (°C): 131-134. Anal. Calcd. for $C_{24}H_{28}Si$: C, 83.66; H, 8.19. Found: C, 83.91; H, 8.01.

3.5.3.1 Synthesis of Xyl$_3$SiBr (3b)

Xyl$_3$SiH (1.02 g, 2.95 mmol) was dissolved in 6 mL of CCl_4 to yield a pale yellow solution. The solution was then cooled to 0 °C, and Br_2 (0.18 mL, 0.56 g, 3.5 mmol) was added. The resulting mixture was stirred for 30 minutes at 0 °C, and then the volatiles were removed *in vacuo* to yield Xyl$_3$SiBr as an analytically pure pale orange (0.94 g, 75 %). ^{1}H NMR (500 MHz, C_6D_6): δ 2.01 (s, 18H, ArC*H*$_3$), 6.83 (s, 3H, p-Ar*H*), 7.62 (s, 6H, o-Ar*H*). ^{13}C{^{1}H} NMR (126 MHz, C_6D_6): δ 21.3 (Ar*C*H$_3$), 133.0 (Ar*C*), 133.6 (Ar*C*), 133.8 (Ar*C*), 137.8 (Ar*C*). Mp (°C): 187-189. Anal. Calcd. for $C_{24}H_{27}SiBr$: C, 68.07; H, 6.43. Found: C, 68.57; H, 6.82.

3.5.3.3 Synthesis of Xyl$_3$SiNH$_2$ (4)

A suspension of $LiNH_2$ (0.051 g, 2.2 mmol) in 4 mL of Et_2O was cooled to -35 °C, and a solution of Xyl$_3$SiBr (0.93 g, 2.2 mmol) in 5 mL of Et_2O was added dropwise. The resultant mixture was stirred for 72 hours, and

then filtered through Celite. The solvent was then removed from the filtrate to yield Xyl_3SiNH_2 as a white crystalline solid (0.75 g, 94 %). ^{1}H NMR (500 MHz, $CDCl_3$): δ 2.30 (s, 18H, ArC*H*$_3$), 7.04 (s, 3H, p-Ar*H*), 7.21 (s, 6H, o-Ar*H*). ^{13}C{^{1}H} NMR (126 MHz, $CDCl_3$): δ 21.6 (Ar*C*H$_3$), 131.4 (Ar*C*), 132.9 (o-Ar*C*), 136.8 (ipso- Ar*C*), 137.13 (Ar*C*). Mp (°C): 131-134. Anal. Calcd. for $C_{24}H_{29}NSi$: C, 80.17; H, 8.13; N, 3.90. Found: C, 80.78; H, 8.42; N, 4.01.

3.5.3.4 Synthesis of $(Xyl_3SiNH)_2Si^iPr_2$ (5)

Xyl_3SiNH_2 (1.107 g, 3.078 mmol) was dissolved in 10 mL of THF and the resultant solution cooled to -35 °C. To this was added ^{n}BuLi (1.6 M solution in hexanes, 1.924 mL, 3.1 mmol) to give a pale yellow solution. The mixture was allowed to stir for 4 hours, and then $^iPr_2SiCl_2$ (0.285 g, 277.6 µL, 1.54 mmol) was added. The resultant mixture was stirred for 18 hours, and then the volatiles were removed *in vacuo*. The crude oily solid was then extracted into 6 mL of Et_2O, and the mixture filtered through Celite to remove lithium salts. Removal of the solvent from the filtrate gave $(Xyl_3NH)_2Si^iPr_2$ as a white crystalline solid (0.950 g, 74 %). ^{1}H NMR (500 MHz, C_6D_6): δ 0.78 (sept, 2H, SiC*H*(CH$_3$)$_2$, $^3J_{HH}$ = 7.2 Hz), 1.11 (d, 6H, SiCH(C*H*$_3$)$_2$, $^3J_{HH}$ = 7.2 Hz), 1.40 (broad s, 2H, N*H*), 2.10 (s, 36H, ArC*H*$_3$), 6.86 (s, 6H, p-Ar*H*), 7.59 (s, 12H, o-Ar*H*). *Need to rerun $^{13}C\{^1H\}$ NMR.* Mp (°C): 93-97. Anal. Calcd. for $C_{54}H_{70}N_2Si_3$: C, 78.01; H, 8.49; N, 3.37; Found: C, 78.63; H, 8.91; N, 2.98.

3.5.3.5 Synthesis of (3,5-Dipp)$_3$SiH (2a)

3,5-DippBr (12.39 g, 51.4 mmol) was dissolved in 200 mL of Et_2O and cooled to 0 °C, and to this solution was added dropwise ^{n}BuLi (1.6 M in hexanes, 40.0 mL, 64 mmol). The mixture was stirred for 20 hours, during which time it was allowed to warm up to room temperature, and a white precipitate formed. The mother liquor was decanted away through a filter cannula, and 200 mL of C_6H_6 was added to the remaining solid. The resultant suspension was cooled to 0 °C and $HSiCl_3$ (2.32 g, 1.73 mL, 17.1 mmol) was added dropwise. The mixture was heated to reflux for 16 hours, and then the volatiles were removed *in vacuo*. The resultant yellow oily solid was extracted into 150 mL of Et_2O, and then filtered. The pale yellow filtrate was concentrated to dryness *in* vacuo and triturated with 3 × 5 mL portions of hexanes to yield (3,5-Dipp)$_3$SiH as a pale yellow crystalline solid (5.21 g, 59 %). ^{1}H NMR (400 MHz, $CDCl_3$): δ 1.24 (d, 36H, ArCH(C*H*$_3$)$_2$, $^3J_{HH}$ = 7.1 Hz), 2.89 (sept, 6H, ArC*H*(C*H*$_3$)$_2$, $^3J_{HH}$ = 7.0 Hz), 5.43 (s with satellites, 1H, Si*H*, $^1J_{SiH}$ = 196 Hz), 7.13 (t, 3H, p-Ar*H*, $^4J_{HH}$ = 2.0 Hz), 7.33 (d, 6H, o-Ar*H*, $^4J_{HH}$ = 2.0 Hz). ^{13}C{^{1}H} NMR (126 MHz, $CDCl_3$): δ 24.2 (ArCH(*C*H$_3$)$_2$), 34.6 (Ar*C*H(CH$_3$)$_2$), 126.3 (Ar*C*), 131.6 (Ar*C*), 133.7 (Ar*C*), 148.2 (Ar*C*). Mp (°C): 122-125. Anal. Calcd. for $C_{36}H_{52}Si$: C, 84.30; H, 10.22. Found: C, 84.86; H, 9.89.

3.5.3.6 Synthesis of [(Me$_2$N)$_2$C=N]$_2$Si^{i}Pr$_2$ (7)

Tetramethylguanidine (**6**) (0.570 g, 4.95 mmol) was dissolved in 10 mL of Et_2O, and the solution was cooled to 0 °C. ^{n}BuLi (2.5 M solution in hexanes, 1.98 mL, 5.0 mmol) was then added dropwise, and the mixture was

allowed to warm to room temperature and stir for 2 hours. The resulting solution was cooled again to 0 °C, and $^{i}Pr_2SiCl_2$ (446.6 μL, 0.458 g, 2.47 mmol) was added with the immediate formation of a white precipitate. The mixture was stirred for 2 hours, and then filtered. Removal of the volatiles from the filtrate yielded **7** as a colourless liquid (0.41 g, 48 %). ^{1}H NMR (400 MHz, C_6D_6): δ 0.82 (sept, 2H, SiC*H*$(CH_3)_2$, $^{3}J_{HH}$ = 7.5 Hz), 0.93 (overlapping d, 12H, SiCH(C*H*$_3)_2$), 2.89 (s, 24H, N(C*H*$_3)_2$). ^{13}C{^{1}H} NMR (126 MHz, C_6D_6): δ 14.2 (Si*C*H$(CH_3)_2$), 17.3 (SiCH(*C*H$_3)_2$), 40.1 (N(*C*H$_3)_2$), 162.9 (N*C*N). ^{29}Si{^{1}H} NMR (99 MHz, C_6D_6): δ -33.9 (*Si*$(CH_3)_2$). HR-MS: [M – H]$^{+}$; Calcd. 343.2927. Obs. 343.2996 (Δ ppm = 1.20). A satisfactory combustion analysis was not obtained; please see Figures 3.5–3.7 for associated NMR spectra.

3.5.3.7 Synthesis of $[(Me_2N)_2C=N(SiMe_2)]_2$ (8)

Tetramethylguanidine (**6**) (0.322 g, 2.80 mmol) was dissolved in 6 mL of Et_2O and a solution of ^{n}BuLi (2.5 M solution in hexanes, 1.12 mL, 2.8 mmol) was added at 0 °C, after which the mixture was allowed to warm to room temperature and stir for 3 hours. This solution was cooled again to 0 °C, and $ClSiMe_2SiMe_2Cl$ (260.4 μL, 0.262 g, 1.40 mmol) was added with the immediate formation of a white precipitate. The resultant mixture was allowed to stir for 1 hour, and then filtered. Removal of the volatiles from the filtrate gave the desired product $[(Me_2N)_2C=N(SiMe_2)]_2$ (**8**) as a colourless liquid (0.380 g, 79 %). ^{1}H NMR (400 MHz, C_6D_6): δ 0.56 (s, 12H, Si(C*H*$_3)_2$), 2.55 (s, 24H, N(C*H*$_3)_2$). ^{13}C{^{1}H} NMR (126 MHz, C_6D_6): δ 4.0 (Si(*C*H$_3)_2$), 40.0 (N(*C*H$_3)_2$). ^{29}Si{^{1}H} NMR (99 MHz, C_6D_6): δ -31.7

($Si(CH_3)_2$). HR-MS: [EI]; Calcd. 344.25400. Obs. 344.25504 (Δ ppm = 3.0). A satisfactory combustion analysis was not obtained; please see Figures 3.8–3.10 for associated NMR spectra.

3.5.3.8 Synthesis of $\{[(Me_2N)_2C{=}N]SiMe_2\}_2O$ (9)

Tetramethylguanidine (**6**) (0.185 g, 1.61 mmol) was dissolved in 4 mL of Et_2O and a solution of ^{n}BuLi (2.5 M solution in hexanes, 644.0 μL, 1.6 mmol) was added at 0 °C, after which the mixture was allowed to warm to room temperature and stir for 3 hours. This solution was cooled again to 0 °C, and $(ClSiMe_2)_2O$ (157.5 μL, 0.164 g, 0.81 mmol) was added, with the immediate formation of a white precipitate. The resultant mixture was allowed to stir for 2 hours, and then filtered. Removal of the volatiles from the filtrate yielded $\{[(Me_2N)_2C{=}N]SiMe_2\}_2O$ (**9**) as a colourless liquid (0.380 g, 79 %). ^{1}H NMR (400 MHz, C_6D_6): δ 0.51 (s, 12H, $Si(CH_3)_2$), 2.59 (s, 24H, $N(CH_3)_2$). $^{13}C\{^{1}H\}$ NMR (126 MHz, C_6D_6): δ 3.9 ($Si(CH_3)_2$), 39.9 ($N(CH_3)_2$). $^{29}Si\{^{1}H\}$ NMR (79 MHz, C_6D_6): δ -21.8 ($Si(CH_3)_2$). HR-MS: [EI]; Calcd. 360.24893. Obs. 360.24874 (Δ ppm = 0.50). A satisfactory combustion analysis was not obtained; please see Figures 3.11–3.13 for associated NMR spectra.

3.5.3.9 Synthesis of $[(Me_2N)_2C{=}N]_2Si(tolyl)_2$ (10)

Tetramethylguanidine (**6**) (0.401 g, 3.48 mmol) was dissolved in 10 mL of Et_2O, and a solution of ^{n}BuLi (2.5 M solution in hexanes, 1.39 mL, 3.5 mmol) was added at -35 °C after which the mixture was allowed to warm to room temperature and stir for 3 hours. The mixture was then cooled to -35

°C, and (p-tolyl)$_2$SiCl$_2$ (445.1 μL, 0.490 g, 1.74 mmol) was added with the immediate formation of a white precipitate. The resultant mixture was allowed to stir for 3 hours, and then filtered. Removal of the volatiles from the filtrate afforded the crude product [(Me$_2$N)$_2$C=N]$_2$Si(tolyl)$_2$ (**10**) as an orange oil (0.515 g, 67 %). Colourless crystals suitable for X-ray crystallographic analysis were obtained by dissolving the product in 1 mL of hexanes, followed by cooling to -35 °C for 5 days. ^{1}H NMR (400 MHz, C$_6$D$_6$): δ 2.18 (s, 6H, ArC*H*$_3$), 2.63 (s, 24H, N(C*H*$_3$)$_2$), 7.19 (d, 4H, Ar*H*, $^3J_{HH}$ = 8.0 Hz), 8.16 (d, 4H, Ar*H*, $^3J_{HH}$ = 8.0 Hz). ^{13}C{^{1}H} NMR (126 MHz, C$_6$D$_6$): δ 21.6 (Ar*C*H$_3$), 40.1 (N(*C*H$_3$)$_2$), 135.2 (Ar*C*), 137.1 (Ar*C*), 142.6 (Ar*C*), 158.3 (Ar*C*). ^{29}Si{^{1}H} NMR (99 MHz, C$_6$D$_6$): δ -55.3 (*Si*(CH$_3$)$_2$). Mp (°C): 35-38. Anal. Calcd. for C$_{24}$H$_{38}$N$_6$Si: C, 65.71; H, 8.73; N, 19.16. Found: C, 66.11; H, 9.13; N, 18.90.

3.5.3.10 Reaction of [(Me$_2$N)$_2$C=N(SiMe$_2$)]$_2$ with Cl$_2$Ge•dioxane; synthesis of [(Me$_2$N)$_2$C=NGeCl]$_2$ (11)

[(Me$_2$N)$_2$C=N(SiMe$_2$)]$_2$ (**8**) (0.101 g, 0.293 mmol) was dissolved in 3 mL of toluene, and this solution was added to a suspension of Cl$_2$Ge•dioxane (0.136 g, 0.587 mmol) in 4 mL of toluene, and the resultant suspension was stirred for 20 hours. The precipitate was allowed to settle, and the mother liquor decanted away. The remaining white solid was washed with 3 mL of hexanes, and then dried *in vacuo* to yield **11** as a white, free-flowing powder (0.108 g, 83 %). Crystals suitable for X-ray diffraction analysis were obtained by dissolving 0.060 g of the solid in 2 mL of CH$_2$Cl$_2$, and then layering with 2 mL of hexanes; the hexanes were allowed to slowly diffuse into the CH$_2$Cl$_2$

layer overnight at room temperature to yield colourless crystals. ^{1}H NMR (400 MHz, CD_2Cl_2): δ 3.04 (s, 24H, N(CH_3)$_2$). ^{13}C{^{1}H} NMR (101 MHz, CD_2Cl_2): δ 40.6 (N(*C*H$_3$)$_2$), 164.8 (N*C*N). Mp (°C): 163-166. Anal. Calcd. for $C_{10}H_{24}Cl_2Ge_2N_6$: C, 27.02; H, 5.44; N, 18.91. Found: C, 26.86; H, 5.81; N, 19.13.

Table 3.1 Crystallographic Data for Compounds **10** and **11**

	10	**11**
empirical formula	$C_{24}H_{38}N_6Si$	$C_{10}H_{24}Cl_2Ge_2N_6$
fw	438.69	444.43
cryst dimens (mm^3)	0.45 × 0.12 × 0.11	0.22 × 0.18 × 0.17
cryst syst	Orthorhombic	Monoclinic
space group	$P2_12_12_1$	$P2_1/c$
unit cell dimensions		
a (Å)	11.9756 (2)	8.6855 (3)
b (Å)	12.1464 (2)	7.3337 (3)
c (Å)	8.8646 (1)	14.6686 (6)
α (deg)		
β (deg)		97.2696 (9)
γ (deg)		
V ($Å^3$)	1289.45 (3)	926.83 (6)
Z	2	2
ρ (g cm^{-3})	1.130	1.593
abs coeff (mm^{-1})	0.960	6.649
T (K)	173 (1)	173 (1)
$2\theta_{max}$ (deg)	140.40	142.61
total data	8848	5954
unique data (R_{int})	2382 (0.0118)	1779 (0.0137)
obs data [$I > 2\sigma(I)$]	2362	1769
Params	147	95
R_1 [$I > 2\sigma(I)$][a]	0.0237	0.0183
wR_2 [all data][a]	0.0669	0.0488
Max/Min $\Delta\rho$ (e$^-$ $Å^{-3}$	0.227/-0.147	0.281/-0.360

[a] $R_1 = \Sigma \| \|F_o\| - \|F_c\| \| / \Sigma |F_o|$; $wR_2 = [\Sigma\, w(F_o^2 - F_c^2)^2 / \Sigma\, w(F_o^4)]^{1/2}$.

Figure 3.5 ^{1}H NMR spectrum ($CDCl_3$) of $[(Me_2N)_2C{=}N(SiMe_2)]_2$ (**7**)

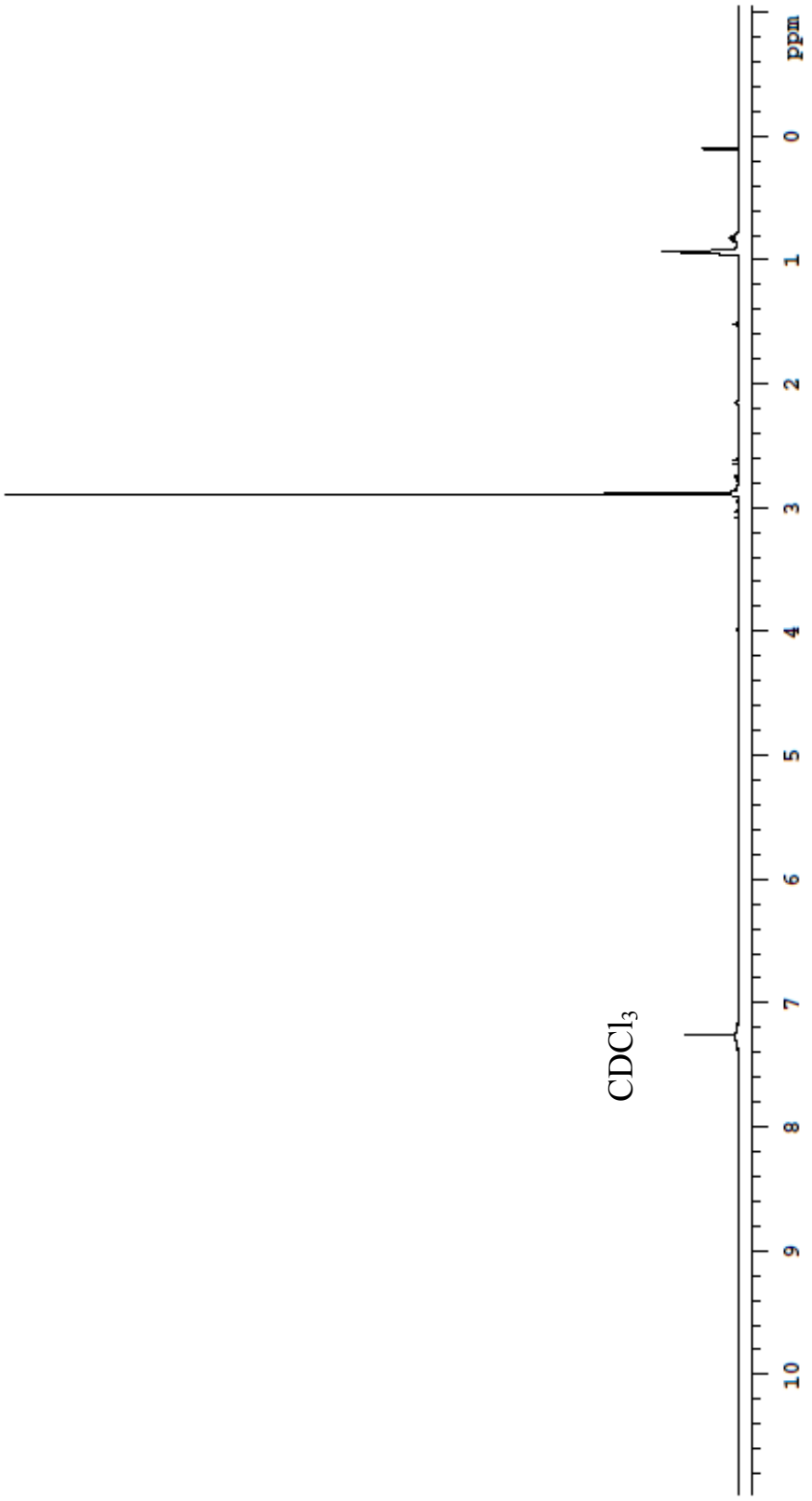

Figure 3.6 $^{13}C\{^{1}H\}$ NMR spectrum ($CDCl_3$) of $[(Me_2N)_2C{=}N(SiMe_2)]_2$ (**7**)

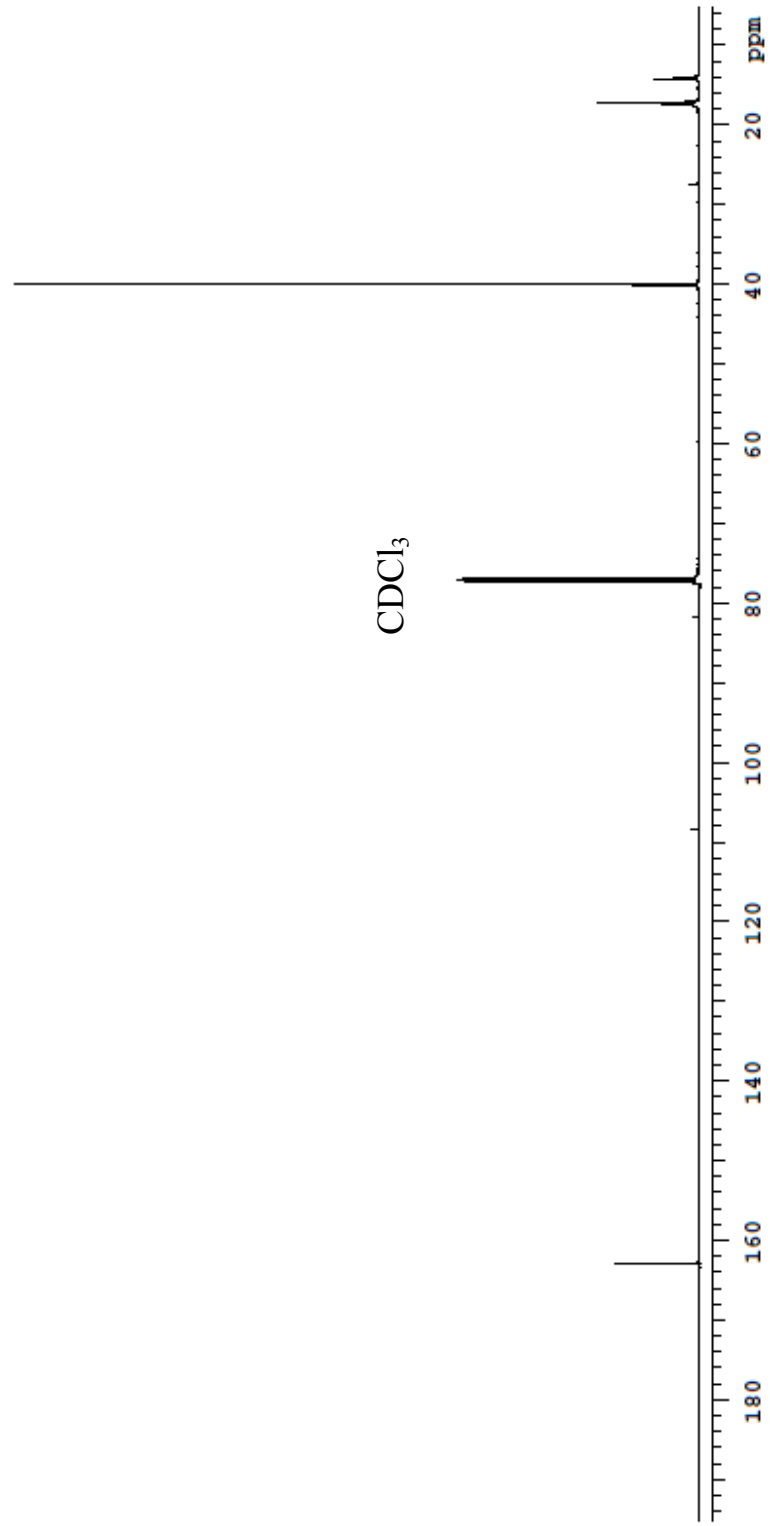

Figure 3.7 $^{29}Si\{^{1}H\}$ NMR spectrum ($CDCl_3$) of $[(Me_2N)_2C{=}N(SiMe_2)]_2$ (**7**)

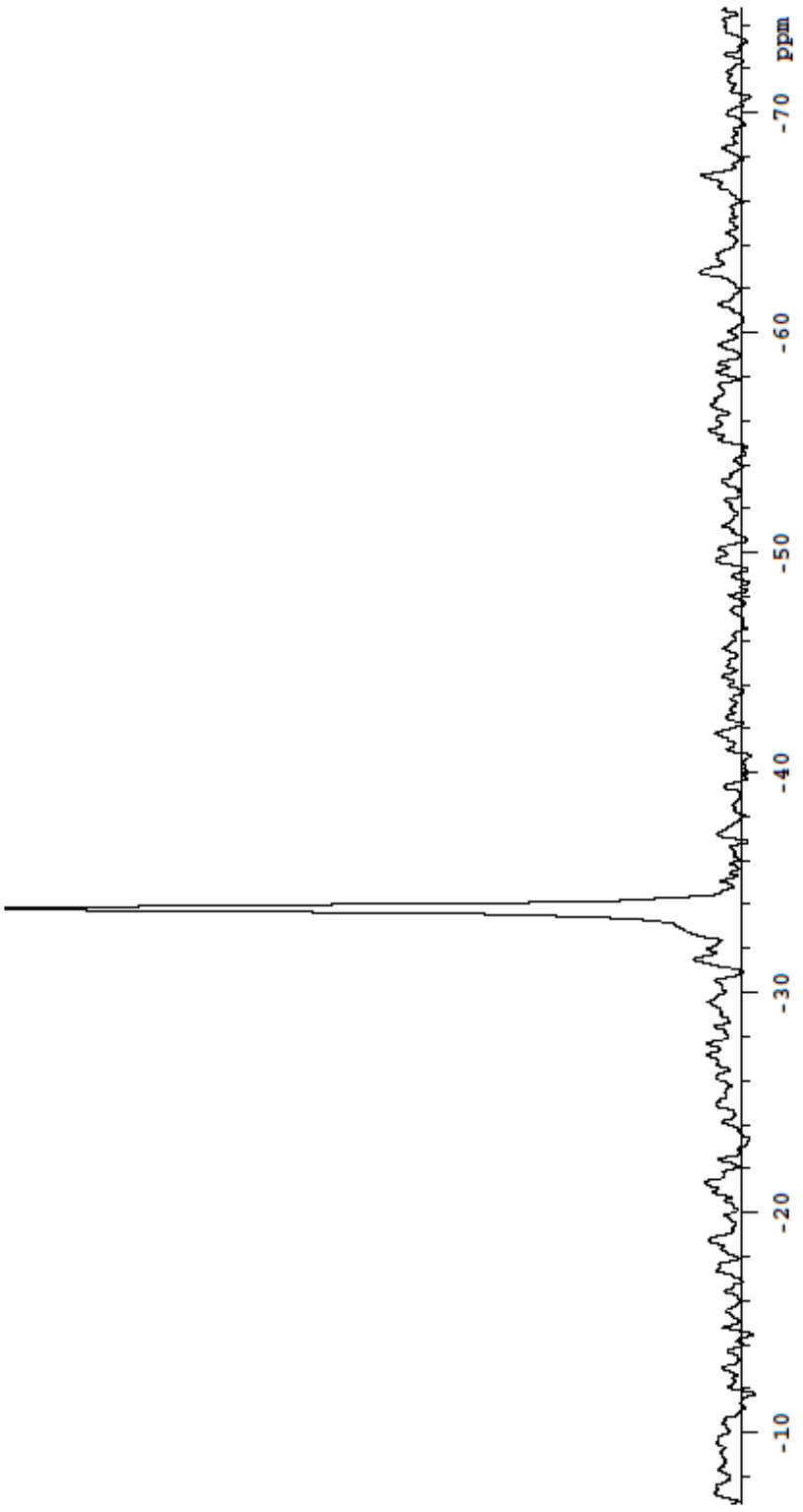

Figure 3.8 ^{1}H NMR spectrum (C_6D_6) of $[(Me_2N)_2C{=}N(SiMe_2)]_2$ (**8**)

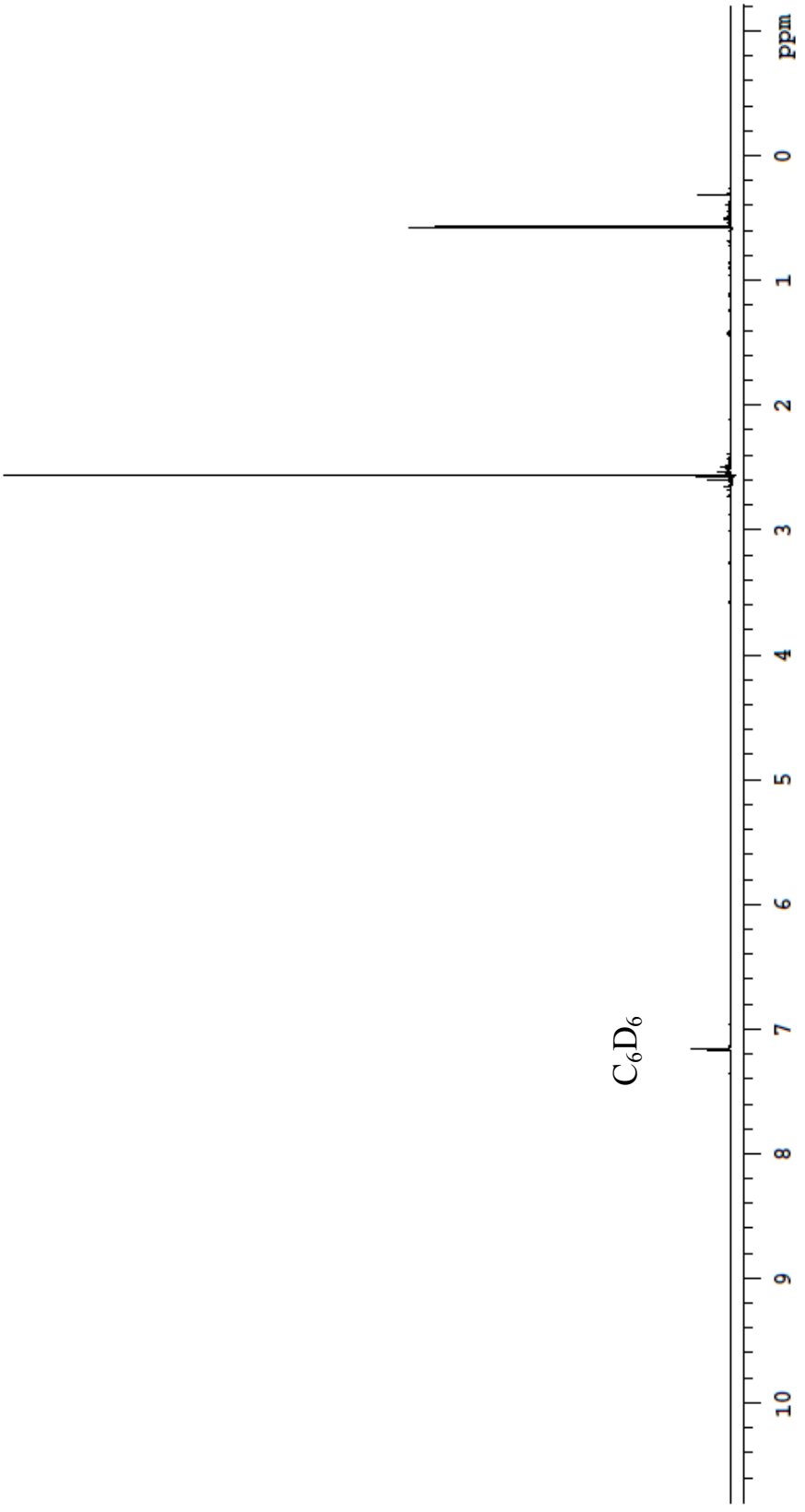

Figure 3.9 $^{13}C\{^{1}H\}$ NMR spectrum (C_6D_6) of $[(Me_2N)_2C{=}N(SiMe_2)]_2$ (**8**)

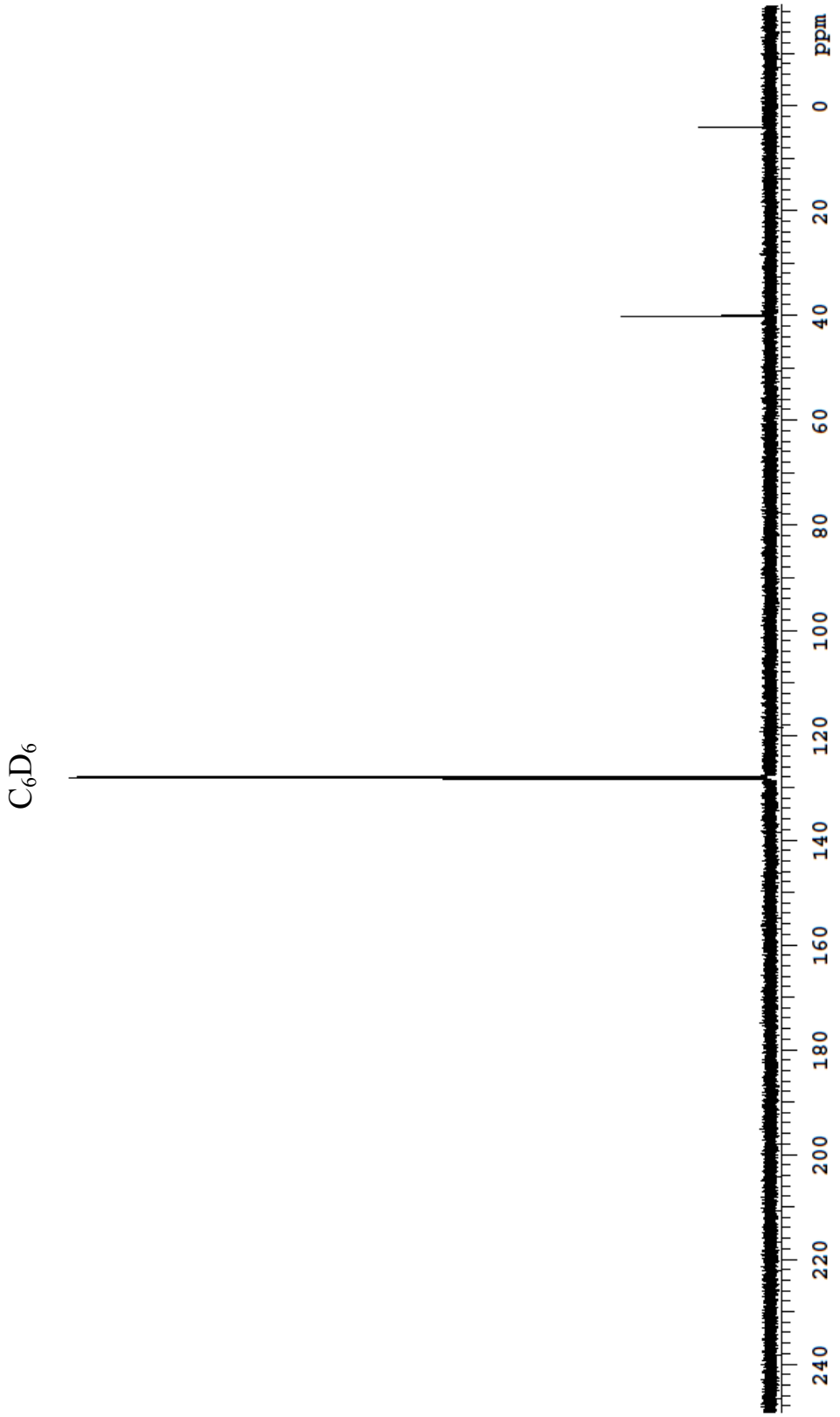

Figure 3.10 $^{29}Si\{^{1}H\}$ NMR spectrum (C_6D_6) of $[(Me_2N)_2C{=}N(SiMe_2)]_2$ (**8**)

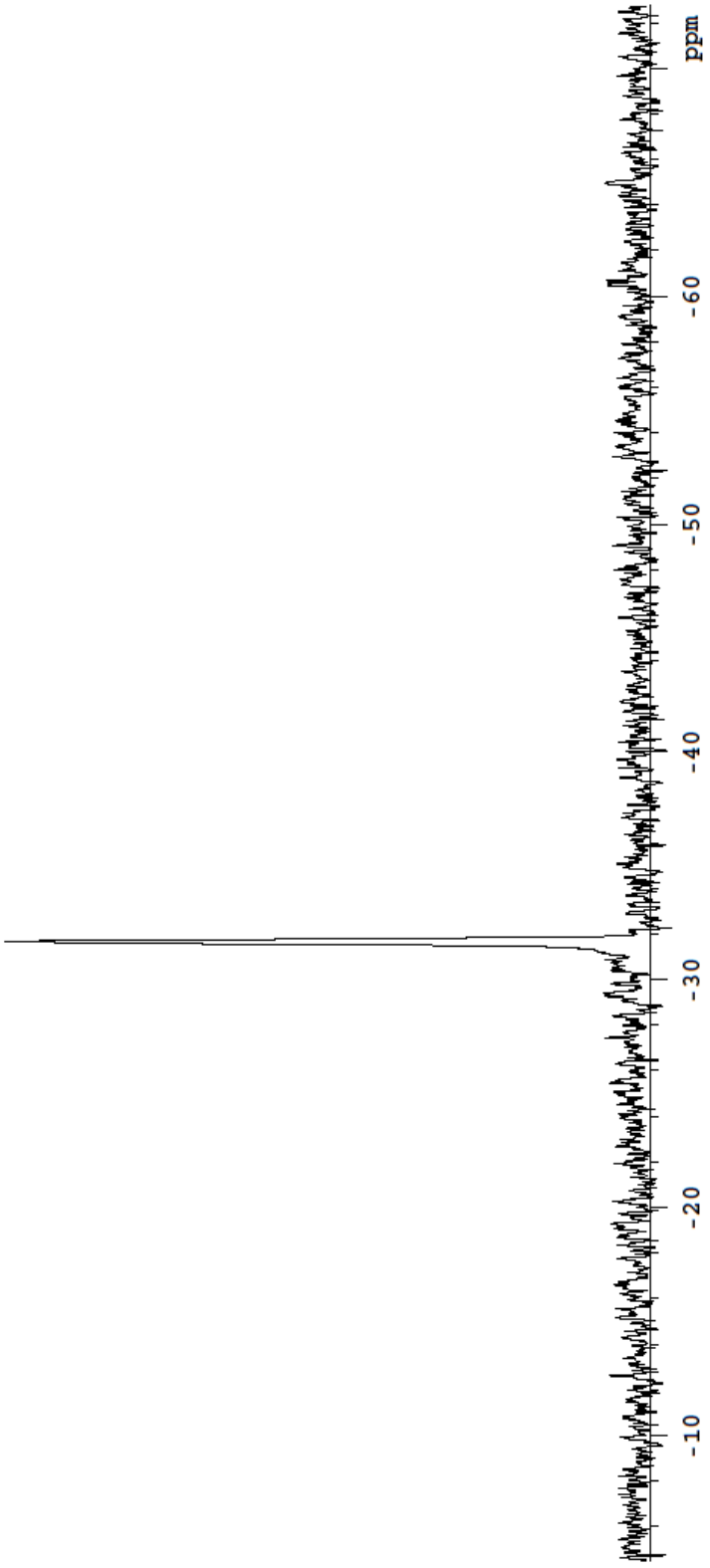

Figure 3.11 ^{1}H NMR spectrum (C_6D_6) of $[(Me_2N)_2C{=}N(SiMe_2)]_2O$ (**9**)

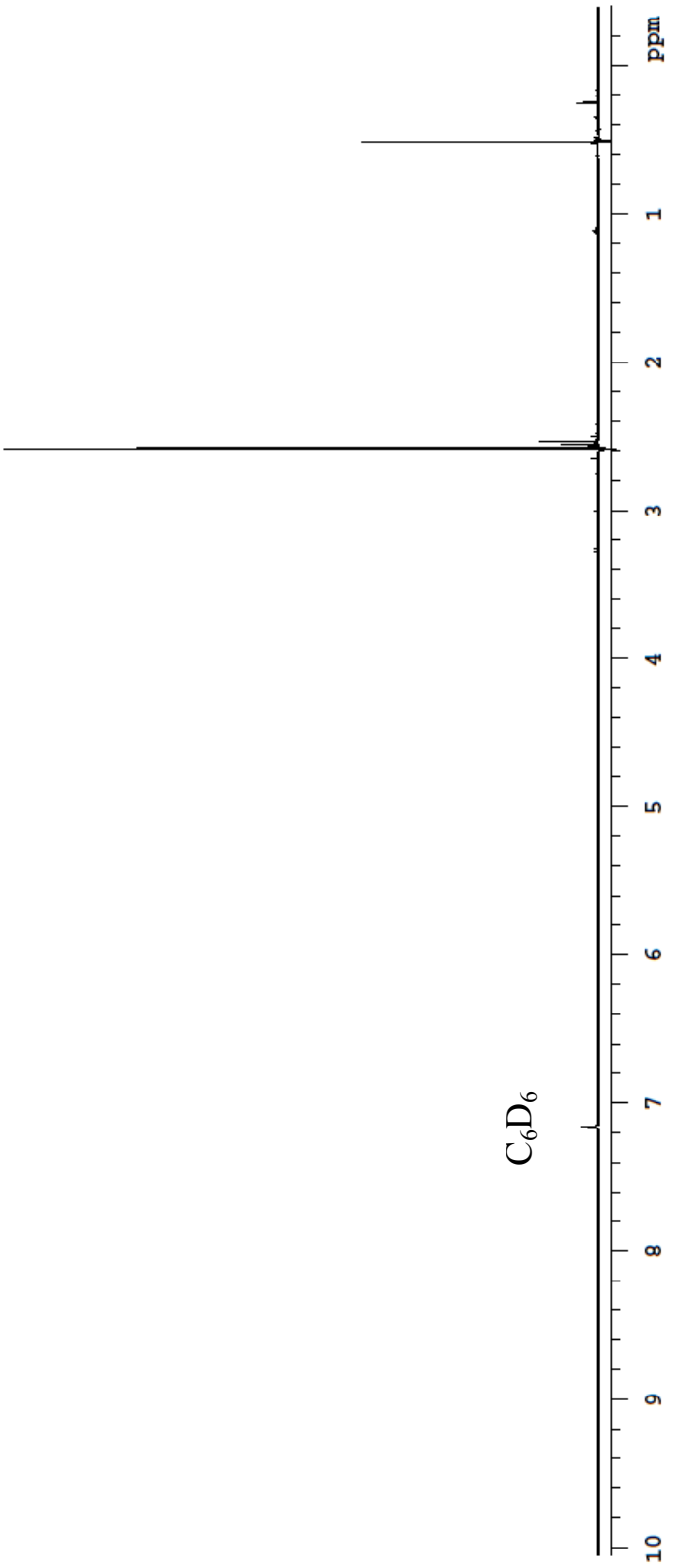

Figure 3.12 $^{13}C\{^{1}H\}$ NMR spectrum (C_6D_6) of $[(Me_2N)_2C{=}N(SiMe_2)]_2O$ (**9**)

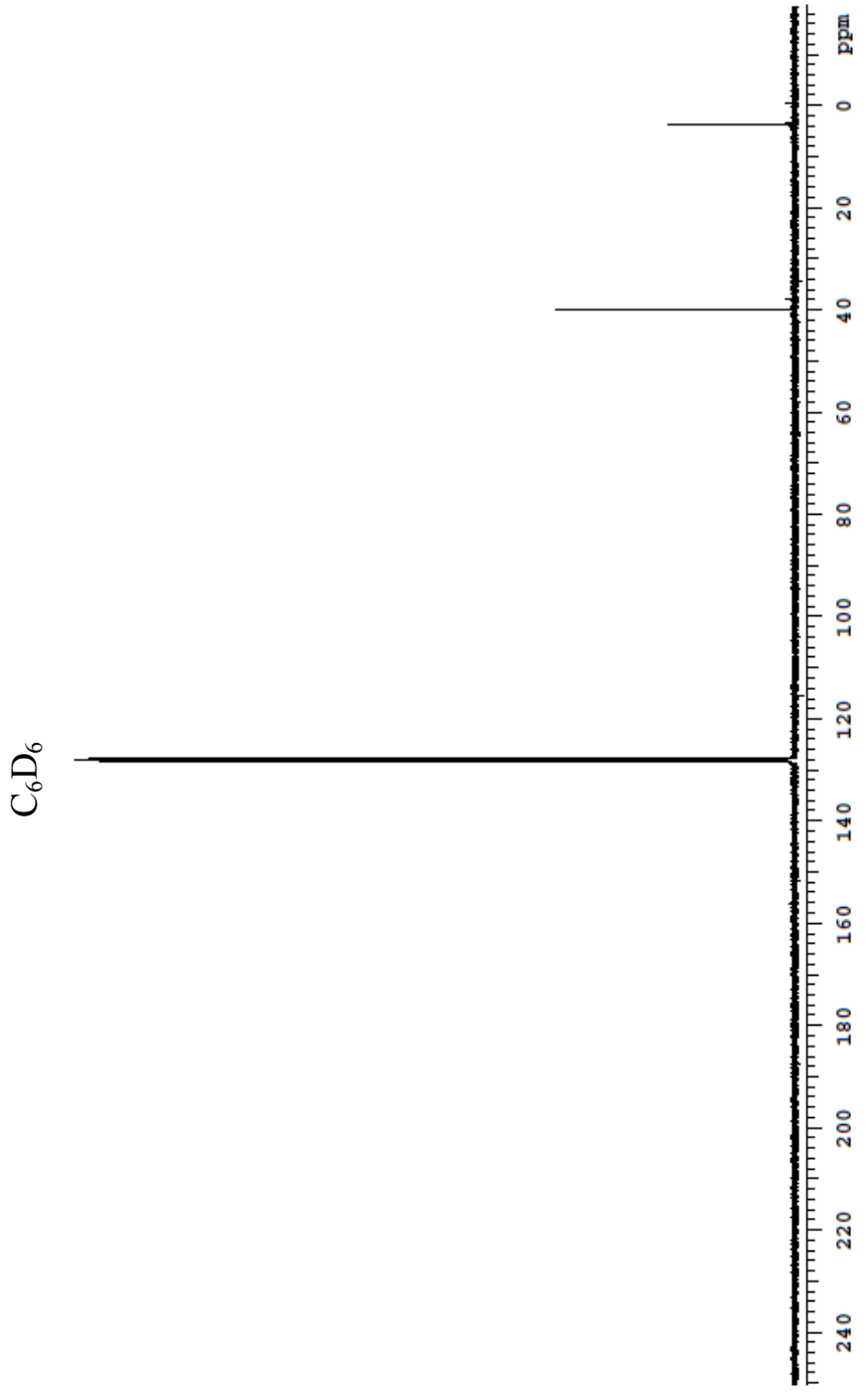

Figure 3.13 $^{29}Si\{^{1}H\}$ NMR spectrum (C_6D_6) of $[(Me_2N)_2C{=}N(SiMe_2)]_2O$ (**9**)

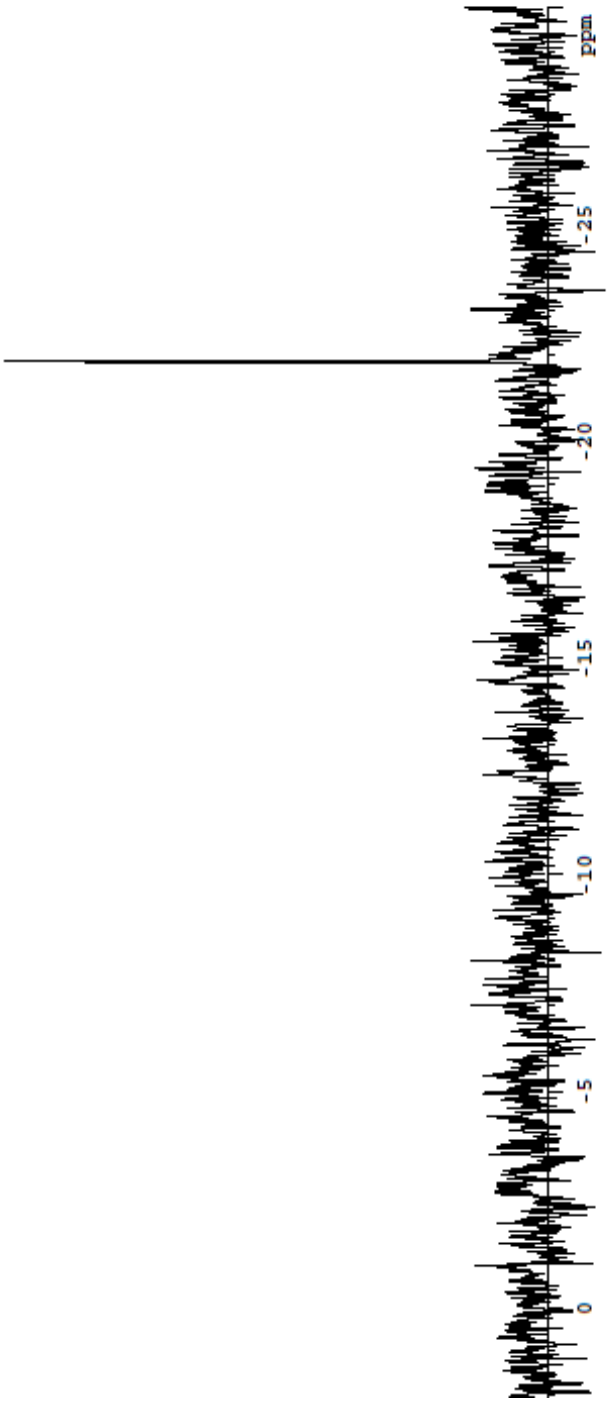

3.6 References

1 (*a*) R. J. Lundgren, M. Stradiotto, *Chem. Eur. J.*, **2012**, *32*, 9758; (*b*) R. D. Hancock, *Chem. Soc. Rev.*, **2013**, *42*, 1500; (*c*) M. M. Watt, M. S. Collins, D. W. Johnson, *Acc. Chem. Res.*, **2012**, *46*, 955.

2 M. Lappert, P. P. Power, A. Protchenko, A. Seeber, *Metal Amide Chemistry*; John Wiley and Sons Ltd.: West Sussex, UK, **2008**.

3 (*a*) D. C. Bradley, M. H. Chisholm, *Acc. Chem. Res.*, **1976**, *9*, 273; (*b*) M. D. Fryzuk, *Can. J. Chem.*, **1992**, *70*, 2839; (*c*) R. R. Schrock, *Acc. Chem. Res.*, **1997**, *30*, 9; (*d*) L. H. Gade, *Acc. Chem. Res.*, **2002**, *35*, 575.

4 D. V. Yandulov, R. R. Schrock, *Science*, **2003**, *301*, 76.

5 A. M. Tondreau, C. C. H. Atienza, K. J. Weller, S. A. Nye, K. M. Lewis, J. G. P. Delis, P. J. Chirik, *Science*, **2012**, *335*, 567.

6 (*a*) E. Niecke, W. Flick, *Angew. Chem., Int. Ed. Engl.*, **1974**, *13*, 134; (*b*) R. West, M. Denk, *Pure Appl. Chem.*, **1996**, *68*, 785; (*c*) L. Stahl, *Coord. Chem. Rev.*, **2000**, *210*, 203; (*d*) Y. Segawa, M. Yamashita, K. Nozaki, *Science*, **2006**, *314*, 113; (*e*) R. J. Wright, M. Brynda, J. C. Fettinger, A. R. Betzer, P. P. Power, *J. Am. Chem. Soc.*, **2006**, *128*, 12498; (*f*) T. J. Hadlington, M. Hermann, G. Frenking, C. Jones, *J. Am. Chem. Soc.*, **2014**, *136*, 3028.

7 T. J. Hadlington, M. Hermann, G. Frenking, C. Jones, *J. Am. Chem. Soc.*, **2014**, *136*, 3028.

8 (*a*) S. M. I. Al-Rafia, P. A. Lummis, M. J. Ferguson, R. McDonald, E. Rivard, *Inorg. Chem.*, **2010**, *49*, 9709; (*b*) S. K. Liew, S. M. I. Al-Rafia,

J. T. Goettel, P. A. Lummis, S. M. McDonald, L. J. Miedema, M. J. Ferguson, R. McDonald and E. Rivard, *Inorg. Chem.*, **2012**, *51*, 5471.

9 V. Diemer, H. Chaumeil, A. Defoin, A. Fort, A. Boeglin, C. Carré, *Eur. J. Org. Chem.*, **2006**, 2727.

10 N. Momiyama, Y. Yamamoto, H. Yamamoto, *J. Am. Chem. Soc.*, **2007**, *129*, 1190.

11 For example of compounds featuring monodentate *N*-heterocyclic guanidine ligands, see: (*a*) M. Tamm, D. Petrovic, S. Randoll, S. Beer, T. Bannenberg, P. G. Jones, J. Grunenberg, *Org. Biomol. Chem.*, **2007**, *5*, 523; (*b*) S. Dastgir, G. G. Lavoie, *Dalton Trans.*, **2010**, *39*, 6943; (*c*) D. Franz, E. Irran, S. Inoue, *Dalton Trans.*, **2014**, *43*, 4451.

12 For a review of the chemistry of bidentate guanidinato complexes, please see: C. Jones, *Coord. Chem. Rev.*, **2010**, *249*, 1857.

13 F. H. Allen, O. Kennard, D. G. Watson, L. Brammer, A. G. Orpen, R. Taylor, *J. Chem. Soc., Perkin Trans.*, **1987**, S1.

14 W. A. Merrill, R. J. Wright, C. S. Stanciu, M. M. Olmstead, J. C. Fettinger, P. P. Power, *Inorg. Chem.*, **2010**, *49*, 7097.

15 C. Stanciu, S. H. Hino, M. Stender, A. F. Richards, M. M. Olmstead, P. P. Power, *Inorg. Chem.,* **2005**, *44*, 2774.

16 A. B. Panghorn, M. A. Giardello, R. H. Grubbs, R. K. Rosen, F. J. Timmers, *Organometallics* **1996**, *15*, 1518.

17 L. E. Manzer, J. Deaton, P. Sharp, R. R. Schrock *Inorg. Synth.*, **1982**, *21*, 135.

18 H. Hope, *Prog. Inorg. Chem.*, **1993**, *41*, 1.

19 G. M. Sheldrick, *Acta. Cryst.,* **2008**, *A64*, 112.

Chapter 4

Accessing soluble complexes of zinc dihydride, and cationic zinc hydride species via *N*-heterocyclic carbene stabilisation

4.1 Abstract

In this chapter, the synthesis of a variety of group 12 element complexes with *N*-Heterocyclic carbenes (NHCs), 4-dimethylaminopyridine (DMAP) and Wittig reagents such as Ph_3PCMe_2 is described. Specifically, the carbene adduct of zinc diiodide IPr•ZnI_2•THF (**1**) [IPr = $(DippNCH)_2C$:; Dipp = 2,6-diisopropylphenyl] was prepared and combined with a variety of hydride sources to eventually yield the carbene-zinc dihydride dimer [IPr•ZnH(μ-H)]$_2$ (**5**). IPr was reacted with $CdCl_2$ in THF, to first yield [IPr•H][IPr•$CdCl_3$] (**2**), which can then be converted to IPr•$CdCl_2$•THF (**3**) following treatment with Tl[OTf].

In the case of [IPr•ZnH(μ-H)]$_2$ (**5**) and its less hindered analogue [$ImMe_2{}^iPr_2$•ZnH(μ-H)]$_2$ (**6b**) [$ImMe_2{}^iPr_2$ = $({}^iPrNCMe)_2C$:], the Zn_2H_2 core is resistant to the addition of neutral Lewis bases, however the terminal Zn-H bonds of 5 are succeptible to electrophilic attack by MeI and MeOTf, which yield the dimeric species [IPr•ZnI(μ-H)]$_2$ (**7**), and monomeric IPr•Zn(H)(OTf)•THF (**8**) respectively. While **7** retains a centrosymmetric Zn_2H_2 unit supported by two bridging, compound **8** is monomeric and sufficiently Lewis acidic to bind two equivalents of the Lewis base, DMAP, leading to the formation of the first example of a formally cationic complex of zinc hydride [IPr•$Zn(DMAP)_2$][OTf] (**9**). The efficacy of **8** as a catalyst for the hydrosilylation and hydroboration of select unsaturated species is also described.

4.2 Introduction

Since the discovery that *N*-heterocyclic carbenes (NHCs) could be synthesised in large quantity as thermally stable materials,[1] researchers have sought to explore this versatile ligand class within the context of catalysis[2] and to intercept novel bonding environments within the main group.[3] In relation to the latter concept, the generation/stabilisation of reactive main group element allotropes such as the tetrylone dimers E_2 (E = Si, Ge and Sn),[4-6] the diboron species B_2,[7] and the parent methylene and ethylene analogues (EH_2 and H_2EEH_2)[8-11] in the form of stable NHC adducts, represent interesting additions to the chemical literature.[12]

In general, the preparation of the abovementioned reactive species necessitates the use of main group element halide adducts of *N*-heterocyclic carbenes as starting reagents. In line with this concept, this chapter reports the synthesis of new group 12 element adducts containing the readily prepared carbenes IPr and $ImMe_2{}^{i}Me_2$ as donors.[13] Added interest for this research endeavour stems from the report that various NHC-zinc adducts (including those of $ZnBr_2$) can act as catalysts for a variety of transformations ranging from the ring-opening polymerisation of lactides to the synthesis of value added products from CO_2.[14]

While zinc dihydride has been known since 1947,[15] this parent species is pyrophoric, insoluble in most solvents and decomposes over time at room temperature, thus counteracting the potential utility of this species as a reducing

agent.[16] With a judicious choice of anionic co-ligand, soluble and more thermally stable examples of zinc(II) hydride complexes $[LZnH]_x$ ($x \geq 1$) have been prepared with varying degrees of nuclearity depending on the steric bulk and denticity of the ligand present (Figure 4.1).[17] Moreover, the use of the hydridic ($H^{\delta-}$) character within Zn-H residues to activate substrates, such as CO_2 and imines, represents a promising low-toxicity avenue for chemical synthesis.[18,19]

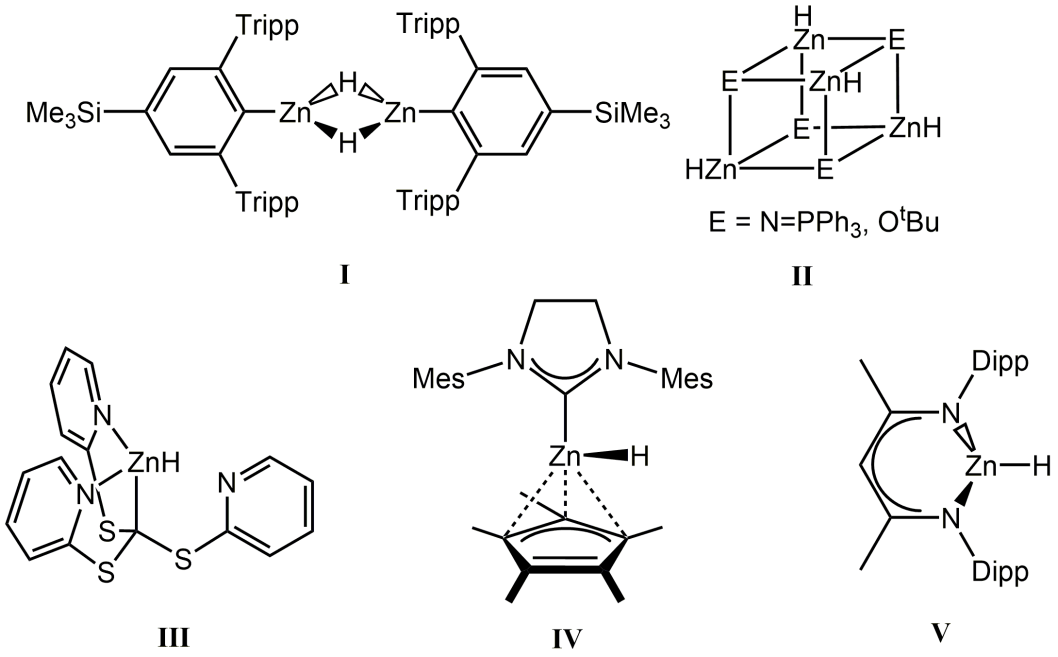

Figure 4.1 Examples of zinc(II) hydride complexes; Ar = sterically hindered aryl group; Mes = 2,4,6-$Me_3C_6H_2$, Tripp = 2,4,6-$^iPr_3C_6H_2$.

One possible way to increase the reactivity of Zn hydrides is to open coordination sites for substrate binding/activation via the synthesis of complexes featuring formally cationic $[ZnH]^+$ moieties, while concurrently retaining the requisite hydridic character. To this end, this chapter describes a mild procedure

to access stable complexes of $[ZnH]^+$ each supported by an *N*-heterocyclic carbene donor.[20]

4.3.1 Carbene complexes of group 12 element dihalides

The use of *N*-heterocyclic carbenes as ligands for group 12 elements is not a new concept, as illustrated by the report of a stable NHC-mercury complex by Wanzlick in 1970.[21,22] The primary motivation for the exploration of carbene coordination to group 12 element halides is the future synthesis of novel hydride species via halide metathesis chemistry.[23] One primary benefit of targeting metal hydride species for metathesis chemistry is that the hydride is usually lost as H_2 gas following protonolysis by an incoming substrate; as such this proves to be an extremely clean and atom economical method to mediate catalytic transformations.

As depicted in Equation 4.1, the thermally stable zinc iodide adduct IPr•ZnI_2•THF (**1**) [Mp = 150-152 °C] was prepared in high yield (86 %) by combining IPr with ZnI_2 in THF. The ^{1}H NMR spectrum of **1** gave expected features for a mono-adduct of IPr including a diagnostic pair of doublet resonances due to the presence of diasterotopically inequivalent Me groups within the peripheral isopropyl groups of the carbene donor. Additional structural authentication of **1** was achieved by single-crystal X-ray crystallography and the refined structure of **1** is shown in Figure 4.2. It should be noted that the attempted synthesis of a carbene adduct of ZnI_2 did not proceed in common aliphatic or aromatic solvents such as hexanes, benzene and toluene due to the inherent insolubility of ZnI_2 in these media.

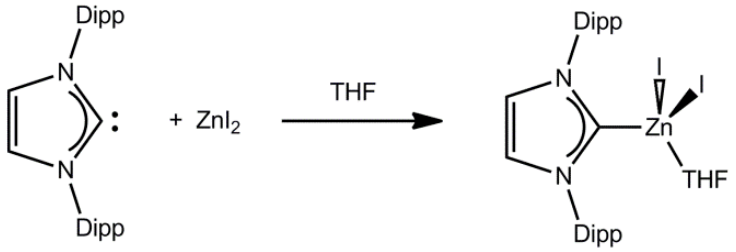

(4.1)

1

As expected, the Zn centre in **1** adopts a slightly distorted tetrahedral geometry with a C_{IPr}-Zn bond length of 2.0419(19) Å. For comparison, the C_{IPr}-Zn distance in the recently reported zinc dichloride adduct IPr•$ZnCl_2$•THF [2.045(6) Å *avg.*] has the same value within experimental error as **1**,[24] while the Zn-O distance in **1** [2.1252(16) Å] is longer than the Zn-O bond length in IPr•$ZnCl_2$•THF [2.093(4) Å *avg.*].[25] Attempts to bind an additional equivalent of IPr to the Zn centre in **1** (to form IPr•ZnI_2•IPr) did not yield any appreciable coordination chemistry.[26]

In addition, we were interested in the attempted formation of complexes of cadmium hydride via similar methodology, however attempts to extend carbene complexation to a cadmium dihalide proved to be more of a challenge.[27] When IPr was directly combined with $CdCl_2$ in a THF/dioxane solvent mixture, a new Cd-containing product was obtained after crystallising the resulting crude material from THF/hexanes at -35 °C. Interestingly, this product contained ^{1}H NMR spectroscopic resonances consistent with the presence of two distinct IPr environments.

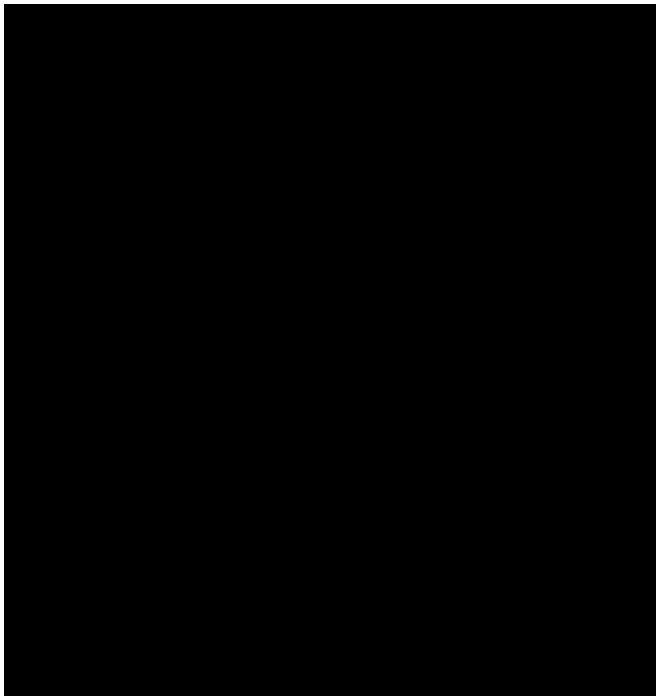

Figure 4.2 Thermal ellipsoid plot (30 % probability level) for IPr•ZnI_2•THF (**1**). All hydrogen atoms have been omitted for clarity. Selected bond lengths [Å] and angles [°]: Zn-C(1) 2.0419(19), Zn-I(1) 2.6120(3), Zn-I(2) 2.5580(3), Zn-O 2.1252(16); I(1)-Zn-I(2) 112.701(10), C(1)-Zn-I(1) 108.10(6), C(1)-Zn-I(2) 120.21(5), C(1)-Zn-O 110.49(7).

For example, a singlet resonance was present at 6.57 ppm (in C_6D_6) due to backbone-positioned C-H groups of the central ring five-membered ring in IPr; this signal was also accompanied by adjoining satellites resonances resulting from long-range coupling (*ca.* J = 5.6 Hz) to NMR active ^{111}Cd and ^{113}Cd nuclei (I = ½).[28] Thus it appeared that one of the IPr units was bound to a Cd centre. A second set of IPr resonances was also detected and were indicative of the known imidazolium cation $[IPrH]^+$ (*e.g.* the backbone C-H groups of the imidazolium heterocycle were located at 9.21 ppm). The composition of the isolated Cd product was corroborated by X-ray crystallography, which identified the product

as [IPrH][IPr•$CdCl_3$] (**2**) (Scheme 4.1, Figure 4.3). The formation of **2** suggests that C-H bond activation of one equivalent of carbene likely transpired[29] to form the imidazolium salt **2**; at this time we are unsure about the fate of the other product(s) generated in this transformation. In chemistry reported by the Jones group, IPr and Cl_2Ge•dioxane combined in THF to give crystals of [IPrH]$GeCl_3$,[5,30] whereas when the same reaction was conducted in either Et_2O[30] or toluene[8] the production of IPr•$GeCl_2$ in high yield occurs. Therefore the stronger donating ability of the THF and dioxane appears to assist in the C-H activation/deprotonation chemistry leading to the formation of **2**.

Figure 4.3 Thermal ellipsoid plot (30 % probability level) for [IPr•$CdCl_3$][IPrH] (**2**). All hydrogen atoms and toluene solvate have been omitted for clarity. Selected bond lengths [Å] and angles [°]: Cd-C(1) 2.246(3), Cd-Cl(1) 2.4790(8), Cd-Cl(2) 2.4650(10), Cd-Cl(3) 2.4573(9); C(1)-Cd-Cl(1) 114.76(7), Cl(1)-Cd-Cl(2) 103.59(3), Cl(2)-Cd-Cl(3) 112.24(4).

As depicted in Figure 4.3, compound **2** consists of discrete cationic $[IPrH]^+$ and anionic $[IPr\text{-}CdCl_3]^-$ units in the solid state. The C_{IPr}-Cd bond length

is 2.246(3) Å and is considerably shorter than the C_{NHC}-Cd distances noted within various *N*-heterocyclic carbene adducts of $CdMe_2$ [2.327(2) to 2.406(4) Å].[27] The Cd centre within the $[IPr•CdCl_3]^-$ anion has a distorted tetrahedral geometry with bond angles at Cd in the range of 103.59(3) to 114.76(7)°, while the metrical parameters for the remaining $[IPrH]^+$ cation match those found in related imidazolium salts present in the literature.[8,32,33]

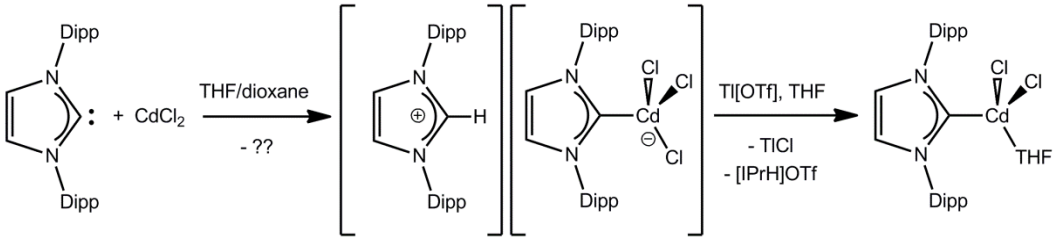

2 **3**

Scheme 4.1 Synthesis of an NHC adduct of $CdCl_2$, **3**, via the imidazolium salt **2**.

As part of our attempts to induce HCl elimination from $[IPrH][IPr•CdCl_3]$ (**2**) and generate a well-defined neutral cadmium dihalide adduct, compound **2** was treated with thallium triflate Tl[OTf] in THF. Upon adding Tl[OTf] to **2**, the immediate formation of a white precipitate (presumably TlCl) was observed; analysis of the resulting filtrate confirmed the presence of [IPrH]OTf and a new carbene containing product (Scheme 4.1). The latter species exhibited diagnostic coupling between the IPr unit and Cd in the form of ^{111}Cd and ^{113}Cd satellites. Fortunately the cadmium-carbene complex could be selectively separated from [IPrH]OTf by extraction with benzene, and crystals of this species could be obtained from THF/hexanes which identified the product as the target adduct

IPr•$CdCl_2$•THF (**3**) (Figure 4.4). Notably, IPr•$CdCl_2$•THF readily underwent loss of THF under vacuum to yield IPr•$CdCl_2$ which was characterised by ^{1}H and $^{13}C\{^{1}H\}$ NMR spectroscopy and elemental analysis (C, H, N).

Figure 4.4 Thermal ellipsoid plot (30 % probability level) for IPr•$CdCl_2$•THF (**3**). All hydrogen atoms and THF solvate have been omitted for clarity. Selected bond lengths [Å] and angles [°]: Cd-C(1) 2.218(2), Cd-Cl(1) 2.4029(6), Cd-Cl(2) 2.4338(6), Cd-O(1) 2.3413(17); Cl(1)-Cd-Cl(2) 114.08(3), C(1)-Cd-Cl(1) 119.97(6), C(1)-Cd-Cl(2) 111.26(6), C(1)-Cd-O(1) 112.14(8).

Compound **3** adopts a similar coordination motif as its lighter group 12 element congener IPr•$ZnCl_2$•THF[24] with Cd-Cl bonds [2.4184(8) Å *avg*.] which are longer than the reported Zn-Cl distances in IPr•$ZnCl_2$•THF [2.257(4) Å *avg*] due to the larger covalent radius of Cd. A C_{IPr}-Cd bond length of 2.218(2) Å was determined in **3** which is contracted in relation to the C_{IPr}-Cd distance within the anionic $[IPr•CdCl_3]^-$ unit in **2** [2.246(3) Å]. Our synthetic investigations did not include the Hg(II) adducts IPr•HgX_2 (X = halide) as efficient routes to these species are already known.[34]

4.3.2 Attempted synthesis of new group 12 hydride complexes using $Li[BH_4]$ and $Li[HBEt_3]$ as hydride sources

Following related protocols used by our group to prepare EH_2 and H_2EEH_2 adducts (E = Si, Ge and/or Sn),[8,9,11] the newly prepared compounds 1-3 were combined with the hydride sources $Li[BH_4]$ and $Li[HBEt_3]$ in ethereal solvents.

To begin, the zinc adduct IPr•ZnI_2•THF (**1**), and the cadmium complexes [IPrH][IPr•$CdCl_3$] (**2**) and IPr•$CdCl_2$ (**3**) were each combined with lithium triethylborohydride, $Li[HBEt_3]$ (2-4 equivalents); in each case, products mixtures were obtained which contained the known species $IPrH_2$[9] and IPr•BEt_3[9] in varying amounts, as determined by ^1H NMR spectroscopy, and presumably Zn and Cd metal as insoluble products. Thus it appears that adduct formation between the Lewis acidic BEt_3 by-product and IPr was a favorable reaction pathway in each case. In addition, competitive hydride-migration to the carbene carbon of either IPr (or transiently generated $IPrH^+$) to form the dihydroaminal $IPrH_2$ was also observed. It should be mentioned that when IPr•ZnI_2•THF (**1**) was combined with $Li[HBEt_3]$, no sign of the formation of the known hydride adduct [IPr•ZnH(μ-H)]$_2$[23e] was observed, confirming that the choice of the hydride reagent is important in dictating the successful formation of carbene-supported hydride complexes.

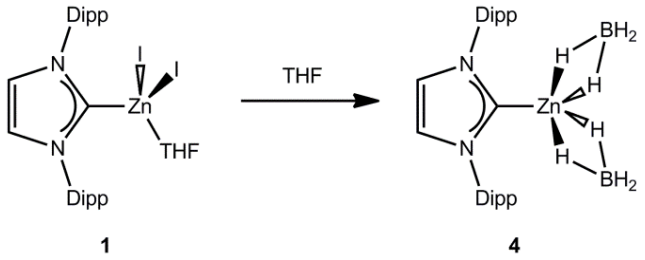

(4.2)

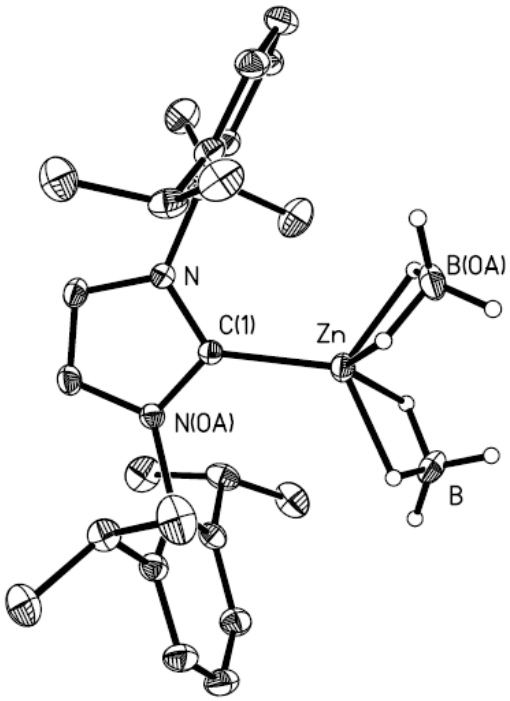

Figure 4.5 Thermal ellipsoid plot (30 % probability level) for IPr•Zn$(BH_4)_2$ (**4**). All carbon-bound hydrogen have been omitted for clarity. Selected bond lengths [Å] and angles [°]: Zn-C(1) 2.013(2), Zn-B 2.252(2), Zn-B′ 2.252(2); C(1)-Zn-B 126.26(7), C(1)-Zn-B′ 126.26(7), B-Zn-B′ 107.48(13).

However the use of Li$[BH_4]$ as a hydride source was able to furnish a new compound, IPr•Zn$(BH_4)_2$ (**4**) (Equation 4.2, Figure 4.5) which displayed a bis(borohydride) functionality; attempts to remove BH_3 and furnish direct Zn-H bonds were unsuccessful. Compound **4** exists as a discreet species with no bound solvent, unlike **1**. This is likely due to the fact that the $[BH_4]^-$ units appear to

coordinate in the solid state via two points of attachment, although the ^{11}B NMR spectrum of **1** in C_6D_6 displays only a well-defined pentet, suggesting that this coordination is fluxional on the NMR timescale.

4.3.3 Synthesis of soluble zinc hydride complexes using K[HB^{s}Bu$_3$] as a hydride source, and generation of stable zinc hydride cations

At the onset of this study, it appeared that the most direct route to form a zinc hydride cation $[ZnH]^+$ would be to begin with an isolable ZnH_2 complex and perform hydride abstraction chemistry. Fortunately, Okuda and coworkers recently prepared the first examples of such species with the assistance of *N*-heterocyclic carbene (NHC) donors.[23e] For example, the metastable dimer [IPr•ZnH(μ-H)]$_2$ (**5**).[23e,37] was shown to be active in the catalytic methanolysis of silanes, as well as being reactive towards CO_2. Okuda's original synthesis involved the use of pyrophoric $ZnEt_2$ as a reagent, with **5** formed by first making the adduct between IPr and $ZnEt_2$, and then treatment of the resulting IPr•$ZnEt_2$ with two equivalents each of methanol and phenylmethylsilane in sequence. In our laboratory it was found that compound **5** could be prepared in a 95 % yield from the direct reaction of the readily available adduct IPr•ZnI_2•THF (**1**) with two equivalents of K[HB^{s}Bu$_3$] (Scheme 4.2).[38] As previously discussed, attempts to generate **5** from the reaction of IPr•ZnI_2•THF with Li[HBEt$_3$] as a hydride source affords IPr•BEt_3, $IPrH_2$[9] and zinc metal as involatile products.[20] In addition, the less hindered Zn(II) dihydride adduct [ImMe$_2$^{i}Pr$_2$•ZnH(μ-H)]$_2$ (**6b**) was prepared in a one-pot procedure, with ImMe$_2$^{i}Pr$_2$•$ZnEt_2$ (**6a**) made without isolation

(Equation 4.3).[23e] Compound **6b** is a colourless solid (Mp = 131-134 °C) that adopts a similar centrosymmetric dimer arrangement as [IPr•ZnH(μ-H)]$_2$ (**5**) with both terminal and bridging Zn-H units present.

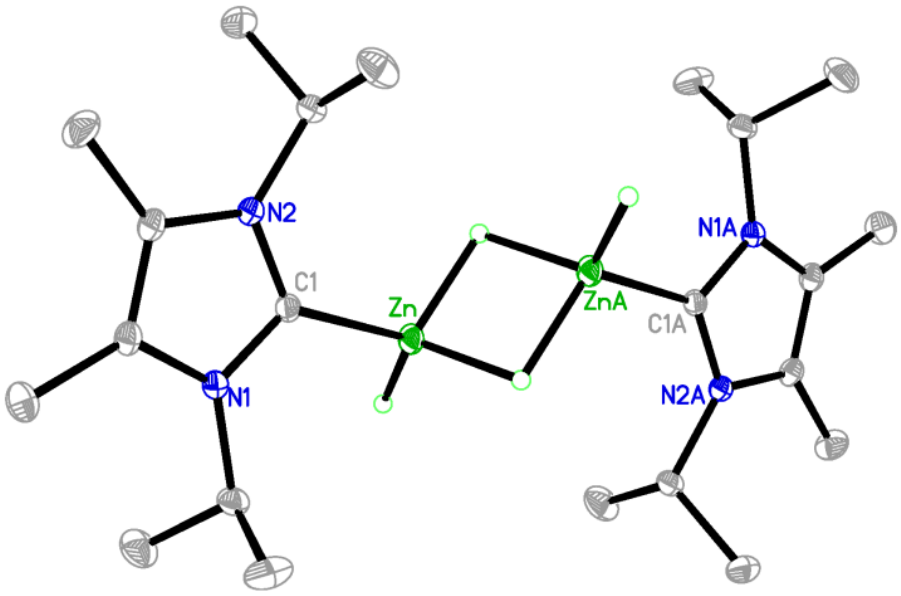

Figure 4.6 Molecular structure of [ImMe$_2$^{i}Pr$_2$•ZnH(μ-H)]$_2$ (**6b**) with thermal ellipsoids at the 30 % probability level; all carbon bound hydrogen atoms have been omitted for clarity. Selected bond lengths [Å] and angles [°]: Zn-C(1) 2.0737(10), Zn-H(1) 1.54(2), Zn-H(2) 1.68(2); H(1)-Zn-H(2) 117.2(10), C(1)-Zn-H(1) 115.9(7), C(1)-Zn-H(2) 111.1(7).

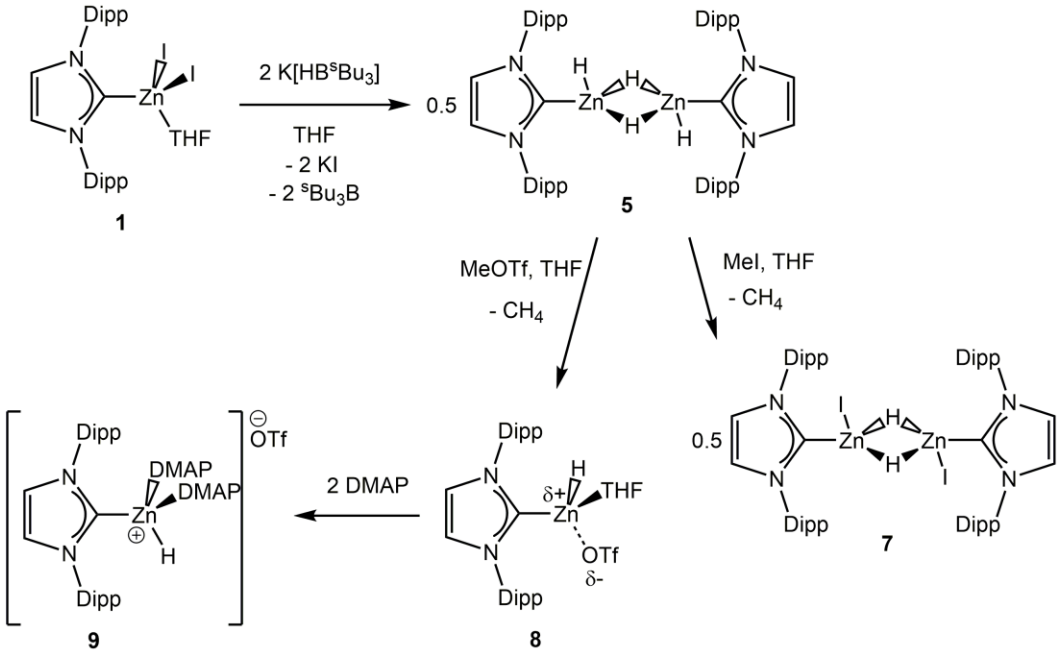

Scheme 4.2 Alternate synthesis of [IPr•ZnH(μ-H)]$_2$ (**5**), preparation of the iodo analogue [IPr•ZnI(μ-H)]$_2$ (**7**) and the formal [ZnH]$^+$ complexes **8** and **9**.

Slightly elongated Zn-C_{IPr} bond lengths [2.0737(10) Å] and Zn···Zn separation [2.5149(2) Å] are present in [Im$Me_2{}^iPr_2$•ZnH(μ-H)]$_2$ (**6b**) in relation to the corresponding values in the IPr analogue **5** (Figure 4.6). While distinct ^{1}H NMR resonances are noted for the terminal and bridging hydrides within [IPr•ZnH(μ-H)]$_2$ (**5**), a single broad resonance for **6b** is present in C_6D_6 at room temperature, suggesting that exchange between terminal and bridging positions occurs in solution. Consistent with this observation, our accompanying computational studies show that the dimerization of Im$Me_2{}^iPr_2$•ZnH_2 to give **6b** in the gas phase (via formation of Zn-H-Zn bridges) is less thermodynamically favorable than for the IPr analogue. Variable temperature (VT) NMR analysis (Figures 4.7 and 4.8) shows a coalescence of the Zn-H resonances in **6b** at *ca.* 0

°C, with the appearance of two distinct peaks upon cooling below this temperature. DOSY NMR experiments (Figures 4.9 and 4.10)[39] suggest that this fluxional process does not involve the formation of large quantities of monomeric $ImMe_2{}^iPr_2{\bullet}ZnH_2$ as detectable on the NMR timescale, but rather that scrambling of the hydrides occurs within dimetallic species with retention of some Zn-H-Zn bridges. The hydrodynamic radii for **6b** in both toluene-D_8 and THF-D_8 (as derived from DOSY) were of similar value (*ca.* 5.4 Å), and match fairly well with the solid state structure of **6b** which shows an overall molecular end-to-end distance of *ca.* 12.3 Å.[41] $[ImMe_2{}^iPr_2{\bullet}ZnH(\mu\text{-}H)]_2$ (**6**) does not interact with the Lewis bases THF, Cy_3P, DMAP (4-dimethylaminopyridine), nor the nucleophilic carbon-based donors Ph_3PCMe_2,[40] $IPrCH_2$[41] and $:C(N{}^iPr_2)_2$.[42]

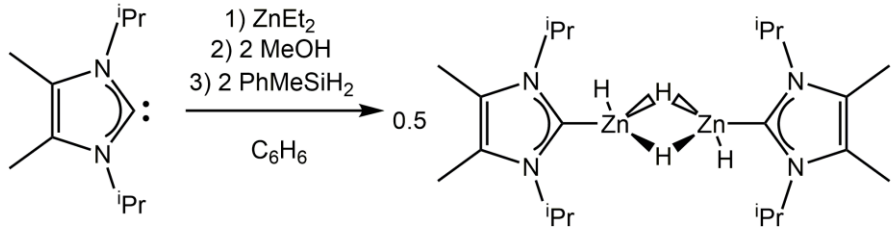

(4.3)

6b

Attempts to convert the known group 12 element halide adducts $[IPr{\bullet}CdI(\mu\text{-}I)]_2$[43] and $IPr{\bullet}HgI_2$[44] to the corresponding metal dihydride complexes, $IPr{\bullet}CdH_2$ and $IPr{\bullet}HgH_2$, using $K[{}^sBu_3BH]$ as a hydride source resulted in the immediate formation of metallic precipitates, and the isolation of free IPr and the aminal $IPrH_2$[9] from solution in both cases (presumably due to the highly reactive nature of Cd-H and Hg-H bonds).[45]

Figure 4.7 Variable temperature ^{1}H NMR spectra for **6b** in THF-D_8 [(Residual protio peaks from solvent denoted with (*)] From top to bottom: 27 °C, 0 °C, -20 °C, -40 °C, -60 °C.

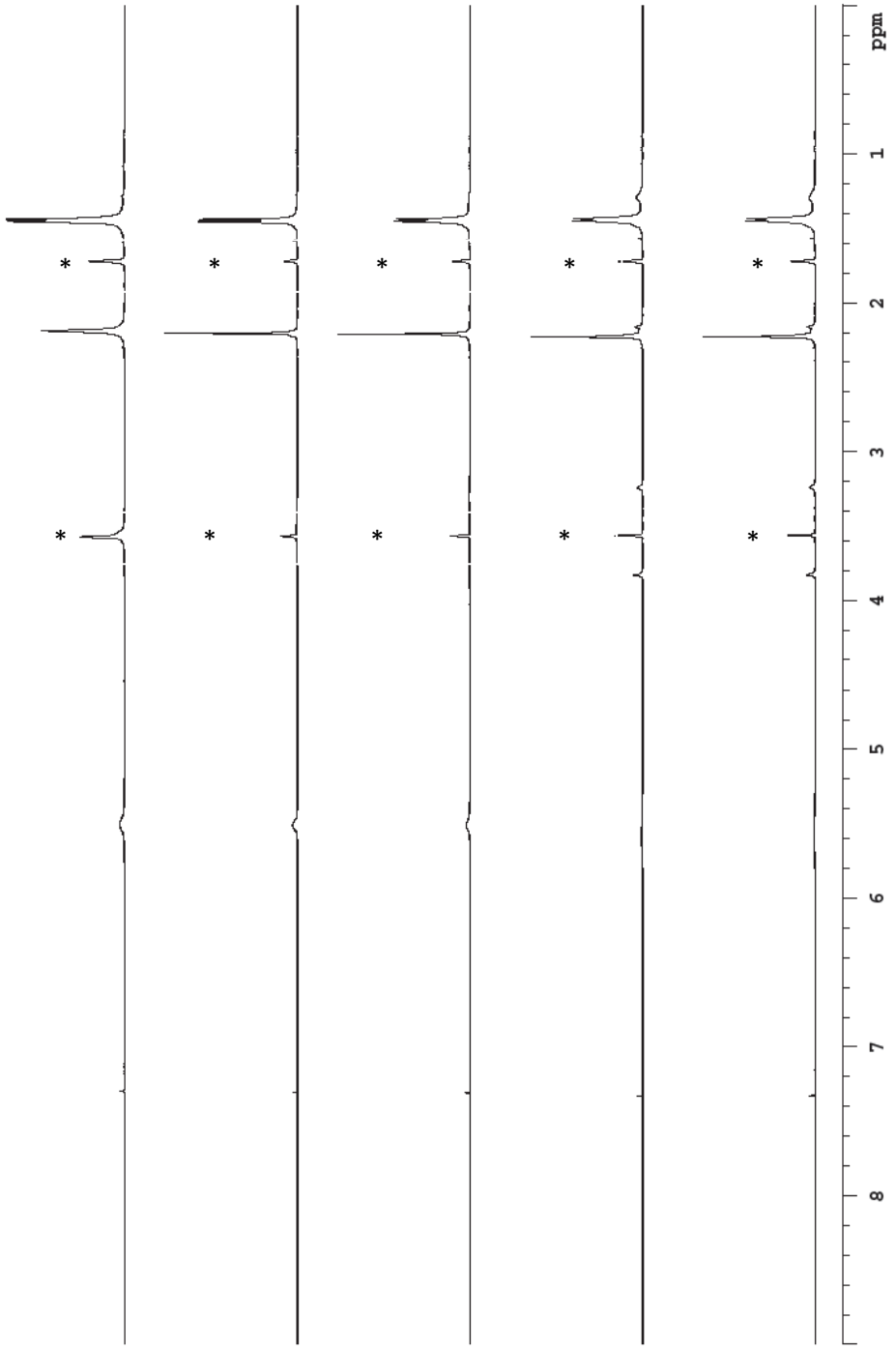

Figure 4.8 Variable temperature ^{1}H NMR spectra for **6b** in toluene-D_8 [(Residual protio peaks from solvent denoted with (*)] From top to bottom: 27 °C, 0 °C, -20 °C, -40 °C, -60 °C.

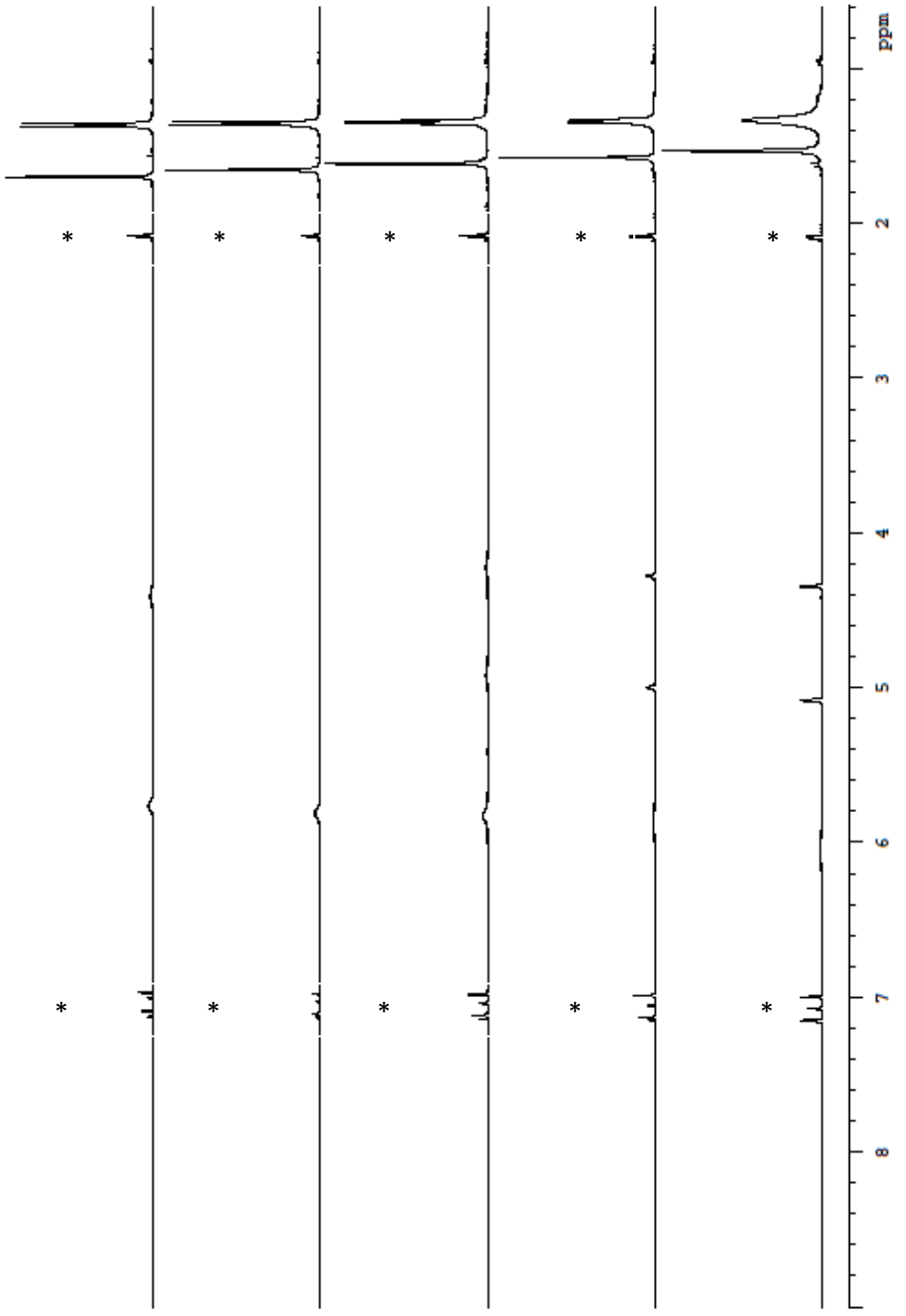

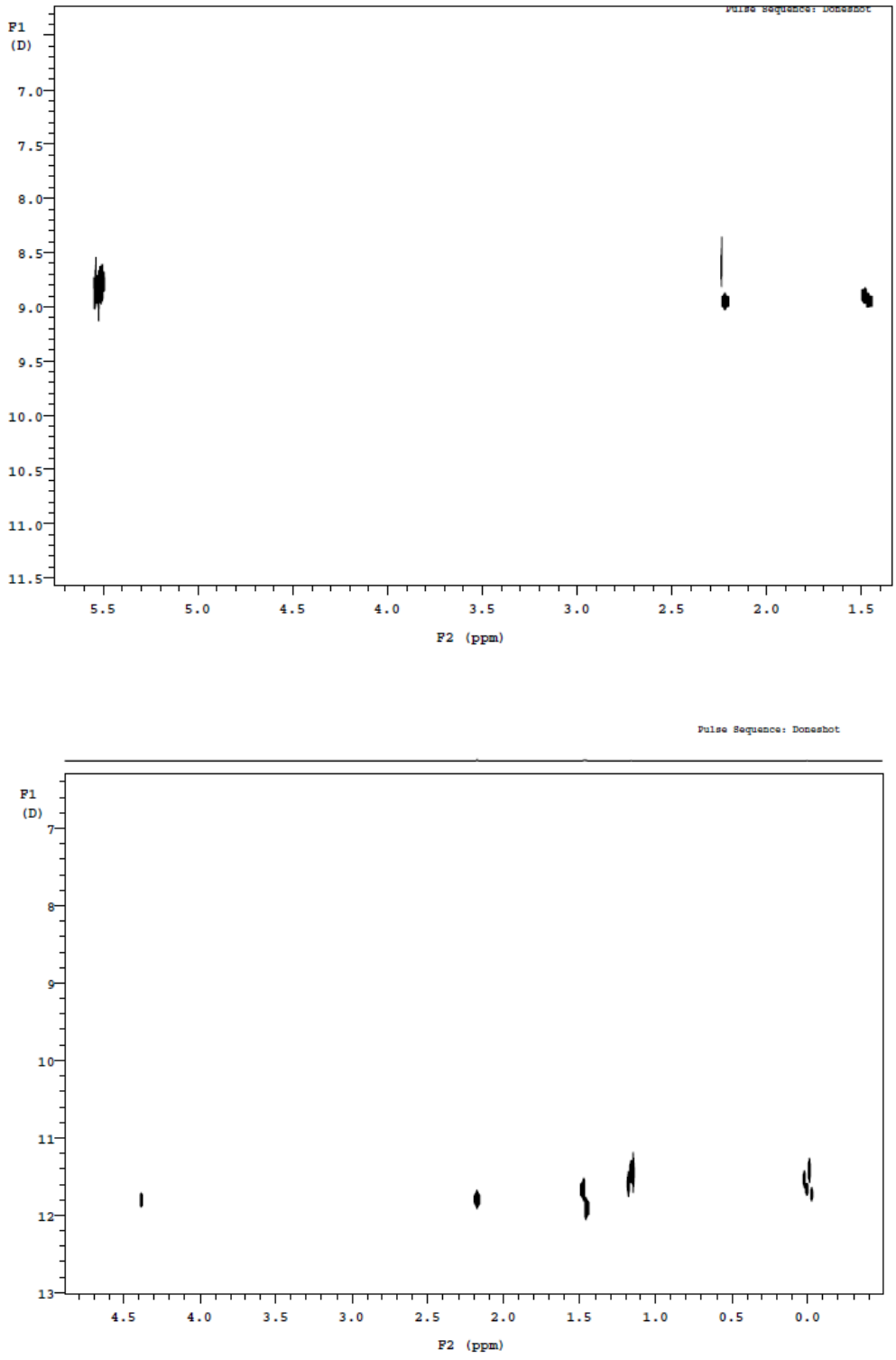

Figure 4.9 DOSY NMR spectra of $[ImMe_2{}^iPr_2{\bullet}ZnH(\mu\text{-}H)]_2$ (**6b**, top) and $ImMe_2{}^iPr_2{\bullet}ZnEt_2$ (**6a**) (bottom) in THF-D_8

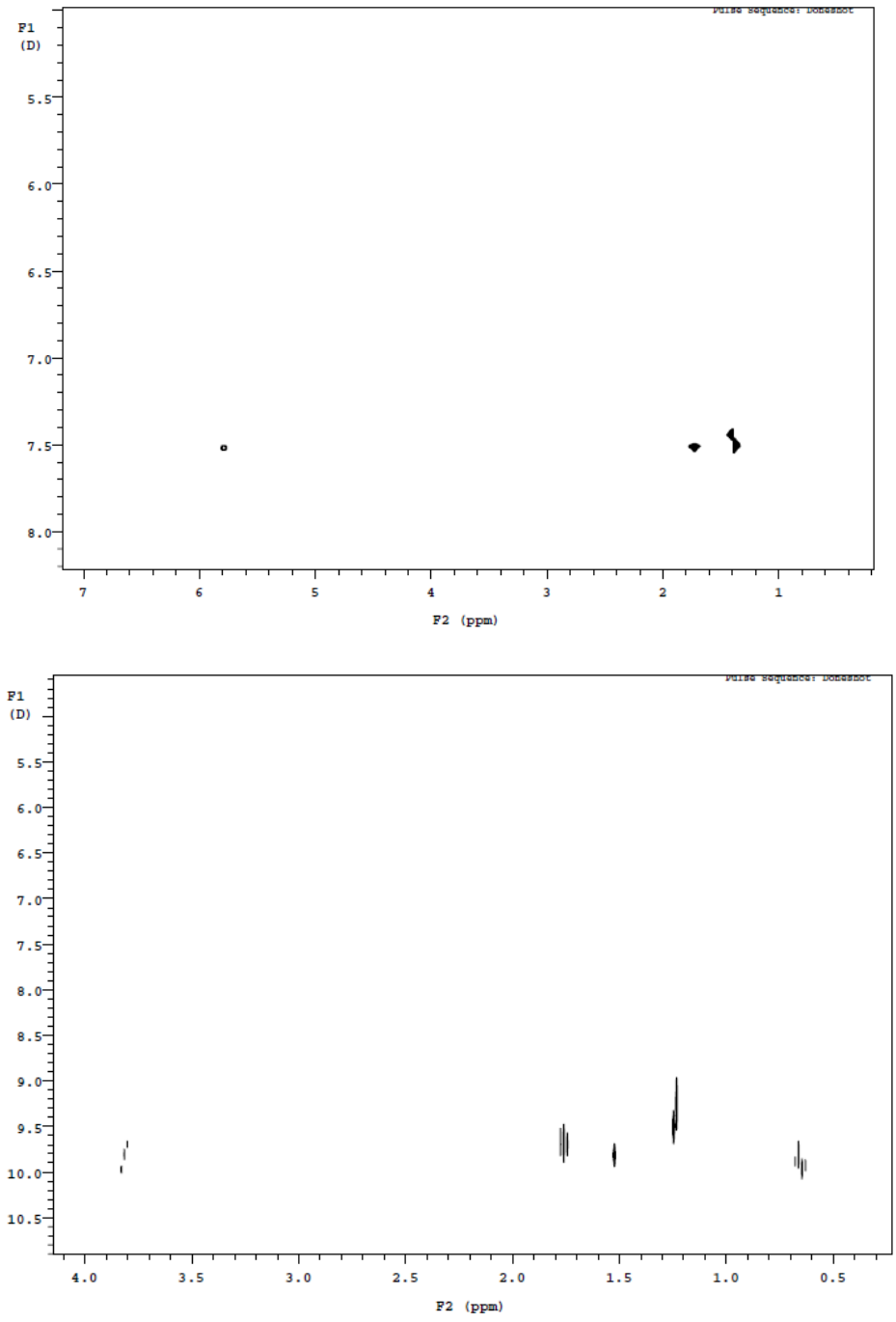

Figure 4.10 DOSY NMR spectra of $[ImMe_2{}^iPr_2{\bullet}ZnH(\mu\text{-}H)]_2$ (**6b**, top) and $ImMe_2{}^iPr_2{\bullet}ZnEt_2$ (**6a**) (bottom) in toluene-D_8

Complementary computational studies were undertaken on the ZnH_2 adducts **5** and **6** at the M06-2X/cc-pVTZ level of theory, with corresponding NBO and AIM analyses, to further understand the bonding and potential reactivity of these species. These studies indicate the presence of significant hydridic character on each zinc-bound hydrogen atom (-0.470/-0.738 to -0.435/-0.646 in **5**/**6b**; NBO charge analysis). Thus it appeared that hydride removal from either complex was a feasible synthetic endeavour.[46] Accordingly, hydride removal in an efficient manner was achieved with the use of methylating agents. For example, MeI interacted with [IPr•ZnH(μ-H)]$_2$ (**5**) to yield the hydrido-iodo product [IPr•ZnI(μ-H)]$_2$ (**7**) in a high yield of 76 % with concomitant loss of methane (Scheme 4.2; Figure 4.11); compound **7** could also be prepared via the treatment of IPr•ZnI$_2$•THF, **1** with one equiv. of K[HB^{s}Bu$_3$] as shown in Equation 4.4.

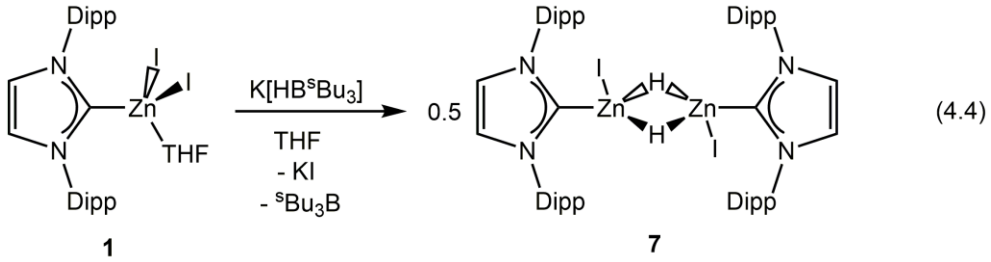

1 **7** (4.4)

[IPr•ZnI(μ-H)]$_2$ (**7**) adopts a dimeric arrangement in the solid state (Figure 4.11) with bridging Zn-H-Zn arrays at its core; the metrical parameters are similar to those observed for [IPr•ZnH(μ-H)]$_2$ (**5**).[23e] The use of MeOTf as an electrophile resulted in clean conversion of **5** in THF into the carbene-ligated zinc hydrido-triflate adduct, IPr•ZnH(OTf)•THF (**8**) in high yield (88 %; Scheme 4.2, Figure 4.12) as a moisture-sensitive, yet thermally stable (up to 260 °C) colourless solid.

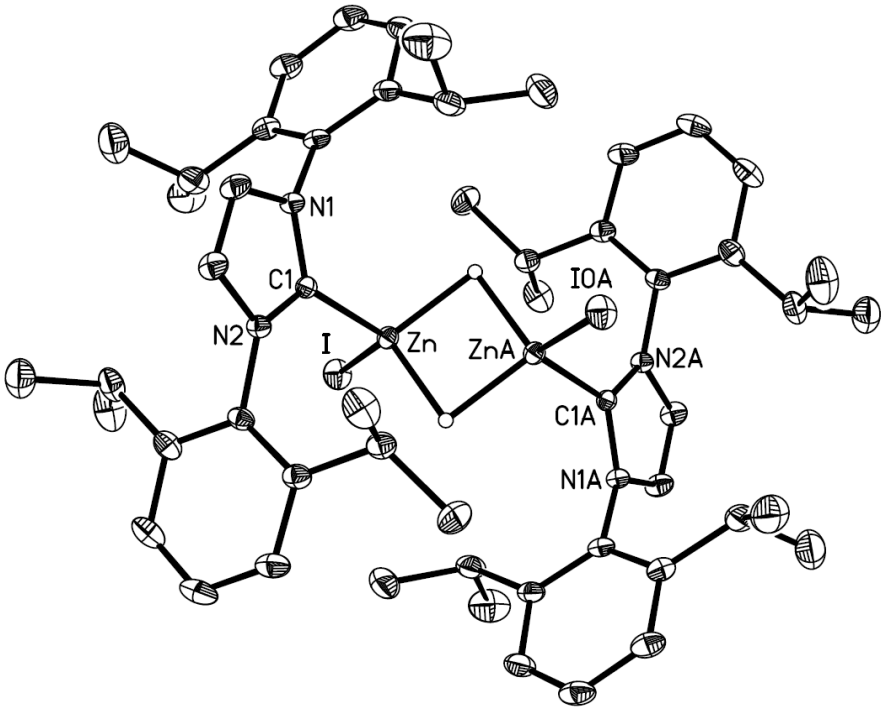

Figure 4.11 Molecular structure of [IPr•ZnI(μ-H)]$_2$ (**7**) with thermal ellipsoids at the 30 % probability level; a crystallographic inversion centre is present in the molecule. All carbon bound hydrogen atoms and THF solvate have been omitted for clarity. Selected bond lengths [Å] and angles [°]: Zn-C(1) 2.018(2), Zn-H(1) 1.79(3), Zn-I 2.5680(4), Zn···Zn 2.4682(5); C(1)-Zn-H(1) 111.9(8), C(1)-Zn-I 118.66(6), I-Zn-H(1) 110.6(8), H(1)-Zn-H(1A) 92(1).

Notably, the NHC-ZnH$_2$ adducts **5** and **6b** do not coordinate THF, while the zinc monohydride unit in **8** binds one equivalent of THF as indicated by both NMR spectroscopy and X-ray crystallography (Figure 4.12). This suggests the presence of increased positive charge at the zinc centre in IPr•ZnH(OTf)•THF (**8**) in relation to its dihydride progenitor **5**; our computations reveal that hydride removal (conversion of **5** into **8**) is accompanied by an increase in charge at Zn from +0.65 to +1.08 (Figure 4.13). A lack of dimerization of **8** might be attributed to mutual repulsion between two [ZnH]$^+$ units: overall charge for each [ZnH]$^+$

unit in **8** = +0.545 by NBO analysis. Steric effects could also be responsible, in the form of the added bulk from a bound OTf˙ group in relation to the H and I groups in dimeric **5** and **7**; however, ^{19}F NMR spectroscopy indicates that the OTf˙ unit in **8** is only weakly bound in THF-D_8 (δ = -78.5 ppm).

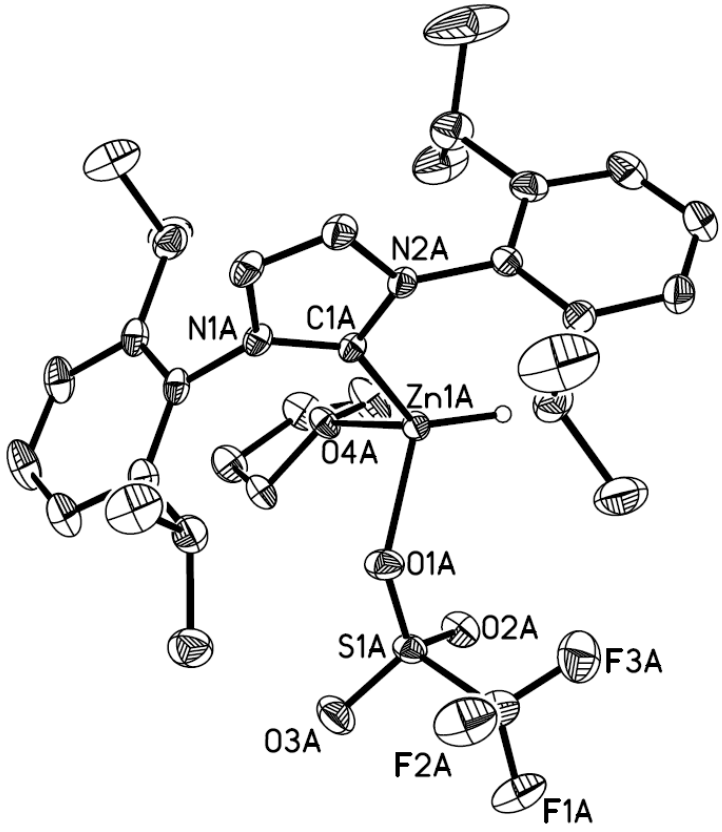

Figure 4.12 Molecular structure of IPr•ZnH(OTf)•THF (**8**) with thermal ellipsoids at the 30 % probability level. All carbon-bound hydrogen atoms have been omitted for clarity. Selected bond lengths [Å] and angles [°] with values belonging to a second molecule in the asymmetric unit listed in square brackets: Zn(1)-O(1) 2.068(3) [2.078(3)], Zn(1)-O(4) 2.156(3) [2.124(3)], Zn(1)-H(1) 1.38(3) [1.36(3)], Zn(1)-C(1) 2.031(3) [2.041(3)]; C(1)-Zn(1)-O(1) 103.43(13) [101.78(12)], C(1)-Zn(1)-O(4) 106.69(12) [107.93(13)], O(1)-Zn(1)-O(4) 94.31(12) [93.93(12)].

A terminal Zn-H stretching band was located in the IR spectrum of **8** at 1766 cm^{-1} which is shifted to higher frequency in relation to the terminal Zn(II) hydride vibrations in the ZnH_2 adducts **5** and **6b** (1625 and 1635 cm^{-1}, respectively). The computed IR spectrum for **8** also contains a prominent Zn-H stretching band at 1765 cm^{-1} which supports our initial assignment. X-ray crystallography confirmed the presence of a monomeric zinc hydride adduct IPr•ZnH(OTf)•THF (**8**) with elongated Zn-O bond lengths involving the THF and OTf units [2.140(4) and 2.073(4) Å, respectively; average of the two molecules in the asymmetric unit]. For comparison, IMes•$Zn(OTf)_2$•THF[47] (IMes = $[(HCNMes)_2C$:; Mes = 2,4,6-$Me_3C_6H_2$) displays significantly shorter Zn-O(Tf) distances of 1.966(2) and 1.973(2) Å. The zinc-bound hydride unit could be located in the electron difference map, however restraints were applied during the refinement thus preventing a detailed discussion of its metrical parameters. The adjacent Zn-C_{IPr} bond length in **8** [2.036(4) Å (*avg.*)] is similar to the corresponding distance in the four-coordinate Zn adduct, IPr•ZnI_2•THF (**1**) [2.0419(19) Å] (*vide infra*).

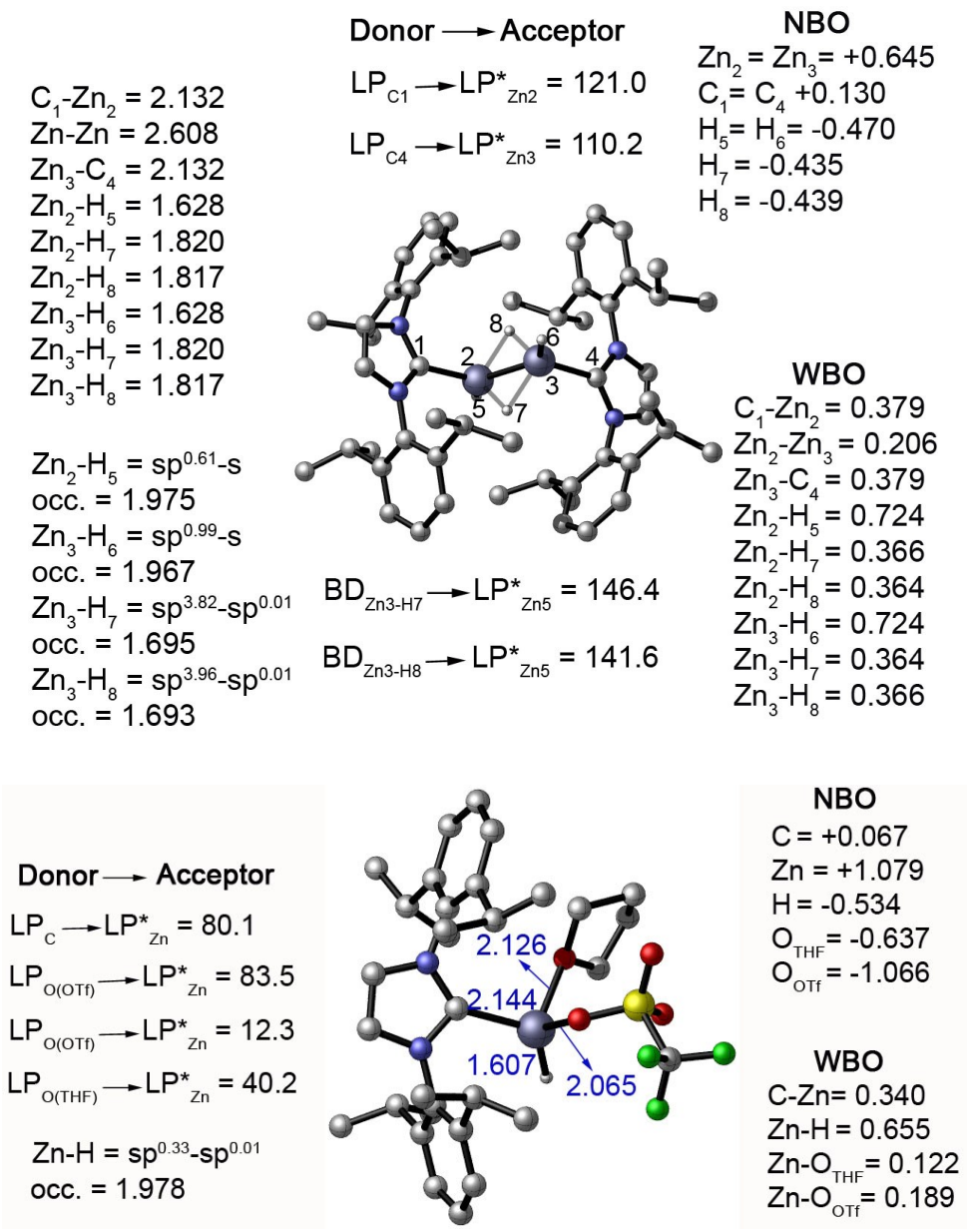

Figure 4.13 Gas phase optimized structures for **5** and **8**. Included are the NBO natural charges and Wiberg bond orders (WBO), computed at the M06-2X/cc-pVTZ level of theory (C-H bonds are omitted in the diagrams for clarity).

In order to further probe the electrophilicity of the zinc centre in IPr•ZnH(OTf)•THF (**8**), this species was treated with the strong donor, DMAP. In

the presence of two equivalents of DMAP, we were able to displace both THF and OTf^- from the coordination sphere of zinc and generate the formal $[ZnH]^+$ complex [IPr•ZnH(DMAP)$_2$]OTf (**9**) (Scheme 4.2; Figure 4.14). Compound **9** contains a tetrahedrally coordinated Zn(II) centre with a slightly elongated C_{IPr}-Zn distance [2.073(5) Å *avg.*] in relation to the triflato precursor **8** [2.036(4) Å *avg.*]. The zinc bound hydride could be located in the electron difference map but again, restraints where applied in the refinement of this residue.

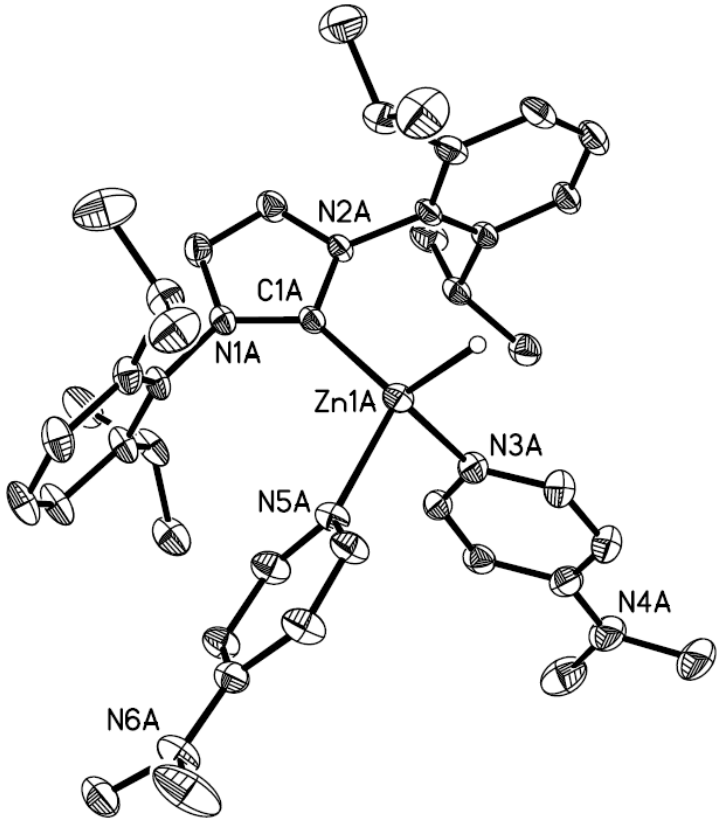

Figure 4.14 Molecular structure of [IPr•ZnH(DMAP)$_2$]OTf (**9**) with thermal ellipsoids at the 30 % probabilty level; all carbon-bound hydrogen atoms and the OTf^- anion have been omitted for clarity. Selected bond lengths [Å] and angles [°] with values due to a second molecule of **9** in the asymmetric unit in square brackets: Zn(1A)-H(1A) 1.92(3) [1.93(3)], Zn(1A)-C(1A) 2.071(4) [2.075(4)],

Zn(1A)-N(3A) 2.074(5) [2.135(4)], Zn(1A)-N(5A) 2.097(3) [2.059(4)]; C(1A)-Zn(1A)-N(3A) 104.92(14) [112.18(15)], C(1A)-Zn(1A)-N(5A) 112.84(14) [110.86(14)], C(1A)-Zn(1A)-H(1A) 122.0(12) [117.2(13)].

The Zn···OTf distances in **9** are > 8.0 Å and thus lie well outside the sum of the van der Waals radii for Zn and O. ^{19}F NMR spectroscopy also supported the presence of an outer sphere OTf^- ion in solution as a shielded resonance for this anion at –78.7 ppm was noted in THF-D_8. The one-electron reduction of IPr•ZnH(OTf)•THF (**8**) was attempted with Na, KC_8, Cp_2Co and sodium naphthalenide in THF, and in each case obtained free carbene IPr and Zn metal in place of the target Zn(I) complex IPr•Zn(H)-Zn(H)•IPr. When the reduction was carried out in Et_2O using the aforementioned reducing agents however, a new product (Equation 4.5) was recovered from the soluble fraction (67 % yield), which was identified as IPr•ZnH(μ-H)$_2$Zn(OTf)•IPr (**10**) by X-ray crystallography (Figure 4.15).

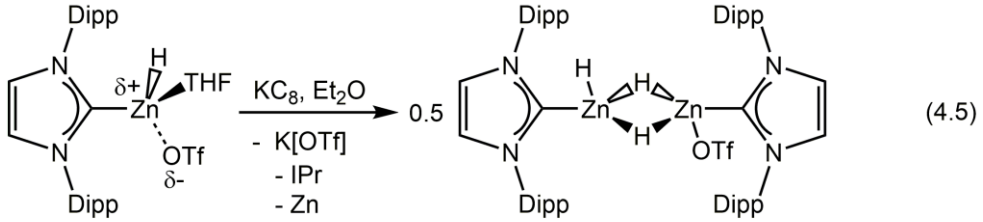

8 **10** (4.5)

Compound **10** features a Zn_2H_2 heterocyclic core, with two μ-hydrido bridges as has been seen previously in compounds **5**, **6b**, and **7**. In the case of **10** however, one zinc centre bears a terminal hydrido ligand, while the other zinc bears a triflate moiety which is bound in the solid state. The ^{19}F{^{1}H} NMR shift

of -79.1 ppm for the OTf⁻ group infers that this is dissociated in solution, similar to what has been observed with IPr•ZnH(OTf)•THF (**8**).

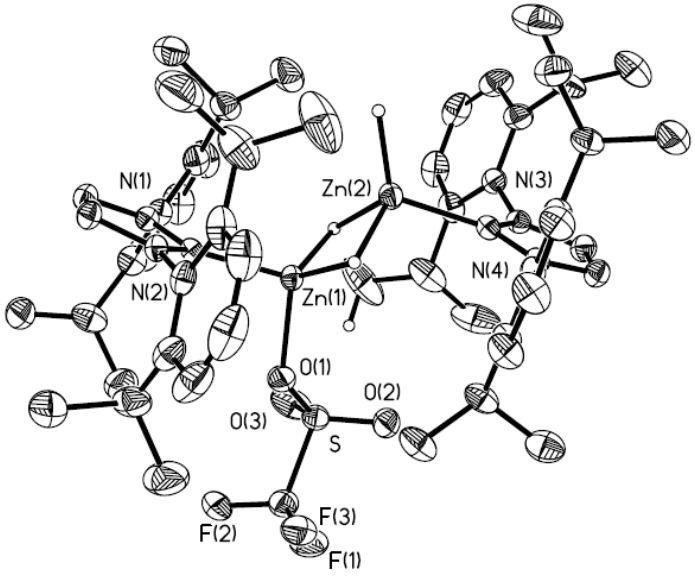

Figure 4.15 Molecular structure of IPr•ZnH(μ-H)$_2$Zn(OTf)•IPr (**10**) with thermal ellipsoids at the 30 % probability level; all carbon bound hydrogen atoms have been omitted for clarity. Selected bond lengths [Å] and angles [°]: Zn(1)-C(1) 2.026(3), Zn(1)-O(1) 2.051(3), Zn(1)-H(1) 1.73(4), Zn(1)-H(2) 1.78(4), Zn(1)•••Zn(2) 2.4689(6), Zn(2)-C(4) 2.032(3), Zn(2)-H(1) 1.85(4), Zn(2)-H(2) 1.82(3), Zn(2)-H(3) 1.67(4); H(1)-Zn-H(2) 95.1(16), C(1)-Zn-H(1) 116.6(12), C(1)-Zn-H(2) 114.6(10), C(4)-Zn-H(1) 107.4(12), C(4)-Zn-H(2) 106.3(10), O(1)-Zn-H(1) 114.1(13), O(1)-Zn-H(2) 114.8(10), O(1)-Zn-C(1) 102.47(12).

Also of note here is that there is just one zinc hydride peak observed by ^{1}H NMR, which infers that the terminal and bridging hydride positions are fluxional on the NMR timescale, as was observed with **6b**. Free IPr can be identified as a byproduct (by ^{1}H NMR spectroscopy; 25 % by integration) when **8** is combined with the reducing agents Na, KC_8 and Cp_2Co. One possible mechanism for the formation of **10** involves the initial reduction of IPr•ZnH(OTf)•THF (**8**) to the

intermediate IPr•Zn(H)Zn(H)•IPr, which then reacts with free **8** in solution, resulting in the addition of the H and OTf groups to the HZn-ZnH unit, followed by elimination of free IPr and Zn metal.

4.3.4 Catalytic activity of IPr•Zn(H)OTf•THF

There has been recent literature precedence for the use of either isolable or transiently generated zinc hydrides to catalyze the hydrosilylation of activated unsaturated compounds.[16b,23e,49] Following the notion that the dual electrophilic and hydridic character within the $[ZnH]^+$ unit in **8** along with the facile access to an open coordination site would encourage substrate binding and hydride transfer from Zn, the catalytic hydrosilylation of benzophenone was investigated. This portion of the study was buoyed by our computational studies which clearly show the retention of hydridic character at the zinc-bound H atom in **8** (Figure 4.13, NBO charge = -0.534).

When benzophenone was combined with a stoichiometric equivalent of $MePhSiH_2$ in the presence of 0.1 mol% of **8** in THF, the rapid and quantitative formation of the reduced product $Ph_2C(H)OSi(H)MePh$ was noted (Equation 4.6, room temperature; TOF = turnover frequency = 475 h^{-1}). A likely mechanism of this transformation involves first the binding of ketone to form $[IPr•Zn(H)OCPh_2]^+$, followed by hydride transfer to the ketonic carbon to yield an alkoxide intermediate $[IPr•Zn(OCPh_2)]^+$ that is later converted into **8** and silylether via known silane-mediated metathesis (Scheme 4.3).[17,52] The presence of strongly donating DMAP groups about Zn in **9** appears to shut down the

activity of this species as no catalytic reduction of benzophenone was observed, thus lending support to the abovementioned mechanism. [IPr•ZnH(μ-H)]$_2$ (**5**) was also found to be active in the hydrosilylation of Ph_2CO under similar conditions albeit with slightly lower activity (TOF = 190 h^{-1}) relative to **8**.

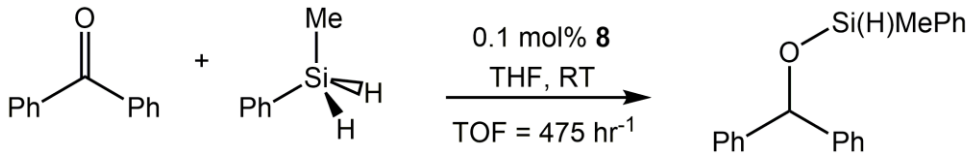

(4.6)

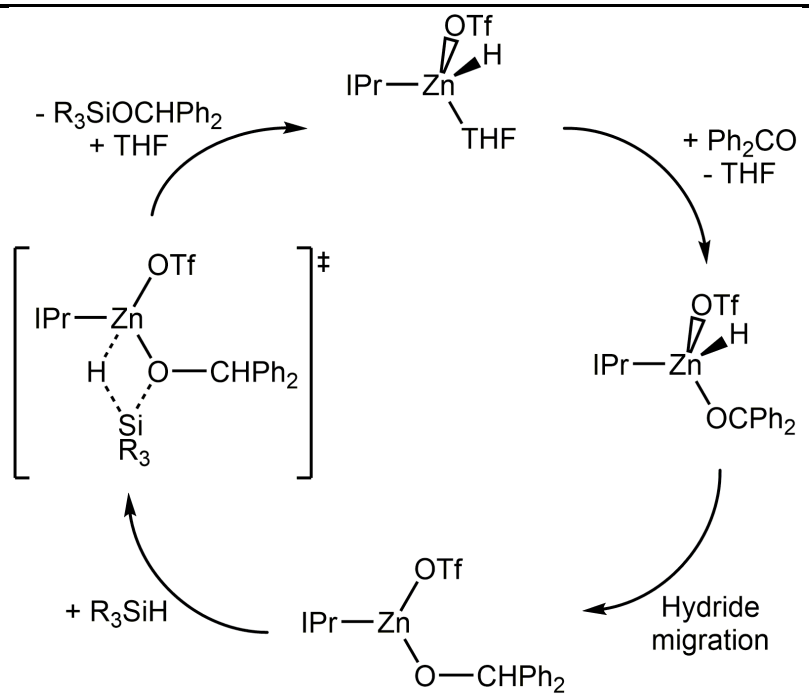

Scheme 4.3 Proposed mechanism for catalytic hydrosilation of benzophenone mediated by IPr•ZnH(OTf)•THF (**8**).

The above is consistent with the increased reactivity of **8** due to the labile nature of the THF and OTf` that encourage substrate (ketone) binding/activation. Somewhat to our surprise, the less hindered ZnH_2 adduct [Im$Me_2^{i}Pr_2$•ZnH(μ-H)]$_2$ (**6b**) was also quite active as a hydrosilylation catalyst and mediated the reduction

of Ph_2CO with a TOF of *ca*. 600 h^{-1}. The high activity of **6b** could be due to the presence of trace quantities of coordinatively unsaturated $ImMe_2{}^iPr_2{\bullet}ZnH_2$ monomer in solution, yet the variable temperature and DOSY NMR studies described already suggest a predominance of the dimeric form in solution. For added comparison, the three-coordinate zinc(II) hydride [$HC(MeCNDipp)_2ZnH$] (*c.f.* **V** in Scheme 4.1) catalyzes the hydrosilylation of Ph_2CO with an approximate TOF 0.6 h^{-1}. Thus our results portent well for the future use of $[ZnH]^+$ in abundant-metal catalysis.[49] Despite reacting quite rapidly with $PhMeSiH_2$, attempts to instigate hydrosilylation (from **8**) using tertiary silanes such as Et_3SiH or $(EtO)_3SiH$ did not yield any catalysis. Further to this work, recent studies by Okuda and coworkers show that a trimetallic zinc cluster [$\{IMes{\bullet}Zn(\mu\text{-}H)\}_2Zn(THF){\bullet}IMes$] is capable of effecting the hydrosilation of aldehydes, ketones and nitriles using tertiary silanes.[50] In addition, IPr•ZnH(OTf)•THF (**8**) was able to effect the hydroboration of in the presence of HBPin [Bpin = $-B(OCMe_2)_2$] with a TOF of 1100 h^{-1} at 25 °C (Equation 4.7). It should also be mentioned that the formal $[ZnH]^+$ complex IPr•ZnH(OTF)•THF (**8**) is significantly more thermally stable than the Zn(II) dihydride adducts **5** and **6b**. Specifically, compounds **5** and **6b** both degrade quantitatively to free carbene and zinc metal upon heating THF solutions to 60 °C for 4 hrs, while compound **8** remains unchanged upon heating to 60 °C in THF for two days. Furthermore, compounds **8** and $[IPr{\bullet}ZnH(DMAP)_2]OTf$ (**9**) can be stored at ambient temperature in the solid state with no decomposition noted over multiple months

of storage;[37] thus IPr•ZnH(OTF)•THF (**8**) represents an easy to handle base-metal hydrosilylation and hydroboration catalyst.

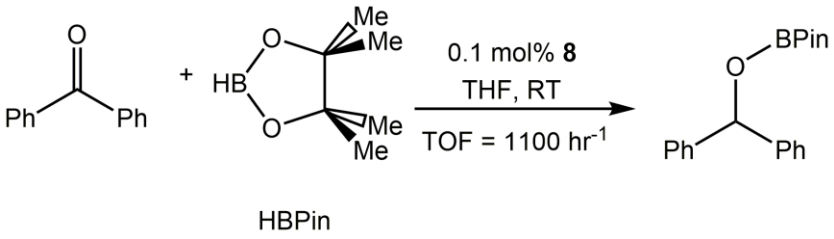

HBPin (4.7)

Future work will expand upon these promising early studies to include a wider range of substrates and catalytic transformations (including the reduction of CO_2) whereby an electrophilic late metal centre and an adjacent hydride unit act in concert to mediate bond activation.

4.3.5 Zinc halide complexes featuring non-carbene ligands and attempted formation of zinc(II) hydrides

In addition to complexes bearing an *N*-heterocyclic carbene ligand, it was identified that Wittig reagents such as Ph_3PCMe_2 might be useful donors, a previously shown within Group 14 EH_2 coordination chemistry (E = Ge and Sn).[34]

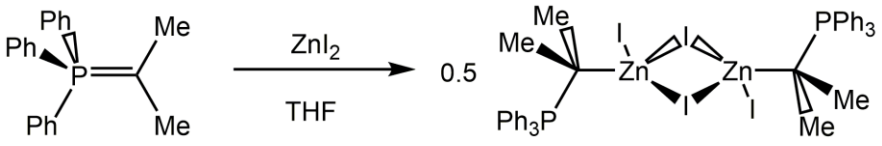

11 (4.8)

To this end, the Wittig adduct $[Ph_3PCMe_2•ZnI(\mu\text{-}I)]_2$ was prepared in THF from Ph_3PCMe_2 and ZnI_2 (Equation 4.8). Of note, the resulting complex existed

as a centro symmetric dimer (Figure 4.16) rather than allowing for the incorporation of one equivalent of THF as was seen with **1**.

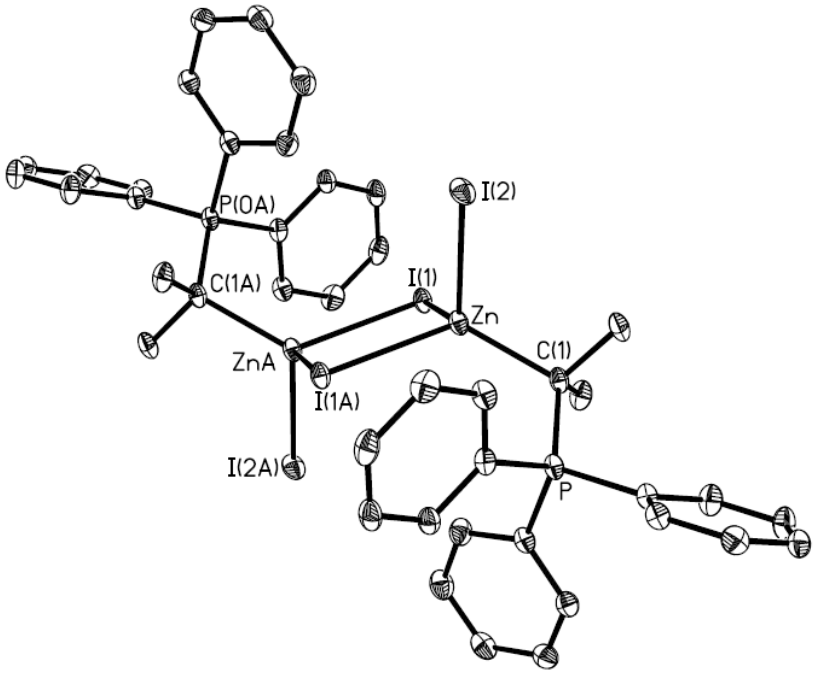

Figure 4.16 Molecular structure of $[Ph_3PCMe_2{\bullet}ZnI(\mu\text{-}I)]_2$ (**11**) with thermal ellipsoids at the 30 % probability level; a crystallographic inversion centre is present in the molecule. All hydrogen atoms and THF solvate have been omitted for clarity. Selected bond lengths [Å] and angles [°]: Zn-C(1) 2.085(2), Zn-I(1) 2.7028(3), Zn-I(2) 2.6111(3), C(1)-P 1.800(2); C(1)-Zn-I(1) 109.18(6), C(1)-Zn-I(2) 113.68(6), I(1)-Zn-I(2) 108.344(10).

This suggests that the Zn centre in this compound is less electrophilic than in compound **5**, which is supported by the fact that when compound **11** was treated with either 2 or 4 equivalents of $K[HB^{S}Bu_3]$, rather than yielding the expected compounds ($[Ph_3PCMe_2{\bullet}ZnI(\mu\text{-}H)]_2$ and $[Ph_3PCMe_2{\bullet}ZnH(\mu\text{-}H)]_2$), the precipitation of zinc metal from solution was observed, and Ph_3PCMe_2 recovered from the soluble fraction.[40] This is in contrast to what was described earlier when using NHC ligands. The crystal structure of $[Ph_3PCMe_2{\bullet}ZnI(\mu\text{-}I)]_2$ (**11**) (Figure

4.16) reveals a similar coordination geometry as described previously for the zinc hydrides [NHC•ZnH(μ-)H]$_2$. The Zn-C(1) distance is shorter by ca. 0.04 Å than the corresponding distance in IPr•ZnI_2•THF (1). This work suggests that in order to obtain soluble complexes of ZnH_2 and derivatives thereof, the choice of ligand is essential to the stability of the resulting compound; this is supported by the observations of Okuda and coworkers who noted that attempts to synthesis phosphine ligated compounds of ZnH_2 were ultimately unsuccessful.[23e]

4.4 Conclusions

In conclusion, the synthesis of a number of *N*-heterocyclic carbene adducts with group 12 metals was achieved. In the case of cadmium, the use of $CdCl_2$ initially yields the [IPr•$CdCl_3$][IPrH] salt (**2**), which can be converted to the neutral adduct, IPr•$CdCl_2$•THF (**3**) following treatment with Tl[OTf]. An analogous species, IPr•ZnI_2•THF (**1**) was obtained via the combination of ZnI_2 with IPr in THF, and this species could be further functionalised with $[BH_4]^-$ groups to yield IPr•$Zn(BH_4)_2$ (**4**) following treatment of **1** with two equivalents of $Li[BH_4]$. While the use of $Li[HBEt_3]$ as a hydride source yielded the known adduct IPr•BEt_3, use of potassium selectride $K[HB^sBu_3]$ yielded instead the desired zinc(II) hydride complexes [IPr•ZnH(μ-H)]$_2$ (**5**) and [IPr•ZnI(μ-H)]$_2$ (**7**). In addition, a complex featuring the less hindered carbene, $ImMe_2{}^iPr_2$ [$ImMe_2{}^i$Pr•ZnH(μ-H)]$_2$ (**6b**) was prepared. Treatment of **5** with MeI and MeOTf yielded dimeric **7** and monomeric IPr•ZnH(OTf)•THF (**8**) respectively. Compound **8** was shown to be reactive towards Lewis bases, with the addition of two equivalents of DMAP yielding [IPr•ZnH(DMAP)$_2$]OTf (**9**), a novel, thermally stable $[ZnH]^+$ species. In addition, **8** was shown to be effective at mediating the catalytic hydrosilylation and hydroboration of simple ketones such as benzophenone. Finally, the attempted reduction of compound **8** yielded the dimeric Zn(II) species IPr•ZnH(μ-H)$_2$Zn(OTf)•IPr (**10**).

4.5 Experimental Procedures

4.5.1 Materials and instrumentation

All reactions were performed using standard Schlenk line techniques under an atmosphere of nitrogen or in an inert atmosphere glove box (Innovative Technology, Inc.). Solvents were dried using a Grubbs-type solvent purification system[52] manufactured by Innovative Technology, Inc., degassed (freeze-pump-thaw method) and stored under an atmosphere of nitrogen prior to use. $CdCl_2$, ZnI_2, $Li[BH_4]$, $Li[HBEt_3]$ (1.0 M solution in THF), thallium (I) trifluoromethane sulfonate (Tl[OTf]), diethylzinc (1.0 M solution in THF), 4-dimethylaminopyridine (DMAP), benzophenone, phenylmethylsilane, $K[HB^sBu_3]$ (1.0 M solution in THF), MeOTF, MeI and HBPin (BPin = $B(OCMe_2)_2$) were purchased from Aldrich and used as received. Ph_3PCMe_2,[40] 1,3-bis-(2,6-diisopropylphenyl)-imidazol-2-ylidene (IPr),[13] and 1,3-diisopropyl-4,5-dimethylimidazole-2-ylidene ($ImMe_2{}^iPr_2$)[53] were prepared according to literature procedures. ^1H, ^{11}B, $^{13}C\{^1H\}$ and $^{19}F\{^1H\}$ NMR spectra were recorded either on a Varian iNova-400 or on a Varian iNova-500 spectrometer running VNMRJ 3.2A and referenced to the residual protonated solvent peak of known chemical shift downfield from $SiMe_4$ for ^1H and $^{13}C\{^1H\}$ or externally to $CFCl_3$ for the ^{19}F NMR data. Variable temperature studies were carried out on a 400 MHz Varian Inova instrument from –60 °C to 27 °C in *ca.* 20 °C steps. All temperatures were calibrated against a standard methanol sample to achieve the desired temperature inside the probe. The spectral window for all experiments was 6 kHz. Spectra

were acquired with 32 scans, a 5 s acquisition time, 0.1 s relaxation delay and a 30 degree flip angle was used for all data sets. Diffusion-Ordered Spectroscopy (DOSY) experiments were performed on the 500 MHz instrument equipped with a Z-gradient broadband probe capable of outputting 61.6 G/cm of gradient strength. All measurements were carried out non-spinning and at a calibrated temperature of 27 °C using the Oneshot45 pulse sequence.[54,55] For all DOSY experiments a spectral window of 6 kHz was used with a 3 s acquisition time and a 2 s relaxation delay with 8 scans for each gradient increment. Pulses widths and gradient strengths were optimized for each sample. For both solvent systems a diffusion delay of 50 ms a diffusion gradient length of 2 ms was used. Gradient strengths of 1.9 G/cm to 47.1 G/cm incremented in 20 steps were used for the toluene solutions and gradient strengths of 1.9 G/cm to 37.6 G/cm also incremented in 20 steps were used for the THF solutions. The spectra were Fourier transformed and baseline corrected prior to discrete processing, fitting the data to a double exponential fit and applying corrections for non-uniform gradients.[56] The diffusion dimension was zero filled to 1024 data points and the directly detected dimension was zero filled to 128k data points. Elemental analyses were performed by the Analytical and Instrumentation Laboratory at the University of Alberta. Melting points were measured in sealed glass capillaries under nitrogen using a MelTemp melting point apparatus and are uncorrected.

4.5.2 Computational Studies

Geometry optimizations were accomplished utilizing density functional theory with the M06-2X[58] functional. The basis sets employed in the computations were cc-pVTZ[59,60] for all atoms (*i.e.*, C, H, N, O, F, S, and Zn) except iodine where a cc-pVTZ-pp[61,62] basis set was used (a combination of cc-pVTZ with the corresponding small core, 28 electrons, effective core potential[63,64]). For convenience, the theoretical level of each computation is labeled as M06-2X/cc-pVTZ throughout the text. "Tight" convergence criteria, *i.e.*, maximum force = 1.5×10^{-5} a.u., RMS force = 1.0×10^{-5} a.u., max displacement = 6.0×10^{-5}, and RMS displacement = 4.0×10^{-5} were applied for all optimizations. The grid used for numerical integration in DFT was set to "Ultrafine," *i.e.*, a pruned grid of 99 radial shells and 370 angular points per shell. Harmonic vibrational frequencies were computed analytically at the same level of theory in order to characterize the stationary points as true minima, representing equilibrium structures on the potential energy surfaces. Heats of formation (ΔH_f) for all systems were computed with the procedure discussed in the Gaussian white paper on thermochemistry available in the Gaussian 09 online manual.[65] The GaussView 5.0[66] program was used for plotting the molecular electrostatic potentials (MEP). The GaussSum 3.0[67] program was also utilized to plot infrared spectra for all species. The NBO[68] population analyses on the optimized structures are accomplished at M06-2X/cc-pVTZ level of theory. All the computations were performed using the Gaussian 09 program package, revision C.01.[69]

4.5.3 X-ray Crystallography

Crystals of appropriate quality for X-ray diffraction studies were removed either from a Schlenk tube under a stream of nitrogen or a vial (glovebox) and immediately covered with a thin layer of hydrocarbon oil (Paratone-N). A suitable crystal was then selected, attached to a glass fibre, and quickly placed in a low-temperature stream of nitrogen.[70] All data were collected using a Bruker APEX II CCD detector/D8 diffractometer using Mo Kα or Cu Kα radiation, with the crystal cooled to −100 °C. Refinements were completed using the program SHELXL-97.[71] Hydrogen atoms were assigned positions based on the sp^2 or sp^3 hybridisation geometries of their attached carbon or nitrogen atoms and were given thermal parameters 20 % greater than those of their parent atoms. See Tables 4.1 to 4.5 for a listing of relevant crystallographic data.

4.5.4 Synthetic procedures

4.5.4.1 Synthesis of IPr•ZnI_2•THF (1)

IPr (0.181 g, 0.466 mmol) and ZnI_2 (0.149 g, 0.465 mmol) were combined in 10 mL of THF at room temperature. The mixture was stirred for 12 hrs giving a pale yellow solution. Removal of the volatiles from the mixture yielded a pale yellow powder (0.310 g, 86 %), which was identified as 1 by ^{1}H NMR spectroscopy. Colourless crystals suitable for X-ray crystallography were obtained by cooling a saturated THF solution of 1 layered with hexanes at -35 °C for 3 days. Mp (°C): 150-152 (dec). ^{1}H NMR (500 MHz, C_6D_6): δ 7.16 (t, 2H,

Ar*H*, $^{3}J_{HH}$ = 7.6 Hz), 7.05 (d, 4H, Ar*H*, $^{3}J_{HH}$ = 7.6 Hz), 6.40 (s, 2H, N–C*H*–), 3.59 (m, 4H, C_4H_8O), 2.81 (septet, 4H, C*H*$(CH_3)_2$, $^{3}J_{HH}$ = 6.8 Hz), 1.52 (d, 12H, CH(C*H*$_3)_2$, $^{3}J_{HH}$ = 6.8 Hz), 1.36 (m, 4H, C_4H_8O), 0.94 (d, 12H, CH(C*H*$_3)_2$, $^{3}J_{HH}$ = 6.8 Hz). ^{1}H NMR (500 MHz, CD_2Cl_2): δ 7.54 (t, 2H, Ar*H*, $^{3}J_{HH}$ = 8.0 Hz), 7.55 (d, 4H, Ar*H*, $^{3}J_{HH}$ = 8.0 Hz), 7.28 (s, 2H, N–C*H*–), 3.58 (m, 4H, C_4H_8O), 2.67 (septet, 4H, C*H*$(CH_3)_2$, $^{3}J_{HH}$ = 7.2 Hz), 1.74 (m, 4H, C_4H_8O), 1.39 (d, 12H, CH(C*H*$_3)_2$, $^{3}J_{HH}$ = 6.5 Hz), 1.15 (d, 12H, CH(C*H*$_3)_2$, $^{3}J_{HH}$ = 6.5 Hz). ^{13}C{^{1}H} NMR (126 MHz, CD_2Cl_2): δ 173.3 (N–*C*–N), 146.2 (Ar*C*), 134.2 (Ar*C*), 131.3 (Ar*C*), 125.7 (Ar*C*), 124.8 (N–*C*H–), 69.3 (C_4H_8O), 29.1 (*C*H$(CH_3)_2$), 26.9 (CH(*C*H$_3)_2$), 25.6 (C_4H_8O), 23.7 (CH(*C*H$_3)_2$). Anal. Calc. for $C_{31}H_{45}I_2N_2OZn$: C, 47.68; H, 5.81; N, 3.59. Found: C, 47.41; H, 5.59; N, 3.59.

4.5.4.2 Synthesis of [IPrH][IPr•$CdCl_3$] (2)

To a solution of $CdCl_2$ (0.14 g, 0.76 mmol) in 4 mL of 1,4-dioxane was added a solution of IPr (0.29 g, 0.76 mmol) in 4 mL of THF. The reaction vial was wrapped in aluminium foil and the mixture was stirred for 18 hrs to give a pale yellow slurry. The volatiles were removed in *vacuo* to yield an off-white powder. This material was dissolved in 3 mL of THF, then 5 mL of hexanes was layered ontop of the solution and the mixture was stored at -35 °C overnight. This afforded 2 as a white microcrystalline solid (0.20 g, 27 %; the yield was calculated assuming a 1:1 mole ratio between the reagents IPr and $CdCl_2$ and the final product 2). Crystals suitable for X-ray crystallography were grown by cooling a THF/hexanes solution of 2 to -35 °C for 7 days. Mp (°C): 227-230. ^{1}H

NMR (500 MHz, C_6D_6): δ 9.21 (s, 2H, N-C*H*-), 7.33 (t, 2H, Ar*H*, $^3J_{HH}$ = 7.5 Hz), 7.25 (d, 4H, Ar*H*, $^3J_{HH}$ = 7.5 Hz), 7.06 (t, 2H, Ar*H*, $^3J_{HH}$ = 7.5 Hz), 6.90 (d, 4H, Ar*H*, $^3J_{HH}$ = 7.5 Hz), 6.57 (s, satellites, 2H, N–C*H*–, $^4J_{H\text{-}Cd}$ = 5.6 Hz), 6.32 (broad s, 1H, N-C*H*-N), 3.01 (septet, 4H, C*H*$(CH_3)_2$, $^3J_{HH}$ = 6.5 Hz), 2.50 (septet, 4H, CH(C*H*$_3)_2$, $^3J_{HH}$ = 6.5 Hz), 1.71 (d, 12H, CH(C*H*$_3)_2$, $^3J_{HH}$ = 6.5 Hz), 1.10 (d, 12H, CH(C*H*$_3)_2$, $^3J_{HH}$ = 6.5 Hz), 1.09 (d, 12H, CH(C*H*$_3)_2$, $^3J_{HH}$ = 6.5 Hz), 0.91 (d, 12H, CH(C*H*$_3)_2$, $^3J_{HH}$ = 6.5 Hz). $^{13}C\{^1H\}$ NMR (126 MHz, C_6D_6): δ 187.9 (N–*C*–N), 146.2 (Ar*C*), 145.9 (Ar*C*), 135.6 (Ar*C*), 133.7 (N–*C*H–N), 131.5 (Ar*C*), 130.8 (Ar*C*), 130.4 (Ar*C*), 124.28 (Ar*C*), 124.32 (Ar*C*), 124.2 (N-*C*H-), 29.1 (*C*H$(CH_3)_2$), 28.8 (*C*H$(CH_3)_2$), 25.8 (CH(*C*H$_3)_2$), 24.4 (CH(*C*H$_3)_2$), 23.8 (CH(*C*H$_3)_2$). Anal. Calc. for $C_{54}H_{73}CdCl_3N_4$: C, 65.06; H, 7.38; N, 5.62. Found: C, 65.00; H, 7.49; N, 5.49.

4.5.4.3 Reaction of [IPrH][IPr•$CdCl_3$] (2) with Tl[OTf]: Isolation of IPr•$CdCl_2$•THF (3)

To a colourless solution of Tl[OTf] (39 mg, 0.11 mmol) in 3 mL of THF was added a colourless solution of [IPrH][IPr•$CdCl_3$] (2) (109 mg, 0.109 mmol) in 3 mL of THF. Immediately upon the addition of 2, the formation of white precipitate was noted. The mixture was stirred for 18 hrs, and then the volatiles removed *in vacuo*. The resulting off-white solid was extracted with 4 mL of benzene, and filtered to remove insoluble byproducts. The volatiles were removed from the resulting filtrate in *vacuo* to yield a white solid, which was washed with 2 x 1 mL of hexanes and dried under vacuum to yield spectroscopically pure

IPr•$CdCl_2$ as a white powder (30 mg, 48 %); note: the data presented below is for the THF-free complex IPr•$CdCl_2$. Crystals suitable for X-ray crystallography were grown by cooling a THF/hexanes solution of 3 to -35 °C for 5 days. Mp (°C): Stable to 260. ^{1}H NMR (500 MHz, C_6D_6): δ 7.21 (t, 2H, Ar*H*, $^3J_{HH}$ = 7.5 Hz), 7.08 (d, 4H, Ar*H*, $^3J_{HH}$ = 7.5 Hz), 6.41 (s, satellites, 2H, N–C*H*–, $^4J_{H\text{-}Cd}$ = 7.2 Hz), 2.70 (septet, 4H, C*H*$(CH_3)_2$, $^3J_{HH}$ = 6.9 Hz), 1.52 (d, 12H, CH(C*H*$_3)_2$, $^3J_{HH}$ = 6.5 Hz), 0.93 (d, 12H, CH(C*H*$_3)_2$, $^3J_{HH}$ = 6.5 Hz). ^{13}C{^{1}H} NMR (126 MHz, C_6D_6): δ 182.8 (N–*C*–N), 145.8 (Ar*C*), 134.4 (Ar*C*), 131.1 (Ar*C*), 129.2 (Ar*C*), 124.6 (N-*C*H-), 29.1 (*C*H$(CH_3)_2$), 25.7 (CH(*C*H$_3)_2$), 23.7 (CH(*C*H$_3)_2$). Anal. Calc. for $C_{27}H_{36}CdCl_2N_2$: C, 56.70; H, 6.34; N, 4.90. Found: C, 57.60; H, 6.51; N, 4.60.

4.5.4.4 Reaction of [IPrH][IPr•$CdCl_3$] (2) with Tl[OTf]: Isolation of IPrH[OTf]

To a colourless solution of Tl[OTf] (73 mg, 0.21 mmol) in 3 mL of THF was added a colourless solution of [IPrH][IPr•$CdCl_3$] (2) (0.205 g, 0.206 mmol) in 3 mL of THF. Immediately upon the addition of 2, the formation of white precipitate was noted. The solution was stirred for 48 hrs, upon which time the mother liquor was filtered. The volatiles were removed from the filtrate *in vacuo* to yield a white powder, which was washed with 2 x 2mL benzene and dried *in vacuo* to afford a pure sample of IPrH[OTf] (52 mg, 47 %). Mp (°C): stable to 260. NMR spectral values for IPrH[OTf] matched those found in the literature.[13] ^{1}H NMR (500 MHz, $CDCl_3$): δ 9.10 (s, 1H, N-C*H*-N), 7.84 (s, 2H, N-C*H*-), 7.59 (t, 2H, Ar*H*, $^3J_{HH}$ = 7.5 Hz), 7.36 (d, 4H, Ar*H*, $^3J_{HH}$ = 7.5 Hz), 2.42 (septet, 4H,

C*H*(CH_3)$_2$, $^3J_{HH}$ = 6.5 Hz), 1.28 (d, 12H, CH(C*H*$_3$)$_2$, $^3J_{HH}$ = 6.5 Hz), 1.22 (d, 12H, CH(C*H*$_3$)$_2$, $^3J_{HH}$ = 6.5 Hz). $^{13}C\{^1H\}$ NMR (126 MHz, $CDCl_3$): δ 144.9 (N–*C*H–), 138.0 (Ar*C*), 132.3 (Ar*C*), 129.7 (Ar*C*), 126.4 (Ar*C*), 29.5 (*C*H(CH_3)$_2$), 24.8 (CH(*C*H$_3$)$_2$), 24.2 (CH(*C*H$_3$)$_2$). $^{19}F\{^1H\}$ NMR (470 MHz, $CDCl_3$): δ -78.0. Anal. Calc. for $C_{28}H_{37}F_3N_2O_3S$: C, 62.43; H, 6.92; N, 5.20. Found: C, 62.44; H, 6.94; N, 5.26.

4.5.4.5 Reaction of IPr•ZnI_2•THF (1) with Li[$HBEt_3$]

To a cold (-35 °C) slurry of 1 (100 mg, 0.128 mmol) in 8 mL of THF was added Li[$HBEt_3$] (0.282 mL, 1.0 M solution in THF, 0.282 mmol). The mixture was allowed to warm at room temperature and stirred for 12 hrs resulting in the formation of a black slurry. The resulting slurry was then filtered through Celite and the volatiles were removed in *vacuo* to yield a pale yellow solid (58 mg), which was identified as a mixture of IPr•BEt_3[9] (*ca.* 90 % by ^1H NMR spectroscopy), $IPrH_2$[9] (*ca.* 2 % by ^1H NMR spectroscopy) and *ca.* 8 % of other unidentified products.

4.5.4.6 Reaction of [IPrH][IPr•$CdCl_3$] (2) with Li[$HBEt_3$]

To a cold (-35 °C) solution of 2 (0.065 g, 0.065 mmol) in 6 mL of THF was added Li[$HBEt_3$] (0.137 mL, 1.0 M solution in THF, 0.137 mmol). The mixture was allowed to warm at room temperature and stirred for 3 hrs to give a black slurry. The resulting slurry was then filtered through Celite and the volatiles were removed to yield a white powder (0.052 g), which was identified as a

mixture of IPr•BEt_3[9] (*ca.* 68 % by ^{1}H NMR spectroscopy) and $IPrH_2$[9] (*ca.* 32 % by ^{1}H NMR spectroscopy).

4.5.4.7 Reaction of IPr•$CdCl_2$ with Li[$HBEt_3$]

To a cold (-35 °C) slurry of IPr•$CdCl_2$ (0.052 g, 0.091 mmol) in 5 mL of benzene was added Li[$HBEt_3$] (0.182 mL, 1.0 M solution in THF, 0.182 mmol). The mixture was allowed to warm at room temperature and stirred for 2 hrs to give a black slurry. The resulting slurry was then filtered through Celite and the volatiles were removed to yield a pale yellow powder (0.019 g), which was identified as a mixture of IPr•BEt_3[9] (*ca.* 50 % by ^{1}H NMR spectroscopy) and $IPrH_2$[9] (*ca.* 50 % by ^{1}H NMR spectroscopy).

4.5.4.8 Synthesis of IPr•$Zn(BH_4)_2$ (4)

To a suspension of $LiBH_4$ (0.013 g, 0.60 mmol) in 2 mL of THF was added a solution of 1 (0.233 g, 0.299 mmol) in 3 mL of THF to yield a pale yellow solution. This mixture was allowed to stir for 18 hrs, and then the volatiles removed *in vacuo*. The resulting pale yellow solid was extracted with 4 mL of toluene, and filtered to remove lithium salts. Removal of the solvent from the filtrate *in vacuo* yielded 4 as an off-white solid (0.138 g, 95 %). Crystals suitable for X-ray diffraction were obtained after 12 hrs by layering 2 mL of hexanes ontop of a solution of 7 dissolved in 1 mL of THF. Mp (°C): 104-107 (decomp). ^{1}H NMR (500 MHz, C_6D_6): δ 7.22 (t, 2H, Ar*H*, $^3J_{HH}$ = 8.0 Hz), 7.10 (d, 4H, Ar*H*, $^3J_{HH}$ = 8.0 Hz), 6.45 (s, 2H, N–C*H*–), 2.76 (septet, 4H, C*H*$(CH_3)_2$, $^3J_{HH}$ = 6.0 Hz),

1.47 (d, 12H, CH(CH_3)$_2$, $^3J_{HH}$ = 6.0 Hz), 0.97 (d, 12H, CH(CH_3)$_2$, $^3J_{HH}$ = 6.8 Hz). ^{13}C{^{1}H} NMR (126 MHz, C_6D_6): δ 144.9 (Ar*C*), 134.0 (Ar*C*), 131.5 (Ar*C*), 124.8 (Ar*C*), 124.7 (N–*C*H–), 29.0 (*C*H(CH$_3$)$_2$), 25.9 (CH(*C*H$_3$)$_2$), 23.4 (CH(*C*H$_3$)$_2$). We were unable to locate the N-*C*-N resonance. ^{11}B NMR (160 MHz, C_6D_6): δ -46.3 (pentet, $^1J_{HB}$ = 83.5 Hz, BH_4^-).

4.5.4.9 One pot synthesis of [IPr•ZnH(μ-H)]$_2$ (5)

IPr (3.103 g, 7.99 mmol) was dissolved in 20 mL of toluene and a solution of $ZnEt_2$ (8.0 mL, 1.0 M solution in THF, 8.0 mmol) was added dropwise, followed by stirring for 30 minutes. Methanol (646.5 μL, 16.0 mmol) was then added dropwise, upon which time immediate vigorous bubbling was noted (presumably due to loss of ethane gas). After 5 minutes, phenylmethylsilane (1.95 mL, 16.0 mmol) was added and the mixture stirred for 30 minutes. Addition of 30 mL of hexanes caused the precipitation of a white solid which was isolated from the filtrate, washed with hexanes (2 × 10 mL) and dried to yield [IPr•ZnH(μ-H)]$_2$ (2.513 g, 69 %). NMR data was consistent with literature values.[23e]

4.5.4.10 Alternative preparation of 5

To a colourless solution of IPr•ZnI_2•THF (0.310 g, 0.398 mmol) in 5 mL of THF at room temperature was added a solution of K[HB^{s}Bu$_3$] (398 μL, 1.0 M solution in THF, 0.40 mmol) which resulted in the formation of a white precipitate. After stirring for 2 hours, the mixture was filtered and the solid discarded, and the soluble fraction was evaporated under reduced pressure to give

the crude product as a white solid. This solid was washed with 2 × 3 mL of hexanes to remove trace amounts of IPr and $IPrH_2$[9] to yield 5 as a fine white spectroscopically pure powder (0.160 g, 88 %).[23e]

4.5.4.11 Synthesis of $ImMe_2^iPr_2$•$ZnEt_2$ (6a)

To a pale yellow solution of $ImMe_2^iPr_2$ (61 mg, 0.340 mmol) in 2 mL of Et_2O was added $ZnEt_2$ (338.4 μL, 1.0 M solution in THF, 0.34 mmol), and the resulting yellow solution was stirred for 30 minutes. At this time, the volatiles were removed *in vacuo* to yield the desired product (95 mg, 93 %). Spectroscopically pure product was obtained by dissolving the product in 2 mL of hexanes, filtering the solution through Celite, and then cooling to -35 °C for 72 h (42 mg, 41 %). ^{1}H NMR (C_6D_6, 500 MHz): δ 3.85 (septet, 2H, NC*H*$(CH_3)_2$, $^3J_{HH}$ = 7.5 Hz), 1.88 (t, 6H, $ZnCH_2CH_3$, $^3J_{HH}$ = 7.0 Hz), 1.51 (s, 6H, NCC*H*$_3$), 1.28 (d, 12H, NCH(C*H*$_3)_2$, $^3J_{HH}$ = 7.5 Hz), 0.79 (q, 4H, $ZnCH_2CH_3$, $^3J_{HH}$ = 7.0 Hz). ^{13}C{^{1}H} NMR (C_6D_6, 126 MHz): δ 123.1 (N*C*CH_3), 49.9 (N*C*H$(CH_3)_2$), 23.4 (NCH(*C*$H_3)_2$), 15.4 ($ZnCH_2CH_3$), 8.9 (NC*C*H_3), 5.4 ($ZnCH_2CH_3$). Mp (°C): 68-71. Despite multiple attempts, a satisfactory value for carbon elemental analysis was not obtained; see Figure 4.17 and 4.18 for the NMR spectra.

4.5.4.12 Synthesis of $[ImMe_2^iPr_2$•$ZnH(\mu\text{-}H)]_2$ (6b)

To a pale yellow solution of $ImMe_2^iPr_2$ (39.0 mg, 0.216 mmol) in 4 mL of toluene was added $ZnEt_2$ (216.0 μL, 1.0 M solution in THF, 0.22 mmol), and the resulting yellow solution was stirred for 30 minutes. Methanol (20.0 μL, 0.493

mmol) was added to the reaction mixture, immediately resulting in gas evolution being observed. After stirring for 5 minutes, phenylmethylsilane (59.5 μL, 0.434 mmol) was added, and the reaction stirred for 1 hour. Addition of 10 mL of hexanes resulted in the precipitation of a white solid, which was isolated and washed with 2 × 2 mL of hexanes to yield the desired product as an off-white solid (54.0 mg, 85 %). Dissolving the product in 3 mL of Et_2O and layering with 2 mL of hexanes, followed by storage at -35 °C for 72 hours yielded X-ray quality crystals of $[ImMe_2^iPr_2•ZnH(\mu\text{-}H)]_2$. ^1H NMR (C_6D_6, 500 MHz): δ 5.86 (septet, 4H, NC*H*$(CH_3)_2$, $^3J_{HH}$ = 8.0 Hz), 4.66 (broad s, 4H, ZnH_2), 1.62 (s, 12H, NCC*H*$_3$), 1.39 (d, 24H, NCH(C*H*$_3)_2$, $^3J_{HH}$ = 8.0 Hz). $^{13}C\{^1H\}$ NMR (C_6D_6, 126 MHz): δ 124.7 (N*C*CH_3), 52.6 (N*C*$H(CH_3)_2$), 22.3 (NCH(*C*$H_3)_2$), 9.9 (NC*C*H_3). IR (cm^{-1}): 1635 (m, Zn-$H_{terminal}$). Mp (°C): 131-134. Anal. Calcd. for $C_{22}H_{44}N_4Zn_2$: C, 53.34; H, 8.95; N, 11.30. Found: C, 53.05; H, 8.89; N, 10.94.

4.5.4.13 Synthesis of $[IPr•Zn(I)(\mu\text{-}H)]_2$ (7)

To a colourless solution of $IPr•ZnI_2•THF$ (0.204 g, 0.262 mmol) in 3 mL of THF at room temperature was added a solution of $K[HB^sBu_3]$ (262 μL, 1.0 M solution in THF, 0.26 mmol) which resulted in the formation of a white precipitate. After stirring for 30 minutes, the mixture was filtered and the solid discarded, and the solvent was removed from the filtrate under vacuum to give the crude product as a white solid (0.145 g, 95 %). Crystals suitable for X-ray diffraction were obtained by dissolution of the product in a minimum amount of THF, before being layered with an equal amount of hexanes, and left at room

temperature overnight to allow mixing of the solvents and crystallization of 7 to transpire. ^{1}H NMR (CD_2Cl_2, 400 MHz): δ 7.46 (t, 4H, p-Ar*H*, $^{3}J_{HH}$ = 8.0 Hz), 7.22 (d, 8H, m-Ar*H*, $^{3}J_{HH}$ = 8.0 Hz), 7.11 (s, 4H, N=C*H*), 2.64 (septet, 8H, C*H*(CH_3)$_2$, $^{3}J_{HH}$ = 6.8 Hz), 1.15 (broad d, 24H, CH(C*H*$_3$)$_2$, $^{3}J_{HH}$ = 6.8 Hz), 1.01 (d, 24H, $^{3}J_{HH}$ = 6.8 Hz, CH(C*H*$_3$)$_2$). *Please note that the Zn-H peak could not be identified.* ^{13}C{^{1}H} NMR (CD_2Cl_2, 126 MHz): δ 146.3 (Ar*C*), 135.2 (Ar*C*), 130.5 (Ar*C*), 125.2 (Ar*C*), 124.6 (Ar*C*), 28.7 (*C*H(CH_3)$_2$), 26.0 (CH(*C*H$_3$)$_2$), 23.9 (CH(*C*H$_3$)$_2$). Mp (°C): 179-182. (decomposes to a black powder). Anal. Calcd. for $C_{54}H_{74}I_2N_4Zn_2$: C, 55.73; H, 6.41; N, 4.81. Found: C, 55.02; H, 6.19; N, 4.07.

4.5.4.14 Alternative preparation of (7)

To a colourless solution of [IPr•ZnH(μ-H)]$_2$ (85 mg, 0.093 mmol) in 3 mL of toluene was added MeI (11.6 μL, 0.186 mmol). Immediate evolution of methane gas was noted, in addition to the formation of a white precipitate. The mixture was stirred for 3 hours, and the precipitate was allowed to settle. The mother liquor was decanted and the remaining solid washed with 2 × 2 mL of cold (-35 °C) toluene, and dried to yield 7 as a white spectroscopically pure solid (83 mg, 76 %).

4.5.4.15 Synthesis of IPr•Zn(H)OTf•THF (8)

To a colourless solution of [IPr•ZnH(μ-H)]$_2$ (0.135 g, 0.148 mmol) in 3 mL of THF was added MeOTf (32.4 μL, 0.296 mmol), which effected the immediate release of methane gas from the solution. The resulting solution was

stirred for 1 hour, and the volatiles were removed under reduced pressure to give IPr•Zn(H)OTf•THF as an off-white solid that was washed with 2 × 3 mL of hexanes and dried under reduced pressure (0.175 g, 88 %). Crystals of IPr•Zn(H)OTf•THF suitable for X-ray crystallographic analysis were obtained by dissolving the product in 2 mL of THF, before being layered with an equal volume of hexanes, and cooled to -35 °C for 20 hours. ^{1}H NMR (THF-D_8, 500 MHz): δ 7.62 (s, 2H, N=C*H*), 7.48 (t, 2H, p-Ar*H*, $^{3}J_{HH}$ = 8.0 Hz), 7.34 (d, 4H, m-Ar*H*, $^{3}J_{HH}$ = 8.0 Hz), 3.62 (m, 4H, OCH_2), 3.39 (s, 1H, Zn*H*), 2.68 (septet, 4H, C*H*(CH_3)$_2$, $^{3}J_{HH}$ = 7.0 Hz), 1.78 (m, 4H, OCH_2CH_2), 1.32 (d, 12H, CH(CH_3)$_2$, $^{3}J_{HH}$ = 7.0 Hz), 1.60 (d, 12H, CH(CH_3)$_2$, $^{3}J_{HH}$ = 7.0 Hz). ^{13}C{^{1}H} NMR (THF-D_8, 126 MHz): δ 168.3 (N*C*N), 145.4 (o-Ar*C*), 133.1 (ipso-Ar*C*), 131.8 (p-Ar*C*), 125.9 (N=*C*H), 124.9 (m-Ar*C*), 68.2 (O*C*H_2), 29.1 (*C*H(CH_3)$_2$), 26.0 (OCH_2*C*H_2), 24.9 (CH(*C*H_3)$_2$), 23.4 (CH(*C*H_3)$_2$). A resonance for the OTf group was not observed. ^{19}F{^{1}H} NMR (THF-D_8, 376 MHz): δ –78.5. IR (cm^{-1}): 1766 (m, Zn-$H_{terminal}$). Mp (°C): Stable to 260. Anal. Calcd. for $C_{32}H_{44}F_3N_2O_4SZn$: C, 56.93; H, 6.57; N, 4.15; S, 4.75. Found: C, 56.23; H, 6.75; N, 3.94; S, 4.01.

4.5.4.16 Synthesis of [IPr•Zn(H)(DMAP)$_2$][OTf] (9)

To a colourless solution of IPr•Zn(H)OTf•THF (80.0 mg, 0.118 mmol) in 3 mL of THF was added a solution of DMAP (29.0 mg, 0.237 mmol) in 2 mL of THF. The mixture was stirred for 4 hours, concentrated to ca. 2 mL, and then 10 mL of hexanes was added to precipitate [IPr•Zn(H)(DMAP)$_2$][OTf] (9) as a white solid. The mother liquor was decanted away and the remaining solid product

washed with 3 × 3 mL of hexanes before being dried under vacuum (75.0 mg, 76 %). The product was recrystallized by dissolution of the crude solid in 2 mL of THF, before layering with an equal volume of hexanes and cooling to -35 °C for 72 hours. ^{1}H NMR (CD_2Cl_2, 400 MHz): δ 7.50 (t, 2H, p-Ar*H*, $^{3}J_{HH}$ = 8.0 Hz), 7.30 (s, 2H, N=C*H*), 7.25 (d, 4H, m-Ar*H*, $^{3}J_{HH}$ = 8.0 Hz), 7.11 (broad s, 4H, DMAP-Ar*H*), 6.22 (broad s, 4H, DMAP-Ar*H*), 3.74 (s, 1H, Zn*H*), 2.97 (s, 12 H, N(CH_3)$_2$), 2.66 (septet, 4H, C*H*(CH$_3$)$_2$, $^{3}J_{HH}$ = 6.8 Hz), 1.15 (d, 12H, CH(CH_3)$_2$, $^{3}J_{HH}$ = 6.8 Hz), 1.10 (d, 12H, CH(CH_3)$_2$, $^{3}J_{HH}$ = 6.8 Hz). ^{13}C{^{1}H} NMR (CD_2Cl_2, 126 MHz): δ 146.2 (Ar*C*), 135.1 (Ar*C*), 131.2 (Ar*C*), 125.9 (DMAP-Ar*C*), 125.4 (Ar*C*), 124.7 (Ar*C*), 107.0 (DMAP-Ar*C*), 39.4 (N(*C*H$_3$)$_2$), 29.2 (*C*H(CH$_3$)$_2$), 25.7 (CH(*C*H$_3$)$_2$), 22.7 (CH(*C*H$_3$)$_2$). A resonance for the OTf group was not observed. ^{19}F{^{1}H} NMR (CD_2Cl_2, 376 MHz): δ -80.1 (THF-D_8, 376 MHz): δ −78.7. IR (cm^{-1}): 1615 (m, Zn-H). Mp (°C): 155-158 (decomposes to a dark brown solid). Anal. Calcd. for $C_{42}H_{57}F_3N_6O_3SZn$: C, 59.46; H, 6.77; N, 9.91; S, 3.78. Found: C, 59.22; H, 6.88; N, 9.69; S, 3.27.

4.5.4.17 Catalytic hydrosilylation of benzophenone using 8

A scintillation vial was charged with 8 (2.0 mg, 3.0 μmol, 1 mol%) and benzophenone (56.0 mg, 0.30 mmol), and 1 mL of THF was added (catalyst concentration: 3.0 M). To this colourless solution was added phenylmethylsilane (40.8 μL, 36.3 mg, 0.30 mmol), and the solution allowed to stir for ten minutes at ambient temperature. At this time, an aliquot of 200 μL was removed, and the volatiles removed *in vacuo*. ^{1}H NMR analysis in C_6D_6 revealed that the reaction

had proceeded to 92 % completion. The remaining solution was allowed to stir for a total of 30 minutes, upon which time the volatiles were removed *in vacuo* to yield $Ph_2C(H)OSi(H)MePh$ as a colourless liquid in a quantitative yield. Similar procedures were employed using 5 and 6b as catalysts; in the case of compound 9, no reaction was observed. Data for $Ph_2C(H)OSi(H)MePh$: ^1H NMR (C_6D_6, 500 MHz): δ 7.54 (d, 2H, Ar*H*, $^3J_{HH}$ = 7.5 Hz), 7.34 (d, 4H, Ar*H*, $^3J_{HH}$ = 8.0 Hz), 7.18-6.99 (m, 9H, Ar*H*), 5.82 (s, 1H, Ph_2C*H*), 5.27 (q with satellites, $^1J_{SiH}$ = 210 Hz, Si*H*, 1H, $^3J_{HH}$ = 3.0 Hz), 0.29 (d, 3H, SiCH_3, $^3J_{HH}$ = 3.0 Hz). $^{13}C\{^1H\}$ (C_6D_6, 126 MHz): δ 138.3 (Ar*C*), 135.9 (Ar*C*), 134.4 (Ar*C*), 132.1 (Ar*C*), 130.4 (Ar*C*), 130.2 (Ar*C*), 128.5 (Ar*C*), 128.4 (Ar*C*), 78.6 (Ph_2*C*H), -2.1(Si*C*H_3). ^{29}Si (99 MHz, C_6D_6): δ -3.0 (d, $^1J_{SiH}$ = 210 Hz). IR (cm^{-1}): 2131 (m, Si-H).

4.5.4.18 Catalytic hydroboration of benzophenone with 8

A scintillation vial was charged with 8 (5.0 mg, 7.4 μmol, 1 mol%) and benzophenone (0.135 g, 0.741 mmol), and 2.5 mL of THF was added (catalyst concentration: 3.0 M). To this colourless solution was added HBPin (107.5 μL, 94.8 mg, 0.741 mmol), and the solution allowed to stir for five minutes at ambient temperature. At this time, an aliquot of 200 μL was removed, and the volatiles removed *in vacuo*. ^1H NMR analysis in C_6D_6 revealed that the reaction had proceeded to 91 % completion. The remaining solution was allowed to stir for a total of 20 minutes, upon which time the volatiles were removed *in vacuo* to yield $Ph_2C(H)OB(OCMe_2)_2$ as a colourless solid in a quantitative yield. Data is consistent with the literature.[57]

4.5.4.19 Synthesis of IPr•ZnH(μ-H)$_2$Zn(OTf)•IPr (10)

A solution of IPr•Zn(H)OTf•THF (0.261 g, 0.387 mmol) in 3 mL of Et_2O was added to a slurry of KC_8 (0.053 g, 0.39 mmol) in 3 mL of Et_2O, and the resulting black suspension was allowed to stir for 10 minutes. At this time, the solid was allowed to settle, and the filtrate decanted and filtered through Celite. Evaporation of the volatiles *in vacuo* yielded the crude product as a white solid. This solid was then washed with 2 × 3 mL of hexanes to remove any free IPr, and the product dried under vacuum to yield a white solid (88 mg, 64 %). ^{1}H NMR (C_6D_6, 400 MHz): δ 7.24 (s, 4H, p-Ar*H*, $^3J_{HH}$ = 8.0 Hz), 7.48 (t, 8H, m-Ar*H*, $^3J_{HH}$ = 8.0 Hz), 6.44 (s, 4H, NC*H*), 3.01 (s, 3H, Zn*H*), 2.77 (septet, 8H, C*H*(CH_3)$_2$, $^3J_{HH}$ = 6.8 Hz), 1.33 (d, 24H, CH(C*H*$_3$)$_2$, $^3J_{HH}$ = 6.8 Hz), 0.99 (d, 24H, CH(C*H*$_3$)$_2$, $^3J_{HH}$ = 6.8 Hz). ^{13}C{^{1}H} NMR (C_6D_6, 126 MHz): δ 168.3 (N*C*N), 145.4 (o-Ar*C*), 133.1 (ipso-Ar*C*), 131.8 (p-Ar*C*), 125.9 (N=*C*H), 124.9 (m-Ar*C*), 29.1 (*C*H(CH_3)$_2$), 24.9 (CH(*C*H$_3$)$_2$), 23.4 (CH(*C*H$_3$)$_2$). A resonance for the OTf group was not observed. ^{19}F{^{1}H} NMR (C_6D_6, 376 MHz): δ -77.0 ppm. Mp (°C): 156-159. Anal. Calcd. for $C_{55}H_{77}F_3N_4O_3SZn_2$: C, 62.20; H, 7.31; N, 5.28; S, 3.02. Found: C, 62.80; H, 7.51; N, 5.41; S, 2.96.

4.4.2.20 Synthesis of $[Ph_3PCMe_2 \bullet ZnI(\mu\text{-}I)]_2$ (11)

To a solution of ZnI_2 (0.103 g, 0.323 mmol) in 3 mL of THF was added dropwise a deep red solution of Ph_3PCMe_2 (0.098 g, 0.32 mmol) in 4 mL of THF. Upon the addition of this solution, the colour faded immediately, and the resultant colourless solution was allowed to stir at room temperature for 2 hours. At this point, 5 mL of hexanes was added to the solution, which caused the immediate precipitation of a white solid. The precipitate was allowed to settle and the filtrate decanted; the remaining solid was washed with 2 × 2 mL portions of hexanes, before being dried *in vacuo*. This solid was identified as analytically pure 11 (0.156 g, 78 %). ^{1}H NMR (THF-D_8, 400 MHz): δ 7.89 (m, 12H, m-Ar*H*), 7.70 (m, 6H, p-Ar*H*), 7.59 (m, 12H, o-Ar*H*), 1.59 (d, 12H, PC(CH_3)$_2$, $^3J_{HP}$ = 21.6 Hz). ^{13}C{^{1}H} NMR (THF-D_8, 101 MHz): δ 135.8 (d, m-Ar*C*, $^3J_{CP}$ = 8.3 Hz), 133.7 (d, p-Ar*C*, $^4J_{CP}$ = 3.0 Hz), 129.6 (d, o-Ar*C*, $^2J_{CP}$ = 11.4 Hz), 123.4 (d, ipso-Ar*C*, $^1J_{CP}$ = 80.9 Hz), 30.1 (d, C(*C*H$_3$)$_2$, $^2J_{CP}$ = 26.5 Hz), 22.5 (C(*C*H$_3$)$_2$). ^{31}P{^{1}H} NMR (THF-D_8, 162 MHz): δ 37.5. Mp (°C): 210-213. Anal. Calcd. for $C_{42}H_{42}I_4P_2Zn_2$: C, 40.45; H, 3.39. Found: C, 40.89; H, 3.64.

Figure 4.17 ^{1}H (500 MHz, C_6D_6) spectrum of $ImMe_2{}^{i}Pr_2{\bullet}ZnEt_2$ (**6a**)

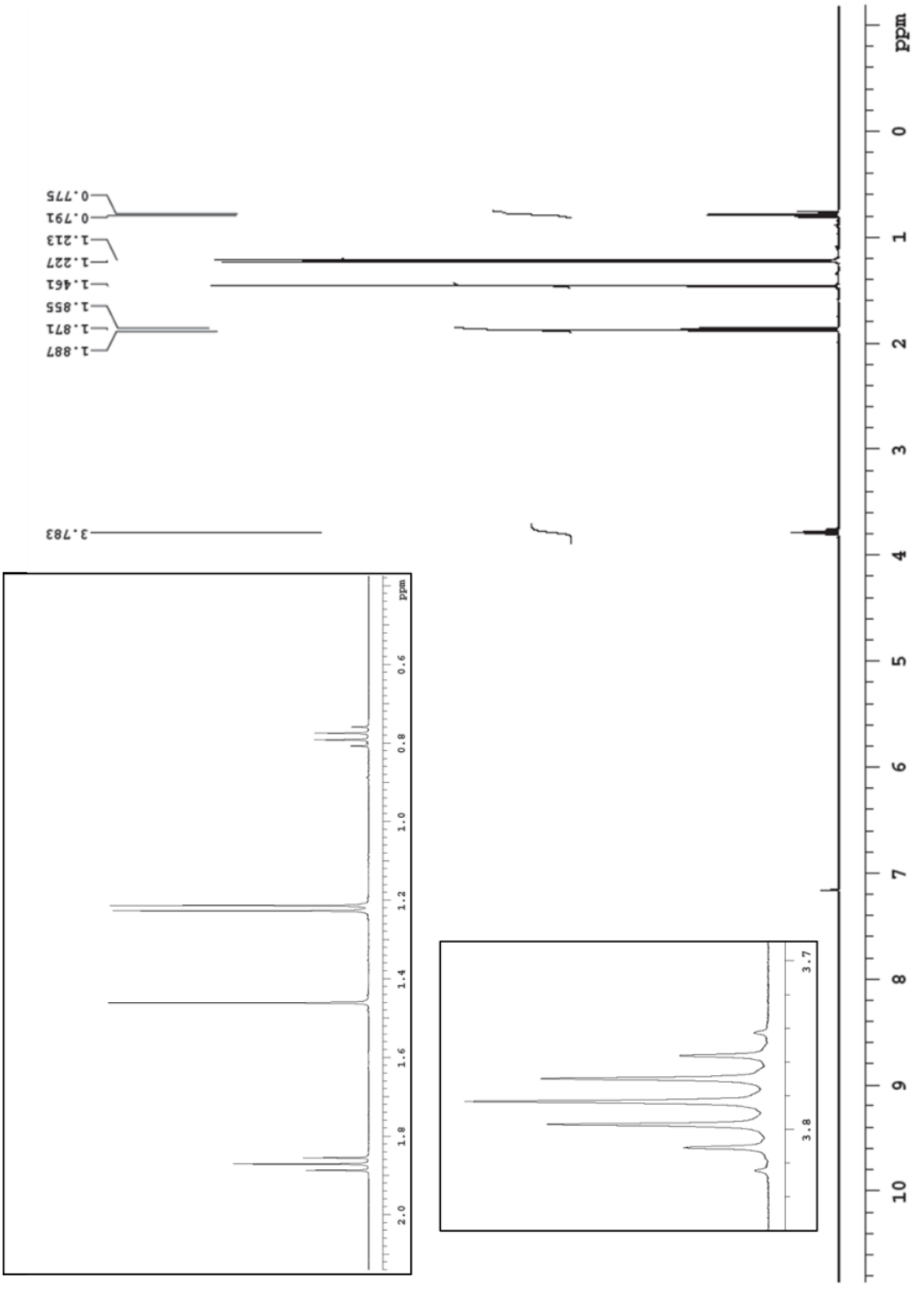

Figure 4.18 $^{13}C\{^{1}H\}$ (126 MHz, C_6D_6) APT spectrum of $ImMe_2{}^{i}Pr_2{\bullet}ZnEt_2$ (**6a**)

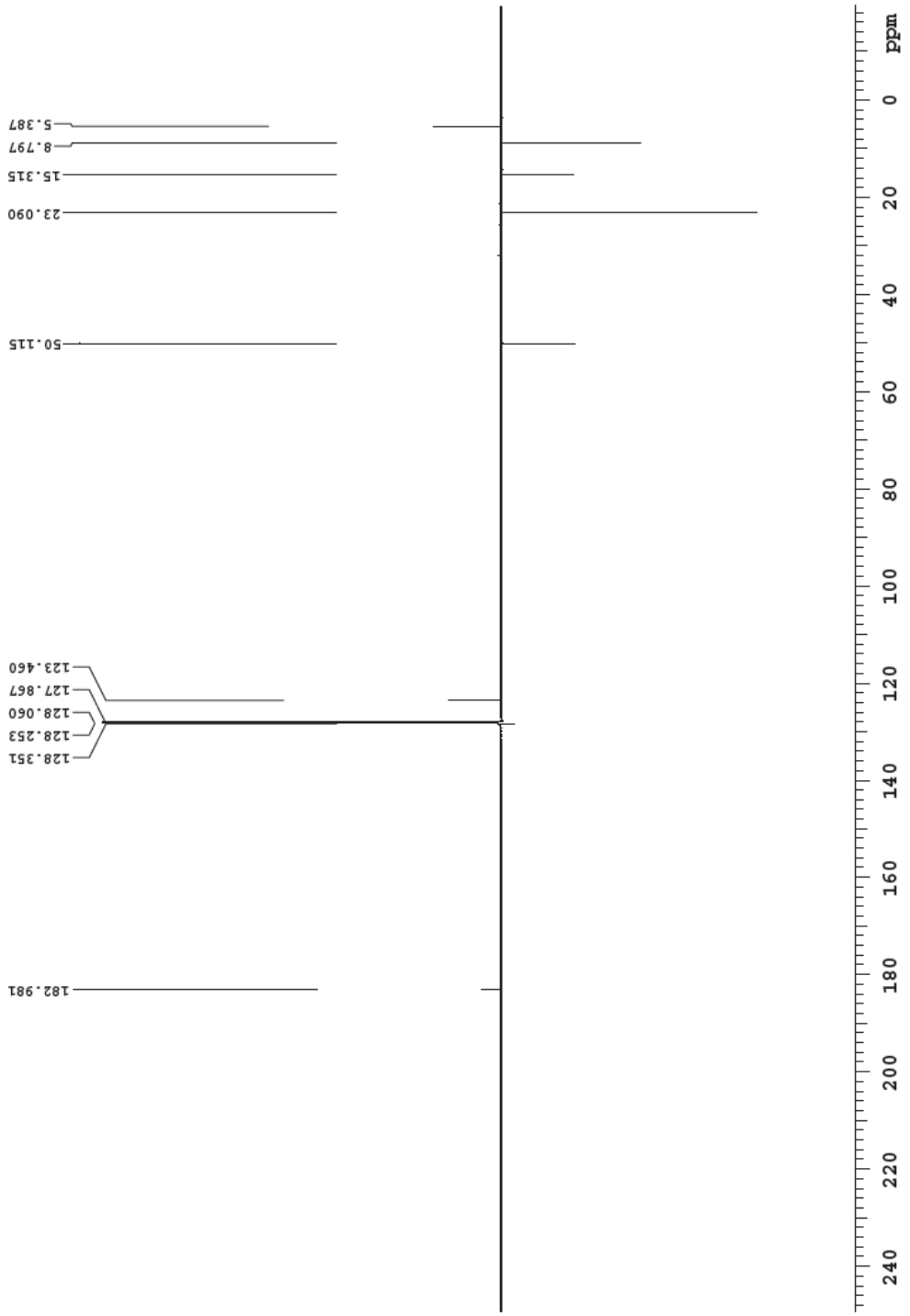

Table 4.1. Crystallographic Data for Compounds **1** and **2**

	1	**2**•2.5 toluene
empirical formula	$C_{31}H_{44}I_2N_2OZn$	$C_{71.5}H_{93}CdCl_3N_4$
fw	779.85	1227.25
cryst dimens (mm^3)	0.48 × 0.31 × 0.15	0.49 × 0.18 × 0.08
cryst syst	monoclinic	triclinic
space group	*C*2/*c*	$P\ \bar{1}$
a (Å)	40.7207(14)	14.985(2)
b (Å)	9.6340(3)	16.849(2)
c (Å)	17.0987(6)	18.063(2)
a(deg)		61.6908(15)
β (deg)	99.7678(3)	73.7219(16)
γ (deg)		58.9672(15)
V ($Å^3$)	6610.6(4)	3436.7(8)
Z	8	2
ρ (g cm^{-3})	1.567	1.186
abs coeff (mm^{-1})	2.635	0.476
T (K)	173(1)	173(1)
$2\theta_{max}$ (deg)	52.76	55.20
total data	25661	67722
unique data (R_{int})	6749 (0.0118)	27625 (0.0702)
R_1 [$I > 2\sigma(I)$][a]	0.0213	0.0602
wR_2 [all data][a]	0.0544	0.1702
Max/Min $\Delta\rho$ (e^- $Å^{-3}$)	1.072/-0.786	1.890/-1.275

[a] $R_1 = \Sigma\,||F_o|-|F_c||/\Sigma|F_o|$; $wR_2 = [\Sigma\, w(F_o^2 - F_c^2)^2/\Sigma\, w(F_o^4)]^{1/2}$.

Table 4.2. Crystallographic Data for Compounds **3** and **4**

	3	**4**
empirical formula	$C_{35}H_{52}CdCl_2N_2O_2$	$C_{27}H_{44}B_2N_2Zn$
fw	716.09	483.63
cryst dimens (mm^3)	0.38 × 0.32 × 0.24	0.21 × 0.12 × 0.07
cryst syst	orthorhombic	monoclinic
space group	$P2_12_12_1$	$C2/c$
a (Å)	13.9468(8)	16.6074(5)
b (Å)	15.8702(9)	9.4081(3)
c (Å)	16.5113(9)	17.7919(5)
a(deg)		
β (deg)		90.3920(10)
γ (deg)		
V ($Å^3$)	3654.6(4)	2779.81(14)
Z	4	4
ρ (g cm^{-3})	1.301	1.156
abs coeff (mm^{-1})	0.774	1.320
T (K)	173(1)	173(1)
$2\theta_{max}$ (deg)	54.88	140.34
total data	32290	9055
unique data (R_{int})	8318 (0.0288)	2600 (0.0196)
R_1 [$I > 2\sigma(I)$][a]	0.0249	0.0338
wR_2 [all data][a]	0.0671	0.0994
Max/Min $\Delta\rho$ (e^- $Å^{-3}$)	0.762/-0.332	1.412/-0.320

[a] $R_1 = \Sigma \| \|F_o\| - \|F_c\| \| / \Sigma |F_o|$; $wR_2 = [\Sigma\, w(F_o^2 - F_c^2)^2 / \Sigma\, w(F_o^4)]^{1/2}$.

Table 4.3. Crystallographic Data for Compounds **6** and **7**

	6	**7**
empirical formula	$C_{22}H_{44}N_4Zn_2$	$C_{70}H_{106}I_2N_4O_4Zn_2$
fw	495.35	1452.12
cryst dimens (mm^3)	0.45 × 0.24 × 0.16	0.34 × 0.19 × 0.18
cryst syst	triclinic	monoclinic
space group	$P\bar{1}$	$P2_1/n$
a (Å)	8.4179(3)	13.4890 (5)
b (Å)	9.1569(3)	17.9912 (7)
c (Å)	9.5467(3)	15.7313 (6)
a(deg)	96.6389(4)	
β (deg)	109.5357(3)	109.9139 (5)
γ (deg)	107.4586(3)	
V ($Å^3$)	642.20	3589.4(2)
Z	1	2
ρ (g cm^{-3})	1.281	1.344
abs coeff (mm^{-1})	1.881	1.575
T (K)	173(1)	173(1)
$2\theta_{max}$ (deg)	56.60	56.61
total data	5940	9055
unique data (R_{int})	3083 (0.0070)	8817 (0.0251)
R_1 [$I > 2\sigma(I)$][a]	0.0191	0.0329
wR_2 [all data][a]	0.0524	0.0906
Max/Min $\Delta\rho$ (e^- $Å^{-3}$)	0.403/-0.178	0.744/-0.762

[a] $R_1 = \Sigma \| \|F_o\| - \|F_c\| \| / \Sigma |F_o|$; w$R_2 = [\Sigma\, w(F_o^2 - F_c^2)^2 / \Sigma\, w(F_o^4)]^{1/2}$.

Table 4.4 Crystallographic Data for Compounds **8** and **9**

	8	**9**
empirical formula	$C_{32}H_{45}F_3N_2O_4SZn$	$C_{42}H_{57}F_3N_6O_3SZn$
fw	676.13	848.36
cryst dimens (mm^3)	0.40 × 0.16 × 0.15	0.24 × 0.19 × 0.15
cryst syst	triclinic	triclinic
space group	$P1$	$P\bar{1}$
a (Å)	10.4513 (10)	16.1713 (3)
b (Å)	11.3209 (11)	17.0038 (3)
c (Å)	15.6761 (15)	17.7430 (3)
a(deg)	90.6516 (12)	90.6070 (9)
β (deg)	105.2853 (12)	96.2563 (8)
γ (deg)	102.7679 (12)	115.2972 (8)
V ($Å^3$)	1740.1(3)	4375.84 (14)
Z	2	4
ρ (g cm^{-3})	1.290	1.288
abs coeff (mm^{-1})	0.817	1.693
T (K)	173(1)	173(1)
$2\theta_{max}$ (deg)	56.83	139.99
total data	15841	28635
unique data (R_{int})	15841 (0.0322)	16014 (0.0201)
obs data [$I > 2\sigma(I)$]	13392	13598
Params	785	1027
R_1 [$I > 2\sigma(I)$][a]	0.369	0.0910
wR_2 [all data][a]	0.0872	0.2733
Max/Min $\Delta\rho$ (e^- $Å^{-3}$)	0.570/-0.315	4.600/-1.816

[a] $R_1 = \Sigma \| \|F_o\| - \|F_c\| \| / \Sigma |F_o|$; $wR_2 = [\Sigma\, w(F_o^2 - F_c^2)^2 / \Sigma\, w(F_o^4)]^{1/2}$.

Table 4.5 Crystallographic Data for Compounds **10** and **11**

	10	**11**
empirical formula	$C_{59}H_{85}F_3N_4O_4SZn_2$	$C_{42}H_{42}I_4P_2Zn$
fw	1134.10	1247.03
cryst dimens (mm^3)	0.23 × 0.20 × 0.13	0.29 × 0.18 × 0.0
cryst syst	monoclinic	monoclinic
space group	*Cc*	*I*2/*a*
a (Å)	20.3116 (4)	21.4940 (8)
b (Å)	15.0498 (3)	9.6728 (4)
c (Å)	21.1766 (4)	21.6828 (8)
a(deg)		
β (deg)	103.5214 (10	108.0769 (4)
γ (deg)		
V ($Å^3$)	6294.0 (2)	4285.5(3)
Z	4	4
ρ (g cm^{-3})	1.197	1.933
abs coeff (mm^{-1})	1.672	4.104
T (K)	173(1)	173(1)
$2\theta_{max}$ (deg)	144.89	56.55
total data	21257	19396
unique data (R_{int})	12316 (0.0174)	5264 (0.0160)
obs data [$I > 2\sigma(I)$]	11905	4863
Params	690	228
R_1 [$I > 2\sigma(I)$][a]	0.0335	0.0199
wR_2 [all data][a]	0.0923	0.0499
Max/Min $\Delta\rho$ (e^- $Å^{-3}$)	0.435/-0.318	0.780/-0.353

[a] $R_1 = \Sigma \| \|F_o\| - \|F_c\| \| / \Sigma |F_o|$; $wR_2 = [\Sigma\, w(F_o^2 - F_c^2)^2 / \Sigma\, w(F_o^4)]^{1/2}$.

4.6 References

1. (*a*) A. J. Arduengo III, R. L. Harlow, M. Kline, *J. Am. Chem. Soc.* **1991**, *113*, 361; (*b*) A. J. Arduengo III, H. V. Rasika Dias, R. L. Harlow, M. Kline, *J. Am. Chem. Soc.* **1992**, *114*, 5530; (*c*) For an early report of a stable acyclic carbene, see: A. Igau, H. Grutzmacher, A. Baceiredo, G. Bertrand, *J. Am. Chem. Soc.* **1988**, *110*, 6463.

2. (*a*) S. Díez-González, N. Marion, S. P. Nolan, *Chem. Rev.* **2009**, *109*, 3612; (*b*) C. M. Crudden, D. P. Allen, *Coord. Chem. Rev.* **2004**, *248*, 2247.

3. (*a*) N. Kuhn, A. Al-Sheikh, *Coord. Chem. Rev.* **2005**, *249*, 829; (*b*) R. Wolf, W. Uhl, *Angew. Chem. Int. Ed.* **2009**, *48*, 6774; (*c*) Y. Wang, G. H. Robinson, *Chem. Commun.* **2009**, 5201; (*d*) Y. Wang, G. H. Robinson, *Inorg. Chem.* **2011**, *50*, 12326; (*e*) D. Martin, M. Melaimi, M. Soleilhavoup, G. Bertrand, *Organometallics* **2011**, *30*, 5304.

4. Y. Wang, Y. Xie, P. Wei, R. B. King, H. F. Schaefer III, P. v. R. Schleyer, G. H. Robinson, *Science* **2008**, *321*, 1069.

5. A. Sidiropoulos, C. Jones, A. Stasch, S. Klein, G. Frenking, *Angew. Chem. Int. Ed.* **2009**, *48*, 9701.

6. C. Jones, A. Sidiropoulos, N. Holzmann, G. Frenking, A. Stasch, *Chem. Commun.* **2012**, *48*, 9855.

7. H. Braunschweig, R. D. Dewhurst, K. Hammond, J. Mies, K. Radacki, A. Vargas, *Science* **2012**, *336*, 1420.

8. K. C. Thimer, S. M. I. Al-Rafia, M. J. Ferguson, R. McDonald, E. Rivard, *Chem. Commun.* **2009**, 7119.

9. S. M. I. Al-Rafia, A. C. Malcolm, S. K. Liew, M. J. Ferguson, E. Rivard, *J. Am. Chem. Soc.* **2011**, *133*, 777.

10. (*a*) M. Y. Abraham, Y. Wang, Y. Xie, P. Wei, H. F. Schaefer III, P. v. R. Schleyer, G. H. Robinson, *J. Am. Chem. Soc.* **2011**, *133*, 8874; (*b*) S. M. I. Al-Rafia, A. C. Malcolm, R. McDonald, M. J. Ferguson, E. Rivard, *Chem. Commun.* **2012**, *48*, 1308.

11. S. M. I. Al-Rafia, A. C. Malcolm, R. McDonald, M. J. Ferguson, E. Rivard, *Angew. Chem. Int. Ed.* **2011**, *50*, 8354.

12. For selected recent advances in this area, see: (*a*) R. Kinjo, B. Donnadieu, M. Ali Celik, G. Frenking, G. Bertrand, *Science* **2011**, *333*, 610; (*b*) B. Inés, M. Patil, J. Carreras, R. Goddard, W. Thiel, M. Alcarazo, *Angew. Chem. Int. Ed.* **2011**, *50*, 8400; (*c*) S. J. Bonyhady, D. Collis, G. Frenking, N. Holzmann, C. Jones, A. Stasch, *Nat. Chem.* **2010**, *2*, 865; (*d*) Y. Xiong, S. Yao, G. Tan, S. Inoue, M. Driess, *J. Am. Chem. Soc.* **2013**, *135*, 5004; (*e*) K. Chandra Mondal, H. W. Roesky, M. C. Schwarzer, G. Freking, B. Niepötter, H. Wolf, R. Herbst-Irmer, D. Stalke, *Angew. Chem. Int. Ed.* **2013**, *52*, 2963.

13. L. Jafarpour, E. D. Stevens, S. P. Nolan, *J. Organomet. Chem.* **2000**, *606*, 49.

14. (*a*) T. R. Jensen, C. P. Schaller, M. A. Hillmyer, W. B. Tolman, *J. Organomet. Chem.* **2005**, *690*, 5881; (*b*) B. Bantu, G. Manohar Pawar,

U. Decker, K. Wurst, A. M. Schmidt, M. R. Buchmeiser, *Chem. Eur. J.* **2009**, *15*, 3103; (*c*) P. L. Arnold, I. J. Casely, Z. R. Turner, R. Bellabarba, R. B. Tooze, *Dalton Trans.* **2009**, 7236; (*d*) Y. Lee, B. Li, A. H. Hoveyda, *J. Am. Chem. Soc.* **2009**, *131*, 11625; (*e*) X. Liu, C. Cao, Y. Li, P. Guan, L. Yang, Y. Shi, *Synlett* **2012**, *23*, 1343; (*f*) For a report of a carbene-zinc catalyst which activates CO_2, see: O. Jacquet, X. Frogneux, C. Das Neves Gomes, T. Cantat, *Chem. Sci.* **2013**, *4*, 2127.

15. (*a*) A. E. Finholt, A. C. Bond, Jr., H. I. Schlesinger, *J. Am. Chem. Soc.* **1947***, 69*, 1199; (*b*) J. J. Watkins, E. C. Ashby, *Inorg. Chem.* **1974**, *13*, 2350; (*c*) For the synthesis of gas phase ZnH_2, see: A. Shayesteh, S. Yu, P. F. Bernath, *Chem. Eur. J.* **2005**, *11*, 4709.

16. For the use of late metal hydrides as reducing agents, see: (*a*) C. Deutsch, N. Krause, B. H. Lipshutz, *Chem. Rev.* **2008**, *108*, 2916; (*b*) C. Boone, I. Korobkov, G. I. Nikonov, *ACS Catal.* **2013**, *3*, 2336 and references therein; (*c*) F. Alonso, P. Riente, M. Yus, *Acc. Chem. Res.* **2011**, *44*, 379; (*d*) T. Vergote, F. Nahra, A. Merschaert, O. Riant, D. Peeters, T. Leyssens, *Organometallics* **2014**, *33*, 1953.

17. For selected examples, see: (*a*) N. A. Bell, P. T. Moseley, H. M. M. Shearer, C. B. Spencer, *J. Chem. Soc., Chem. Commun.* **1980**, 359; (*b*) A. Looney, R. Han, I. B. Gorrell, M. Cornebise, K. Yoon, G. Parkin, A. L. Rheingold, *Organometallics* **1995**, *14*, 274; (*c*) M. Krieger, B. Neumüller, K. Dehnicke, *Z. Anorg. Allg. Chem.* **1998**, *624*, 1563; (*d*)

H. Hao, C. Cui, H. W. Roesky, G. Bai, H. –G. Schmidt, M. Noltemeyer, *Chem. Commun.* **2001**, 1118; (*e*) Z. Zhu, R. J. Wright, M. M. Olmstead, E. Rivard, M. Brynda, P. P. Power, *Angew. Chem. Int. Ed.* **2006**, *45*, 5807; (*f*) W. Marcinak, K. Merz, M. Moreno, M. Driess, *Organometallics* **2006**, *25*, 4931; (*g*) M. P. Coles, S. M. El-Hamruni, J. D. Smith, P. B. Hitchcock, *Angew. Chem., Int. Ed.* **2008**, *47*, 10147; (*h*) J. Spielmann, D. Piesik, B. Wittkamp, G. Jansen, S. Harder, *Chem. Commun.* **2009**, 3455; (*i*) I. L. Fedushkin, O. V. Eremenko, A. A. Skatova, A. V. Piskunov, G. K. Fukin, S. Yu. Ketkov, E. Irran, H. Schumann, *Organometallics* **2009**, *28*, 3863; (*j*) D. Mukherjee, A. Ellern, A. D. Sadow, *J. Am. Chem. Soc.* **2010**, *132*, 7582; (*k*) G. Bendt, S. Schultz, J. Spielmann, S. Schmidt, D. Bläser, C. Wölper, *Eur. J. Inorg. Chem.* **2012**, 3725; (*l*) A. Rit, T. P. Spaniol, L. Maron, J. Okuda, *Organometallics*, **2014**, *33*, 2039; (*m*) K. Revunova, G. Nikonov, *Dalton Trans.* **2015**, *44*, 840.

18. (*a*) P. Jochmann, D. W. Stephan, *Angew. Chem.* **2013**, *125*, 10014; *Angew. Chem., Int. Ed.* **2013**, *52*, 9831; (*b*) W. Sattler, G. Parkin, *J. Am. Chem. Soc.* **2011**, *133*, 9708; (*c*) W. Sattler, G. Parkin, *J. Am. Chem. Soc.* **2012**, *134*, 17462; (*d*) N. J. Brown, J. E. Harris, X. Yin, I. Silverwood, A. J. P. White, S. G. Kazarian, K. Hellgardt, M. S. P. Shaffer, C. K. Williams, *Organometallics* **2014**, *33*, 1112.

19. ZnH^+ has been identified at 4K: M. Kajita, M. Abe, M. Hada, Y. Moriwaki, *J. Phys. B* **2011**, *44*, 025402.

20. S. M. I. Al-Rafia, P. A. Lummis, A. K. Swarnakar, K. C. Deutsch, M. J. Ferguson, R. McDonald, E. Rivard, *Aus. J. Chem.* **2013**, *66*, 1235.

21. H. –J. Schönherr, H. –W. Wanzlick, *Chem. Ber.* **1970**, *103*, 1037.

22. For a recent review of Group 12 element carbene complexes, see: S. Budagumpi, S. Endud, *Organometallics* **2013**, *32*, 1537.

23. (*a*) N. P. Mankad, D. S. Laitar, J. P. Sadighi, *Organometallics* **2004**, *23*, 3369; (*b*) E. Y. Tsui, P. Müller, J. P. Sadighi, *Angew. Chem. Int. Ed.* **2008**, *47*, 8937; (*c*) C. H. Lee, T. R. Cook, D. G. Nocera, *Inorg. Chem.* **2011**, *50*, 714; (*d*) C. D. Abernethy, R. J. Baker, M. L. Cole, A. J. Davies, C. Jones, *Transition Met. Chem.* **2003**, *28*, 296; (*e*) A. Rit, T. P. Spaniol, L. Maron, J. Okuda, *Angew. Chem. Int. Ed.* **2013**, *52*, 4664.

24. A. Doddi, C. Gemel, R. W. Siedel, M. Winter, R. A. Fischer, *Polyhedron* **2013**, *52*, 1103.

25. For the synthesis of IMes•$ZnCl_2$•THF (IMes = [$(HCNMes)_2C$:, Mes = 2,4,6-$Me_3C_6H_2$), see : D. Wang, K. Wurst, M. Buchmeiser, *J. Organomet. Chem.* **2004**, *689*, 2123.

26. In one case, crystals of the THF-free adduct IPr•ZnI_2 were isolated from a reaction mixture containing **1** and unreacted IPr. (CCDC 934972).

27. A. J. Arduengo III, J. R. Goerlich, F. Davidson, W. J. Marshall, *Z. Naturforsch.* **1999**, *54b*, 1350.

28. Z. Zhu, R. C. Fischer, J. C. Fettinger, E. Rivard, M. Brynda, P. P. Power, *J. Am. Chem. Soc.* **2006**, *128*, 15068.

29. For related examples of backbone C-H activation in NHCs, see: (*a*) J. I. Bates, P. Kennepohl, D. P. Gates, *Angew. Chem. Int. Ed.* **2009**, *48*, 9844; (*b*) Y. Wang, Y. Xie, M. Y. Abraham, R. J. Gillard Jr., P. Wei, H. F. Schaefer III, P. v. R. Schleyer, G. H. Robinson, *Organometallics* **2010**, *29*, 4778.

30. We have noted that IPr and Cl_2Ge•dioxane do react in THF to give spectroscopically pure IPr•$GeCl_2$ (by ^1H NMR) when the reaction times are limited to 30 min.

31. (*a*) R. J. Baker, A. J. Davies, C. Jones, M. Kloth, *J. Organomet. Chem.* **2002**, *656*, 203; (*b*) E. D. Blue, T. B. Gunnoe, J. F. Peterson, P. D. Boyle, *J. Organomet. Chem.* **2006**, *691*, 5988.

32. R. S. Ghadwal, R. Azhakar, H. W. Roesky, K. Pröpper, B. Dittrich, C. Goedecke, G. Frenking, *Chem. Commun.* **2012**, *48*, 8186.

33. S. Pelz, F. Mohr, *Organometallics* **2011**, *30*, 383.

34. (*a*) A. K. Swarnakar, S. M. McDonald, K. C. Deutsch, P. Choi, M. J. Ferguson, R. McDonald, E. Rivard, *Inorg. Chem.* **2014**, *53*, 8662; (*b*) E. Rivard, *Dalton Trans.* **2014**, *43*, 8577

35. J. Monot, M. Makhlouf Brahmi, S. -H Ueng, C. Robert, M. Desage-El Murr, D. P. Curran, M. Malarcia, L. Fensterrbank, E. Lacôte, *Org. Lett.* **2009**, *11*, 4914. Note: The ^1H and ^{11}B NMR data for IPr•BEt_3 is

listed as being in $CDCl_3$, but in fact all NMR data for this species were acquired in C_6D_6.

36. S. M. I. Al-Rafia, M. R. Momeni, M. J. Ferguson, R. McDonald, A. Brown, E. Rivard, *Organometallics* **2013**, *32*, 6658.

37. In our hands, compounds **5** and **6b** show signs of decomposition into Zn metal over time in the solid state (including upon storage at -35 °C under nitrogen in the absence of light).

38. For the use of Li[^{s}Bu$_3$BH] as a mild source of hydride, see: A. F. Richards, A. D. Phillips, M. M. Olmstead, P. P. Power, *J. Am. Chem. Soc.* **2003**, *125*, 3204.

39. A. R. Waldeck, P. W. Kuchel, A. J. Lennon, B. E. Chapman, *Prog. Nucl. Magn. Reson. Spectrosc.* **1997**, *30*, 39. The diffusion coefficients of **2** and ImMe$_2$iPr$_2$•ZnEt$_2$ were determined to be 8.9×10^{-10} and 1.2×10^{-9} m^2 s^{-1} respectively in THF-D_8, and 7.4×10^{-10} and 9.8×10^{-10} m^2 s^{-1} respectively in toluene-D_8.

40. H. J. Bestmann, O. Kratzer, *Chem. Ber.* **1963**, *96*, 1899.

41. S. M. I. Al-Rafia, A. C. Malcolm, S. K. Liew, M. J. Ferguson, R. McDonald, E. Rivard, *Chem. Commun.* **2011**, *47*, 6987.

42. R. W. Alder, P. R. Allen, M. Murray, A. G. Orpen, *Angew. Chem., Int. Ed. Engl.* **1996**, *35*, 1121.

43. M. Ma, A. Sidiropoulos, L. Ralte, A. Stasch, C. Jones, *Chem. Commun.* **2013**, *49*, 48.

44. S. Peltz, M. Mohr, *Organometallics* **2011**, *30*, 383.

45. In the presence of sterically encumbered anionic ligands both Cd-H and Hg-H units can be isolated, see: (*a*) D. L. Reger, S. S. Mason, A. L. Rheingold, *J. Am. Chem. Soc.* **1993**, *115*, 10406; (*b*) Z. Zhu, M. Brynda, R. J. Wright, R. C. Fischer, W. A. Merrill, E. Rivard, R. Wolf, J. C. Fettinger, M. M. Olmstead, P. P. Power, *J. Am. Chem. Soc.* **2007**, *129*, 10847; (*c*) Z. Zhu, J. C. Fettinger, M. M. Olmstead, P. P. Power, *Organometallics* **2009**, *28*, 2091.

46. For the synthesis of the metal hydride cation $[IPr•Cu(\mu\text{-}H)Cu•IPr]^+$ via an alternate route, see: C. M. Wyss, B. K. Tate, J. Basca, T. G. Gray, J. P. Sadighi, *Angew. Chem., Int. Ed.* **2013**, *52*, 12920.

47. D. Wang, K. Wurst, M. R. Buchmeiser *J. Organomet. Chem.* **2004**, *689*, 2123.

48 We have investigated the structure of the intended Zn(I) hydride product, $ImMe_2{}^iPr_2•Zn(H)\text{-}Zn(H)•ImMe_2{}^iPr_2$ (and its isomers) by computational methods. It was found that the direct dehydrogenation of **6b** to yield $ImMe_2{}^iPr_2•Zn(H)\text{-}Zn(H)•ImMe_2{}^iPr_2$ is endergonic ($\Delta G_{dehydro}$ = +18.4 kcal/mol).

49. S. Enthaler, *ACS Catal.* **2013**, *3*, 150.

50. A. Rit, A. Zanardi, T. P. Spaniol, L. Maron, J. Okuda, *Angew. Chem. Int. Ed.* **2014**, *53*, 13273

51. It is likely that THF is present within the coordination sphere of the proposed Zn intermediates during catalytic hydrosilylation.

52. A. B. Pangborn, M. A. Giardello, R. H. Grubbs, R. K. Rosen, F. J. Timmers, *Organometallics*, **1996**, *15*, 1518.

53. N. Kuhn, T. Kratz, *Synthesis*, **1993**, 561.

54. M. D. Pelta, G. A. Morris, M. J. Stchedroff, S. J. Hammond, *Magn*. *Reson*. *Chem*., **2002**, *40*, S147.

55. A. Botana, J.A. Aguilar, M. Nilsson, G.A. Morris, *J. Magn*. *Reson*., **2011**, *208*, 270.

56. M.A. Connell, P.J. Bowyer, P.A. Bone, A. L. Davis, A.G. Swanson, M. Nilsson, G.A. Morris, *J. Magn*. *Reson*., **2009**, *198*, 121.

57. M. Arrowsmith, T. J. Hadlington, M. S. Hill, G. Kociok-Kohn, *Chem. Commun.* **2012**, *48*, 4567.

58. Y. Zhao, D. G. Truhlar, *Theor. Chem. Acc.*, **2008**, *120*, 215.

59. T. H. Dunning Jr., *J. Chem. Phys.* **1989**, *90*, 1007.

60. D. E. Woon, T. J. Dunning, Jr. *J. Chem. Phys.* **1993**, *98*, 1358.

61. K. A. Peterson, C. Puzzarini, *Theor. Chem. Acc.* **2005**, *114*, 283.

62. D. Figgen, K. A. Peterson, M. Dolg, H. Stoll, *J. Chem. Phys.* **2009**, *130*, 164108.

63. D. Feller, *J. Comput. Chem.* **1996**, *17*, 1571.

64. K. L. Schuchardt, B. T. Didier, T. Elsethagen, L. Sun, V. Gurumoorthi, J. Chase, J. Li, T. L. Windus, *J. Chem. Inf. Model.* **2007**, *47*, 1045; https://bse.pnl.gov/bse/portal.

65. http://www.gaussian.com/g_whitepap/thermo.htm, Thermochemistry in Gaussian.

66. GaussView, Version 5, R. Dennington, T. Keith, J. Millam *Semichem Inc.*, Shawnee Mission KS, 2009.

67. N. M. O'Boyle, A. L. Tenderholt, K. M. Langner *J. Comp. Chem.*, **2008**, *29*, 839.

68. NBO 5.9. E. D. Glendening, J. K. Badenhoop, A. E. Reed, J. E. Carpenter, J. A. Bohmann, C. M. Morales, and F. Weinhold (Theoretical Chemistry Institute, University of Wisconsin, Madison, WI, 2012); http://www.chem.wisc.edu/~nbo5.

69. M. J. Frisch, G. W. Trucks, H. B. Schlegel, G. E. Scuseria, M. A. Robb, J. R. Cheeseman, G. Scalmani, V. Barone, B. Mennucci, G. A. Petersson, H. Nakatsuji, M. Caricato, X. Li, H. P. Hratchian, A. F. Izmaylov, J. Bloino, G. Zheng, J. L. Sonnenberg, M. Hada, M. Ehara, K. Toyota, R. Fukuda, J. Hasegawa, M. Ishida, T. Nakajima, Y. Honda, O. Kitao, H. Nakai, T. Vreven, J. A. Montgomery, Jr., J. E. Peralta, F. Ogliaro, M. Bearpark, J. J. Heyd, E. Brothers, K. N. Kudin, V. N. Staroverov, T. Keith, R. Kobayashi, J. Normand, K. Raghavachari, A. Rendell, J. C. Burant, S. S. Iyengar, J. Tomasi, M. Cossi, N. Rega, J. M. Millam, M. Klene, J. E. Knox, J. B. Cross, V.

Bakken, C. Adamo, J. Jaramillo, R. Gomperts, R. E. Stratmann, O. Yazyev, A. J. Austin, R. Cammi, C. Pomelli, J. W. Ochterski, R. L. Martin, K. Morokuma, V. G. Zakrzewski, G. A. Voth, P. Salvador, J. J. Dannenberg, S. Dapprich, A. D. Daniels, O. Farkas, J. B. Foresman, J. V. Ortiz, J. Cioslowski, D. J. Fox, Gaussian 09, Revision C.01, Gaussian, Inc., Wallingford CT, 2010.

70. H. Hope, *Prog. Inorg. Chem.*, **1993**, *41*, 1.

71. G. M. Sheldrick, *Acta. Cryst.,* **2008**, *A64*, 112.

Chapter 5

Towards thermally stable carbonyl complexes of zinc and the utilisation of carbene-stabilised zinc complexes for the deposition of crystalline zinc metal

5.1 Abstract

In the first half of this chapter, the synthesis of a variety of cationic zinc compounds featuring hemilabile ligands to accommodate the potential binding of carbon monoxide directly at zinc is discussed. While this is not successful for all species, spectroscopic evidence was presented for the first thermally stable carbon monoxide adduct of zinc, featuring a Zn^{2+} centre that is also stabilised by *N*-heterocyclic carbene ligands.

In the second half of this chapter, the development of one-pot precursors for the generation of crystalline zinc materials is detailed. By gently heating Lewis-base stabilised adducts of zinc(II)dihydrides in solution, the liberation of crystalline zinc metal was possible; in addition this process releases the carbene ligand which can potentially be reused later deposition processes. Furthermore, the use of this methodology towards forming uniform zinc coatings on silicon nanocrystals is discussed.

5.2 Introduction

Metal complexes of carbon monoxide, or *metal carbonyl complexes*, form a ubiquitous part of the chemistry of the transition elements. Indeed, the first isolated example of a metal carbonyl complex was dicarbonyldichloroplatinum(II), $Cl_2Pt(CO)_2$, which was synthesized in 1868 by Schützenberger.[1] Shortly thereafter, the first example of a neutral homoleptic metal carbonyl complex, $Ni(CO)_4$, was discovered by Ludwig Mond.[2] Later Mond used the preparation of $Ni(CO)_4$ from the interaction of nickel metal with carbon monoxide as a method of purification (Mond Process) of Ni metal from the corresponding nickel oxide impurities. This pioneering work paved the way for unlocking key guiding principles behind chemical and biological processes; in particular, an understanding of metal carbonyl complexes is essential when considering that such complexes are shown to be important intermediates in hydroformylation and hydrocarboxylation catalysis,[3] as well as biologically in enzymes such as carbon monoxide dehydrogenase.[4]

One of the major concepts involved when considering the chemistry of neutral metal carbonyl complexes is that of *synergistic bonding* (see Figure 5.1), which involves not only the σ-donation of the CO-bound lone-pair into an empty metal orbital, but also the donation of electron density from an occupied d-orbital on the metal centre to the $\pi^*_{(CO)}$ of the bound carbonyl. This second π-backbonding interaction serves to strengthen the M-C bond, but also weakens the C-O bond, and the decrease in C-O bond order can be conveniently monitored via

infrared (IR) spectroscopy, with lower $\nu_{(CO)}$ values relative to free CO (2143 cm^{-1}) when backbonding transpires. It is of particular interest however that when considering metal carbonyl cations, such as $[Hg(CO)_2][Sb_2F_{11}]_2$ and $[Pt(CO)_4][Sb_2F_{11}]_2$, we observe an increase in $\nu_{(CO)}$ relative to that of free CO (*cf.* 2248 cm^{-1} and 2261 cm^{-1} respectively).[5] This is due to a decrease in π-backbonding observed from many metal cations due to a constriction of the d-orbitals.[5] This increased positive charge on the metal serves to polarize the M-C bond, inducing a more electropositive carbon centre. This in turn leads to an increased Coulombic contribution within the C-O bond, rendering the bond somewhat stronger than is normally observed within free C-O; moreover the CO-lone pair used to coordinate to the metal centre has a slight net σ–antibonding contribution, and this removal of electron density leads to additional strengthening of the C-O bond.[5] It is also noted that the $\nu_{(CO)}$ frequency will increase with increasing formal positive charge on the metal centre, and will also decrease with increasing number of bound CO ligands.[6]

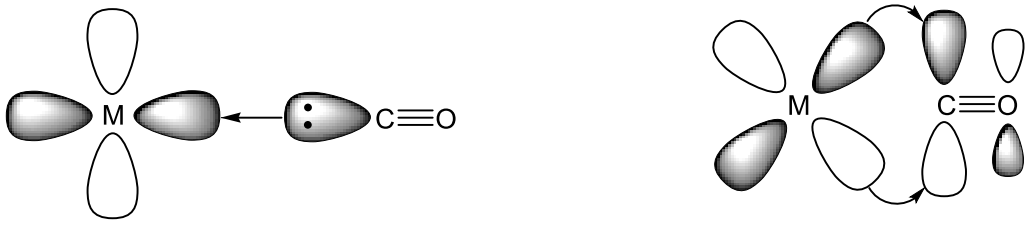

Figure 5.1 (left) Donation of lone-pair of electrons from CO to empty metal d-orbital (left), and (right) π back-bonding from occupied metal d-orbital to π* of CO.

Despite the many advances in the chemistry of metal carbonyl compounds, there is a very conspicuous absence with regard to the isolation of well-defined molecular compounds of zinc featuring carbonyl ligands. The homoleptic 18-electron species $Zn(CO)_3$ was recently proposed as a stable species at 7 K based on IR spectroscopy *via* matrix isolation, and calculations performed at the BP86/6-311++ level;[7] a more recent study however suggests that the proposed species is neither a genuine thermodynamic minima, nor is kinetically stable.[8] In particular, the authors note that the basis sets for calculation used in reference 7 often are inappropriate for ligands that feature multiple bonds such as the triple bond observed in CO, and that further calculations using a variety of different basis sets reveal the proposed product to be unstable by approximately 40 kcal mol^{-1} relative to the constituent molecular and atomic fragments. Despite this instability, there is some evidence for the interaction between zinc and CO, with Haw and coworkers reporting the $^{13}C\{^1H\}$ solid state NMR spectroscopic observation of ^{13}CO adsorbed on a ZnO and Zn zeolite surfaces at 148 K and 98 K, respectively, with a peak at 165 ppm in each case attributed to bound CO.[9] It should be noticed that at 298 K, there was no evidence of CO binding to either ZnO or the Zn zeolite, and that elevating the temperature to 498 K resulted in the formation of CO_2, however the mechanism for the formation of CO_2 is not discussed. In addition, reports by the Ghiotti[10] and Lavalley[11] groups reveal an IR band at 2187 cm^{-1} following the low temperature adsorption of CO onto ZnO surfaces. Despite this, all reports cite the absence of any well-defined molecular Zn-CO complex of any kind within the literature, in addition to the lack of any

evidence for room-temperature stable Zn-CO adducts. As ZnX_2 species (X = F, Cl, Br, OTf) are typically regarded as being strong Lewis acids, this would suggest that the backbonding interaction that is ubiquitous with many metal carbonyls must be quite small in the case of zinc, potentially due to Zn experiencing a higher Z_{eff} than most other transition metals, and thus having more compact d-orbitals which have poor overlap with the CO π* orbitals. Computational studies by Frenking and coworkers suggest that for $[Zn(CO)_n]^{2+}$ cations, there is a sharp dropoff in average M-CO bond strength as n is increased from 1 to 6;[12] as such it was decided that the synthesis of a species that featured just one carbonyl moiety, with coordinative saturation achieved through the addition of other σ-donor ligands with limited π-acidity would be optimal in isolating a stable Zn-CO complex.

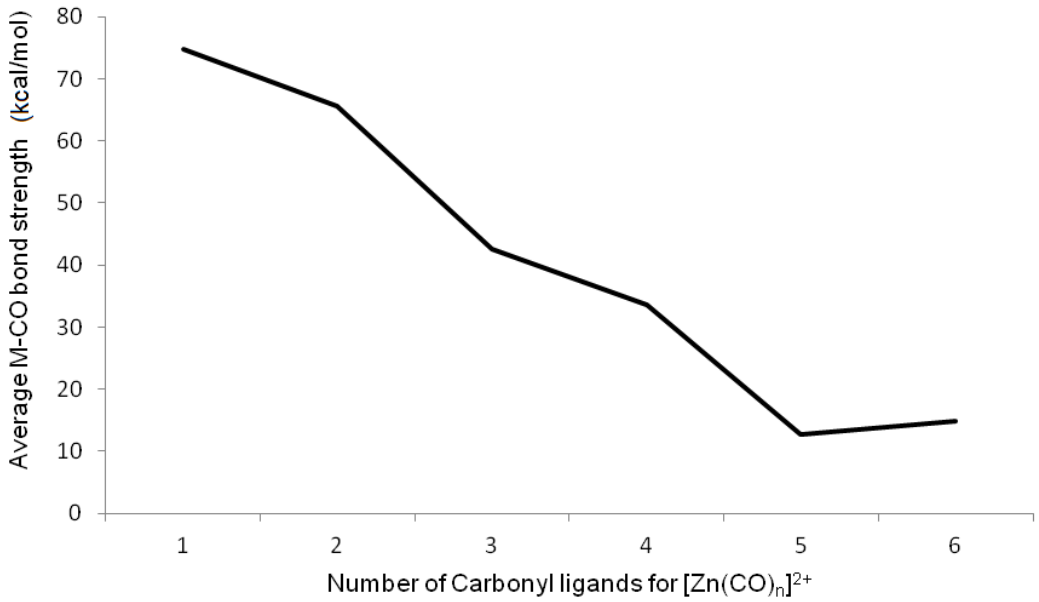

Figure 5.2 Average energy of metal-carbonyl bond in $[Zn(CO)_n]^{2+}$ fragments, calculated at CCSD(T)/I/MP2/I level of theory.[12]

5.2.2 The use of N-heterocyclic carbene complexes of zinc as precursors to crystalline zinc for materials applications.

The generation of metal nanoparticles (MNPs) with low-dimensionality have long been of interest due to their ability to display novel chemical and physical properties.[13,14] The origin of these properties can be attributed to their small size, and current literature shows a variety of ways to synthesise such materials such as laser irradiation of ZnO,[15] thermal evaporation,[16] or vapour deposition.[17] Of note, ZnO materials often possess novel properties such as metal-enhanced fluorescence[16] or emission of blue light under UV irradiation.[17] Despite these properties however, access to these species usually calls for either specialised equipment, or high temperature synthetic routes, sometimes with the hot-injection addition of strong reducing agents or the *in situ* addition of hydride sources to metal halides.[18] In addition, submicron hexagonal plates of zinc that were deposited on a Si wafer via vapour deposition techniques were shown to exhibit size dependent properties and could be either semi-conducting or metallic in character, in addition to displaying photoluminescence in the UV-Vis region similar to that of their ZnO analogues.[19]

Despite often needing harsh conditions for the synthesis of these materials, the interesting properties displayed often mitigate some of the drawbacks associated with their synthesis. In this chapter, lower temperature, solution-based materials synthesis that utilise only a single molecular precursor are explored. In addition to phase-pure zinc materials, it was hypothesised that the methodology

investigated could potentially open the door to obtaining useful binary zinc-containing materials such as zinc sulphide,[20] zinc oxide[21] and zinc phosphide.[22]

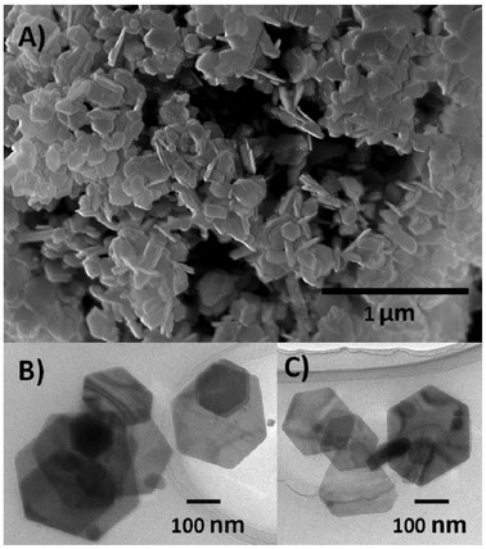

Figure 5.3 SEM (A) and TEM (B, C) images of crystalline blue-emitting Zinc hexagons formed via the reaction of $ZnCl_2$ with $Li[HBEt_3]$ at 200 °C.[18]

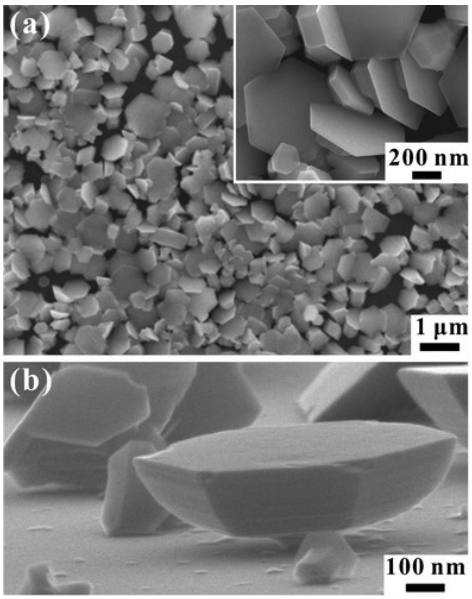

Figure 5.4 (a) SEM images showing the top views of a large area array of 2D pure Zn-metal nanoplates on a Si substrate following reduction of $ZnCl_2$ with $Li[BH_4]$. (b) High-magnification SEM image showing the side view of 2D pure Zn-metal nanoplates.[19]

It should be noted that for many metals, especially the noble metals, there are a wide variety of chemical synthetic methods to access these types of materials, and these routes offer excellent control over morphology and size.[25] For metals that are easily oxidised such as zinc however, there are fewer methods to obtain these materials via chemical synthesis.[24]

One particular type of material of interest is that of the core-shell nanoparticle. These comprise of an internal core consisting of a quantum dot, around which a shell of different material has been deposited. The advantages of this type of structure include: the ability to stabilise an internal material for which oxidisation or reactivity with the atmosphere is problematic; the ability to utilise a toxic core material and protect it with a benign shell, and the ability to attach a shell to a nanoparticle to improve the bio-recognition of the particle for medicinal applications. As discussed in chapter 1, ZnS and ZnO are of interest due to their semiconducting properties, and as such the deposition of zinc onto previously synthesised nanoparticles and quantum dots is investigated.

5.3 Results and discussion

5.3.1 Evidence for a thermally stable Zn-CO complex

With the above in mind, a suitable starting point for our efforts would be to generate a highly Lewis acidic Zn(II) species capable of forming a σ-complex with CO. Earlier in this thesis the stabilization of a formal $[ZnH]^+$ complex IPr•ZnH(OTf)•THF (IPr = $[(HCNDipp)_2C:]$; Dipp = 2,6-diisopropylphenyl)[25] was

demonstrated. It was observed that while the OTf^- anion is coordinated in the solid state, ^{19}F NMR spectroscopy shows that it is weakly coordinated to zinc in solution, and indeed the addition of two equivalents of strongly Lewis basic 4-dimethylaminopyridine (DMAP) was sufficient to displace both the THF and triflato moieties to outside of the coordination sphere of the metal, yielding the $[ZnH]^+$ complex $[IPr•ZnH(DMAP)_2]OTf$.[26] Inspired by this work, we decided to target *N*-heterocyclic carbenes adducts of ZnX_2 (x = I, OTf) using IPr[25] and the less hindered analogue $ImMe_2^iPr_2$[15] ($ImMe_2^iPr_2$ = [(MeCN^{i}Pr)$_2$C:]). As we were previously able to demonstrate the synthesis of Zn^{2+} complexes featuring multiple Lewis basic ligands around a zinc centre,[26,27] it was hypothesised that we could utlise this strategy to provide additional coordinative saturation to the zinc centre, and potentially allow access for the binding of CO with displacement of one of the anionic ligands. Pleasingly, it found that the reaction of 3 equivalents of $ImMe_2^iPr_2$ (**1**) with $Zn(OTf)_2$ was able to generate $[(ImMe_2^iPr_2)_3Zn(OTf)][OTf]$ (**2**) cleanly and in high yield (85%). Likewise, the reaction between three equivalents of $ImMe_2^iPr_2$ and ZnI_2 proceeds smoothly, with the rapid formation of $[(ImMe_2^iPr_2)ZnI][I]$ (**3**) which precipitates from THF solution.

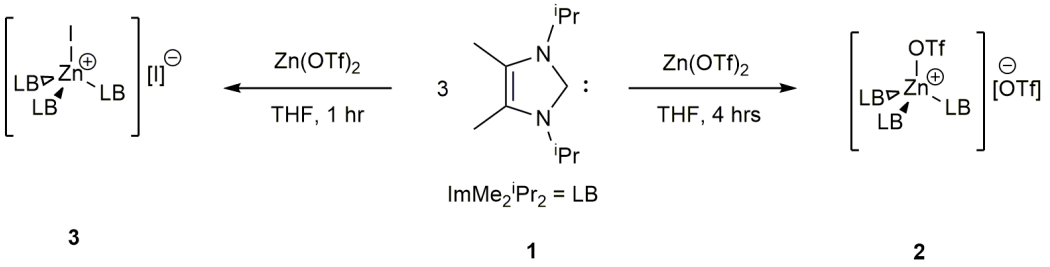

Scheme 5.1 Synthesis of tris(carbene)zinc salts from ZnX_2 (X = OTf^-, I^-)

Compound **2** is an air-sensitive off-white solid which features one singlet in its ^{19}F NMR spectrum at -78.9 ppm, which suggests that either there is an exchange between one bound and one unbound triflate, or that both triflate anions do not substantially interact with Zn^{2+} when in solution. While compound **2** is stable in dichloromethane, sufficiently so that NMR analysis could be performed, prolonged storage (> 2 hours) causes the decomposition of the complex into multiple unidentified products by ^{1}H NMR spectroscopy, in addition to imidazolium salt [$ImMe_2{}^{i}Pr_2H$]OTf. The attempted use of $CDCl_3$ as an NMR solvent with the same sample led to immediate decomposition of **2** to yield a dark red solution followed by significant fuming and heat generation. Multiple unidentified products were present according to ^{1}H NMR analysis and the observed spectrum is congruent with the spectrum obtained following the reaction between $ImMe_2{}^{i}Pr_2$ and $CDCl_3$.

It should also be pointed out that due to the hygroscopic nature of $Zn(OTf)_2$, drying of this reagent by heating under vacuum (20 mTorr) at 150 °C for 24 hours followed by recrystallization from THF/hexanes at -35 °C yielded an optimal yield of **2** later on. The crystal structure of **2** reveals a slightly distorted tetrahedral arrangement around Zn, with Zn-C bond length [avg. 2.084(3) Å] being longer than observed for IPr•ZnH(OTf)•THF [*cf.* 2.031(3) Å], and the Zn-O_{OTf-} distance [2.144(2) Å] being somewhat longer than observed for IPr•ZnH(OTf)•THF [*cf.* 2.069(3) Å]; whether this lengthened Zn-O interaction is due to the electronic effects of the different carbene ligands, or due to steric effects has yet to be determined.

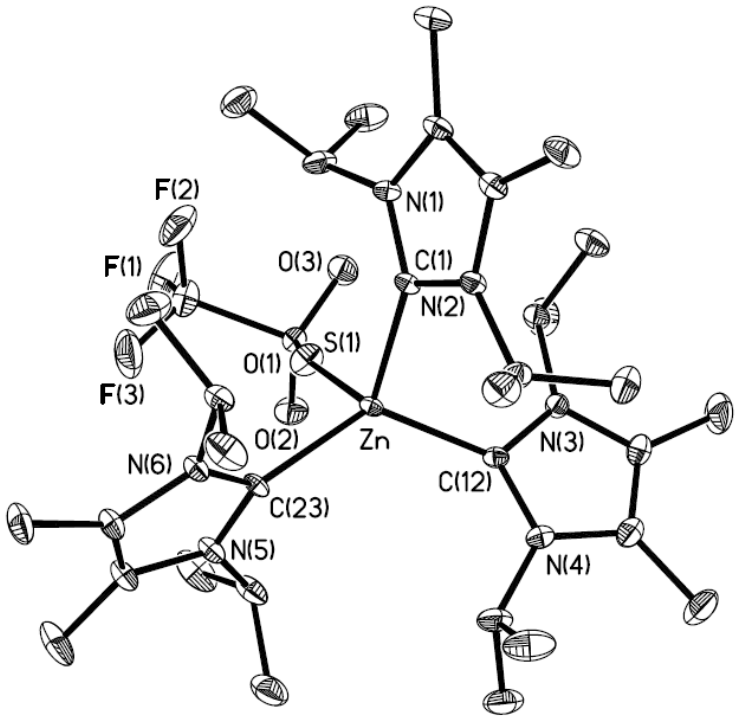

Figure 5.5 X-ray structure of $[(ImMe_2{}^iPr_2)_3Zn(OTf)]OTf$ (**2**) with thermal ellipsoids at the 30 % probabilty level; all carbon-bound hydrogen atoms and the outer sphere OTf⁻ anion have been omitted for clarity. Selected bond lengths [Å] and angles (°): Zn-C(1) 2.099(3), Zn-C(12) 2.082(3), Zn-C(23) 2.072(3), Zn-O(1) 2.144(2); O(1)-Zn-C(1) 105.63(11), O(1)-Zn-C(12) 105.16(10), O(1)-Zn-C(23) 93.96(11), C(1)-Zn-C(12) 104.34(10), C(1)-Zn-C(23) 118.04(11), C(12)-Zn-C(23) 126.39(12).

In the case of $[(ImMe_2{}^iPr_2)_3ZnI]I$ **3**, the insolubility of this species in THF coupled with the high solubility of starting materials in the same solvent allowed for its facile synthesis and isolation. Upon obtaining the product via filtration, cold (-35 °C) THF could be used to wash the product and yield analytically pure **3** as determined by NMR spectroscopy and elemental analysis. As with **2**, the use of $CDCl_3$ as an NMR solvent with analytically pure samples of **3** led to rapid decomposition of the product, which would indicate that this sensitivity is inherent to these tris(carbene) complexes featuring the $ImMe_2{}^iPr_2$ carbene; in our

hands, Zn compounds bearing the larger, more donating IPr ligand do not display this sensitivity towards $CDCl_3$.[28]

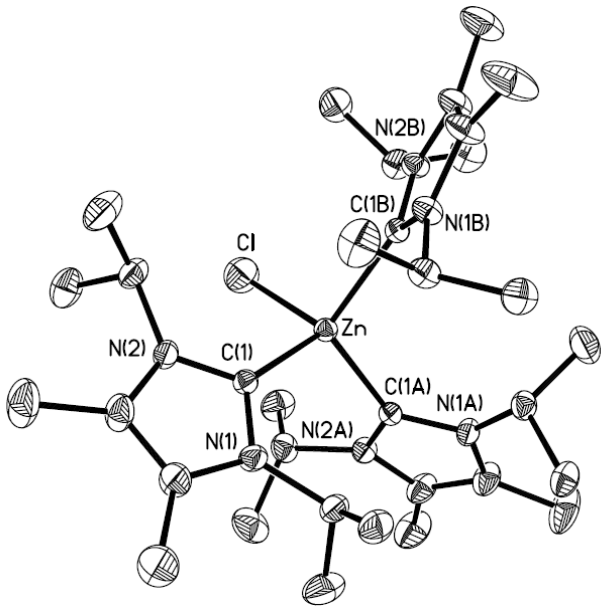

Figure 5.6 X-ray structure of $[(ImMe_2{}^iPr_2)_3ZnCl]I$ with thermal ellipsoids at the 30 % probabilty level; all carbon-bound hydrogen atoms and the I^- anion have been omitted for clarity. Selected bond lengths [Å] and angles (°): Zn-C(1) 2.101(4), Zn-C(1′) 2.101(3), Zn-C(1″) 2.101(3), Zn-Cl 2.349(3); Cl-Zn-C(1) 104.69(10), Cl-Zn-C(1′) 104.69(10), Cl-Zn-C(1″) 104.69(10), C(1)-Zn-C(1′) 113.80(8), C(1)-Zn-C(1″) 113.80(8), C(1′)-Zn-C(1″) 113.80(8).

As with **2** however, the use of dichloromethane allowed for the NMR analysis of **3**, which revealed one dominant product in solution. It should be noted also that long-term exposure of compound **3** to CH_2Cl_2 led to the interchange of iodine with chlorine, and as such, when samples of **3** were stored in DCM layered with hexanes at room temperature with the intent of growing X-ray quality crystals, the resultant product identified by X-ray analysis was $[(ImMe_2{}^iPr_2)ZnCl]I$, suggesting that the bound iodine can be exchanged in solution, thus making it a potential precursor for binding one equivalent of CO.

Despite this, elemental analysis of samples that had not been exposed to halogenated solvents were identified as being of the desired composition, ruling out the possibility of any contamination in the starting materials. The solid state structure of the chloringated congener [($ImMe_2{}^iPr_2$)ZnCl]I shows similar structural features as **2**, with Zn-C bond length [2.101(3) Å] being the same within error as the average of the Zn-C bond lengths for [($ImMe_2{}^iPr_2$)Zn(OTf)]OTf [*cf*. 2.084(3) Å].

In addition, possible zinc precursors for the potential binding of CO that incorporated the more sterically hindered carbene ligand IPr were studied.[25] As a starting point, the corresponding compound [IPr•Zn(OTf)($DMAP)_2$][OTf] (**4**) was prepared as this species could yield an open site for CO binding upon OTf^- dissociation. The aforementioned complex (**4**) could be prepared easily via the sequential addition of one equivalent of IPr to $Zn(OTf)_2$, followed by the addition of two equivalents of DMAP to the intermediate species IPr•$Zn(OTf)_2$ after two hours. The resultant mixture was allowed to stir for 16 hours, and then the desired product obtained by first removing all of the volatiles from the solution under vacuum, and then washing the product with cold Et_2O (Equation 5.1).

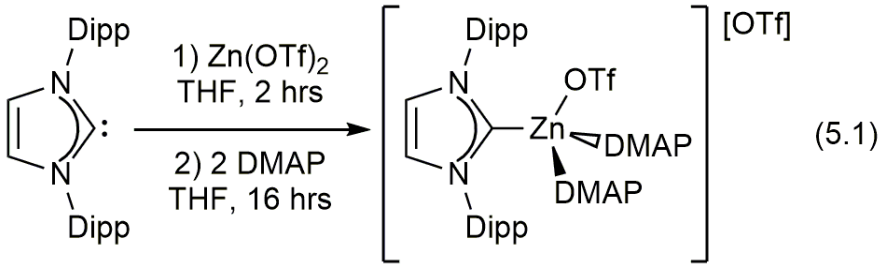

(5.1)

Dipp = 2,6-$^iPr_2C_6H_3$ **4**

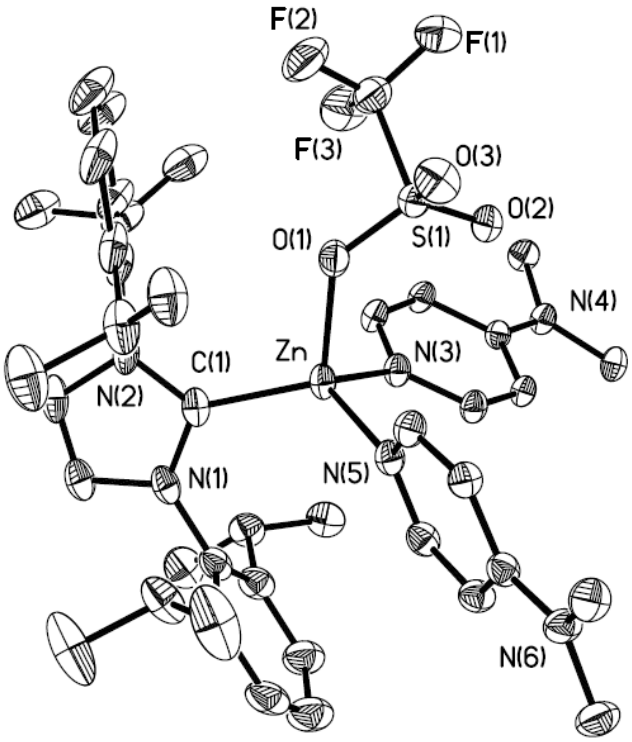

Figure 5.7 X-ray structure of [(IPr•Zn(OTf)(DMAP)$_2$]OTf (**4**) with thermal ellipsoids at the 30 % probabilty level; all carbon-bound hydrogen atoms and the OTf$^-$ anion have been omitted for clarity. Selected bond lengths [Å] and angles(°): Zn-C(1) 2.017(2), Zn-N(3) 2.008(2), Zn-N(5) 2.008(2), Zn-O(1) 2.0261(19); O(1)-Zn-C(1) 109.81(9), O(1)-Zn-N(3) 102.55(8), O(1)-Zn-N(5) 99.73(8), N(3)-Zn-C(1) 114.57(8), N(3)-Zn-N(5) 108.11(8), C(1)-Zn-N(5) 119.72(9).

Compound **4** is a thermally stable off-white solid, and crystals of sufficient quality for X-ray crystallographic analysis were obtained from a THF/toluene mixture that was stored at -35 °C overnight. The X-ray structure of **4** reveals a slightly distorted tetrahedral arrangement around the central zinc atom, however the Zn-C bond length [2.017(2) Å] and Zn-O_{OTf-} bond length [2.0261(19) Å] are shorter than was observed for either [(ImMe$_2$^{i}Pr$_2$)Zn(OTf)]OTf (**2**) or [(ImMe$_2$^{i}Pr$_2$)ZnCl]I.

With adducts **2**-**4** in hand, the propensity of these complexes to bind CO was investigated; **2**-**4** all feature a cationic, Lewis acidic Zn centre, and all which possessed coordinatively labile I^- and OTf^- substituents which could be displaced by a Lewis base. In order to carry out the addition of CO, solutions of all three compounds (**2**-**4**) were each placed into sealed Schlenk flasks fitted with septa under nitrogen in the glove box, and then connected to a vacuum line from which CO gas was introduced by a needle, and bubbled directly though the solutions for twenty minutes. The resulting mixtures were then allowed to stir for one hour at ambient temperature under CO atmosphere, before being placed under vacuum to remove all of the volatiles. In the case of **3** and **4**, ^{1}H NMR analysis revealed that no reaction had occurred, even when the reaction was monitored *in situ*. In the case of compound 2 however, a significant change was noted (Equation 5.2). ^{1}H NMR spectroscopy revealed the formation of a new product, with the presence of three distinct proton environments being similar to that observed with [($ImMe_2{}^iPr_2$)Zn(OTf)]OTf (**2**) and [($ImMe_2{}^iPr_2$)ZnI]I (**3**). This would suggest that the new product was of a similar structure to **2** and **3**, with all carbenes being in equivalent environments. The product, which was isolated as a white powder was then analysed via IR spectroscopy as a solid on a KBr plate, and a very strong absorption at 2149 cm^{-1} was noted. This data is very much consistent with what is expected from a metal carbonyl complex without appreciable π-backbonding, with the $\nu_{(CO)}$ being observed at a higher wavenumber relative to that observed in free CO (2143 cm^{-1}).

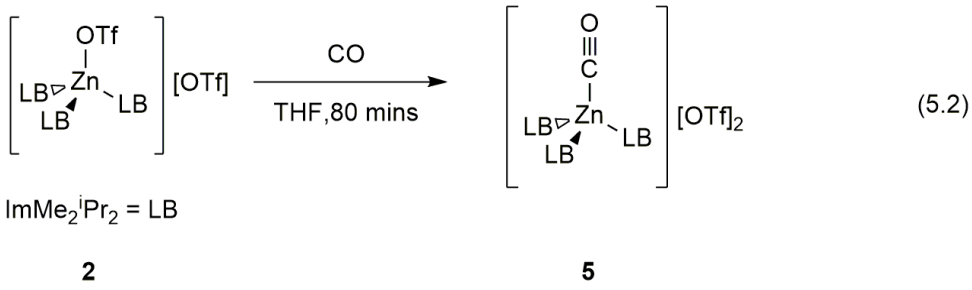

(5.2)

$ImMe_2{}^iPr_2$ = LB

2 **5**

Despite repeated attempts, analysis by X-ray crystallography was not possible due to a lack of X-ray quality crystals being produced. The product proved to be extremely sensitive to moisture, and even brief exposure to less than rigorous anhydrous conditions yielded the corresponding imidazolium salt, $[ImMe_2{}^iPr_2H]OTf$, which was routinely obtained during our crystallisation attempts. Despite the lack of X-ray crystallographical analysis, IR analysis and the presence of a peak by $^{13}C\{^1H\}$ NMR analysis at 164.1 ppm, which is similar to the peak observed at 165 ppm by Haw and co-workers for Zn-*C*O within ZnO at 148 K,[9] provide significant evidence for the formation of this unprecedented complex. Unfortunately, the presence of residual moisture within all sources of ^{13}C labelled CO yielded only the hydrolysis product $[ImMe_2{}^iPr_2H]OTf$ upon its reaction with **2**, despite all attempts at drying the gas with in-line drying tubes containing CaH_2, P_2O_5 and activated alumina.

5.3.2 The formation of crystalline zinc from N-heterocyclic carbene (NHC) stabilised molecular zinc species

Inspired by earlier work in our group,[29] the previously reported NHC-stabilised zinc hydride species $[IPr{\bullet}ZnH(\mu\text{-}H)]_2$[13,30] was examined as a single-

source precursor to zinc due to the documented low temperature at which this species decomposes.[25] As such a C_6D_6 solution (20 mg/mL) of the previously reported [IPr•ZnH(μ-H)]$_2$[25] was heated at 60 °C inside a sealed J-Young NMR tube. Upon heating for 3 hours, a zinc mirror was observed on the inner walls of the J-Young tube, which could easily be dispersed upon sonication for 30 seconds. ^{1}H NMR analysis of the resulting supernatant in the NMR tube revealed the presence of free IPr (85 % by integration), in addition to the known dihydroaminal IPrH$_2$,[31] and trace amounts of dissolved H_2 gas. This suggests that not only can [IPr•ZnH(μ-H)]$_2$ be used to synthesise the desired material, but also that the carbene ligands can be recycled and reused to regenerate [IPr•ZnH(μ-H)]$_2$, and ultimately, more crystalline zinc.

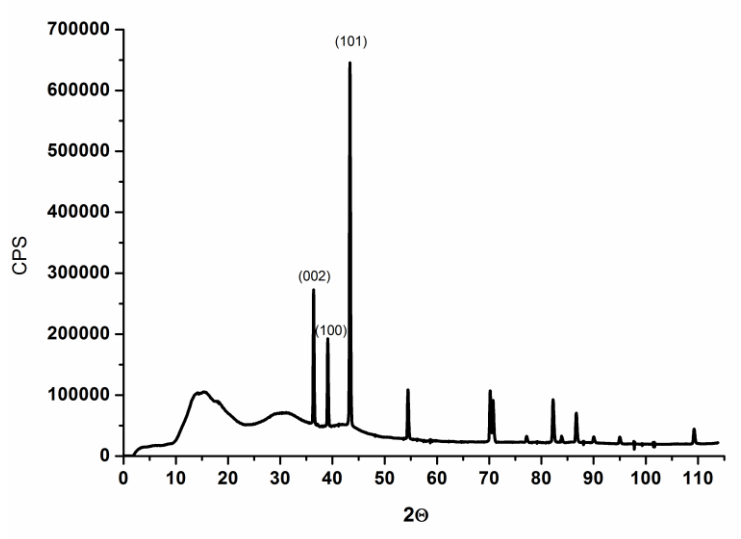

Figure 5.8 PXRD analysis of Zn metal generated via thermolysis of [IPr•ZnH(μ-H)]$_2$. Labelled are (002), (100) and (101) planes matching literature precedent.[32]

Analysis of the generated zinc metal precipitate by PXRD shows crystalline material, along with less-ordered, amorphous zinc; the presence of amorphous product could be due to the lower temperatures during the heating process. In addition to powder XRD (PXRD) analysis, SEM analysis was performed (Figure 5.9) on the generated Zn material. In addition, transmission electron microscopy (TEM) (Figure 5.10) shows that the generated Zn plates have well-defined features, with sharp edges and regular angles between the faces, in line with what was found in the literature (see also Figures 5.3 and 5.4).[22,23] By refining the procedure, comparable materials can be formed within 4 hours from the start of heating. Unfortunately, the known cationic $[ZnH]^+$ compounds, [IPr•Zn(H)(OTf)•THF] or $[IPr•Zn(H)(DMAP)_2][OTf]$,[13] do not yield any zinc, even when heated to 110 °C due to their higher thermal stability relative to $[IPr•ZnH(\mu\text{-}H)]_2$.

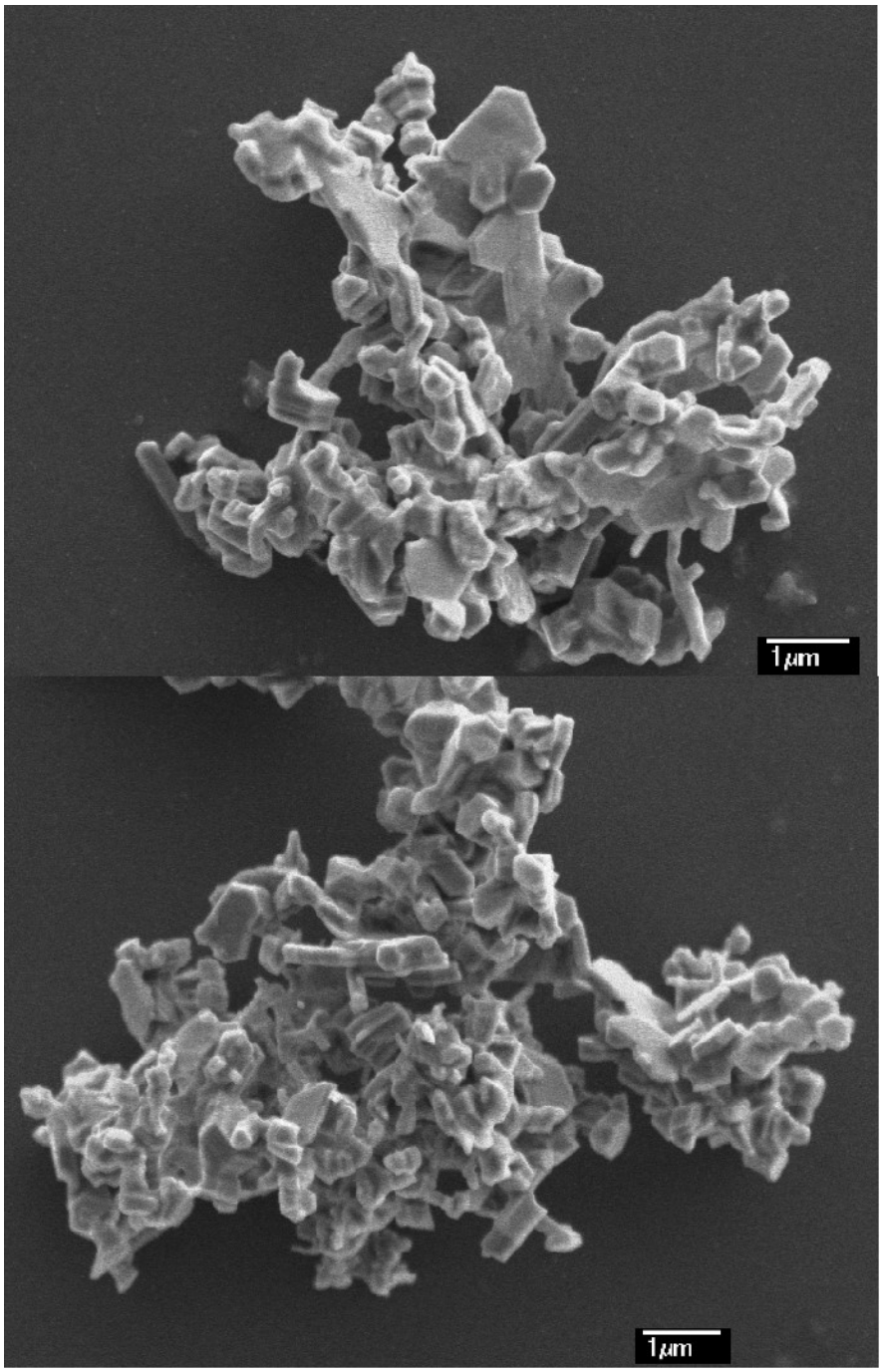

Figure 5.9 SEM image of crystalline Zn metal generated via thermolysis of $[IPr•ZnH(\mu\text{-}H)]_2$.

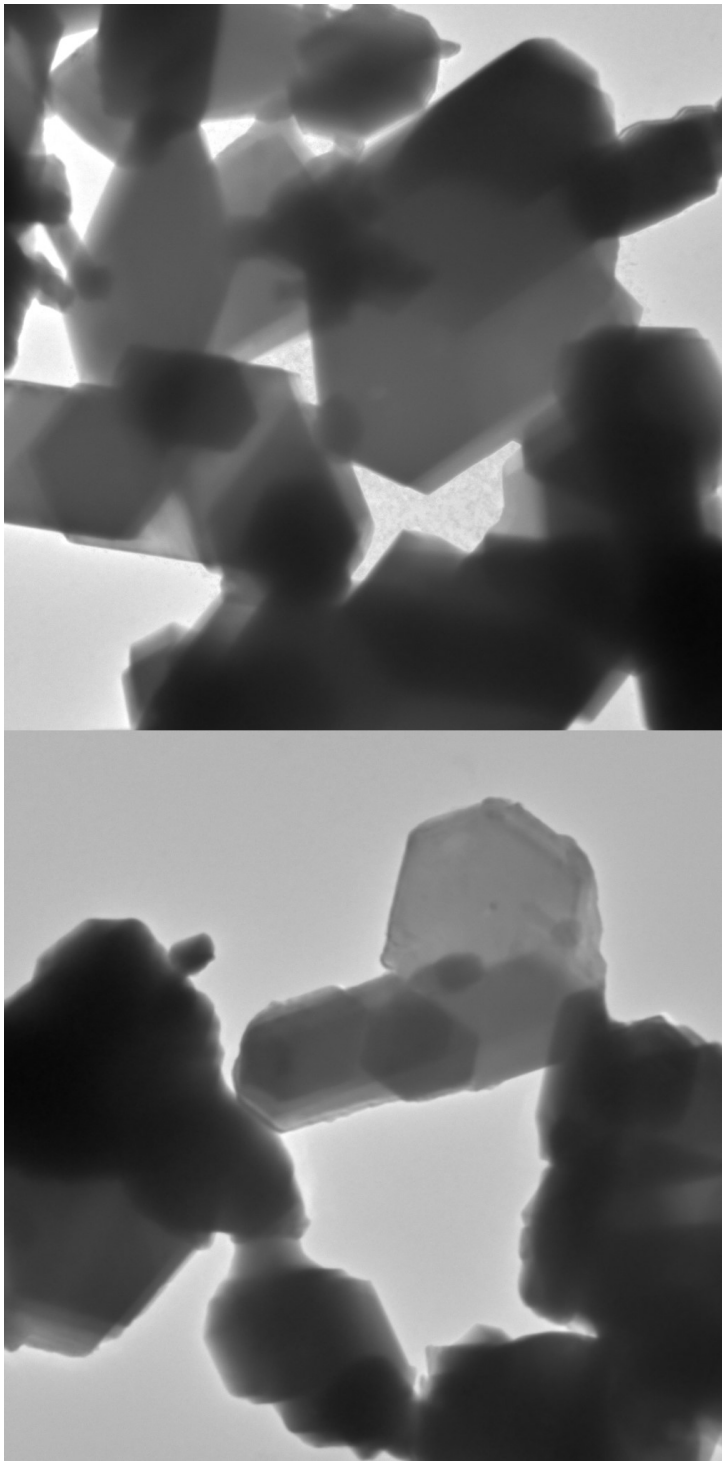

Figure 5.10 TEM images of crystalline Zn metal generated via thermolysis of $[IPr\bullet ZnH(\mu\text{-}H)]_2$.

The synthesis of zinc-coated silicon nanocrystals (Si-NCs) was also examined. As there is literature precedent for the formation of zinc oxide nanoparticles via microwave-assisted thermolysis, it was decided that this would be an appropriate place to start out investigations.[33,34] Diphenyl ether was chosen as a solvent due to its high boiling point (121 °C) and strong microwave absorbing properties. In order to enhance the stability and improve emission characteristics, the Si-NCs studied were prepared in the presence of N,N-dimethylpropargylamine as a capping agent.[29] The diphenyl ether and N,N-dimethylpropargylamine were dried rigorously prior to use, to ensure that no hydrolysis would occur and that any materials generated would be directly from our precursors, especially since $Zn(OH)_2$ (a possible hydrolysis product) has already been shown as an effective precursor to ZnO nanoparticles.[34]

For this work, we chose to work with 3 nm Si-NCs which were synthesised as described previously; these nanoparticles were available as either the unfunctionalised particles, or the dodecylamine capped nanoparticles. [35] In an attempt to form core-shell particles featuring a silicon core and zinc outer layer capped by N,N-dimethylpropargylamine, the Si-NCs, both unfunctionalised and capped, were separately combined with $[IPr{\bullet}ZnH(\mu\text{-}H)]_2$ in diphenyl ether, and N,N-dimethylpropargylamine was added to the solution, which was then sealed in a microwave reaction tube and irradiated for 1 hour at 190 °C. The resultant solutions displayed weak yellow emission upon being exposed to UV light, and the resultant nanoparticles could be recovered from the solution following the addition of ethanol to precipitate them from solution. Analysis of these

nanoparticles was performed via X-ray Photoelectron Spectroscopy (XPS) and Transmission Electron Microroscopy (TEM) (Figures 5.11 to 5.14), and revealed the formation of relatively uniform nanoparticles that not only contained silicon, but also zinc (and potentially zinc oxide).

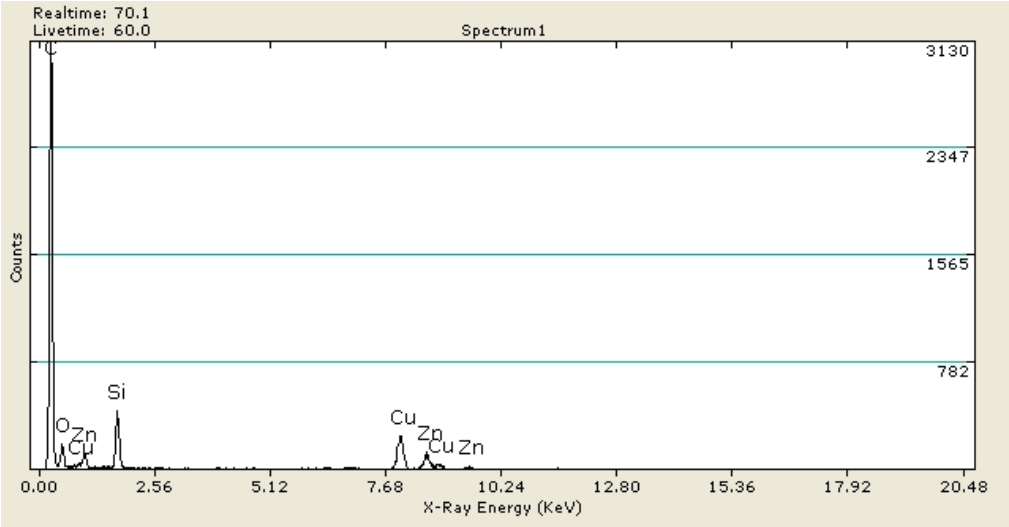

Figure 5.11 XPS analysis of Zn-coated nanoparticles following deposition of Zn on dodecylamine functionalised Si-NCs

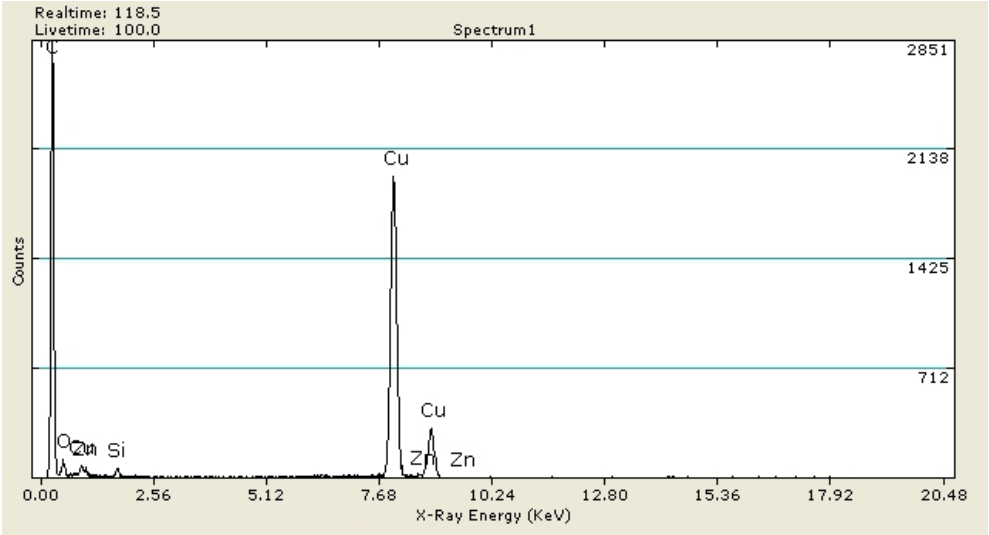

Figure 5.12 XPS analysis of Zn-coated nanoparticles following deposition of Zn on non-functionalised Si-NCs

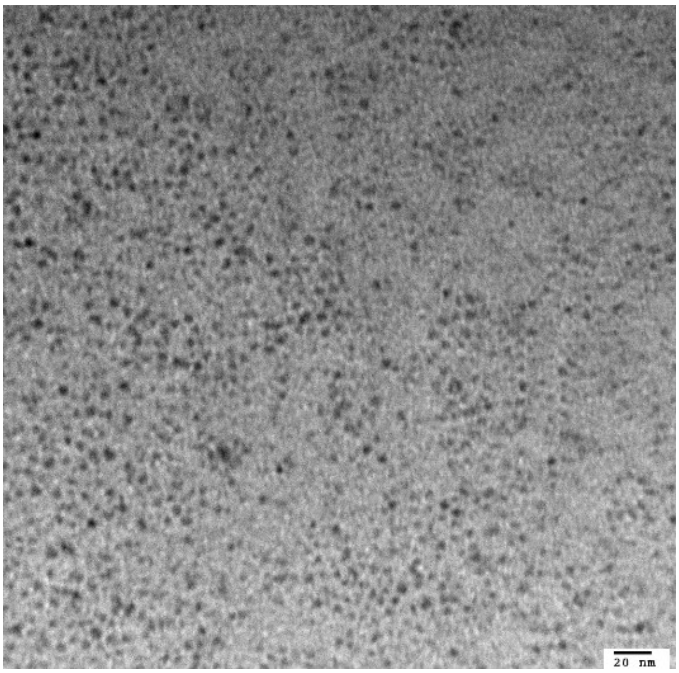

Figure 5.13 TEM image of Zn-coated nanoparticles following deposition of Zn on dodecylamine functionalised 3 nm Si-NCs

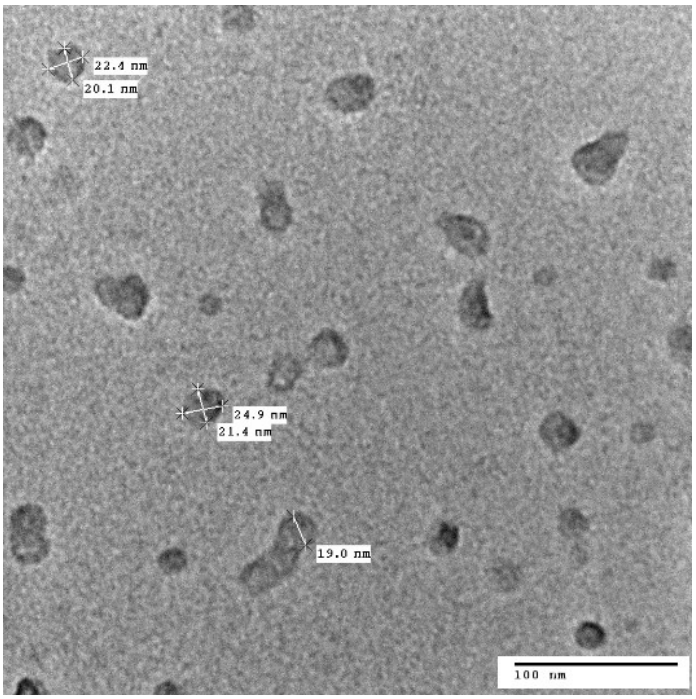

Figure 5.14 TEM image of Zn-coated nanoparticles following deposition of Zn on non-functionalised 3nm Si-NCs

The preliminary XPS and TEM data supports the presence of zinc on the surface of the silicon nanoparticles (to form core-shell structures), although some agglomeration of the resultant material is noted in the TEM images. Despite this early success, only weak yellow fluorescence was noted for both types of particle upon illumination with UV light, and no significant change from what was observed with the non-coated Si-NCs. As such, future work in this area will involve the optimisation of reaction conditions as a means to investigate whether the addition of Zn can tailor the properties of the Si-NCs in a controlled fashion. Moreover, the described microwave/capping ligand route could be used to generate pure zinc nanoparticles (Zn-NPs), leading to possibly novel size- and shape-dependent properties; the controlled oxidation of these Zn-NPs using O_2 or S_8 could yield ZnO and ZnS materials in an *in situ* manner, which are of interest as wide band-gap semiconductors, as previously described.

5.4 Conclusions

In the first part of this chapter, the synthesis of cationic zinc complexes stabilised by *N*-heterocyclic carbene ligands was described. These complexes were evaluated with regards to their propensity to bind CO, and while $[(ImMe_2{}^iPr_2)_3ZnI]I$ (**3**) and $[IPr{\bullet}ZnOTf(DMAP)_2]OTf$ (**4**) do not show any evidence of CO binding, $[(ImMe_2{}^iPr_2)_3ZnOTf]OTf$ (**2**) combines with CO to yield a new product, presumably $[(ImMe_2{}^iPr_2)_3Zn(CO)][OTf]_2$ (**5**, structure inferred from NMR and IR spectroscopy). While compounds **2**-**4** were crystallographically characterised, suitable crystals of **5** for X-ray crystallographic analysis were not obtained despite repeated attempts.

In the second part of this chapter, the mild thermolysis of $[IPr{\bullet}ZnH(\mu\text{-}H)]_2$ to yield samples crystalline zinc, with loss of free carbene IPr and H_2 as observed by NMR spectroscopy was demonstrated. In addition, the preliminary synthesis of Si-Zn core-shell nanomaterials was outlined.

5.5 Experimental section

5.5.1 Materials and instrumentation

All reactions were performed using standard Schlenk line techniques under an atmosphere of nitrogen or in an inert atmosphere glove box (Innovative Technology, Inc.). Solvents were dried using a Grubbs-type solvent purification system[36] manufactured by Innovative Technology, Inc., degassed (freeze-pump-thaw method) and stored under an atmosphere of nitrogen, plus filtered through an approximately 2 cm plug of activated alumina immediately prior to use. IPr,[14] $ImMe_2{}^iPr_2$,[15] $[IPr{\bullet}ZnH(\mu\text{-}H)]_2$[30] and 3 nm Si-NCs[35] were synthesized via literature procedures, with the synthesis of the Si-NCs being performed by Ms. Christina Gonzalez. ZnI_2 was purchased from Sigma Aldrich and used without further purification. $Zn(OTf)_2$ was purchased from Sigma Aldrich, and dried under vacuum (20 mTorr) at 150 °C for 8 hours, before being recrystallized from THF/Hexanes at -35 °C prior to use. N,N-dimethylpropargylamine and diphenyl ether were purchased from Sigma Aldrich, dried over CaH_2 and distilled under nitrogen prior to use.

^1H, $^{13}C\{^1H\}$ and $^{19}F\{^1H\}$ NMR spectra were recorded either on a Varian iNova-400 or on a Varian iNova-500 spectrometer running VNMRJ 3.2A and referenced to the residual protonated solvent peak of known chemical shift downfield from $Si(CH_3)_4$ for ^1H and $^{13}C\{^1H\}$ or externally to $CFCl_3$ for the ^{19}F NMR data. Fourier Transform Infrared Spectroscopy (FT-IR) was performed using a Nicolet Magna 750 IR spectrophotometer by drop coating CH_2Cl_2

solution of the desired compound onto a KBr plate, followed by solvent evaporation in a glovebox. Transmission Electron Microscopy (TEM) analysis was performed using a JEOL-2010 (LaB6filament) electron microscope with an accelerating voltage of 200 keV. TEM samples were prepared by drop casting a toluene solution of Si-NCs onto a 200 μm mesh carbon coated copper grid and allowing the solvent to evaporate under vacuum prior to imaging. Size information was obtained by counting no fewer than 200 particles using Image J program. Elemental analyses were performed by the Analytical and Instrumentation Laboratory at the University of Alberta. Melting points were measured in sealed glass capillaries under nitrogen using a MelTemp melting point apparatus and are uncorrected.

5.5.2 X-ray Crystallography

Crystals of appropriate quality for X-ray diffraction studies were removed either from a Schlenk tube under a stream of nitrogen or a vial (glovebox) and immediately covered with a thin layer of hydrocarbon oil (Paratone-N). A suitable crystal was then selected, attached to a glass fibre, and quickly placed in a low-temperature stream of nitrogen.[37] All data were collected using a Bruker APEX II CCD detector/D8 diffractometer using Mo Kα or Cu Kα radiation, with the crystal cooled to −100 °C. Refinements were completed using the program SHELXL-97.[38] Hydrogen atoms were assigned positions based on the sp^2 or sp^3 hybridisation geometries of their attached carbon or nitrogen atoms and were

given thermal parameters 20 % greater than those of their parent atoms. See Tables 5.1 and 5.2 for a listing of relevant crystallographic data.

5.5.3 Synthetic procedures

5.5.3.1 Synthesis of $[(ImMe_2{}^iPr_2)_3Zn(OTf)][OTf]$ (2)

$ImMe_2{}^iPr_2$ (0.204 g, 1.13 mmol) was dissolved in 3 mL of THF to yield a pale yellow solution. This solution was then added dropwise over ca. 2 minutes to a suspension of $Zn(OTf)_2$ (0.137 g, 0.377 mmol) in 3 mL of THF. The resultant mixture was allowed to stir for 4 hours, before being filtered through a 1 cm plug of Celite in a pipette, and the solvents removed *in vacuo*. This yielded an off-white solid which was washed with 2 × 2mL of hexanes prior to being allowed to dry under high vacuum for 2 hours (0.286 g, 84% yield). Crystals of suitable quality for X-ray crystallography were obtained by dissolving the product in 2mL of THF, and allowing 3mL of toluene to slowly diffuse into this solution overnight. ^{1}H NMR (CD_2Cl_2, 500 MHz): δ 4.59 (sept, 6H, NC*H*$(CH_3)_2$, $^3J_{HH}$ = 8.0 Hz), 2.30 (s, 18H, NCC*H*$_3$), 1.41 (d, 36H, NCH(C*H*$_3)_2$, $^3J_{HH}$ = 8.0 Hz). ^{13}C{^{1}H} NMR (CD_2Cl_2, 126 MHz): δ 167.7 (N*C*N), 128.7 (N*C*CH_3), 121.2 (q, $^1J_{CF}$ = 321 Hz, O_3SCF_3), 54.2 (N*C*$(CH_3)_2$), 22.7 ((NC(*C*$H_3)_2$), 10.8 (NC*C*H_3). ^{19}F{^{1}H} NMR (CD_2Cl_2, 469 MHz): δ -78.3 (O_3SCF_3). Mp (°C): 145 – 148. Anal. Calcd. for $C_{35}H_{60}F_6N_6O_6S_2Zn$: C, 46.48; H, 6.69; N, 9.29; S, 7.09. Found: C, 46.21; H, 6.51; N, 8.95; S, 6.53.

5.5.3.2 Synthesis of [($ImMe_2{}^iPr_2)_3ZnI$][I] (3)

$ImMe_2{}^iPr_2$ (0.310 g, 1.72 mmol) was dissolved in 4 mL of THF to yield a pale yellow solution. This solution was then added dropwise over ca. 3 minutes to a suspension of ZnI_2 (0.183 g, 0.573 mmol) in 5 mL of THF. Within ca. 5 minutes of addition, a noticeable amount of additional white precipitate had formed. The resultant mixture was allowed to stir for 1 hour, before the precipitate was allowed to settle, and the mother liquor decanted. The resultant colourless solid was washed with 2 × 4 mL cold (-35 °C) THF prior to being allowed to dry under high vacuum for 2 hours (0.401 g, 81% yield). Crystals suitable for X-ray diffraction were obtained by dissolving 60 mg of solid in 2 mL of CH_2Cl_2, before allowing 2 mL of hexanes to slowly diffuse through the solution at room temperature for 24 hours. X-ray analysis revealed that the terminal iodine on the Zn cation had swapped with chlorine from the solvent to yield [($ImMe_2{}^iPr_2)_3ZnCl$][I]. ^{1}H NMR (CD_2Cl_2, 400 MHz): δ 5.59 (sept, 6H, NC*H*$(CH_3)_2$, $^3J_{HH}$ = 7.6 Hz), 2.22 (s, 18H, NCC*H*$_3$), 1.39 (d, 36H, NCH(C*H*$_3)_2$, $^3J_{HH}$ = 7.6 Hz). ^{13}C{^{1}H} NMR (CD_2Cl_2, 126 MHz): δ 171.7 (N*C*N), 126.3 (N*C*CH_3), 53.1 (N*C*$(CH_3)_2$), 21.9 ((NC(*C*$H_3)_2$), 10.5 (NC*C*H_3). Mp (°C): 213-215. Anal. Calcd. for $C_{33}H_{60}I_2N_6Zn$: C, 46.08; H, 7.03; N, 9.77. Found: C, 46.37; H, 6.81; N, 9.38.

5.5.33 Synthesis of [IPr•Zn(OTf)$(DMAP)_2$][OTf] (4)

A solution of IPr (0.198 g, 0.510 mmol) in 2 mL of THF was added to a suspension of $Zn(OTf)_2$ (0.185 g, 0.509 mmol) in 3 mL of THF. The resultant

pale yellow solution was allowed to stir for 2 hours, upon which time a solution of 4-dimethylaminopyridine (DMAP; 0.126 g, 1.03 mmol) in 3 mL of THF was added, with no visible change to the mixture noted. This solution was allowed to stir for an additional 16 hours, upon which time the solution was concentrated to half its original volume *in vacuo*. 10 mL of hexanes was then added, which resulted in the formation of white precipitate from the solution. This insoluble solid was allowed to settle, the filtrate decanted away, and the residual solid washed with 2 × 4 mL diethyl ether prior to being allowed to dry under high vacuum for 2 hours, to yield **4** as a fine, white powder (0.397 g, 78 %). Crystals of suitable quality for X-ray diffraction were obtained by dissolving the solid in 2 mL of THF, before layering with 3 mL of toluene, and allowing the two layers to diffuse together overnight at room temperature. ^{1}H NMR ($CDCl_3$, 500 MHz): δ 7.58 (t, 2H, p-Ar*H*, $^{3}J_{HH}$ = 8.0 Hz), 7.47 (s, 2H, NC*H*), 7.30 (d, 4H, m-Ar*H*, $^{3}J_{HH}$ = 8.0 Hz), 7.02 (broad s, 4H, DMAP-Ar*H*), 6.38 (broad s, 4H, DMAP-Ar*H*), 3.04 (s, 12H, N(C*H*$_3$)$_2$), 2.54 (sept, 4H, ArC*H*(CH$_3$)$_2$, $^{3}J_{HH}$ = 7.0 Hz), 1.16 (d, 2H, ArCH(C*H*$_3$)$_2$, $^{3}J_{HH}$ = 7.0 Hz), 1.06 (d, 2H, ArCH(C*H*$_3$)$_2$, $^{3}J_{HH}$ = 7.0 Hz). ^{13}C{^{1}H} NMR ($CDCl_3$, 126 MHz): δ 171.4 (N*C*N), 155.5 (Ar*C*), 147.3 (DMAP-Ar*C*), 145.6 (Ar*C*), 133.7 (Ar*C*), 131.9 (Ar*C*), 125.0 (Ar*C*), 120.3 (q, $^{1}J_{CF}$ = 320 Hz, O$_3$S*C*F$_3$), 107.5 (DMAP-Ar*C*), 39.4 (N(*C*H$_3$)$_2$), 29.1 (Ar*C*H(CH$_3$)$_2$), 25.9 (ArCH(*C*H$_3$)$_2$), 22.5 (ArCH(*C*H$_3$)$_2$). Mp (°C): 184-188. Anal. Calcd. for $C_{43}H_{56}F_6N_6O_6S_2Zn$: C, 51.83; H, 5.66; N, 8.43; S, 6.43. Found: C, 51.12; H, 5.58; N, 8.41; S, 6.02.

5.5.5.4 Synthesis of $[(ImMe_2{}^iPr_2)_3Zn(CO)][OTf]_2$ (5)

Compound **2** (0.251 g, 0.278 mmol) was dissolved in 3 mL of THF to yield a pale yellow solution. CO gas was allowed to bubble through this solution for 20 minutes, and the resultant mixture was allowed to stir for 1 hour. At this point, the volatiles were removed *in vacuo*. This yielded pale yellow solid which was washed with 2 × 2mL of diethyl ether prior to being allowed to dry under high vacuum for 2 hours. (0.235 g, 91% yield). The product could be further purified by dissolving in 4 mL of fluorobenzene and layering with 5 mL of hexanes before allowing the two layers to diffuse together overnight, yielding **5** as an analytically pure white solid after drying for 3 hours *in vacuo*. ^{1}H NMR (CD_2Cl_2, 500 MHz): δ 4.30 (sept, 6H, NC*H*$(CH_3)_2$, $^3J_{HH}$ = 7.0 Hz), 2.10 (s, 18H, NCC*H*$_3$), 1.48 (d, 36H, NCH(C*H*$_3)_2$, $^3J_{HH}$ = 7.0 Hz). ^{13}C{^{1}H} NMR (CD_2Cl_2, 126 MHz): δ 164.2 (Zn-*C*O) 162.3 (N*C*N), 126.5 (N*C*CH$_3$), 120.9 (q, O_3SCF_3, $^1J_{CF}$ = 320 Hz), 51.4 (N*C*$(CH_3)_2$), 22.8 ((NC(*C*H$_3)_2$), 8.8 (NC*C*H$_3$). ^{19}F{^{1}H} NMR (CD_2Cl_2, 469 MHz): δ -79.1 (O_3SCF_3). IR (cm^{-1}): $\nu_{(CO)}$ = 2149. Mp (°C): 144-147. Anal. Calcd. for $C_{36}H_{60}F_6N_6O_7S_2Zn$: C, 46.37; H, 6.49; N, 9.01. Found: C, 46.01; H, 6.83; N, 8.89.

5.5.2.5 Thermolysis of $[IPr{\bullet}ZnH(\mu\text{-}H)]_2$ to afford crystalline Zn

A solution of $[IPr{\bullet}ZnH(\mu\text{-}H)]_2$ (0.103 g, 0.113 mmol) was dissolved in 4 mL of benzene, and sealed inside a Teflon-capped Schlenk flask. The resultant pale yellow solution was heated to 60 °C for four hours, by which time visible Zn metal formation was observed in the form of a Zn mirror on the inside of the glass

wall of the flask. The reaction was cooled to room temperature, sonicated for 30 seconds, and then brought into a nitrogen-filled glovebox and the filtrate decanted away. Removal of the volatiles from the filtrate *in vacuo* yielded 0.053 g of colourless solid, which was shown by 1H NMR spectroscopy to be a mixture of IPr[14] (85%) and [IPr]H_2[31] (15%). The resulting Zn metal was collected and dried *in vacuo* to yield 12.0 mg of crystalline Zn (81% yield).

5.5.2.6 Microwave assisted Thermolysis of [IPr•ZnH(μ-H)]$_2$ in the presence of Si-NCs

In a glovebox, a solution of [IPr•ZnH(μ-H)]$_2$ (40 mg, 44 μmol) in 3 mL of Ph_2O and 2 mL (18.6 mmol) of dry N,N-dimethylpropargylamine was added to a suspension of 18 mg of Si-NCs in 2 mL of toluene in a microwave vial, and the vial was capped. This was heated to a maximum of 190 °C for 1 hour via microwave-assisted thermolysis, upon which time the mixture was allowed to cool. The resultant solution was decanted from the microwave vial, concentrated by removal of solvent *in vacuo* to half its original volume, and precipitated with 20 mL EtOH to yield 15 mg of Zn-coated Si-NCs for analysis.

Table 5.1 Crystallographic Data for Compounds **2** and **3**

	2	**3**
empirical formula	$C_{35}H_{60}F_6N_6O_6S_2Zn$	$C_{33}H_{60}ClIN_6Zn$
fw	904.38	768.59
cryst dimens (mm^3)	0.48 × 0.11 × 0.06	0.27 × 0.19 × 0.15
cryst syst	orthorhombic	cubic
space group	*Fdd*2	$P2_13$
unit cell dimensions		
a (Å)	23.6554 (6)	16.7243 (7)
b (Å)	70.6934 (19)	
c (Å)	10.4508 (3)	
α (deg)		
β (deg)		
γ (deg)		
V ($Å^3$)	17476.7 (8)	4677.8 (6)
Z	16	4
ρ (g cm^{-3})	1.375	1.091
abs coeff (mm^{-1})	2.313	1.266
T (K)	173 (1)	173 (1)
$2\theta_{max}$ (deg)	148.18	55.05
total data	30819	75499
unique data (R_{int})	8753 (0.0396)	3608 (0.0371)
obs data [$I > 2\sigma(I)$]	8644	3418
Params	523	133
R_1 [$I > 2\sigma(I)$][a]	0.0350	0.0324
wR_2 [all data][a]	0.0903	0.0937
Max/Min $\Delta\rho$ (e^- $Å^{-3}$)	0.790/-0.726	1.178/-0.927

[a] $R_1 = \Sigma \left| \left| F_o \right| - \left| F_c \right| \right| / \Sigma \left| F_o \right|$; $wR_2 = [\Sigma\, w(F_o^2 - F_c^2)^2 / \Sigma\, w(F_o^4)]^{1/2}$.

Table 5.2 Crystallographic Data for Compound **4**

	4•$2CH_2Cl_2$
empirical formula	$C_{45}H_{60}Cl_4F_6N_6O_6S_2Zn$
fw	1166.28
cryst dimens (mm^3)	0.28 × 0.28 × 0.28
cryst syst	monoclinic
space group	*C*2/*c*
unit cell dimensions	
a (Å)	29.8125 (14)
b (Å)	11.6623 (5)
c (Å)	34.8201 (15)
α (deg)	
β (deg)	110.316 (2)
γ (deg)	
V ($Å^3$)	17353.3 (9)
Z	8
ρ (g cm^{-3})	1.365
abs coeff (mm^{-1})	3.602
T (K)	173 (1)
$2\theta_{max}$ (deg)	148.42
total data	39821
unique data (R_{int})	11545 (0.0223)
obs data [$I > 2\sigma(I)$]	10009
Params	613
R_1 [$I > 2\sigma(I)$][a]	0.0497
wR_2 [all data][a]	0.1405
Max/Min $\Delta\rho$ (e^- $Å^{-3}$)	0.524/-0.414

[a] $R_1 = \Sigma \left| \left| F_o \right| - \left| F_c \right| \right| / \Sigma \left| F_o \right|$; $wR_2 = [\Sigma\, w(F_o^2 - F_c^2)^2 / \Sigma\, w(F_o^4)]^{1/2}$.

Figure 5.15 ^{1}H NMR spectrum (CD_2Cl_2, 500 MHz) of **5** [(*) = residual proton peak within NMR solvent]

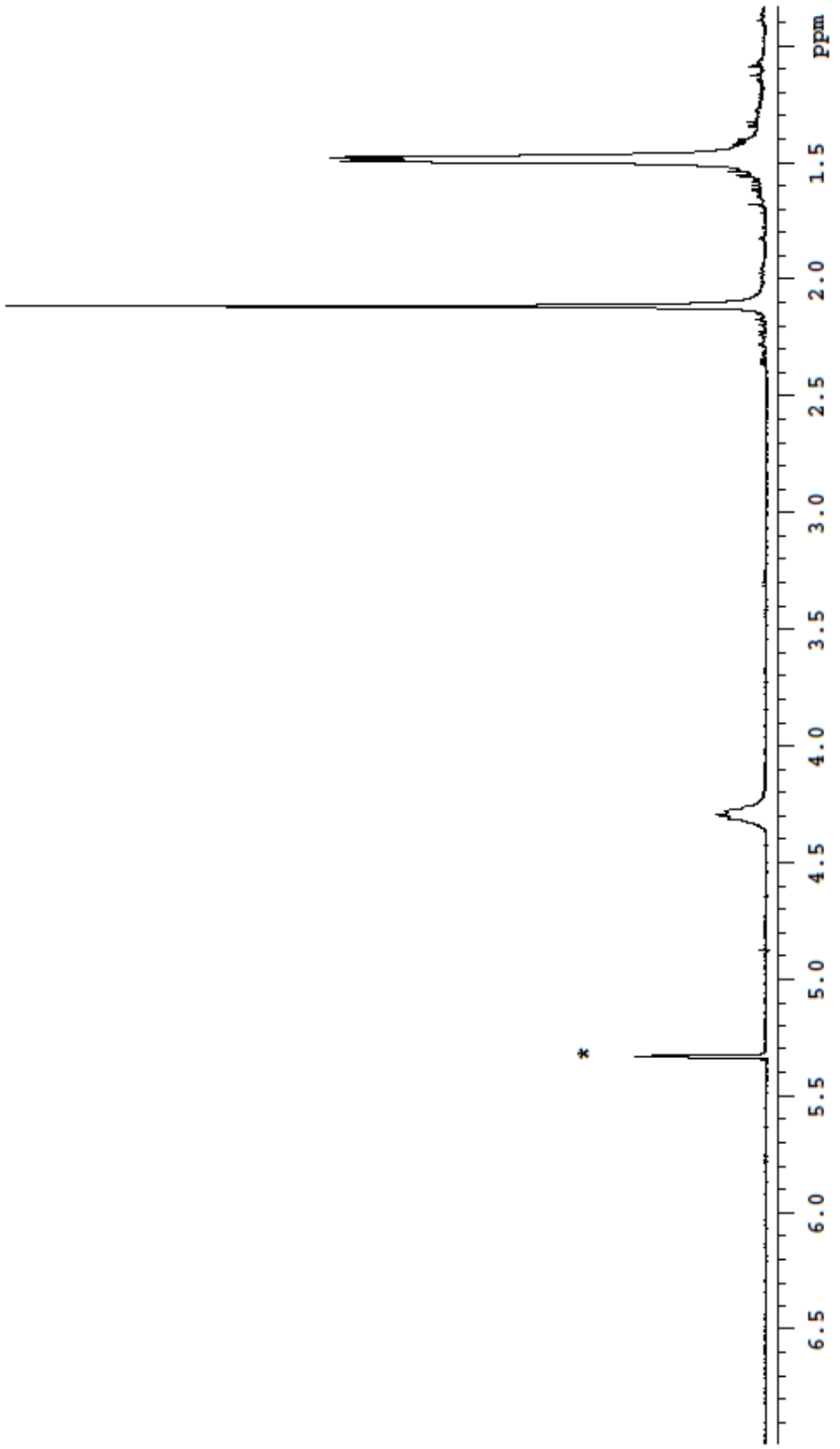

Figure 5.16 $^{13}C\{^{1}H\}$ NMR spectrum (CD_2Cl_2, 126 MHz) of **5** [(*) Denotes residual protio peak from NMR solvent; # Denotes residual solvent within solvent]

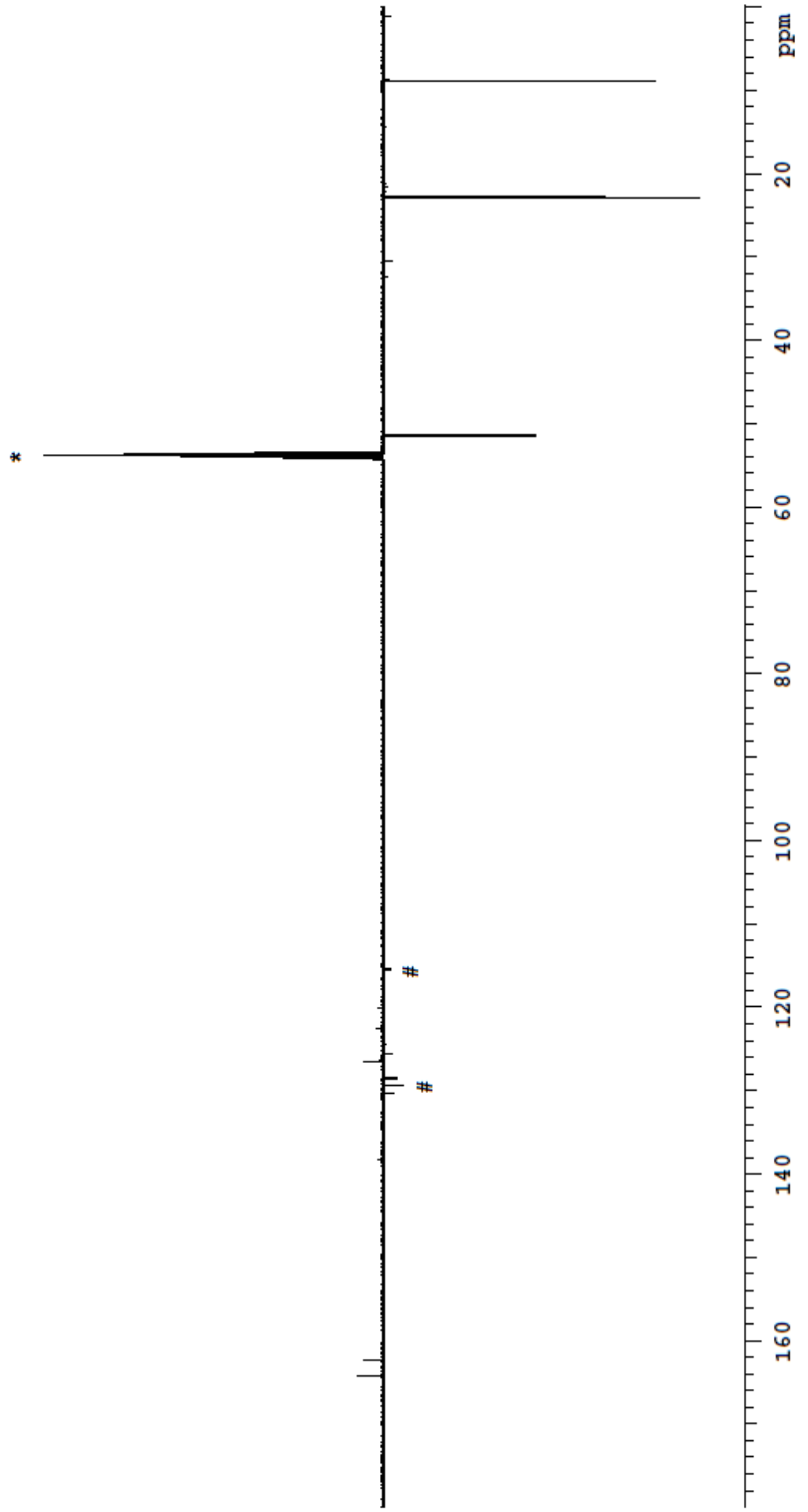

Figure 5.15 ^{19}F NMR spetrum (CD_2Cl_2, 475 MHz) of **5**.

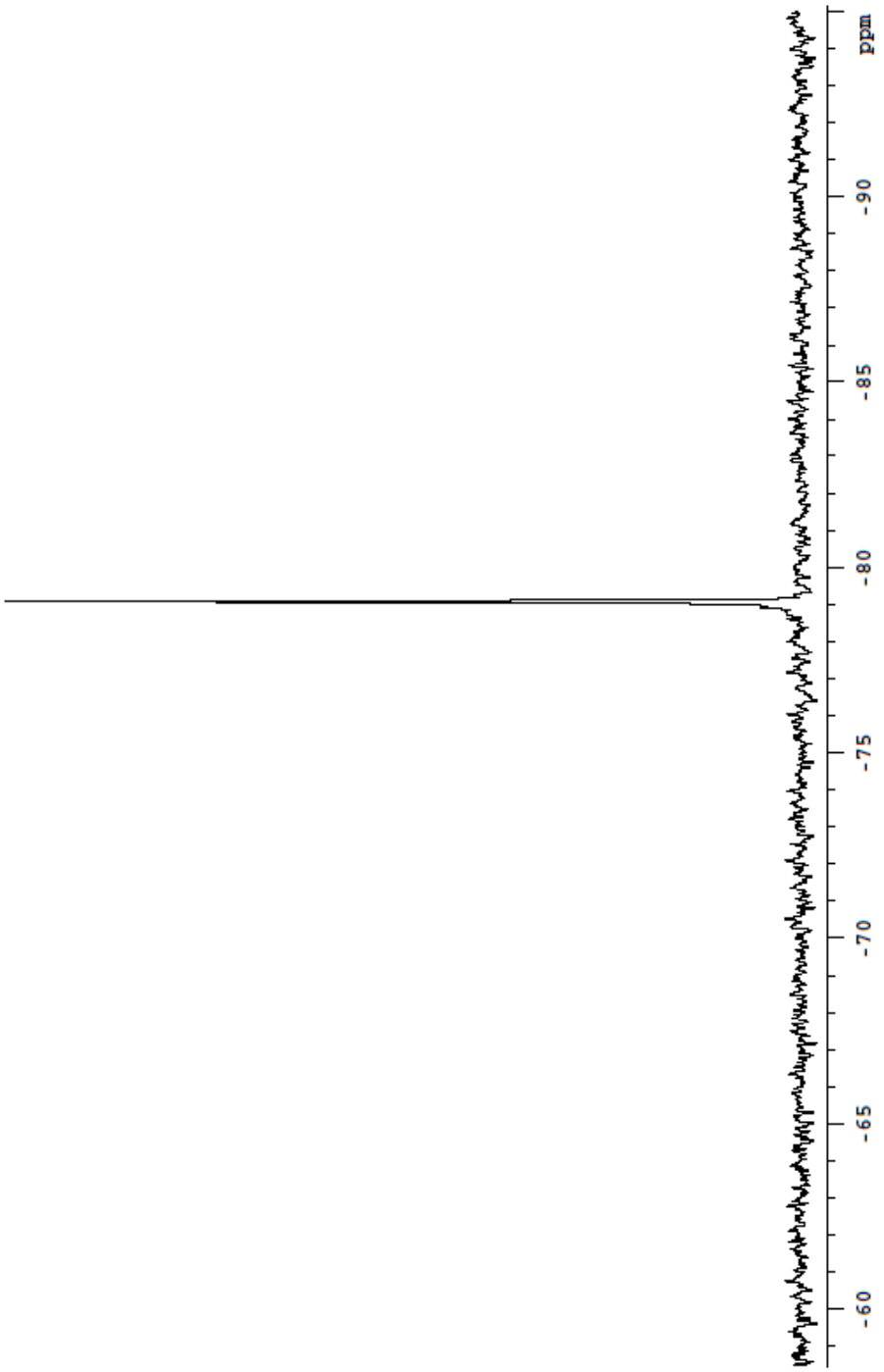

Figure 5.18 IR spectrum (prepared from evaporation of a DCM solution on IR plate) of **5**.

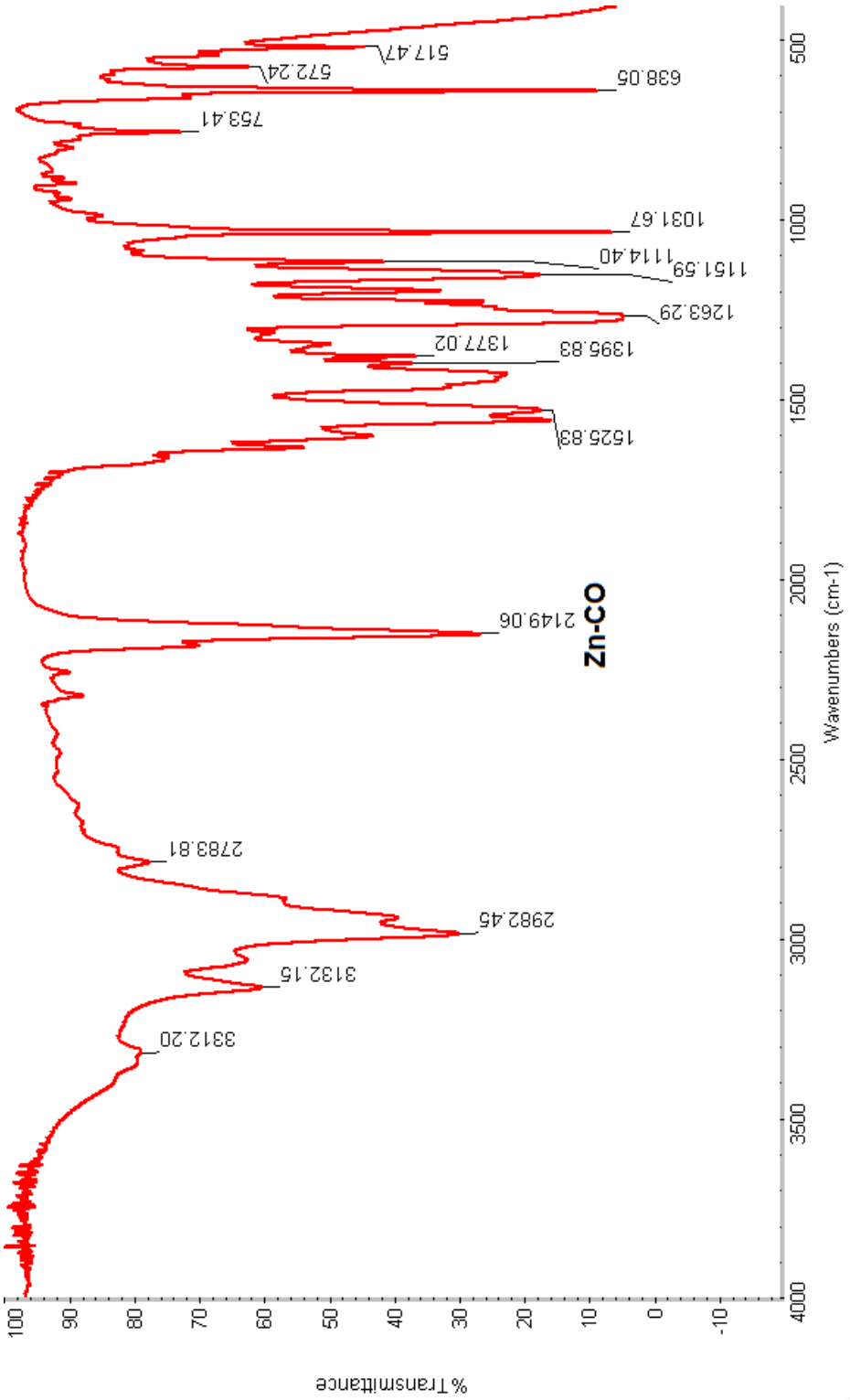

5.6 References

1. P. Schützenberger *Bull. Soc. Chim. Paris,* **1868**, *10*, 188.
2. L. Mond, C. Langer, F. Quincke, *J. Chem. Soc., Trans.* **1890**, *57*, 749.
3. R. Franke, D. Selent, A. Borner, *Chem. Rev.* **2012**, *112*, 5675.
4. S. W. Ragsdale, *Chem. Rev.* **2005**, *106*, 3317.
5. (*a*) F. Aubke, *J. Fluorine Chem.*, **1995**, *72*, 195; (*b*) H. Willner, F. Aubke, *Chem. Eur. J.* **2003**, *9*, 1669.
6. A. S. Goldman, K. Krough-Jesperson, *J. Am. Chem. Soc.* **1996**, 118, 12159.
7. L. Jiang, Q. Xu, *J. Am. Chem. Soc.* **2005**, 127, 8906.
8. L. Jin, L. –J. Fu, Y. –H. Ding, *Phys. Chem. Chem. Phys.,* **2010**, *12*, 10956.
9. T. R. Krawietz, D. H. Barich, L. W. Beck, T. Howard, T. Xu, J. F. Haw, *J. Am. Chem. Soc.* **1995**, *117*, 10407.
10. G. Ghiotti, F. Boccuzzi, R. Scala, *J. Catal.* **1985**, *92*, 79.
11. J. C. Lavalley, J. Saussey, R. Rais, *J. Mol. Catal*. **1982**, *17*, 289.
12. A. J. Lupinetti, V. Jonas, W. Thiel, S. H. Strauss, G. Frenking, *Chem. Eur. J.* **1999**, *5*, 2573.
13. K. Watanabe, D. Menzel, N. Nilius, H. J. Freund, *Chem. Rev.* **2006**, *106*, 4301.
14. C. N. R. Rao, G. U. Kulkarni, P. J. Thomas, P. P. Edwards, *Chem. Soc. Rev.* **2000**, *29*, 27.

15. E. H. Khan, S. C. Langford, J. T. Dickinson, L. A. Boatner, W. P. Hess, *Langmuir* **2009**, *25*, 1930.

16. K. Aslan, M. J. R. Previte, Y. Zhang, C. D. Geddes, *J. Phys. Chem. C* **2008**, *112*, 18368.

17. R. S. Devan, J.-H. Lin, Y.-J. Huang, C.-C. Yang, S. Y. Wu, Y. Liou, Y.-R. Ma, *Nanoscale* **2011**, *3*, 4339

18. N. T. Mai, T. T. Thuy, D. M. Scott, S. Maenosono, *Cryst. Eng. Comm.* **2013**, *15*, 6606.

19. J.-H. Lin, Y.-J. Huang, Y.-P. Su, C.-A. Liu, R. S. Devan, C.-H. Ho, Y.-P. Wang, H.-W. Lee, C.-M. Chang, Y. Liou, Y.-R. Ma, *RSC Adv.* **2012**, *2*, 2123.

20. N. A. Dhas, A. Zaban, A. Gedanken, *Chem. Mater.* **1999**, *11*, 806.

21. M. L. Kahn, M. Monge, V. Colliere, F. Senocq, A. Maisonnat, B. Chaudret, *Adv. Funct. Mater.* **2005**, *15*, 458.

22. M. H. Mobarok, E. J. Luber, G. M. Bernard, L. Peng, R. Wasylischen, J. M. Buriak, *Chem. Mater.* **2014**, *26*, 1925.

23. B. Wiley, Y. Sun, Y. Xia, *Acc. Chem. Res.* **2007**, *40*, 1067.

24. C. S. Birkel, E. Mugnaioli, T. Gorelik, U. Kolb, M. Panthöfer, W. Tremel, *J. Am. Chem. Soc.* **2010**, *132*, 9881.

25. L. Jafarpour, E. D. Stevens, S. P. Nolan, *J. Organomet. Chem.* **2000**, *606*, 49.

26. P. A. Lummis, M. R. Momeni, M. W. Lui, R. McDonald, M. J. Ferguson, M. Miskolzie, A. Brown, E. Rivard, *Angew. Chem. Int. Ed.*, **2014**, *53*, 9347.

27. N. Kuhn, T. Kratz, *Synthesis,* **1993**, 561.

28. S. M. I. Al-Rafia, P. A. Lummis, A. K. Swarnakar, K. C. Deutsch, M. J. Ferguson, R. McDonald, E. Rivard, *Aus. J. Chem.* **2013***, 66,* 1235.

29. T. K. Purkait, A. K. Swarnakar, G. B. De Los Reyes, F. A. Hegmann, E. Rivard, J. G. C. Veinot, *Nanoscale*, **2015**, *7*, 2241.

30. A. Rit, T. P. Spaniol, L. Maron, J. Okuda, *Angew. Chem. Int. Ed.* **2013**, *52*, 4664.

31. S. M. I. Al-Rafia, A. C. Malcolm, S. K. Liew, R. McDonald, E. Rivard, *J. Am. Chem. Soc.* **2011**, *133*, 777.

32. M. S. Chandrasekar, S. Srinivasan, M. Pushpavanan, *J. Mater. Sci.* **2010**, *45*, 1160.

33. A. Irzh, I. Genish, L. Klein, L. A. Solovyov, A. Gedanken, *Langmuir*, **2010**, *26*, 5976.

34. S. Sanctis, R. C. Hoffmann, J. J. Schneider, *RSC Adv.* **2013**, *3*, 20071.

35. C. M. Hessel, E. J. Henderson, J. G. C. Veinot, *Chem. Mater.* **2006**, *18*, 6139.

36. A. B. Pangborn, M. A. Giardello, R. H. Grubbs, R. K. Rosen, F. J. Timmers, *Organometallics*, **1996**, *15*, 1518.

37. H. Hope, *Prog. Inorg. Chem.*, **1993**, *41*, 1.

38. G. M. Sheldrick, *Acta. Cryst.,* **2008**, *A64*, 112.

Chapter 6

Summary and future work

6.1 Summary and future work

Chapter 2 described the synthesis of a series of zirconium compounds featuring the bis(amido)silyl ligand, $[(DippN)_2Si^iPr_2]^{2-}$ ($[NSiN]^{Dipp}$). To our surprise, the protonated analogue, $H_2[(DippN)_2Si^iPr_2]$ did not undergo a protonolysis reaction with $Zr(NMe_2)_4$ which would have yielded the potential dehydrogenation catalyst $[NSiN]^{Dipp}Zr(NMe_2)_2$. This may be due to the lone-pair on nitrogen within $H_2[NSiN]^{Dipp}$ interacting preferentially with the adjacent Si-C σ* orbitals which reduces the nucleophilicity of the nitrogen centres. Despite this set back, the corresponding dilithio salt $Li_2[NSiN]^{Dipp}$ was prepared and nucleophilic substitution chemistry was utilised to generate the zirconium halide complex $[NSiN]^{Dipp}ZrCl(\mu\text{-}Cl)_2Li(THF)_2$; from this species amido, borohydride and methyl-substituted variants could be made. The goal of these synthetic explorations was to obtain suitable catalysts for the dehydrocoupling of amine-boranes. In addition, the previously reported compound $Cl_2Zr(NMe_2)_2(THF)_2$[1] was employed to gain access to the di-substituted complex $[NSiN]^{Dipp}Zr(NMe_2)_2{\bullet}ClLi(THF)_3$. This compound proved to be effective as a pre-catalyst for the dehydrocoupling of select amine-boranes, with the implied catalytically active species being the corresponding hydride $[NSiN]^{Dipp}ZrH_2$, although this species was not detected by NMR or IR spectroscopy. Indirect evidence for the formation of a transient, catalytically active zirconium hydride comes from the sensitivity of the generated active catalyst towards chlorinated solvents (despite $[NSiN]^{Dipp}Zr(NMe_2)_2{\bullet}ClLi(THF)_3$ being stable over time in chlorinated solvents).[2] The more hindered bis(amido)silyl ligand, $[(Ph_3SiN)_2Si^iPr_2]^{2-}$

([NSiN]^{SiPh3}) was also bound to zirconium via salt metathesis between the *in situ* generated dilithio salt Li_2[NSiN]^{SiPh3} and $Cl_4Zr(THF)_2$, to form the bis(amido)zirconium species [NSiN]$^{SiPh3}ZrCl_2(THF)_2$. Future work in this area would include preparing the corresponding bis(dimethylamido)zirconium complex [NSiN]$^{SiPh3}Zr(NMe_2)(THF)_x$ (x = 1 or 2), and testing the activity of this species towards the catalytic dehydrocoupling of amine-boranes as a means of investigating whether these complexes show enhanced thermal or photostability, in addition to the effect of the increased steric bulk of the ligand on the catalytic dehydrocoupling chemistry. Next, it would also be of interest to explore the previously reported 1,2-bis(2,6-diisopropylphenylamino)benzene (**1**)[3] as a ligand precursor (Figure 6.1) as the C-N linkage is more robust than the corresponding Si-N bond, in addition to the potential to employ the protonolysis methodology that did not work for the aforementioned silylamine ligand precursors. To this end, Hahn and coworkers demonstrated the synthesis of low valent group 14 element complexes [1,2-(DippN)$_2$-C_6H_4]E: (E = Ge and Sn) via the reaction of **1** with E(N(SiMe$_3$)$_2$)$_2$ with concomitant loss of two equivalents HN(SiMe$_3$)$_2$.[4] In addition, the bulkier derivative 1,2-bis(triphenylmethylamino)benzene (**2**), first reported in 1952 by Van Leeuwen and coworkers,[5] might be able to support catalytically active Zr(IV) hydride complexes. These bulkier ligands would serve to provide an enhanced degree of kinetic stabilisation to the zirconium hydride motif, and also prevent the dimerisation of these species (as dimerisation might lead to a reduction in activity in dehydrocoupling catalysis).

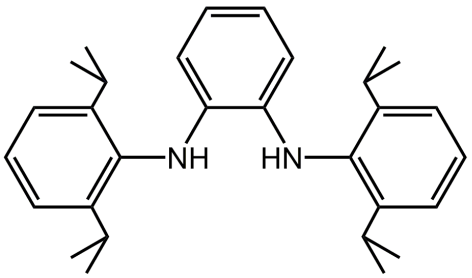

1

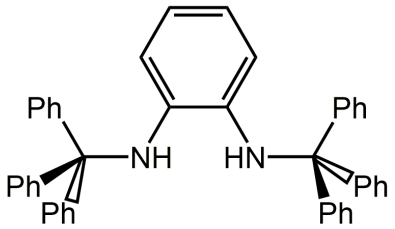

2

Figure 6.1 Previously reported ligand precursors 1,2-$(DippNH)_2C_6H_4$ (**1**) and 1,2-$(Ph_3CNH)_2C_6H_4$ (**2**).

Chapter 3 describes the synthesis of a new, bulky silylbis(amine), $[(Xyl_3SiNH)_2Si^iPr_2]$ ($H_2[NSiN]^{SiXyl3}$), which is a possible pre-ligand for the formation of low coordinate main group and transition metal-based complexes. Initial attempts to attach a $[NSiN]^{SiXyl3}$ unit onto germanium via the reaction of the *in situ* generated dilithio salt $Li_2[NSiN]^{SiXyl3}$ with Cl_2Ge•dioxane did not yield clean products. Future work would include optimisation of the conditions (solvent, temperature etc.) to yield low coordinate E[NSiN] complexes (E = Si, Ge and Sn). One possible application of these hindered [NSiN] ligands would be to kinetically stabilise reactive bonding environments, such as group 14–group 16 element multiple bonds (e.g. in $[NSiN]^{SiXyl3}Si{=}O$, $[NSiN]^{SiXyl3}Ge{=}O$). The second part of chapter 3 describes the synthesis of bis(tetramethylguanidine) ligands bridged by silane, disilane and disiloxane linkages. Most of these species are air sensitive oils, however the tolyl-substituted silane $[\{(Me_2N)_2C{=}N\}_2Si(p\text{-}tolyl)_2]$ can be obtained as a low-melting white, crystalline solid. Unfortunately these compounds proved to be relatively poor ligands, and in the reaction between $[\{(Me_2N)_2C{=}N\}SiMe_2]_2$ and Cl_2Ge•dioxane, Si-N backbone cleavage occurred to form $[\{(Me_2N)_2C{=}N\}GeCl]_2$ and $ClSiMe_2SiMe_2Cl$. In the future,

similar ligands featuring -CH_2CH_2- and C_6H_4 linkages between the capping R_2C=N units should be investigated, due to the increased stability of the N-C bonds relative the N-Si linkages described herein (as mentioned previously). Furthermore, there are more sterically demanding *N*-heterocyclic guanidine derivatives derived from *N*-heterocyclic carbenes that would allow for the development of a large variety of guanidine ligands (Scheme 6.2). As there have been a wide range of previously reported *N*-heterocyclic carbene ligands, this offers access to a significant number of potential ligands, which can be easily tuned to obtain the desired steric and electronic properties (via reaction of the free carbene with Me_3SiN_3 and subsequent work-up as previously described by Tamm and coworkers).[6]

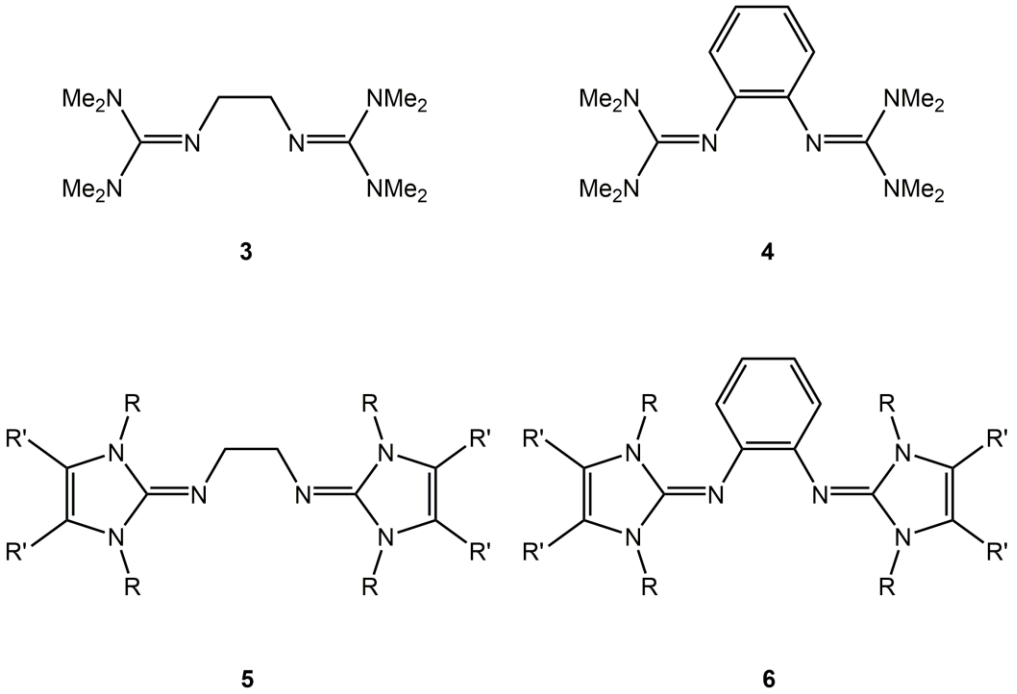

Figure 6.2 Bidentate bis-guanidine ligands featuring acyclic guanidine [$(Me_2N)_2C$=N] units (**3**, **4**) and cyclic guanidines derived from *N*-heterocyclic carbene moieties (**5**, **6**: R = Aryl, alkyl; R′ = H, Me).

As mentioned, previous examples of tethered bis(guanidine) ligands have been previously reported in the literature,[6] however there still remains significant scope to expand the library of these bis(guanidine) species, and further their use towards low-valent main group and transition metal complexes such as LB•ZnH_2 (LB = Lewis Base) complexes and derivatives thereof, where ligands such as phosphines were not sufficiently donating to stabilise the desired species. These ligands may prove to be particularly versatile due to their enhanced σ-donation strength relative to similar imine ligands due to the resonance stabilisation of an increased negative charge on the donor nitrogen atoms.

In Chapter 4, the preparation of *N*-heterocyclic carbene (NHC) adducts of group 12 element dihalides, hydrides and triflates (MX_2; M = Zn, Cd; X = I, H, OTf) is described. An optimised procedure to access the zinc dihydride adducts [NHC•ZnH(μ-H)]$_2$ (NHC = IPr[7] and $ImMe_2{}^iPr_2$;[8] IPr = [(DippNCH)$_2$C:]; $ImMe_2{}^iPr_2$ = [(MeCN^{i}Pr)$_2$C:]), and a new route to these species from the reaction between NHC•ZnI_2 complexes and two equivalents of the commercially available hydride source K[HB^{s}Bu$_3$] are presented. In the case of the hydride complex [IPr•ZnH(μ-H)]$_2$ it was shown that the terminal hydrides within the zinc hydride core are susceptible to electrophilic attack by MeOTf, which gives access to the previously unreported $[ZnH]^+$ complex IPr•ZnH(OTf)•THF. It was shown that this species is more thermally robust than the known neutral carbene ZnH_2 adducts, and that they can function as efficient catalysts for the hydrosilylation and hydroboration of simple ketones such as benzophenone. Next, it was demonstrated that 4-

dimethylaminopyridine (DMAP) can displace both THF and OTf^- from the coordination sphere of the zinc centre in IPr•ZnH(OTf)•THF to yield the formal $[ZnH]^+$ complex $[IPr•ZnH(DMAP)_2][OTf]$. In addition the synthesis of the mixed zinc iodohydride dimer $[IPr•ZnI(\mu\text{-}H)]_2$ was reported. Future work in this area will focus upon the preparation of hydrido element zinc adducts IPr•ZnH(R) (R = amides, alkynes, thiolates and alkoxides) and their use in hydrosilylation and dehydrocoupling catalysis. This may be achieved either via a protonolysis reaction between $[IPr•ZnH(\mu\text{-}H)]_2$ and the desired amine, alkyne thiol or alcohol, or via the reaction of the salt of one of these aforementioned species with the mixed iodohydride species $[IPr•ZnI(\mu\text{-}H)]_2$. This may also provide an appropriate avenue to study carbene-tethered complexes featuring Zn-element multiple bonds (e.g. Zn=NR, Zn=O, Zn=S) and to study the reactivity of these species. Additionally, it would be of interest to investigate the effect of the anion on the reactivity of these complexes, especially as the triflato anion has the ability to bind to the metal centre and block a coordination site more than other anions such as $[B(3,5\text{-}CF_3\text{-}C_6H_3)_4]^-$ or $[B(C_6F_5)_4]^-$.

The final research chapter of this thesis outlines the synthesis of tris(NHC) adducts of ZnX_2 $[(NHC)_3ZnX][X]$ (NHC = $ImMe_2{}^iPr_2$, X = I, OTf). Preliminary evidence for the ability of the $[(NHC)_3Zn(OTf)][OTf]$ species to bind carbon monoxide to form $[(NHC)_3ZnCO][OTf]_2$ was presented; this is notable as the isolation of a thermally stable zinc carbonyl species has yet to be reported. Future work here would involve the preparation of crystals of a Zn-CO complex that are of sufficient quality for single crystal X-ray

diffraction analysis, in addition to the preparation of the ^{13}C labelled CO analogues for IR and NMR spectroscopic investigations. In addition, it would be interesting to investigate the reactivity of the resultant cationic zinc hydride complexes with CO, to first determine whether these species will bind CO, and furthermore then convert CO into H_2CO and H_3COH. In order to fully realise this reactivity, it is likely that the triflato ligand in IPr•ZnH(OTf)•THF would be replaced with different weakly coordinating anions (such as the aforementioned $[B(C_6F_5)_4]^-$) that would interact less with the Zn centre, and thus be less likely to compete with the CO for binding.

The second half of Chapter 5 outlined the controlled thermolysis of $[IPr•ZnH(\mu\text{-}H)]_2$ to yield oxide-free, crystalline zinc from solution with loss of H_2 and regeneration of the IPr ligand; the free IPr formed can then be recovered and reused in the same process. Future work in this area would involve the optimisation of this deposition process (with respect to time, temperature, solvent etc.), in addition to the controlled oxidation of the deposited Zn to form ZnO and ZnS materials which hold promise as potential optoelectronic materials as the bulk materials for each are wide band-gap semi-conductors. Another area of focus here would be to utilise the functionalised zinc hydride species proposed earlier to determine how the physical properties of these complexes can be controlled with addition of alternative functional groups to yield a $[LB•ZnH(R)]_n$ arrangement (LB = Lewis base; R = alkyl, amido, alkoxy, siloxy). Finally, there have been reported in the literature other Lewis-base adducts of first row transition metal hydrides for metals such as Cu[9] and Fe[10], therefore it would be of interest to

expand this methodology to these (and similar) compounds to determine whether the proposed mild thermolysis of Lewis-base metal hydride species to yield metal-containing surfaces and nanomaterials can be expanded beyond the realm of zinc hydride chemistry, particularly for lost cost metals such as those mentioned.

6.2 References

1 S. Brenner, R. Kempe, P. Arndt, *Z. Anorg. Allg. Chem.*, **1995**, *621*, 2021.

2 P. C. Wailes, H. Weigold, *J. Organomet. Chem.*, **1970**, *24*, 405.

3 T. Wenderski, K. M. Light, D. Ogrin, S. G. Bott, C. J. Harlan, *Tetrahedron Lett.*, **2004**, *45*, 6851.

4 S. Krupski, R. Pöttgen, I. Schellenberg, F. E. Hahn, *Dalton Trans.*, **2014**, *43*, 173.

5 P. E. Verkade, H. Nijon, F. D. Tollenaar, J. H. Van Rij, M. Van Leeuwen, *Recl. Trav. Chim. Pays-Bas*, **1952**, *71*, 1007.

6 D. Petrovic, T. Glöge, T. Bannenberg, C. G. Hrib, S. Randoll, P. G. Jones, M. Tamm, *Eur. J. Inorg. Chem.*, **2007**, *22*, 3472.

7 L. Jafarpour, E. D. Stevens, S. P. Nolan, *J. Organomet. Chem.* **2000**, *606*, 49.

8 N. Kuhn, T. Kratz, *Synthesis*, **1993**, 561.

9 S. A. Bezman, M. R. Churchill, J. A. Osborn, J. Wormald, *J. Am. Chem. Soc.*, **1971**, *93*, 2063.

10 W. Hieber, F. Leutert, *Naturwissenschaften*, **1931**, *19*, 360.